DOCTORATE SCHOOL
UNIVERSITÀ DEGLI STUDI DI MILANO-BICOCCA

Department of Biotechnology and Biosciences (BtBs)

PhD program in Converging Technologies for Biomolecular Systems (TeCSBi)
Cycle XXXVI

# Leveraging Recombinant Vault Nanoparticles Produced in *Komagataella phaffii* for Targeted Delivery of siRNAs as therapeutic molecules

*Joint PhD*


Surname: **Tomaino** Name: **Giulia**
Registration number: 791182

Tutor: Marco Vanoni
Co-tutor: Domenico Flagiello
Supervisor: Gianni Frascotti
Coordinator: Paola Branduardi


**Academic year 2022/2023**

# Contents

## Summary

In recent years, nanotechnology have made a significant impact in the field of medicine through the remarkable therapeutic and diagnostic potential of nanoparticles (NPs). Among these, protein-based NPs have gained considerable attention as drug delivery systems and vaults emerge as ideal candidates. Vaults are the largest known ribonucleoprotein particles naturally occurring in higher eukaryotic cells. 78 copies of the dominant component Major Vault Protein (MVP) assemble into a barrel-like "nano-capsule", enclosing other proteins like poly (ADP-ribose) polymerase, telomerase-associated protein-1, and some small untranslated RNAs. While the precise physiological roles of this nanocomplex are not completely understood, it has been associated with numerous cellular functions that promote cell survival and provide cytoprotective effects. Vaults possess unique properties, including non-immunogenicity, biodegradability, dynamic structure, and a spacious cavity, making them highly attractive for delivery of therapeutic molecules, often targeted to cancer cell lines. However, existing production and purification protocols for vault are complex, partly due to their reliance on higher eukaryotes as expression systems. In **Chapter 1**, a newly published simplified procedure is presented, combining human vault expression in the yeast *Komagataella phaffii* and a purification process involving RNase pretreatment followed by size-exclusion chromatography, significantly streamlining the process. The study also addresses the challenge of protein aggregation and identifies optimal storage conditions. One remarkable vault feature is its ability to encapsulate cargo proteins by fusing them with the INT domain, derived from the vault-interacting vPARP protein. **Chapter 2** explores the encapsulation of GFP-INT as a reporter cargo within vaults expressed and purified using the simplified procedure. Encapsulation of GFP-INT was achieved through a straightforward mixing process, harnessing vaults' "breathing" property. The stoichiometry of GFP-INT

loading into vault lumen was found to saturate the binding site with about 20 copies of GFP-INT. Furthermore, the study confirms the ability of vaults to deliver cargo molecules inside cancer cells, particularly the Melanoma A375 cell line. The rise of nucleic acid-based therapeutics has demanded better delivery systems, leading researchers to rely on NPs to tackle this issue. Leveraging recombinant vault particles as nano-drug delivery systems shows significant promise. **Chapter 3** investigates the potential of using vaults for siRNA delivery, focusing on siRNAs targeting *LADON*, a lncRNA associated with tumor progression in melanoma. Two strategies were pursued: one involving chemical conjugation of siRNA to the INT domain, and the other aiming for the direct loading of siRNA into vaults. While progress is made in crosslinking GFP-INT, the construction of the final product, GFP-INT-siRNA, is still ongoing. With the other approach, the study demonstrates that recombinant vaults can mediate the delivery of naked siRNA molecules, without additional formulation aiding the transfection, causing a biological effect. To achieve specific targeting, NPs can be conjugated to antibodies (Ab) on the surface by different chemical methods. Yet these methods do not necessarily guarantee the correct orientation of the Ab to be active. **Chapter 4** addresses this challenge with the construction of an engineered vault variant carrying the protein A-derived Z peptide - tightly binding Fc portion of human IgG1 - allowing for direct and oriented Ab-vault conjugation. Vault-Z, produced and purified in *K. phaffii* with the optimized procedure, maintains the same morphology and size as the wild-type vault. A comprehensive characterization of vault-Z:Ab binding reveals the capacity to bind up to 10-12 Ab molecules per vault-Z. Lastly, we shown that vault-Z uptake in cancer cells, significantly increases upon conjugation with a targeting Ab.

# Riassunto

Le nanotecnologie stanno rivoluzionando il settore medico grazie al potenziale terapeutico e diagnostico delle nanoparticelle (NP). Le NP proteiche hanno ottenuto particolare attenzione come veicoli per la somministrazione di farmaci. Tra di esse spicca la NP vault, la più grande particella ribonucleoproteica conosciuta e presente naturalmente nelle cellule degli eucarioti superiori. La NP vault è costituita da 78 copie della Proteina Major Vault (MVP) che forma una struttura a barile, in grado di racchiudere altre proteine, come la poli (ADP-ribosio) polimerasi, la proteina 1 associata alla telomerasi e alcuni RNA non tradotti. I ruoli fisiologici della vault non sono del tutto chiari ma si riporta essere coinvolta in diverse funzioni cellulari per la sopravvivenza di citoprotezione. La NP vault presenta caratteristiche uniche: non è immunogenica, è biodegradabile e ha una struttura dinamica e una cavità spaziosa, che la rendono idonea per la somministrazione mirata di molecole terapeutiche, spesso destinate alle linee cellulari tumorali. Tuttavia, la produzione e la purificazione di vault rappresentano un processo complesso. Nel **Capitolo 1**, è presentata una procedura semplificata che combina l'espressione di vault nel lievito *Komagataella phaffii* con una procedura di purificazione che coinvolge il pretrattamento con RNasi seguito da cromatografia a esclusione molecolare. Lo studio affronta anche il problema dell'aggregazione proteica, identificando le condizioni di conservazione ottimali. La NP vault è capace di incapsulare proteine cargo se fuse con il dominio INT, derivato dalla proteina vPARP. Nel **Capitolo 2**, viene esplorata l'incapsulazione di GFP-INT come proteina cargo all'interno di vault, prodotte con una procedura semplificata. L'incapsulazione di GFP-INT sfrutta la proprietà di "respirazione" delle vault. Il lavoro ha anche valutato la stechiometria del carico di GFP-INT nella vault, evidenziando una saturazione con circa 20 copie di GFP-INT. Inoltre, è stata confermata l'efficacia delle vault nel trasportare molecole cargo all'interno delle cellule tumorali, come le cellule di melanoma A375. Nell'ultimo decennio, l'aumento delle terapie basate su acidi nucleici ha creato la necessità di sviluppare metodi di somministrazione più efficaci, spingendo i ricercatori a esplorare l'uso di nanoparticelle (NP) come potenziali strumenti. Nel **Capitolo 3**, è stata esaminata la possibilità di utilizzare le vault come veicoli per la

somministrazione di siRNA, concentrando l'attenzione sugli siRNA diretti contro *LADON*, un lungo RNA non codificante associato alla progressione e all'invasione tumorale nel melanoma. Due strategie sono state perseguite: una coinvolge il potenziale caricamento di siRNA nel lume delle vault tramite la coniugazione chimica al dominio INT, mentre l'altra mira al caricamento diretto di siRNA all'interno delle vault. Anche se il completamento del prodotto finale, GFP-INT-siRNA, è ancora in corso, lo studio ha dimostrato che le vault ricombinanti possono mediare con successo la somministrazione di siRNA non rivestiti senza richiedere formulazioni aggiuntive. La coniugazione, mediante metodi chimici, di anticorpi (Ab) sulla superficie di NPs ne permette il targeting attivo. Questa però non sempre garantisce il corretto orientamento dell'Ab. Nel **Capitolo 4**, questa sfida è stata affrontata con la creazione di vault-Z: variante ingegnerizzata che esprime il peptide Z derivato dalla proteina A in grado di legarsi saldamente alla porzione Fc delle IgG1 umane. Vault-Z, ottenuta utilizzando la procedura ottimizzata in *K. phaffii*, mantiene la stessa morfologia e dimensione della vault selvatica. Un'analisi approfondita ha rivelato la capacità di Vault-Z di legare fino a 10-12 molecole di Ab. Lo studio ha dimostrato un significativo aumento dell'endocitosi di Vault-Z nelle cellule tumorali SKBR3 quando essa è coniugata con anticorpi, suggerendo che tale NP rappresenta un potente strumento per il targeting mirato.

# Résumé

Au cours des dernières années, la nanotechnologie a eu un impact significatif dans le domaine de la médecine grâce au remarquable potentiel thérapeutique et diagnostique des nanoparticules (NP). Parmi elles, les NP à base de protéines ont attiré une attention considérable en tant que systèmes de délivrance de médicaments, et les vaults se présentent comme des candidats idéaux. Les vaults sont les plus grandes particules ribonucléoprotéiques naturellement présentes dans les cellules eucaryotes supérieures. 78 unités de la protéine Major Vault Protein (MVP), le composant dominant, s'assemblent pour former une "nano-capsule" en forme de tonneau, renfermant d'autres protéines telles que la poly(ADP-ribose) polymérase, la protéine 1 associée à la télomérase et de petits ARN non traduits. Bien que les rôles physiologiques précis de ce nanocomplexe ne soient pas entièrement compris, il a été associé à de nombreuses fonctions cellulaires favorisant la survie et offrant des effets cytoprotecteurs. Les vaults possèdent des propriétés uniques, notamment la non-immunogénicité, la biodégradabilité, la structure dynamique et une cavité spacieuse, ce qui les rend très attrayants pour la délivrance de molécules thérapeutiques, souvent ciblées vers les lignées cellulaires cancéreuses.

Cependant, les protocoles de production et de purification existants pour les vaults sont complexes, en partie en raison de leur dépendance vis-à-vis des eucaryotes supérieurs en tant que systèmes d'expression. Dans le **Chapitre 1**, une procédure simplifiée récemment publiée est présentée, combinant l'expression des vaults humains dans la levure *Komagataella phaffii* et un processus de purification comprenant un prétraitement par RNase suivi de chromatographie d'exclusion de taille, simplifiant considérablement le processus. L'étude aborde également le défi de l'agrégation des protéines et identifie les conditions de stockage optimales.

Une caractéristique remarquable des vaults est leur capacité à encapsuler des protéines cargo en les fusionnant avec le domaine INT, dérivé de la protéine vPARP interagissant avec les vaults. Le **Chapitre 2** explore l'encapsulation de GFP-INT en tant que protéine cargo témoin à l'intérieur des vaults exprimés et purifiés à l'aide de la procédure simplifiée. L'encapsulation de GFP-INT a été obtenue par un processus de mélange

simple, en exploitant la propriété de "respiration" des vaults. La stœchiométrie du chargement de GFP-INT dans la lumière des vaults sature le site de liaison avec environ 20 exemplaires de GFP-INT. De plus, l'étude confirme la capacité des vaults à délivrer des molécules cargo à l'intérieur des cellules cancéreuses, en particulier dans la lignée cellulaire du mélanome A375.

La montée en puissance des thérapies basées sur les acides nucléiques a exigé une meilleure délivrance, incitant les chercheurs à recourir aux NP pour relever ce défi. L'utilisation de particules de vault recombinantes en tant que systèmes de délivrance de nanomédicaments présente un potentiel significatif. Le **Chapitre 3** explore la possibilité d'utiliser les vaults pour la délivrance de siARN, en se concentrant sur les siARN ciblant *LADON*, un lncARN associé à la progression tumorale dans le mélanome. Deux stratégies ont été poursuivies : l'une impliquant la conjugaison chimique de siARN au domaine INT, et l'autre visant le chargement direct de siARN dans les vaults. Bien que des progrès aient été réalisés dans la liaison de GFP-INT, la construction du produit final, GFP-INT-siARN, est encore en cours. Avec l'autre approche, l'étude démontre que les vaults recombinants peuvent assurer la délivrance de molécules de siARN nues, sans nécessiter de formulation supplémentaire pour favoriser la transfection, conduisant à un effet biologique.

Pour obtenir un ciblage spécifique, la surface des NP peut être conjuguée à des anticorps (Ac) en utilisant différentes méthodes chimiques. Cependant, ces méthodes ne garantissent pas nécessairement une orientation correcte de Ab maintenant son activité. Le **Chapitre 4** relève ce défi avec la construction d'une variante de vault ingénierisée portant le peptide Z dérivé de la protéine A, qui se lie étroitement à la portion Fc de l'IgG1 humaine, permettant une conjugaison directe et orientée de l'anticorps aux vaults. Vault-Z, produit et purifié dans *K. phaffii* avec la procédure optimisée, conserve la même morphologie et la même taille que les vaults sauvages. Une caractérisation complète de la liaison des anticorps à Vault-Z révèle la capacité de lier jusqu'à 12 exemplaires d'Ac par Vault-Z. De plus, l'absorption de Vault-Z par les cellules tumorales SKBR3, qui surexpriment le récepteur à l'Ac Trastuzumab (Tz), augmente de manière significative lorsqu'il est conjugué à Tz.

# List of abbreviations

| | |
|---|---|
| **Ab** | Antibody |
| **AcGFP1** | *Aequorea Coerulescens* Green Fluorescent Protein |
| **AcMNPV** | The Multicapsid Nucleopolyhedro-Virus *Autographa Californica* |
| **ADP** | Adenosine diphosphate |
| **AGO2** | Endonuclease Argonaute 2 |
| **ASO** | Antisense oligonucleotides |
| **ATR** | Attenuated Total Reflection |
| **ATRA** | Hydrophobic All-Trans Retinoic Acid |
| **BCA** | Bicinchoninic Acid |
| **CaPi** | Co-Transfected Calcium Phosphate Precipitated |
| **cDNA** | Complementary DNA |
| **CFE** | Cell Free Extract |
| **CHRONOS** | Chronical Multifactorial Disorders Explored by Novel Integrated Strategies |
| **COVID-19** | Coronavirus Disease 2019 |
| **CP** | Cysteine-Rich Domain |
| **$Cy_3$** | Cyanine 3 |
| **$Cy_5$** | Cyanine 5 |
| **DDS** | Drug Delivery Systems |
| **DEPC** | Diethyl Pyrocarbonate |
| **DLS** | Dynamic Light Scattering |
| **DMEM-HG** | Dulbecco's Modified Eagle's Medium High Glucose |
| **DNA** | Deoxyribonucleic Acid |
| **DTT** | Dithiothreitol |
| ***E. coli*** | *Escherichia coli* |
| **EGF** | Epidermal Growth Factor |
| **EGFP** | Enhanced GFP |
| **EGFR** | Epidermal Growth Factor Receptor |
| **EPR** | Enhanced permeation and retention |
| **EtBr** | Ethidium Bromide |
| **Fc** | Fragment Crystallizable |
| **FDA** | Food And Drug Administration |
| **FTIR** | Fourier-Transform Infrared Spectroscopy |
| **GalNAc** | N-Acetylgalactosamine |
| **GFP** | Green Fluorescent Protein |
| **HCD** | High-Energy Collision-Induced Dissociation |

| | |
|---|---|
| **HER2 receptor** | Human Epidermal Growth Factor Receptor 2 |
| **$His_6$ tag** | Polyhistidine Tag |
| **HIV** | Human Immunodeficiency Virus |
| **IgG1** | Type 1 Immunoglobulins |
| **IMAC** | Immobilized Metal Affinity Chromatography |
| **INT** | Interaction Domain |
| **IPTG** | Isopropyl B-D-1-Thiogalactopyranoside |
| ***K. phaffii*** | *Komagataella phaffii* |
| **lnRNAs** | Long Non-Coding RNAs |
| **MCT** | Mercury Cadmium Telluride |
| **MDR** | Multidrug Resistance |
| **mRNA** | Messenger RNA |
| **MVP** | Major Vault Protein |
| **$NH_2$** | Amine Group |
| **NHS** | N-Hydroxysuccinimide |
| **NP** | Nanoparticles |
| **O/N** | Overnight |
| **PBS** | Phosphate Buffer Saline |
| **PDI** | Polydispersity Index |
| **PDT** | Photodynamic Therapy |
| **PEG** | Polyethylene Glycol |
| **PGA** | Polyglycolic Acid |
| **pGAP** | Glyceraldehyde 3-Phosphate Dehydrogenase Promoter |
| **PI3K** | Phosphatidylinositol-3-Kinase |
| **PLA** | Polylactic Acid |
| **pVI** | Protein VI |
| **Q-PCR** | Quantitative PCR |
| **RISC** | RNA-Induced Silencing Complex |
| **RNA** | Ribonucleic Acid |
| **RNAi** | RNA Interference |
| **RT** | Reverse Transcription |
| **RU** | Response Units |
| **SARS-CoV-2** | Severe Acute Respiratory Syndrome Coronavirus 2 |
| **SDS-PAGE** | Sodium Dodecyl Sulfate-Polyacrylamide Gel Electrophoresis |
| **SEC** | Size-Exclusion Chromatography |
| **SH** | Sulfhydryl Group |
| **siRNA** | Small Interfering RNA |
| **SN** | Supernatants |

| | |
|---|---|
| **SPR** | Surface Plasmon Resonance |
| **sulfo-LC-SPDP** | Sulfosuccinimidyl-6-(3′-(2-Pyridyldithio)Propionamido)Hexanoate |
| **TBE** | Tris-Borate-EDTA |
| **TEM** | Transmission Electron Microscopy |
| **TEP1** | Telomerase-Associated Protein-1 |
| **Tz** | Trastuzumab |
| **UNIMIB** | University Of Milan Bicocca |
| **VLPs** | Virus Like Particles |
| **vPARP** | Poly (ADP-Ribose) Polymerase |
| **VVF** | Void-Volume Fraction |
| **WB** | Western Blot |

# General Introduction

# 1 Nanotechnology and Nanomedicine

The Physics Nobel laureate Richard Feynman is considered the father of modern nanotechnology. In his famous speech to the American Physical Society in 1959, entitled 'There's Plenty of Room at the Bottom', Feynman laid the foundations for this field by proposing a method for manipulating atoms and molecules on nanoscales, where unique phenomena enable novel applications. Nanotechnology classically refers to matter in the size range of 1–100 nm, but it is often extended to include materials below 1 μm in size (Jeevanandam *et al*., 2018). Materials at the nanometric scale were found to exhibit extraordinary chemical, physical, magnetic, and optical properties, that differ from those governing the "macro" world, due to their higher surface-to-volume ratio (Burda *et al*., 2005). This understanding has sparked interest in various fields, including electronics, computer science, and medicine (Albanese *et al*., 2012).

The implementation of nanotechnology for medical needs has been termed 'nanomedicine' and consists in the application of nanomaterials for diagnosis, monitoring, screening, preventing, and curing diseases (Lu *et al*. 2016, Choi and Han 2018). The main tools of nanomedicine are NPs (NPs), defined as solid colloidal particles ranging in size from 10 nm to 1 μm (McNamara & Tofail, 2017). The nanometric size makes NPs especially capable of interacting with biological systems and increases their bioavailability within the body, as they are less susceptible to clearance systems; also increasing the speed of diffusion and response to stimuli (Riehemann *et al*., 2009). Moreover, their high surface-to-volume ratio, allow for more efficient loading of therapeutic molecules onto their surface. All these features combined with the possibility of being modified to be non-toxic and biocompatible make them a versatile and attractive tool for diverse biomedical applications.

NPs became a key tool for the development of innovative technology for diagnostic, molecular imaging, regenerative medicine, theranostic (defined as the combination of diagnosis and treatment), implanted devices and biosensors and mostly for therapy, aiming at setting up new strategy for the treatment of different diseases, cardiovascular, neurodegenerative, and chronic ones, including cancer (Abdel-Mageed *et al*., 2021; McNamara &

Tofail, 2017; Pelaz *et al*., 2017) (Figure 1). Currently, the application of nanotechnology in the design of new drug delivery systems (DDSs) is one of the most active fields in nanomedicine research (Pelaz *et al*., 2017).

Here, we will focus on the application of NPs for the delivery of drugs and RNA therapeutics, providing an overview of the main class of NPs for medical application on drug delivery, to finally introduce the vault NP.

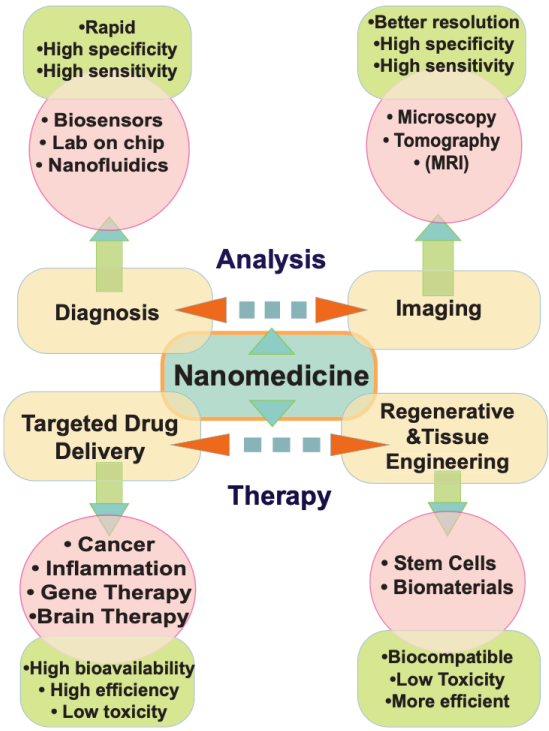


***Figure 1.*** *The diverse application areas of nanomedicine. Illustration indicating various field of application of nanomedicine and the benefits of integrating nanotechnology into analytical, diagnostic, therapeutic, and imaging methods (Abdel-Mageed et al., 2021)*

## 1.1 Nanoparticle-based delivery systems

Conventional routes of drug administration encounter various issues related to the use of large quantities of active principle, resulting in high costs, unwanted side effects, limited biodistribution in tissues, decreased half-life and lack of selectivity for a specific tissue or cell and consequent induction of drug resistance (De Jong & Borm, 2008). In this respect, the case of chemotherapy is particularly illustrative, in that it is the only viable

therapeutic option to control the size and spread for non-resectable or metastatic tumors (Yahya & Alqadhi, 2021). It is worth mentioning that cancer is still a major public health concern and one of the leading causes of death globally, with 18.1 million cancer-associated death in 2018 and 30 million of death per year expected by 2030 (Alshehri *et al*., 2020). In this context, NPs can be used to overcome the limitation of the conventional drug administration by providing a more efficient delivery of chemotherapic drugs, reducing toxicity, and improving stability, biodistribution, and tissue penetration (Alshehri *et al*., 2020) (Figure 2). It is also important to establish NPs' safety in biological systems. Particle design and material selection are crucial, as they must be safe for the body, biocompatible, and non-immunogenic (Alexis *et al*., 2008). NPs can incapsulate the therapeutic agent, protecting it and increasing its half-life. The size and surface characteristics of NPs must be carefully controlled. They should be between 50 nm and 200 nm, large enough to prevent rapid leakage into blood capillaries and renal clearance, but small enough to escape capture by macrophages in the reticuloendothelial system. In case of cancer treatment, NPs can be passively targeted to tumors, by entering via tumor-localized leaky vasculature and being retained due to poor lymphatic drainage in the tumor microenvironment, an effect called enhanced permeation and retention (EPR) (Carissimi *et al*., 2021). However, EPR effect is not common in all tumors and presents high pathophysiological heterogeneity, limiting the penetration of NPs. Thus, NPs can be designed to escape immune clearance but also to be able to actively target tissues. This could be achieved with by functionalizing their surface with targeting agents such as antibodies, peptides or oligonucleotide sequences (Jiang *et al*., 2007). By leveraging these characteristics, as represented in Figure 2, NPs can improve the pharmacokinetic profile of traditional medicine, making them more effective, increasing patient compliance, and reducing healthcare costs and side effects (Hong *et al*., 2020).

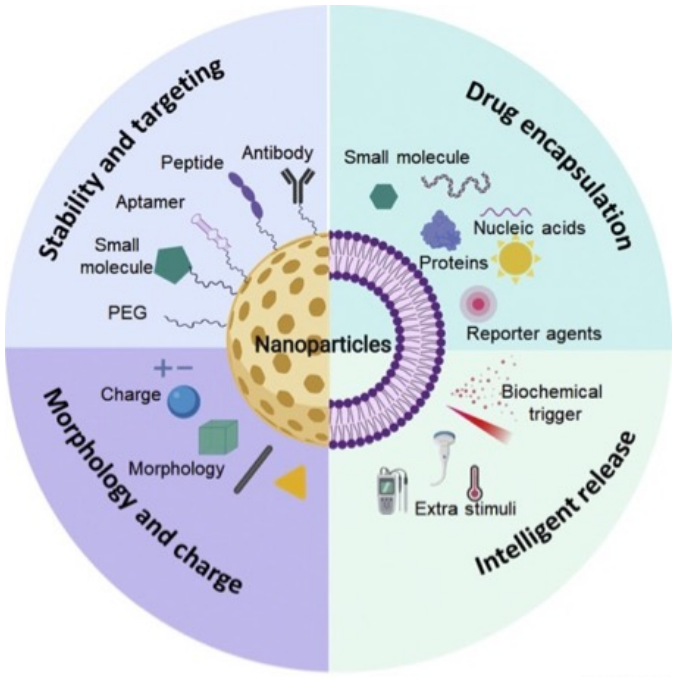


***Figure 2.*** *Nanoparticles with optimized properties for drug delivery. The surface of the nanoparticles can be modified to make them suitable for the desired application for example for enhancing the stability and targeting capabilities of nanoparticles the surface can be modified with polyethylene glycol (PEG) or various targeting ligands. Various types of molecules can be encapsulated within nanoparticles to improve solubility, stability, and reduce exposure to the bloodstream. The morphology and surface charge can be adjusted to optimize the nanoscale effects (Song et al., 2020).*

## 1.2 Nanoparticles as non-viral vector for the delivery of RNA therapeutics

As mentioned in the previous paragraph, NPs can be used for the delivery of small hydrophobic molecules like chemotherapeutic drugs, reducing the toxicity and increasing their solubility (Yahya & Alqadhi, 2021). However, the application of NPs is not limited to the delivery of small molecules: several nanostructures have been designed for the delivery of different types of therapeutic molecules such as hydrophobic and hydrophilic molecules, peptides proteins (Perera *et al*., 2023).

Currently, NPs are being exploited for novel, RNA-based therapeutic approaches, whose notoriety has been increasing in recent years.

RNA therapeutics are a class of gene therapy treatments based on ribonucleic acid (RNA). Gene therapy is considered one of the most revolutionary medical technologies, developed along with recombinant

DNA and gene cloning technologies (Pan *et al*., 2021). It consists in the introduction of a therapeutic genetic material, like DNA or RNA into the cell to transfer gene, for example by introducing a different gene that provides instructions for a protein that helps the cell function normally or to silence genes, increase or decrease the expression of RNA (Bulcha *et al*., n.d.). Over the last 10–20 years, gene therapy drugs have been gaining significant attention in the world of medical science for the cure of genetic diseases, cancer, autoimmune diseases and infections (Butt *et al*., 2022; Zhang *et al*., 2022). The rapid global spread of COVID-19 has pushed the research into the field of RNA technology giving it a boost, a process that typically takes several years to be accomplished (Xu *et al*., 2020).

Figure 3 schematically represents RNA therapeutics including antisense oligonucleotides (ASO), aptamers, small interfering RNAs (siRNA), microRNAs, and messenger RNA (mRNA) (Niazi, 2023).

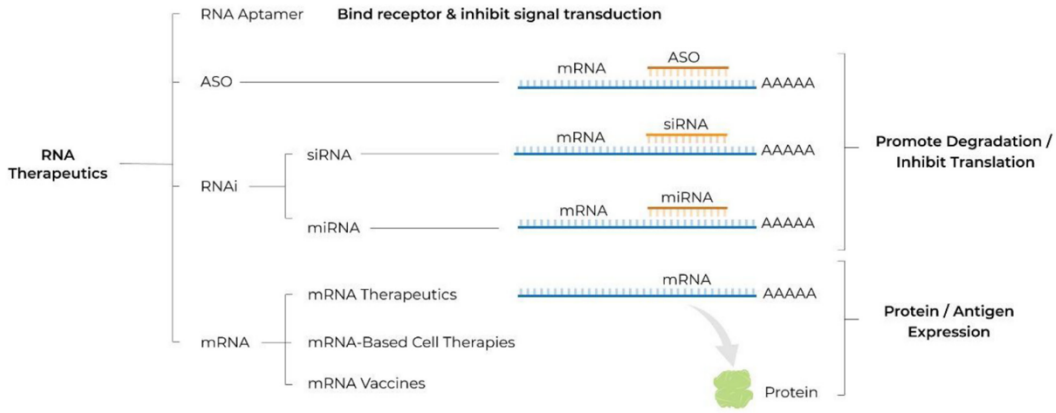


***Figure 3.*** *Schematic illustrating different classes of RNA therapeutics. ASO: antisense oligonucleotide, RNA: ribonucleic acid, RNAi: RNA interference, siRNA: small interfering RNA, miRNA: microRNA, mRNA: messenger RNA, A: adenosine, AAAAA: poly A tail (Damase et al., 2021).*

*mRNA*

mRNA is the transient intermediary between genes and protein (Hou *et al*., 2021). Some therapeutic approaches are based on mRNAs encoding proteins or peptides that elicit their transient expression in the cytoplasm, to replace defective proteins or present an antigen (De*et al*., 2021). The development of mRNA therapeutics was made possible by the insights into mRNA structure and the development of in vitro-transcription (IVT). Applications of mRNA include: vaccines (e.g., for SARS-CoV2); individualized medicine (e.g., cancer immunotherapy); cellular treatments; the replacement of proteins; gene editing (e.g., CRISPR CAS9); rare developllnesses treatment (e.g., enzyme replacement). Fundamental for application of mRNA therapeutic are the modifications on in-vitro transcripted mRNAs, that enabled the development of effective mRNA vaccines against COVID-19 (*Noble Nanomedicine: Celebrating Groundbreaking MRNA Vaccine Innovations*, n.d.). This great achievement has been awarded with Nobel Prize in Physiology or Medicine to Katalin Karikó and Drew Weissman (Karikó *et al*., 2008; Nobel, 2023)

*Antisense RNA, focus on siRNA*

Approaches have been developed, which are based on short antisense RNA that recognize and hybridize to complementary sequences in endogenous RNA transcripts and alter their processing by exploiting, for example, the RNA interference (RNAi) machinery (as for siRNA) or other mechanisms (miRNA, ASO). Few words can be spent on RNAi and siRNA. RNAi is a phenomenon discovered in 1990s in Nematodes, based on a conserved cellular machinery that uses small interfering RNAs (siRNAs) to suppress the expression of target genes specifically by binding complementary sequences in mRNA transcripts (Amreddy *et al*., 2018). This mechanism that also occurs naturally in mammals, represents a cellular strategy for post-transcriptional genome control, and begins when the precursor siRNA duplex of 200 bp is processed by the endogenous Dicer enzyme into 20-30 bp siRNA, characterized by two-bases overhangs at the 3′ end. These short molecules then interact with the RNA-induced silencing complex (RISC) inducing RNA interference: the endonuclease argonaute 2

(AGO2) component of the RISC cleaves the sense strand, leaving the antisense strand intact. The antisense strand serves as a guiding molecule, leading the active RISC to the desired mRNA or untranslated RNA target. Once located, the AGO2 enzyme breaks down the target RNA. Being the antisense strand fully complementary to the target, siRNA knocks down one specific target gene (Dana *et al*., 2017; Wittrup & Lieberman, 2015).

The knowledge of this RNAi pathway mechanism has made develop possible designing synthetic 19-23 bp siRNA molecules (with a 2-nucleotide 3′ overhang) that could utilize the same machinery after being taken up by the cells. Synthetic siRNAs are gaining interest for the treatment of various infectious and genetic diseases, including cancer (Jeong *et al*., 2009; Roberts *et al*., 2020). siRNA can target mRNA but also long non-coding RNAs (lnRNAs), as for instance in the case of *LADON*, a lncRNA whose expression has been associated with invasive behavior in melanoma (Dutriaux *et al*., 2021). Two siRNAs have been identified and their capability of decreasing *LADON* expression has been demonstrated.

*The need of a suitable delivery system*

RNA therapeutics comprise a rapidly expanding category of drugs that will change the paradigm of health care, and allow for treating and preventing diseases, mostly untreatable ones (Niazi, 2023). The development of RNA therapeutics is driven by some advantages: they can act on "undruggable" targets for small molecules or protein, their development is rapid and cost effective in comparison to drugs and they can be used for personalized treatments (Damase *et al*., 2021). Moreover, unlike DNA therapies that perform their function in the nucleus, RNA therapeutics act in the cytoplasm, thus avoiding one of the key intracellular barriers that hampers DNA-based gene therapy (Huang *et al*., 2015).

Nevertheless, despite the great clinical potential, nucleic acid drugs such as RNA therapeutics, face different challenges, mostly given by the fact that to be effective in vivo, they must overcome several biological barriers and eventually enter the cell, so as to reach the target site (S. Hou *et al*., 2022). RNA therapeutics are typically large, hydrophilic polyanions (double-stranded siRNAs are ~14 kDa, mRNA 300–1500 kDa), so they are subject to repulsion

by the negatively charged cell membrane, which prevents them from readily passing through it. Moreover, they must be protected from degradation by ribonucleases in biological sera and must escape the activation of immune responses and rapid clearance from the body (Edwardson *et al*., 2018). All these hurdles could be overcome by designing efficient delivery systems. Different strategies for delivery nucleic acid drugs exist, including viral and nonviral vectors (Butt *et al*., 2022). Viral vectors consist of viruses carrying in their genome therapeutic nucleic acids modified so as to be replication-deficient (Pan *et al*., 2021). Thanks to these properties they provide good transfection efficiency and sustainable gene expression. However, a major drawback is that gene transfer can occur nonspecifically to cells other than the targeted ones, leading to a decrease in the efficacy and increase in immunogenicity and toxicity.

Thanks to the rapid progress of nanotechnology, nanosized materials for gene delivery have attracted attention as promising nonviral vector to accomplish a safe and effective delivery of several gene therapy-based drugs (Mirón-Barroso *et al*., 2021). Besides, both viral and non-viral vector present advantages and disadvantages, but the interest in nonviral vectors has grown in that they promise to be simpler to use, less toxic, capable of transferring large quantities of materials, easy to prepare and to be produced in large-scale, and able to avoid an immune response (Liu *et al*., 2018; H. Wang *et al*., 2015). Nonviral gene delivery strategies also include physical methods that enable cell disruption, naked plasmid DNA injection, gene gun technology, electroporation. Besides being attractive for its simplicity, the therapeutic effect is limited to the injection site and one major limitation is associated to the risk of tissue damaging (Du *et al*., 2018).

In this context, NPs are an important tool for the delivery of nucleic acid drugs such as RNA therapeutics. NPs can be designed to be combined with negatively charged nucleic acids by electrostatic interaction, associated with the membrane and cross it, leading to cell internalization. Most importantly, the delivery systems carrying the drug must escape degradation by endosomes, a process known as endosomal escape that can occur in different way (Voltà-Durán *et al*., 2023) to finally deliver the therapeutic molecules to

the target site (Hidai & Kitano, 2018; Jones *et al*., 2015). This type of nonviral mechanism is represented in Figure 4.

A brief overview on the different NPs that have been developd for the delivery of drugs and nucleic acid therapeutics is following.

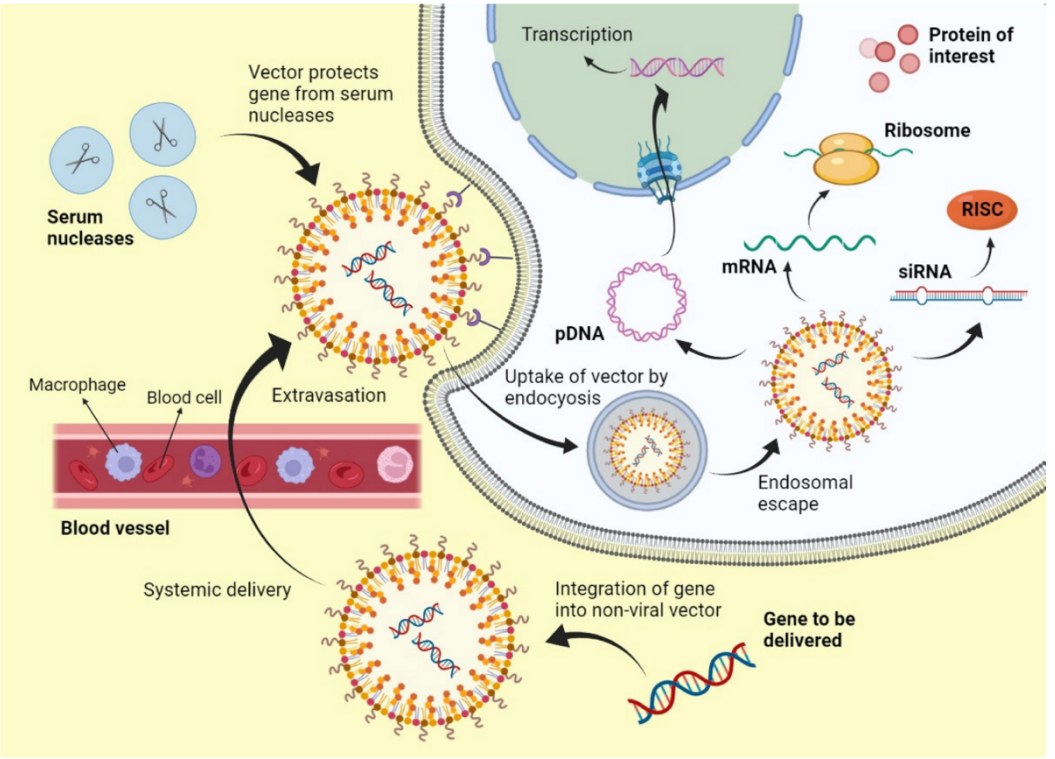


***Figure 4.*** *Mechanism of nonviral gene delivery (Butt et al., 2022).*

### 1.3 A survey of past and current nano-delivery systems.

Over the years, many types of NPs have been developed for applications in the field of nanomedicine. Some of these have been approved by FDA and are illustrated in Figure 5.

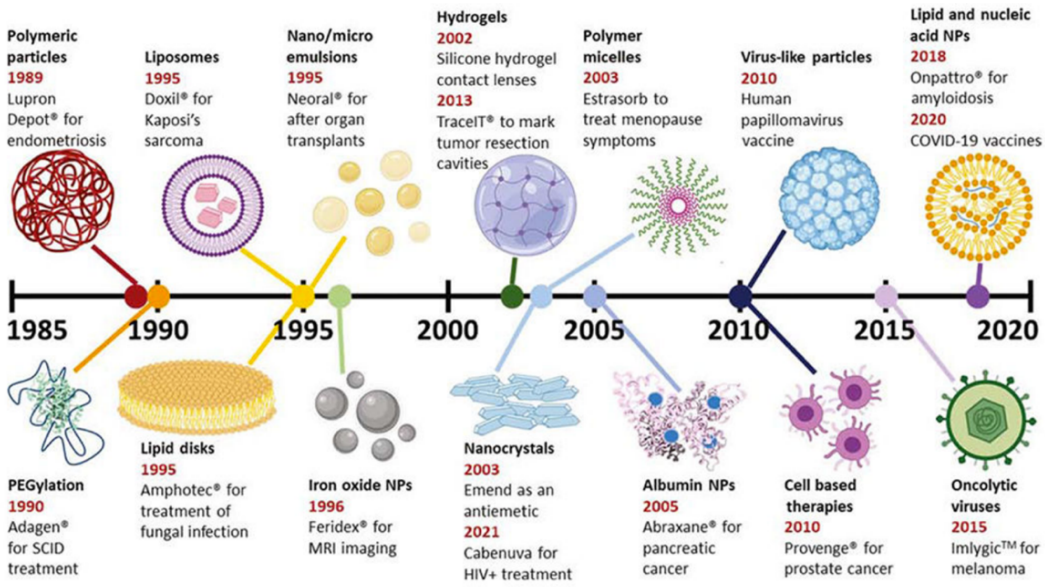


***Figure 5.*** *Timeline illustrating the historical FDA approval of therapeutic nano-drug delivery systems, with key milestones indicating the types of nano-formulations employed. Figures are not to scale with each other. COVID-19: coronavirus disease 2019, MRI: magnetic resonance imaging, SCID: severe combined immunodeficiency disease (Batty et al., 2021).*

NPs are classified on the base of morphology, size, and shape, which also determine their properties. Depending on their composition, NPs can be classified in inorganic and organic.

### 1.4.1 Inorganic nanoparticles

Inorganic NPs are characterized by the absence of carbon atoms in their composition and are generally more stable compared to organic NPs. This category includes metallic NPs, the most important being made of iron or gold, and NPs based on metal-oxides, such as iron or silicon oxides (Ijaz *et al.*, 2020). These structures can vary in shapes and sizes, depending on the synthesis method. Thanks to their metallic composition they possess optical, magnetic, and electronic properties that can be harnessed in the field of nanomedicine (Farooqi *et al.*, 2021). For instance, gold NPs can be used in the development of new technology in the field of theranostics that combines diagnosis and therapy. There are also hybrid NPs, consisting of a core and a shell made of two different materials (core-shell NPs). An example are

nanostructures with a metal or metal oxide core and a silica coating. The outer coating may serve to increase the bioavailability of the NP and reduce the toxicity of the material that makes up the core of the structure, and also can facilitate the conjugation of the NP with specific ligands. They find application in cancer treatment: NPs with a silica core and a gold shell which, when exposed to infrared light, can cause through thermal ablation the death of cancer cells that have internalized them (Anselmo *et al*., 2016). Silica NPs have been thought of as outstanding materials that can offer solutions to many of the current drug-protein-enzyme-gene-RNA delivery problems (Abdel-Mageed *et al*., 2021; Pu *et al*., 2019). However, despite the potential and partial success of inorganic NPs in diagnostics, imaging, and photo-thermal therapies, they present unresolved issues regarding low solubility and toxicity issues, especially in formulations using heavy metals, that have so far limited their use in clinical applications (Mitchell *et al*., 2021).

### 1.4.2 Organic nanoparticles

The class of organic NPs is heterogeneous and includes polymeric NPs, liposome and lipid NPs, dendrimers, and protein-based NPs. Organic NP are characterized for being more biocompatible, non-toxic, and biodegradable and more easily functionalized on the surface with biological molecules. Thanks to these characteristics, they are considered more suitable for therapeutic proposes and they have been extensively applied in drug and gene delivery (Ijaz *et al*., 2020).

The first organic NP to be studied were liposomes, spherical lipid vesicles of macro or nano size (size between 20 and ~ 1,000 nm) composed essentially by phospholipids, sphingolipids, and cholesterol, that self-assemble to form one or more lipid bilayers surrounding an aqueous core. Thanks to the amphiphilic nature of these lipids, liposomes encapsulate molecules both hydrophilic and hydrophobic, such as drugs but also nucleic acids (Liu *et al*., 2022). They can perform active targeting if properly functionalized but also passive targeting, exploiting the EPR effect that enrich the drug in tumor tissue, due to poor vessel integrity (Batty *et al*., 2021; Voltà-Durán *et al*., 2023). They have emerged as the first nanomedicine delivery platform to be

introduced in clinics, and several liposome formulations have been approved and applied to medical practice (Aleandri *et al*., 2023). An example is Doxil®, approved in 1995, that consists of a liposome encapsulating doxorubicin with a surface PEG corona, that reduces protein adsorption and uptake into cells, prolonging circulation time (Figure 5).

With the rise of nucleic acid-based therapeutics demanding better delivery, focus has turned to NPs to overcome this challenge. Starting from 1990s, new generations of lipid nanocarriers were developed with improved characteristics in terms of both kinetic and structural stability (Tenchov *et al*., 2021) or the encapsulation of various nucleic acids (RNA and DNA). Licensed therapies for nucleic acid delivery have predominantly consisted of lipid NPs (LNPs), liposome-like structure in complex with their nucleic acid cargo. LNPs are characterized by having different types of lipids in their composition, carrying cationic and ionizable groups or PEG polymer that serve multiple roles in delivering nucleic acids. An example is ONPATTRO®, the first PEGylated lipid NP containing siRNA (Patisiran) that was FDA-approved in 2018 for the treatment of transthyretin-mediated amyloidosis (Figure 5) (Adams *et al*., 2018). The presence of ionizable lipids that are neutral at physiological pH but positively charged at acidic pH enable the escape from the endosomal compartment characterized by acidic pH.

Notably, the use of lipid NPs for RNA delivery skyrocketed during the coronavirus disease 2019 (COVID-19) pandemic: two vaccines (mRNA-1273 from Moderna and BNT162b2 from Pfizer/BioNTech (Polack *et al*., 2020) were used to deliver mRNA encoding severe acute respiratory syndrome coronavirus 2 (SARS-CoV-2) spike protein and were issued Emergency Use Authorization by the FDA (Figure 5).

Another type of organic NPs are the polymeric ones, obtained from natural or synthetic polymers such as polylactic acid (PLA), polyglycolic acid (PGA). Examples of natural occurring polymers includes chitosan, hyaluronic acid, gelatine and agarose (Madej *et al*., 2022). The peculiarity of polymeric NPs is their high stability that greatly increases the half-life in the body of drug either immobilized or encapsulated within them, allowing also for a gradual release (Amoabediny *et al*., 2018). They are used for drug

delivery, especially for anti-cancer drugs and some of them have been approved by FDA (Figure 5). Indeed, the first FDA-approved synthetic NP therapy, Lupron Depot ®, comprises the therapeutic drug Leuprorelin (for the treatment of endometriosis) encapsulated within a spherical particle made of PLGA (Figure 5) (Batty *et al*., 2021).

Besides conventional polymer particles, there is a particular type of NPs called dendrimers, made up of a distinct core and a series of branches (dendrons) with various functional groups attached at their terminations, that determine the properties and biocompatibility of the NP itself (Bharali *et al*., 2009). The main advantages are the presence of these exposed functional groups, which increases the number of possible interactions and, consequently, the biological activity. Also, their small size allows high penetrability through the cellular membrane resulting in augmented cellular uptake level. They find application in cancer treatment with photodynamic therapy (PDT) and in the delivery of intramuscular self-amplifying mRNA-based vaccination against *Toxoplasma gondii*, Ebola and H1N1 influenza virus (Chahal *et al*., 2016; Chowdhury *et al*., 2022).

*Protein nanoparticles*

Other notable organic NPs are protein-based ones. Protein NPs have the advantage of being biocompatible, safe, biodegradable, low in immunogenicity, cost-effective and easy to be produced. They are capable of binding or encapsulating various molecules, thanks to the abundance of functional groups and amphiphilic properties of proteins, which allow for interactions with both hydrophobic and hydrophilic substances. Although they are easily metabolized by enzymes within the body, they are characterized by having a greater stability compared to liposomes (Jain *et al*., 2018). Additionally, the solubility of protein NPs in aqueous environments reduces the risk of aggregation, a common issue with inorganic NPs. The protein nature of these NPs also allows for targeted modification of their structure by standard genetic engineering techniques.

Thanks to all these features, protein-based NPs are endowed with several advantages relative to the others, which also involves various advantages,

especially in the mode of material delivery, such as genetic materials, anticancer drugs, peptide hormones, growth factors, DNA and RNA (Hong *et al*., 2020).

Some protein-based NPs are capable of self-assembling: this is the case of polymeric proteins, protein cages and desolvated NPs. Desolvation is accomplished by adding dropwise an organic precipitant to a protein solution while stirring, and subsequently crosslinking the particles to stabilize them (Herrera Estrada & Champion, 2015). Examples of desolvated NPs are gelatin and albumin. The latter is the most abundant protein in the blood and physiologically mediates the reversible transport of hydrophobic molecules in the circulatory system (Elzoghby *et al*., 2012). This has led to the successful use of albumin NPs in clinical settings, particularly in chemotherapy formulations to reduce common side effects. A notable example is Abraxane, a drug composed of albumin NPs and a taxane (paclitaxel), which has been approved for clinical use (Gradishar *et al*., 2005) (Figure 5).

A relevant class of protein NPs that is worthy of note for the delivery are the so called "protein cages" or protein boxes (Herrera Estrada & Champion, 2015). Most of these NPs occur in nature and are characterized by their hollow three-dimensional structure and complex designs, which cannot be replicated through artificial means. They peculiarity is their ability to load, contain and release other molecules by different modalities depending on the type (Molino & Wang, 2014). Their regular structure allows for the engineering of specific regions and surfaces of the cage, like the exterior or interior (Diaz *et al*., 2018). Moreover, they can be engineered at the amino acid level to incorporate different type of molecules (proteins, nucleic acids) (Edwardson *et al*., 2022). Due to these features, protein cage NPs have been explored as nanocarriers for the delivery of different therapeutic drugs.

The three most studied protein cage NPs are: Virus Like Particles (VLPs), ferritin, and vault (Herrera Estrada & Champion, 2015) (Figure 6).

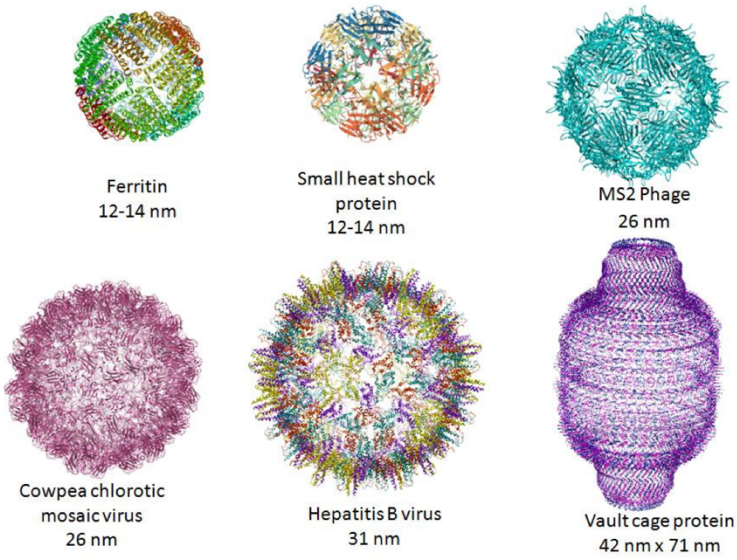


***Figure 6.*** *Illustration of protein cages used as nanocarriers for medical applications. VLPs are derived from natural viruses, so they have variable shapes, sizes, and characteristics. Ferritin and vault are protein complexes naturally expressed in cells. Other types of protein cages, not discussed in the text, originate from cellular protein complexes, such as heat shock proteins or chaperonins. The internal diameter of each protein is indicated (Krayem, 2017; Molino & Wang, 2014).*

VLPs are NP structures that are derived from natural viruses but lack the genome and viral replication-related proteins. Due to their inherent ability to target specific tissues or cell lines, each VLP has a unique tropism. Leveraging the affinity of viral proteins for nucleic acids, these particles have been used effectively in gene therapy for cancer therapy i.e., for the delivery of siRNA(Edwardson *et al*., 2018). VLPs have also found application in the creation of vaccines (Iravani & Varma, 2023; Molino & Wang, 2014). An example is the vaccine for Papilloma virus that has been approved (J. W. Wang & Roden, 2013) (Figure 5).

The term ferritin refers to a group of proteins found in various organisms that are responsible for storing iron (Meyron-Holtz *et al*., 2011). These proteins have a spherical, hollow shape and a diameter of approximately 12 nm. There are several methods for loading drugs in ferritin, including breaking down and rebuilding the protein or utilizing recently discovered thermo-responsive channels. The presence of the transferrin receptor 1, which is highly expressed in tumor cells, also makes ferritin a favorable option for drug delivery (Song *et al*., 2020).

One key advantage of using protein cages as drug delivery systems is given by their internal cavity, whose size determines the number of molecules that can be internalized. Among protein cages, the eukaryotic vaults are protein NPs characterized by a large internal cavity. This is just one of the features that makes vault attractive as nanocarrier for diverse type of molecules. Being vault the main topic of this dissertation, an in-depth, specific discussion will follow.

## 2 Vault protein

Vaults are natural ribonuclear-protein cytoplasmatic complexes, first observed in 1986 as contaminants of rat liver coated vesicles (Kedersha & Rome, 1986). They appear as ovoid bodies whose morphology is reminiscent of the "vaulted ceilings" of medieval cathedrals (Suprenant, 2002). With their molecular mass of 13 MDa and the size of 72.5 × 41 × 41 nm, vaults are considered the largest cytosolic eukaryotic ribonucleoprotein particles ever described (Figure 7). It is estimated that there are $10^4$ to $10^5$ particles per cell (Kickhoefer *et al*., 1998; Steiner *et al*., 2006). Although not ubiquitous, vaults are highly conserved and widespread among animals, like mammals but also protozoa (*Dictyostelium discoideum*), molluscs and echinoderms (*Strongylocentrotus pupuratus*), amphibians (*Rana catesbeiana* and *Xenopus laevis*), birds (*Gallus gallus*) and fish (*Torpedo marmorata*) (Daly *et al*., 2013; Kedersha *et al*., 1990; Llauró *et al*., 2016; Z. Yang & Zhang, 2018). Nevertheless, the gene coding for the major component of vault particle was not found in fungi, insects, nematodes, and possibly in plants (Kolev *et al*., 2019; Suprenant, 2002).

A vault complex encloses proteins and nucleic acids. The main component is the 97-kDa major vault protein (MVP), which represents more than the 70% of the total protein mass (Tanaka & Tsukihara, 2012). The assembly of 78 copies of MVP generates a barrel-like structure enclosing a large internal cavity of $5 \times 10^7$ Å$^3$, wherein vault minor components like small nontranslated RNAs (Kickhoefer *et al*., 1998) and other proteins, i.e., the 193 kDa vault poly(ADP-ribose) polymerase (vPARP) (Kickhoefer, Siva, *et al*., 1999) and the 290 kDa telomerase-associated protein-1 (TEP1) are

accommodated, although a fraction of these molecular components is also free in the cytoplasm.

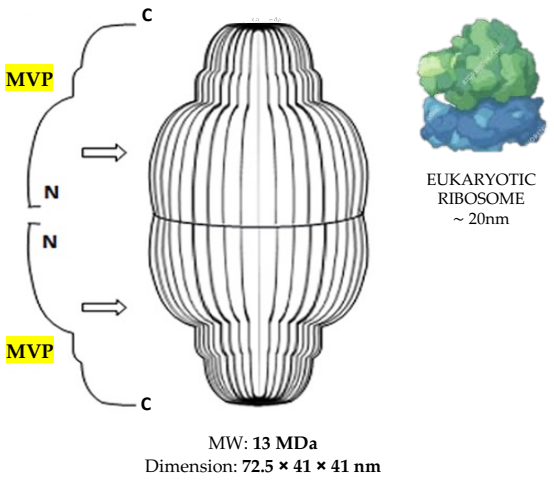


***Figure 7.*** *Representation of vault. Vault impressive dimension can be point out by comparison with a eukaryotic ribosome (image from Biorender). Adapted from Han et al., 2011.*

### *Structure and major vault protein*

The assembly of the MVP protein give rise to the outer shell of the vault NP (Kong *et al.*, 1999) endowed with its natural morphology even in the absence of the other relevant molecular components. This has been achieved by recombinant expression of the sole MVP in insect cells (Mrazek *et al.*, 2014; Stephen *et al.*, 2001).

Structural studies of vault particles have been performed using x-ray diffraction, electron microscopic, and NMR methods. From the first structural studies of vaults, performed using electron microscopy by Rome and his co-workers, vaults appeared as homodimers with each half resembling a barrel-like structure formed by 8 rectangular "petals" hypothesized to consist of 6 molecules of MVP, that open into a flowerlike structure (Kedersha *et al.*, 1991). Cryo-EM revealed that vault is a hollow, barrel-like structure with a constriction in the waist and two protruding caps at both ends. Although some evidence has confirmed Kedersha's initial hypothesis of a 48-fold symmetry, more recent investigations using NMR spectroscopy and crystallographic analysis at higher resolution suggested

that the particle exhibits a 39-fold dihedral symmetry, where each half is formed by 39 MVPs.

Each MVP monomer folds into 12 domains (Figure 8): at the N-terminal, 9 repeating structural domains (R1- R9), a single region called the 'shoulder' domain consisting of four $\alpha$-helices and four $\beta$-sheets, a 155-amino-acid $\alpha$-helix domain that forms the first part of the end (cap-helix) and, at the C-terminal, a random coli ring domain called cap-ring forming a short and thin hook. The N-terminus localizes to the vault's equator, protruding interiorly to create the waistline and forming the sidewalls via noncovalent interactions. Hydrophobic interactions between the C-terminal cap-helix domains are considered the strongest of the structure and are the key to stabilizing the particle, forming the hemispheres of vault (Buehler *et al*., 2014; Tanaka, 2009).

The MVP protein is encoded on chromosome 16p11.2; the gene consists of 15 exons, coding for 893 amino acids. The sequence is highly conserved, having a homology of 90% in mammals and 40-60% in the other organisms in which it is present (Rome and Kickhoefer, 2012).

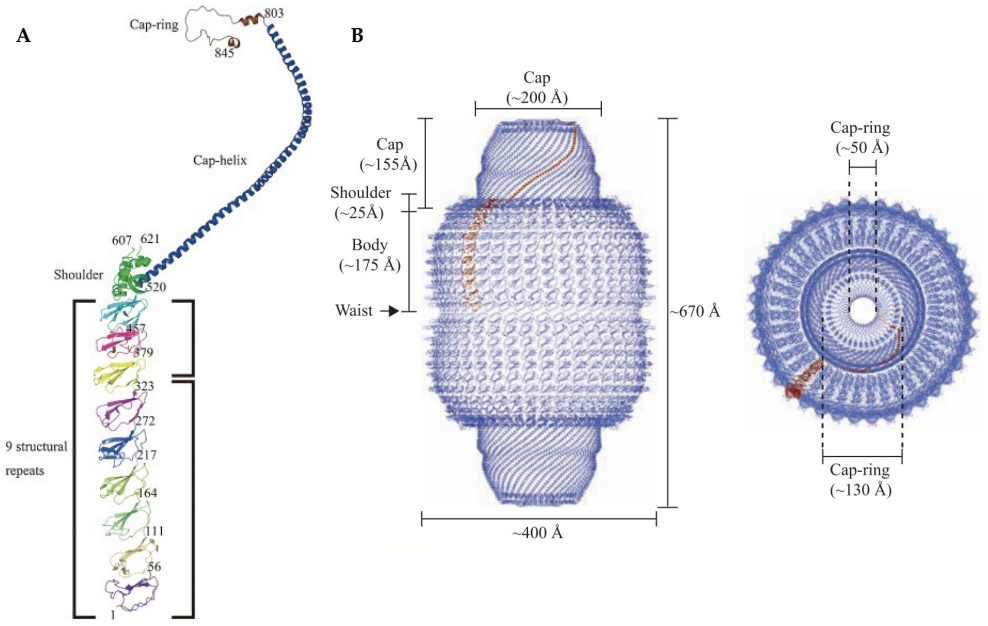


***Figure 8**: On the left, representation of the MVP structure with various domains highlighted (as described in the text); on the right, representation of the vault with the monomer and its structural features highlighted. Modified from Tanaka & Tsukihara, 2012*

*Vault dynamics*

Freeze-etch revealed that each half of the vault can "open up", into flower-like structures composed of eight rectangular petals, each being joined to a central ring by a thin hook. Through cryoelectronic microscopy it has also been observed that the protein is often found in a conformation where the two halves are dissociated but not completely open. Different models have been proposed for elucidating the phenomenon of vault opening, suggesting a dynamic behavior resulting from the protein's pH sensitivity (Figure 9). One possibility is that an acidification of the medium destabilizes the bonds between monomers, except for the strong hydrophobic joints between the head-helix domains, giving rise to a "flower-like" structure (Llauró *et al*., 2016; Matsumoto *et al*., 2015). According to this model, the breathing of the vault is given by single pairs of opposing petals (made up of multiple MVPs) on each half-vault that temporarily separate and then close at the particle waist, without disrupting the integrity of the particle (Kong *et al*., 1999). Another model suggests that under physiological conditions there is a balance between closed and open conformations. The pH decrease leads to the protonation of aspartic acid and glutamic acid residues present at the interface between the two halves of the protein, with consequent repulsion of positively charged residues present in this region (Goldsmith *et al*., 2007; Querol-Audí *et al*., 2009). As a result, the two halves of the vault dissociate and when the acidity of the medium is particularly high the vault is found totally and irreversibly dissociated (Querol-Audí *et al*., 2009).

Regardless of the exact mechanism of reversible opening of the vault, this is a phenomenon that is believed to occur naturally inside the cell, and it has been observed that it can be affected by variations of the pH value. This dissociation triggered at low pH can be exploited for drug delivery: the vault protein, when endocytosed by target cells, ends up in endosomes, characterized by their acidic internal pH. Under these conditions, the two halves of the protein disassemble, and the cargo is released. Thus, this phenomenon is being studied in order to achieve a controlled release of cargo drugs (Matsumoto *et al*., 2015; Muñoz-Juan *et al*., 2019) (Muñoz-Juan *et al*., 2019).

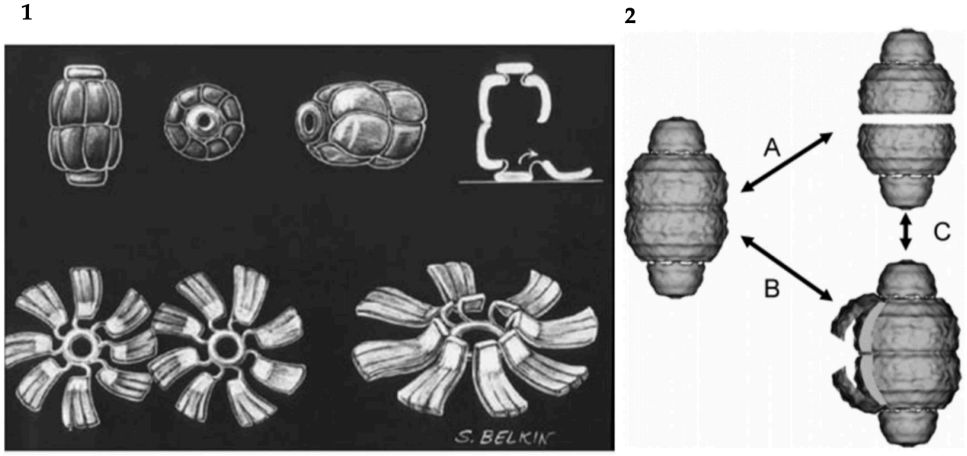


***Figure 9.*** *Vault dynamics. 1) Model of vault flowers folding into vaults. (top row) Side, end, and angled views of an intact vault, with a cross- sectional view showing one of two possible pathways leading to unfolding. (bottom row Left) Paired vault flowers (bottom row, right) three-dimensional rendering of a single vault flower viewed at an angle (Kedersha et al., 1991) 2) The opening of the vault particle might be initiated either by the reversible separation of vault petals at the particle waist (B) or by the temporary division of the particle into two half-vaults (A). In certain cases, this could lead to transitions between these two forms (C) (Poderycki et al., 2006).*

### *Assembly of vault particles*

As just described, when the acidity of the medium is particularly high, the dissociation of the vault protein is irreversible (Querol-Audí *et al*., 2009), thus disparaging the common thinking of vault ability of self-assembly. Nevertheless, vault size, complexity, and homogeneity of the well-assembled particle, together with the fact that MVP monomers have not been found to reassemble into vaults, suggested the occurrence of significant assembly assistance during MVP synthesis, which only recently was clarified (Mrazek *et al*., 2014). It has been demonstrated that the assembly of vault NPs can only occur during the translational progress and that the process is mediated by the presence of polyribosomes. These macromolecular structures formed by chains of ribosomes act as a 3D printer of nanometric size: several ribosomes are associated with a single molecule of MVP mRNA and couple the translation mechanism with the assembly process. They ensure an organized interaction of MVP chains and their protection from degradation or aggregation events.

As represented in Figure 10, in the initial phase, polyribosomes mediate the formation of dimers between monomers in progressive growth from two opposite halves. The interaction occurs through the N-terminal end, particularly the "shoulder" domain guarantees this association. As their translation nears completion, the newly synthetized MVP dimers interact with nearby MVP dimers. The interactions between individual monomers are hydrophobic. The cap helix domain ensures the stability of the particle, imposing a tension favourable for assembly.

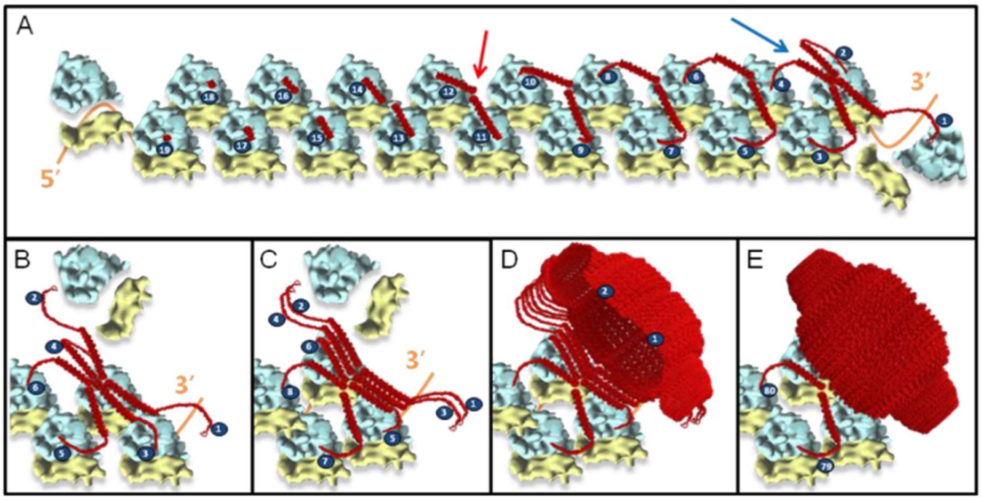


***Figure 10.*** *Model for co-translational assembly of the vault; the first step (A) involves the synthesis of two MVP chains that, by interacting at their N-terminal domains (red arrow), lead to the formation of a dimer (blue arrow); (B) a new dimer is formed and associates with the previously formed one; (C and D) the newly synthesized dimers join the tetramer, gradually forming the complex; (E) the formed complex will spontaneously dissociate from the polyribosome. All components of the model (MVP, vaults, and the 80S ribosome) were drawn to scale. (Mrazek et al., 2014)*

## *Vault minor components*

Two minor protein components of the vault NP are vPARP and TEP1 protein. These proteins, together with the ribonucleic component, do not influence the correct assembly of the protein, and they are considered to play a functional rather than structural role.

The 193 kDa protein vPARP belongs to a class of enzymes PARP, encompassing at least 18 members that catalyse the poly-ADP ribosylation of multiple protein substrates. All members of this protein family share a catalytic domain, which shows high homology. The rest of the structure is quite variable and can contain a N-terminal DNA-binding domain and nuclear localization sequence and an auto modification domain containing a breast cancer susceptibility protein C-terminus motif (BRCT), which is common in many DNA repair and cell cycle proteins, denoting diverse physiological roles among the various PARPs (Nguewa *et al*., 2005). In fact, the post-translational modification catalysed by the different PARPs is fundamental in a multitude of cellular functions, such as the maintenance of genomic stability, DNA damage repair, and chromatin remodelling, and also plays an important role in cell proliferation, apoptotic pathways, metabolism, and even transcription (Morales *et al*., 2014). The vPARP is also known as PARP-4 and has been identified for the first time thanks to its interaction with the MVP through a yeast two-hybrid assay (Kickhoefer *et al*., 1999). The gene encoding vPARP is on the chromosome 13q11 and it is constituted by 34 exons that form a protein of 1724 aa. Unlike other members of the family, vPARP has no DNA-binding domain and instead displays, in addition to a BRCT domain, a catalytic domain, other structural domains, a 162 amino acid domain called INT at its C-terminus. Thanks to this domain, vPARP can interact with the N-terminal domain of MVP with high affinity, localizing within the vault at level of the waist (Figure 11). Around eight-nine vPARP copies can be found associated within the vault. However, this number is quite variable depending on the cell's physiological conditions (Frascotti *et al*., 2021). This suggests that the protein is present in the cell both associated with the vault and free in the cytoplasm (Kickhoefer, Siva, *et al*., 1999).

The TEP1 is encoded by a gene located on chromosome 14q11.2 and consists of 2629 amino acids. It has been identified through its N-terminal region homologous to *Tetrahymena* p80 and was shown to be a subunit of both vault and mammalian telomerases (Collins *et al*., 1995; Kickhoefer, Stephen, *et al*., 1999). In the telomerase complex, reverse transcriptase (hTERT) is the catalytic subunit, whereas TEP1 is catalytically inactive (Kickhoefer *et al*.,

2001) as observed in knockout mice (Y. Liu *et al*., 2000, 2004). Cryo-electron microscopy studies have shown that, unlike vPARP, TEP1 is localized in the vault at the cap (Figure 11). No interaction between this protein and MVP has been observed using the two-hybrid assay, indicating that its association occurs with multiple monomer units at the same time (Frascotti *et al*., 2021). Although its physiological role remains unclear, the presence of the evolutionarily conserved TROVE domain responsible for RNA binding, suggest that TEP1 may be involved in RNA binding (Bateman & Kickhoefer, 2003). TEP1 interact with non-coding RNAs that are found inside the vault (vtRNA) and this interaction is confirmed by the absence of vtRNAs in vaults from TEP1-deleted mouse animal models (Kickhoefer *et al*., 2001)

Lastly, the vault protein contains non-coding RNA species, known as vRNA. vtRNAs are small, noncoding RNAs, 80–140 nt in size, quite likely evolutionarily related to tRNAs since both RNA types are transcribed by RNA polymerase III, and the encoding genes contain a split promoter containing elements known as box A and box B (Hahne *et al*., 2021; Stadler *et al*., 2009). Like the minor vault proteins, vtRNAs are largely not associated with the NP, the bound fraction representing about 5% of the total vault mass, which suggests that they are involved in diverse cellular interactions (Kickhoefer *et al*., 1998).

In the human genome, four vtRNAs are encoded on chromosome 5q31 in two different loci. At the VTRNA1 locus, three vtRNAs are encoded, i.e., vtRNA1-1, vtRNA1-2 and vtRNA1-3, whereas at the VTRNA2 locus, the sole vtRNA 2-1 is encoded. Two other vtRNA pseudogenes are located on chromosomes 2 and X (Büscher *et al*., 2020; Stadler *et al*., 2009). Generally, vtRNA1-1 is the most represented vtRNA variant, although diverse vtRNA expression levels are detected in different tissues.

vRNAs from different species have variable lengths and show low sequence homology, but the secondary structure is highly conserved (van Zon *et al*., 2003). Additionally, the in vivo secondary structure is more open compared to what is observed in vitro. The function of these non-coding RNAs associated with the vault is still unclear, although there is evidence

that their expression levels vary depending on the cells' physiological status (Berger *et al*., 2009).

Since the incorporation of vRNA into the vault depends on TEP1, it is not surprising that vRNA also localizes to the cap (Figure 11). Cryo-EM analysis performed on vaults extracted from Tep1-/- mice showed a reduction in density in this region compared to vaults extracted from wild-type mice (Kickhoefer *et al*., 2001). This same decrease is observed when native vaults are treated with RNase. It is worth noting, in this regard, that the use of only RNase A is not sufficient to completely degrade the vRNA present in the vault, which is instead achieved by adding high concentrations of two different RNases. This suggests that the vault complex has a protective role against the incorporated molecules, including RNA, allowing entry into its cavity only for specific molecules and acting as an insulator against the external environment (Kong *et al*., 2000).

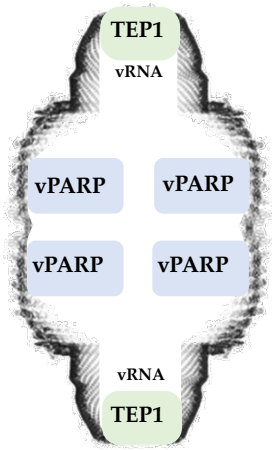


***Figure 11.*** *Vault cross-section including a schematic representation and location of the minor vault molecular components. Adapted from Frascotti et al., 2021*

*Localization and physiological roles*

Plenty of investigations on vault NPs have focused on its intracellular localization, which has helped better understand its biological roles.

Vault particles are mainly located in the cytoplasm (90%). The protein found in the cytoplasm interacts with elements of the cytoskeleton (van Zon *et al*., 2003) and its distribution in the cytoplasm is not random but depends on the metabolic and mitotic state of the cell. For example, in stationary fibroblasts, the protein forms clusters at the ends of actin fibers, while in circulating fibroblasts these clusters are located at the lamellipodia region. Vault has been observed moving at a speed of approximately 10μm/s, in line with the fast anterograde axonal transport of synaptic vesicles along microtubules, suggesting that its movement withing the cell is mediated by its ability to interact with the cytoskeleton (Slesina *et al*., 2006). A smaller amount of protein (approximately 5%) has been found to associate with the nucleus, particularly with the nucleoli, nuclear membrane, and nuclear pore complex (Chugani *et al*., 1993). Despite its large size, the passage through nuclear pores is possible thanks to its great flexibility, deformability, and self-repair capabilities, as recently observed in atomic force microscopy experiments (Llauró *et al*., 2014). Its interaction with the nuclear pore indicates a potential role in the transport of molecules to and from the nucleus (Kickhoefer *et al*., 1998). In humans, the estimated number of vault particles per cell is in the range $10^4$-$10^5$, but their number can vary depending on the cell type and functional state. Basal levels of vault expression have been observed in many tissues, such as the heart, pancreas, kidney, placenta, and central nervous system. Vaults are more abundant in macrophages and epithelial cells (Izquierdo *et al*., 1996), as well as in cells that cells that are chronically exposed to xenobiotics (Scheffer *et al*., 2000), such as enterocytes, hepatocytes, bronchial cells, and lung cells (Herrmann *et al*., 1999; Ikeda *et al*., 2014) but also in muscles.

Vaults' physiological role has not yet been fully characterized and although their structure is highly conserved and are synthetized in large amounts in the cells, they are not essential for survival, as MVP knock-out mice do not seem to present any phenotypic alterations (Frascotti *et al*., 2021).

In the last two decades, the understanding of the roles of the vault NP has greatly expanded revealing a complex and multifaceted involvement in various cellular processes. Mostly, vault works to maintain cell viability by protecting against diverse cellular stresses such as detoxification, infection, DNA damage, radiation, lack of oxygen, high osmotic pressure and oxidative stress. These functions are achieved through different mechanisms, including gene expression changes controlled by the MVP, activation of pathways that promote cell growth and survival, removal of DNA-damaging drugs from the nucleus, and import of specific proteins. The MVP can interact with a multitude of cellular proteins, all involved in survival and proliferation. One of the cellular pathways most influenced is that of the epidermal growth factor (EGF) /phosphatidylinositol-3-kinase (PI3K) /protein kinase B (protein kinase B/AKT). Several studies have shown, in fact, that MVP mediates the activation of AKT with a consequent increase in growth, proliferation, and anti-apoptotic effects (Hahne *et al*., 2021). However, this pro-survival function can also lead to multidrug resistance (MDR) that is the main cause of the failure of chemotherapy-based therapies in treatments against cancer. In 1995, vault has been identified as the lung resistance-related protein (Scheffer *et al*., 1995). In a recent study, it was demonstrated that the increased expression of MVP in mouse cardiomyocytes resulted in increased resistance to doxorubicin (Nandy *et al*., 2009). However, despite strong correlation, overexpression of vaults alone is not sufficient to produce the multidrug resistant phenotype (Kickhoefer *et al*., 1997). In Figure 12 the proposed physiological roles of vault are depicted.

Another area requiring further investigation regards how different components of the vault may complement each other in their functions. vRNA plays a concomitant role promoting cell survival and proliferation. In addition, vRNAs can intervene in the regulation of oncogenes (Lötsch *et al*., 2013).

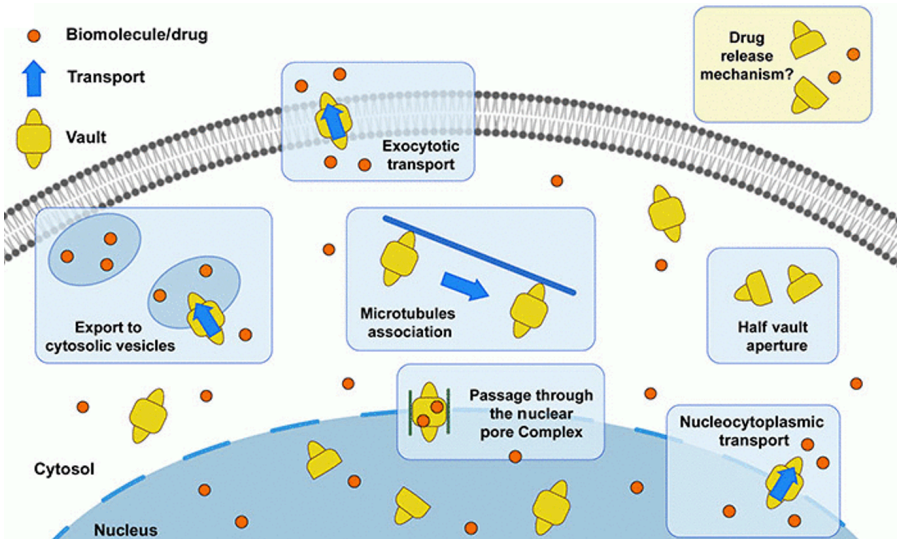


***Figure 12.*** *Representation of suggested vault functions associated with the transportation of diverse cargo within the cell. Adapted from Guerra et al., 2022.*

### 2.1 Recombinant vault as a tool for drug delivery

As previously mentioned, the production of a well-assembled vault structure has been achieved expressing the sole MVP in insect cells (Stephen *et al*., 2001). The pursuit of producing a recombinant vault particle is driven by vault's intrinsic features and structural characteristics that make it a promising candidate for the delivery of therapeutic molecules.

The primary advantage of using vaults for this purpose is their inherent lack of immunogenicity, observed in both mice and rabbits (Champion *et al*., 2009). Indeed, the production of the initial MVP antibody proved to be difficult and ultimately required the crosslinking of vaults before administration, suggesting that an immune response was only possible against a modified/altered particle. Unlike polymers and liposomes that can display size variability and a propensity for aggregation, vaults possess a regular and consistent size of 72 x 41 x 41 nm. This is ideal for circulation within the body by preventing them from being taken up by kidney or liver, as well as for taking advantage of the already mentioned EPR effect, resulting in an accumulation of NP in leaky tumor tissues and in free access to the draining lymph nodes when injected intradermally (Frascotti *et al*., 2021; Muñoz-Juan *et al*., 2019).

Furthermore, its large internal cavity of $5 \times 10^7$ Å$^3$ can potentially allow the incorporation of hundreds of molecules. This internal space not only can encapsulate therapeutic molecules but also offer some degree of protection from degradation by external proteases and can act as insulator towards external environment. For example, by incorporating a variant of a green fluorescent protein (GFP) inside the vault and adding an oxidizing agent to the solution, a gradual decrease in fluorescence can be detected, unlike the rapid decline encountered by free GFP (Kickhoefer *et al*., 2005). This way, pharmacologically active molecules, both hydrophilic and hydrophobic, when subject to poor pharmacokinetics can be encapsulated and protected in vault inner cavity, allowing for extended half-life.

Molecules can be incorporated into vault by exploiting the interaction domain (INT) derived from vPARP. This domain has been identified from structural studies of vPARP and MVP interaction based on yeast two hybrid assay. As already described, it corresponds to the 162 aa C-terminal portion (amino acids 1563 to 1724) of vPARP and it is responsible for the interaction of vPARP with MVP (van Zon *et al*., 2003). Fusion proteins with INT domain can be internalized into the vault complex thanks to the dynamic behavior of vault, without requiring co-translation with MVP (Goldsmith *et al*., 2009; Kickhoefer *et al*., 2005; Querol-Audí *et al*., 2009). Cryo-EM analysis, conducted on INT-luciferase and INT-GFP encapsulated within vault, has demonstrated that INT-fusion proteins are stored inside the vault cavity in two rings of higher density above and below the waist of the protein (Kickhoefer *et al*., 2005) as represented in Figure 13A.

Despite the need of fusing INT to a protein sequence, INT-mediated packaging strategy holds a tremendous potential, ensuring a specific and stable association of the cargo within the vault NP. In principle, any protein recombinantly fused with the INT domain could be internalized within vault, and so far several have been already encapsulated, including luminescent reporter properties (luciferase-INT), immune-stimulatory (MOMP-INT) and chemokines (e.g. chemokine (C–C motif) ligand 21 to treat lung cancer), His-T7, VSG-V tag and HIV- epitope tag (Muñoz-Juan *et al*., 2019). By exploiting INT domain not only proteins can be loaded into vault. An interesting

example is the internalization of a nanodisk-INT into vault that enabled hydrophobic drugs to be loaded within vault. The INT domain was fused to a truncated form of apolipoprotein-AI containing amphipathic alpha-helices. This construct spontaneously associated with phospholipids, forming a unique double lipid layer structure (Nanodisk), intrinsically capable of incorporating hydrophobic molecules (Ryan, 2008). This is the case of many chemotherapeutic agents that are small, hydrophobic molecules difficult to administer for their low solubility in blood and that cannot be fused with the INT domain to be loaded within the vault. In the study from Buehler *et al*. the hydrophobic all-trans retinoic acid (ATRA), a natural derivative of vitamin A used to treat various pathologies, ranging from acne to certain types of tumors (e.g. acute promyelocytic leukemia) was incorporated in the nanodisk-INT structure and subsequently loaded into vault (Buehler *et al*., 2011; Redmond *et al*., 2007). The encapsulation into vault allowed overcoming some issues related to the nature of this therapeutic molecule, including insolubility, teratogenicity, and the potential onset of the retinoic acid syndrome (Muñoz-Juan *et al*., 2019). The loading of hydrophobic drugs into vault can be achieved also without the use of external Nanodisck structure but by modification of the internal vault cavity. For example, the vault lumen was engineered to create a more hydrophobic interior environment, by covalent attachment of an amphipathic $\alpha$-helix peptide, originally from the NS5A protein of hepatitis C virus to the N-terminal end of MVP, naturally protruding inside the lumen, thus allowing the encapsulation of >2000 molecules (such as bryostatin 1, amphotericin B, or ATRA) per single vault (Buehler *et al*., 2014).

The INT domain can also be exploited to encapsulate inorganic molecules. Recombinant INT containing an additional 31 amino acids at the N-terminus, including a $His_6$ tag, was used to load Ni-NTA nanogold, leveraging the affinity between Nickel and the $His_6$ tag (Goldsmith *et al*., 2009). This study has also opened the possibility of using vault protein in imaging.

Recently, a new Adeno-associated virus (AAV) delivery system has emerged, utilizing INT-decorated AAV packaged inside vault NP to shield it from neutralizing serum (Collins *et al*., 2023). As demonstrated in this study,

the high affinity of the INT domain has allowed for the encapsulation of an entire virus within the vault, demonstrating the advantages offered by the INT-mediated packaging strategy.

Another important aspect of vault for its application in drug delivery relies on the possibility of genetically engineering the MVP-encoding sequence to confer specific and additional functionality. Engineering of MVP can involve both N- and C-termini (Rome & Kickhoefer, 2013) (Figure 13B). Since the C-terminus of MVP is localized at the caps and exposed on the surface (Figure 13B in blue), the genetic fusion on MVP C-terminus with suitable peptides can be an ideal approach to increase the protein's specificity towards certain cell lines, thus enabling a targeted delivery (Rome & Kickhoefer, 2013). Indeed, the ability of cells to internalize vault particles has been shown to vary depending on the cell type. Unfunctionalized vaults were reported to enter macrophages and dendritic cells, likely via micropinocytosis or phagocytosis (Lai *et al*., 2009; Nagasawa *et al*., 2020). Vaults are also taken up neither specifically nor efficiently by HeLa (Kickhoefer *et al*., 2005, 2009) and glioblastoma cell lines (Galbiati *et al*., 2018), in the latter case through a process sustained by clathrin- but not caveolae-mediated endocytosis. Nevertheless, in other cell lines such as various adenocarcinoma and breast cancer cells, the degree of vault uptake was much lower. Enabling the vault to perform selective targeting is a good strategy for increasing its potential in the field of drug delivery. As already discussed in previous paragraphs, NPs exploited in the drug delivery can be equipped with antibodies, proteins or peptides that selectively direct them to cancer cell lines (Avvakumova *et al*., 2014; D Friedman *et al*., 2013; Marques *et al*., 2020). One common approach implies the use of specific antibodies, attached to the surface of NPs trough chemical conjugation and other techniques that can be complex, time-consuming, and may not always ensure the correct orientation of the antibody (Marques *et al*., 2020). Based on these considerations, one of the most promising vault modifications for improving its selective targeting, was achieved by fusing MVP C-terminal portion with the Z peptide, a short, acidic sequence 33 amino acids long, derived from the bacterial protein A, known for its ability to interact with the constant portion

(Fragment Crystallizable (Fc) region) of any antibody (Braisted & Wells, 1996). The Protein A-derived Z peptide was engineered to substantially increase its affinity for the Fc compared with the original sequence. The resulting vault-Z fusion product exposes the Z peptides at the two caps, one for each MVP, and is therefore potentially capable of binding with very high affinity to the constant region of human type 1 immunoglobulins (IgG1), as well as rabbit antibodies and, although with lower affinity, mouse antibodies (Kickhoefer *et al*., 2009). By conjugating this peptide with an antibody that recognizes the Epidermal Growth Factor receptor (EGFR), active targeting towards the A431 tumor epithelial cell line was achieved (Kickhoefer *et al*., 2009).

Alternatively, the vault C-termini were fused with a cell-penetrating peptide (13 aa basic fragment, of TAT protein from HIV1) that strongly boosted vault binding and internalization by a variety of cell types (J. Yang *et al*., 2013).

Due to the vault structure, N-terminal modifications are located at the interface between the two halves, protruding in the internal cavity (Figure 13B in pink). Among such modifications, the most promising so far developed are essentially two. One involves the addition of a cysteine-rich domain called CP, which gives the monomers the ability to form disulfide bridges, greatly increasing the stability of the structure (Mikyas *et al*., 2004). The other important modification at the N-terminus was designed to increase the release of the vault protein from the endosome, once it has been endocytosed by the target cells (Han *et al*., 2011). Study on adenovirus cell internalization have shown its capability of escaping the endosomal compartment thanks to the presence of protein VI (pVI), whose N-terminal region presents an amphipathic $\alpha$-helical domain that exhibits potent membrane lytic activity (Wiethoff *et al*., 2005). This membrane-lytic peptide has been initially fused to the INT domain to be loaded into vault, to explore the feasibility of improving vault penetration into target cells. One problem with this approach was that relatively large numbers of vault/pVI-INT particles (>$10^6$/cell) were needed to facilitate the uptake of the co-administered ribotoxin saporin and a GFP-encoding plasmid by a

macrophage cell line (Lai *et al*., 2009). Later, an even more efficient membrane lytic vault was produced by fusing the 20 amino acid membrane lytic domain of pVI directly to the N-terminus of MVP, resulting in several copies of pVI per vault. Although being advantageous in view of enhanced endosomal escape activity, high concentrations of this peptide resulted however in unwanted cellular apoptosis (Han *et al*., 2011).

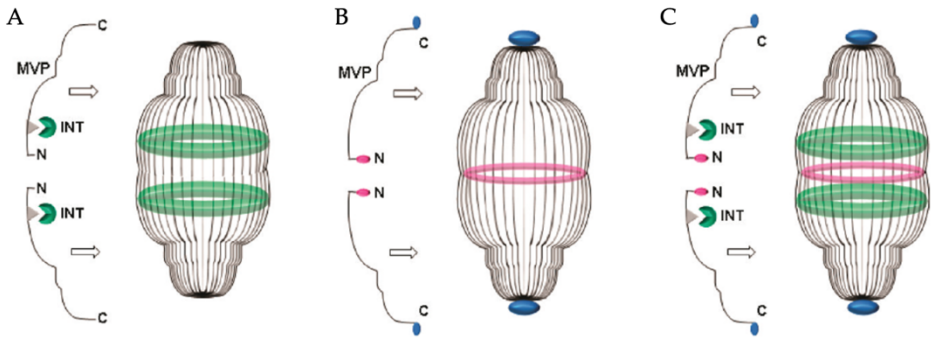


***Figure 13.*** *Schematic diagrams of engineered vault structures. (A) Vaults engineered with exogenous protein fused to the INT. gray triangle: The INT binding site on MVP, located above and below the waist of the vault facing the inside of the particle. Green: Packaged proteins fused to the INT domain, displayed as two rings bound to the INT binding sites on the interior of vaults. (B) Vaults engineered with fused sequences at the N-termini (pink) and C-termini (blue) of the MVP. N-terminal peptide extensions (pink) are located on the interior surface of the engineered vault particles at the waist. C-terminal peptide extensions (blue) fused to MVP are located on the exterior surface of the particles at the end of the caps. (C) Diagram of multifunctional engineered vaults containing INT fusion proteins. Adapted from Han et al., 2011*

These peculiar features, together with other interesting aspects of vault are summarized in Figure 14 by Munoz *et al*. as the vault's hallmarks (Muñoz-Juan *et al*., 2019).

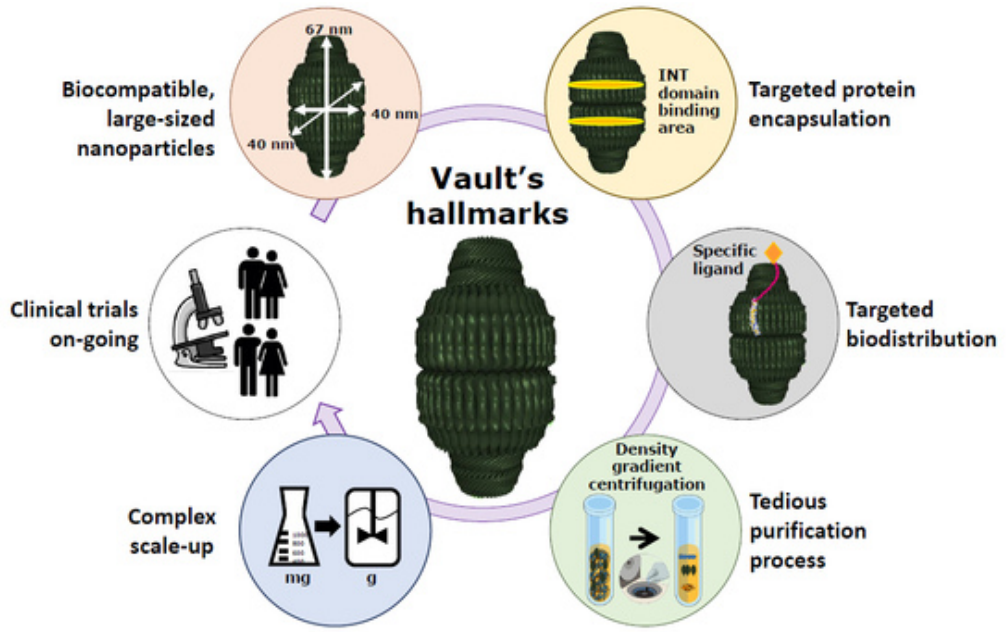


***Figure 14.*** *Vault's hallmarks from Muñoz-Juan et al., 2019.*

An important aspect highlighted in this graph regards vault NPs production and purification, which are regarded as complex and tedious, respectively. In view of the findings presented in this dissertation, a more detailed picture of these concepts is presented below.

*Heterologous vault protein expression system and purification process.*

The development an efficient expression system was essential for the employment of vault in drug delivery. It was necessary to find a cell factory that did not possess endogenous vault and given the occurrence of this protein in several eukaryotes, the number of usable biological systems was reduced.

Until few years ago, the only expression system for the vault protein was the Baculovirus-insect system. The choice on this cell factory was driven by the production efficiency of this system already seen for viral vectors, and of course by the absence of endogenous vault. Expression of rat vault protein was carried out by *Spodoptera frugiperda* Sf9 insect cells, following infection by a baculovirus vector carrying the complementary DNA (cDNA) sequence of MVP (Stephen *et al*., 2001). Within the Baculoviridae family, the

multicapsid nucleopolyhedro-virus *Autographa californica* (AcMNPV) was the best-characterized virus and the one most frequently used for the production of recombinant proteins, partly due to the broad spectrum of infection it possesses (Jarvis, 2009). The MVP-coding sequence was inserted under the control of the promoter of the gene coding for polyhedrin (a protein expressed towards the end of the infection cycle, required for the formation of the inclusion bodies of the virus), since it contains a burst sequence that can increase the expression levels (Stephen *et al*., 2001). This system was proved effective in vault production, also allowing high protein yields (approximately 10 mg/L). However, it also has with several drawbacks:

- The method is complex and expensive, significantly thwarting its scalability for industrial purposes.
- The production process is time-consuming (spanning 3 to 6 months)
- Infection-induced cell lysis can hamper production by releasing intracellular proteins and rendering the heterologous protein vulnerable to protease attack during downstream processing.

Efforts to address these challenges have included the use of Sf9 larvae cells instead of insect cells, which can offer higher yields and cost efficiency, thus favoring scale-up. Nevertheless, this approach has encountered limited adoption due to the unfamiliarity with insect larvae and the difficulty in sourcing these cell lines (Muñoz-Juan *et al*., 2019).

Additionally, to this complex production method has been associated a tedious purification process, developed by the same authors and that is still being employed (Stephen *et al*., 2001). This method involves several steps: after insect cell lysis, it comprises, in particular, several ultracentrifugation steps, RNAse A and RNAse Ti treatment to degrade ribosomes, and centrifugation in a sucrose gradient. While ensuring a high level of protein purity, this procedure is long, expensive, cumbersome, and not scalable (Muñoz-Juan *et al*., 2019).

The limitations implicated in both production and purification methods, prompted scientists to search for new cell factories and alternative purification methods.

As far as the vault purification process is concerned, a simpler and faster purification method has been previously developed in our laboratory, characterized to be simpler, straightforward, and potentially suitable for a possible scale-up. This process involves dialysis with a membrane with a 1000 kDa cut-off of the insect cell lysate, followed by molecular exclusion chromatography with a 4 MDa cut-off resin, whereby the vault protein eluted in the empty volume (Galbiati *et al*., 2018)

Shortly afterwards, a different production system for vault production was set up, which exploited the methylotrophic yeast *Komagataella phaffii* (formerly *Pichia pastoris*) as an alternative cell factory for vault production (M. Wang *et al*., 2018).

The yeast *Pichia pastoris*, now reclassified as *Komagataella phaffii,* is a widely utilized heterologous protein expression system in the industrial context. Around 1950 it gained prominence for its ability to efficiently grow using methanol as its sole carbon and energy source, leading to high yields in biomass and heterologous protein production. As the utilization of methanol in *K. phaffii* production encountered environmental, health, and scale-up concerns, an alternative approach emerged still taking advantage of the properties of this versatile yeast (Güneş & Çalık, 2016). Specifically, a non-methanol-based production system was adopted, which exploited the GAP promoter derived from the glycolytic enzyme glyceraldehyde-3-phosphate dehydrogenase. Unlike the inducible pAOX1 promoter used for production with methanol, the GAP promoter is constitutive, thus ensuring continuous protein expression (Güneş & Çalık, 2016). Moreover, although *K. phaffii* shares several similarities with the well-known yeast *Saccharomyces cerevisiae*, in that they both are budding yeast, exist in both haploid and diploid states and are subject to easy genetical manipulation, *K. phaffii* is often preferred due to its higher protein secretion efficiency, related to the peculiar properties of its Golgi apparatus, and due to a glycosylation pattern more similar to that of mammalian cells, which leads to the incorporation of fewer mannose molecules. This results in the production of heterologous proteins that are less immunogenic to humans.

Even if vault expression is cytosolic thus not subdued to post-translational modification, the above considerations justify the adoption of *K.*

*phaffii* as an expression system for vault production, as accomplished in the aforementioned report (Wang *et al*., 2018). In particular, the human MVP monomer sequence was inserted into the integrative pGAPZ A vector (Invitrogen, Carlsbad, CA) under the control of the robust and constitutive GAP promoter, allowing for a continuative vault production during the entire growth, impossible to be achieved under control of pAOX1 promoter. This vector was then employed to transform the protease-deficient strain SMD1168 of *K. phaffii* and the produced vault protein was purified by the traditional sucrose gradient-based method (Stephen *et al*., 2001), with a protein yield of 7-11 mg/L over a production period of 30 hours. Transmission electron microscopy (TEM) of the vault purified form the transformed yeast demonstrated identical morphology to its insect-produced counterpart (M. Wang *et al*., 2018).

# 3 Scope of the thesis

As we align with the objectives of this dissertation, it becomes apparent that vaults present all the intrinsic features necessary to surmount the constraints encountered by alternative delivery systems: they are nonimmunogenic and nontoxic, they can be modified to encapsulate therapeutic molecules within their internal cavity and target specific cells or tissues, resulting in more effective delivery of therapeutic molecules. Nevertheless, the pivotal challenge of achieving a straightforward, effective, and cost-efficient production process for vaults remains, and with it also numerous uncharted possibility and directions to explore to harness the potential of vaults (Muñoz-Juan *et al*., 2019).

These considerations set the basis of my PhD project, a Joint PhD, conducted in a framework of Cotutelle agreement between the University of Milan Bicocca (UNIMIB) and Université Paris Cité and founded the "CHROnical multifactorial disorders explored by NOvel integrated Strategies (CHRONOS)" project of the Department of Biotechnology and Biosciences (BtBs) of UNIMIB.

The first aim of this project was to optimize the procedure for obtaining recombinant vaults to then apply them in the delivery of therapeutic molecules. As mentioned before, the available methods for the production and purification of vault are complex, time consuming and onerous. The utilization of other cell factory as *K.phaffii* has been proposed (M. Wang *et al*., 2018) as well as new method for vault purification essentially based on a SEC. Thus, we first set up to develop a simple and straightforward one, starting from the combination of these two novel methods. This is reported in **Chapter 1**, where our recently published results are presented. This also includes investigations that led to the identification of the best storage conditions, essential to detach vault use from its production that occurred in Milan, thus allowing vault shipping to Paris.

Following the production and subsequent characterization of the recombinant vault from *K. phaffii*, this project has been particularly intended to focus on two important aspects, relevant to the potential of vault in the field of drug delivery: its capability of loading and delivering proteins and nucleic acids such as siRNA, and the development and characterization of a

variant suitable for targeted delivery. First it was crucial to establish the capacity of our vault to transport cargo molecules, thus validating its functionality. Thus, **Chapter 2**, mainly conducted in Paris, aimed at verifing the vault's ability to encapsulate proteins fused to the INT domain, which tightly binds to the interior of the NP. For this purpose, the protein GFP-INT, was chosen as a reporter cargo, with the aim of also identifying the maximal amount of bound cargo molecules.

Interest in nucleic acids as a new category of therapeutics is growing significantly in recent years, and the use of NPs is at the forefront to achieve safe and effective delivery (Abdel-Mageed *et al*., 2021). The investigations in **Chapter 3**, were intended to explore the potential of using vaults for siRNA delivery, pursuing two different strategies: one exploiting the interaction of INT domain with vault, thus requiring chemical conjugation of siRNA to the GFP-INT and taking advantage of the achievements of the previous chapter. The other is aimed at directly loading a siRNA into vaults, in the expectation that it might directly bind to their positively charged internal lumen.

Moreover, the development of engineered vaults capable of targeted cell delivery is set as the final goal, which is addressed in **Chapter 4** and relies upon the construction of a vault variant carrying the Z peptide. This variant is able to tightly and directly bind antibody's constant portion, which might circumvent the constraints associated with the common chemical methods, in that they are typically complex and time consuming and not necessarily guarantee the correct orientation of the antibody to be active (Marques *et al*., 2020). The investigations also aimed at assessing whether and how the number of bound antibodies per vault, which can be easily tuned, modulates vault endocytosis.

Summing up, the overall goal was the development of a vault-based platform, of ease production and purification, suitable for being loaded with nucleic acids and proteins and for being selectively targeted to selected cell lines via a predetermined number of bound, correctly oriented antibodies.

# References


Abdel-Mageed, H. M., AbuelEzz, N. Z., Radwan, R. A., & Mohamed, S. A. (2021). Nanoparticles in nanomedicine: a comprehensive updated review on current status, challenges and emerging opportunities. *Journal of Microencapsulation*, *38*(6), 414–436. https://doi.org/10.1080/02652048.2021.1942275

Adams, D., Gonzalez-Duarte, A., O'Riordan, W. D., Yang, C.-C., Ueda, M., Kristen, A. V, Tournev, I., Schmidt, H. H., Coelho, T., Berk, J. L., Lin, K.-P., Vita, G., Attarian, S., Planté-Bordeneuve, V., Mezei, M. M., Campistol, J. M., Buades, J., Brannagan, T. H. 3rd, Kim, B. J., … Suhr, O. B. (2018). Patisiran, an RNAi Therapeutic, for Hereditary Transthyretin Amyloidosis. *The New England Journal of Medicine*, *379*(1), 11–21. https://doi.org/10.1056/NEJMoa1716153

Aleandri, S., Fong, W.-K., Manni, L. S., Seo, Y., Lim, H., Park, H., Yu, J., An, J., Yoo, H. Y., & Lee, T. (2023). Recent Progress of Lipid Nanoparticles-Based Lipophilic Drug Delivery: Focus on Surface Modifications. *Pharmaceutics*, *15*(3), 772. https://doi.org/10.3390/pharmaceutics15030772

Alexis, F., Pridgen, E., Molnar, L. K., & Farokhzad, O. C. (2008). Factors Affecting the Clearance and Biodistribution of Polymeric Nanoparticles. *Molecular Pharmaceutics*, *5*(4), 505–515. https://doi.org/10.1021/mp800051m

Alshehri, S., Sarim Imam, S., Rizwanullah, M., Akhter, S., Mahdi, W., Kazi, M., & Ahmad, J. (2020). *Progress of Cancer Nanotechnology as Diagnostics, Therapeutics, and Theranostics Nanomedicine: Preclinical Promise and Translational Challenges*. https://doi.org/10.3390/pharmaceutics13010024

Amoabediny, G., Haghiralsadat, F., Naderinezhad, S., Helder, M. N., Akhoundi Kharanaghi, E., Mohammadnejad Arough, J., & Zandieh-Doulabi, B. (2018). Overview of preparation methods of polymeric and lipid-based (niosome, solid lipid, liposome) nanoparticles: A comprehensive review. *International Journal of Polymeric Materials and Polymeric Biomaterials*, *67*(6), 383–400. https://doi.org/10.1080/00914037.2017.1332623

Amreddy, N., Babu, A., Muralidharan, R., Panneerselvam, J., Srivastava, A., Ahmed, R., Mehta, M., Munshi, A., & Ramesh, R. (2018). Recent Advances in Nanoparticle-Based Cancer Drug and Gene Delivery. In *Advances in Cancer Research* (1st ed., Vol. 137). Elsevier Inc. https://doi.org/10.1016/bs.acr.2017.11.003

Anselmo, A. C., Mitragotri, S., & Samir Mitragotri, C. (2016). *Nanoparticles in the clinic*. https://doi.org/10.1002/btm2.10003

Avvakumova, S., Colombo, M., Tortora, P., & Prosperi, D. (2014). Biotechnological approaches toward nanoparticle biofunctionalization. *Trends in Biotechnology*, *32*(1), 11–20. https://doi.org/10.1016/j.tibtech.2013.09.006

Bateman, A., & Kickhoefer, V. (2003). The TROVE module: A common element in Telomerase, Ro and Vault ribonucleoproteins. *BMC bioinformatics*, *4*(1), 1-5. http://www.vaults.arc.ucla.edu/

Batty, C. J., Bachelder, E. M., & Ainslie, K. M. (2021). Historical Perspective of Clinical Nano and Microparticle Formulations for Delivery of Therapeutics HHS Public Access. *Trends Mol Med*, *27*(6), 516–519. doi.org/10.1016/j.molmed.2021.04.002

Berger, W., Steiner, E., Grusch, M., Elbling, L., & Micksche, M. (2009). Vaults and the major vault protein: Novel roles in signal pathway regulation and immunity. In *Cellular and Molecular Life Sciences* (Vol. 66, Issue 1, pp. 43–61). https://doi.org/10.1007/s00018-008-8364-z

Bharali, D. J., Khalil, M., Gurbuz, M., Simone, T. M., & Mousa, S. A. (2009). Nanoparticles and cancer therapy: A concise review with emphasis on dendrimers. *International Journal of Nanomedicine*, *4*(1), 1–7.

Braisted, A. C., & Wells, J. A. (1996). Minimizing a binding domain from protein A. *Proceedings of the National Academy of Sciences*, *93*(12), 5688–5692.

Buehler, D. C., Marsden, M. D., Shen, S., Toso, D. B., Wu, X., Loo, J. A., Zhou, Z. H., Kickhoefer, V. A., Wender, P. A., Zack, J. A., & Rome, L. H. (2014). Bioengineered vaults: Self-assembling protein shell-lipophilic core nanoparticles for drug delivery. *ACS Nano*, *8*(8), 7723–7732. https://doi.org/10.1021/nn5002694

Buehler, D. C., Toso, D. B., Kickhoefer, V. A., Zhou, Z. H., & Rome, L. H. (2011). Vaults engineered for hydrophobic drug delivery. *Small*, *7*(10), 1432–1439. https://doi.org/10.1002/smll.201002274

Bulcha, J. T., Wang, Y., Ma, H., Tai, P. W. L., & Gao, G. (n.d.). Viral vector platforms within the gene therapy landscape. *Signal transduction and targeted therapy*, *6*(1), 53. https://doi.org/10.1038/s41392-021-00487-6

Büscher, M., Horos, R., & Hentze, M. W. (2020). 'High vault-age': Non-coding RNA control of autophagy. *Open Biology*, *10*(2). https://doi.org/10.1098/rsob.190307

Butt, M. H., Zaman, M., Ahmad, A., Khan, R., Mallhi, T. H., Hasan, M. M., Khan, Y. H., Hafeez, S., Massoud, E. E. S., Rahman, M. H., & Cavalu, S. (2022). Appraisal for the Potential of Viral and Nonviral Vectors in Gene Therapy: A Review. *Genes*, *13*(8). https://doi.org/10.3390/genes13081370

Carissimi, G., Montalbán, M. G., Fuster, M. G., & Víllora, G. (2021). Nanoparticles as Drug Delivery Systems. In P. V Pham (Ed.), *21st Century Nanostructured Materials*. IntechOpen. https://doi.org/10.5772/intechopen.100253

Chahal, J. S., Khan, O. F., Cooper, C. L., McPartlan, J. S., Tsosie, J. K., Tilley, L. D., Sidik, S. M., Lourido, S., Langer, R., Bavari, S., Ploegh, H. L., & Anderson, D. G. (2016). Dendrimer-RNA nanoparticles generate protective immunity against lethal Ebola, H1N1 influenza, and *Toxoplasma gondii* challenges with a single dose. *Proceedings of the National Academy of Sciences*, *113*(29), E4133–E4142. https://doi.org/10.1073/pnas.1600299113

Champion, C. I., Kickhoefer, V. A., Liu, G., Moniz, R. J., Freed, A. S., Bergmann, L. L., Vaccari, D., Raval-Fernandes, S., Chan, A. M., Rome, L. H., & Kelly, K. A. (2009). A vault nanoparticle vaccine induces protective mucosal immunity. *PLoS ONE*, *4*(4). https://doi.org/10.1371/journal.pone.0005409

Chowdhury, S., Toth, I., & Stephenson, R. J. (2022). Dendrimers in vaccine delivery: Recent progress and advances. *Biomaterials*, *280*, 121303. https://doi.org/10.1016/j.biomaterials.2021.121303

Chugani, D. C., Rome, L. H., & Kedersha, N. L. (1993). Evidence that vault ribonucleoprotein particles localize to the nuclear pore complex. *Journal of Cell Science*, *106 ( Pt 1*, 23–29. https://doi.org/10.1242/jcs.106.1.23

Collins, K., Kobayashi, R., & Greider, C. W. (1995). Purification of tetrahymena telomerase and cloning of genes encoding the two protein components of the enzyme. *Cell*, *81*(5), 677–686. https://doi.org/10.1016/0092-8674(95)90529-4

Collins, L. T., Beatty, W., Moyo, B., Alves-Bezerra, M., Hurley, A., Lagor, W., Bao, G., Ponnazhagan, S., Mcnally, R., Rome, L., & Curiel, D. T. (2023). Encapsulation of AAVs into protein vault nanoparticles as a novel solution to gene therapy's neutralizing antibody problem. *bioRxiv*, 2023-11.

D Friedman, A., E Claypool, S., & Liu, R. (2013). The smart targeting of nanoparticles. *Current Pharmaceutical Design*, *19*(35), 6315–6329.

Daly, T. K., Sutherland-Smith, A. J., & Penny, D. (2013). In silico resurrection of the major vault protein suggests it is ancestral in modern eukaryotes. *Genome Biology and Evolution*, *5*(8), 1567–1583. https://doi.org/10.1093/gbe/evt113

Dana, H., Chalbatani, G. M., Mahmoodzadeh, H., Karimloo, R., Rezaiean, O., Moradzadeh, A., Mehmandoost, N., Moazzen, F., Mazraeh, A., Marmari, V., Ebrahimi, M., Rashno, M. M., Abadi, S. J., & Gharagouzlo, E. (2017). Molecular Mechanisms and Biological Functions of siRNA. *International Journal of Biomedical Science : IJBS*, *13*(2), 48–57.

Damase, T. R., Sukhovershin, R., Boada, C., Taraballi, F., Pettigrew, R. I., & Cooke, J. P. (2021). The Limitless Future of RNA Therapeutics. *Frontiers in Bioengineering and Biotechnology*, *9*, 628137. doi.org/10.3389/fbioe.2021.628137

Diaz, D., Care, A., & Sunna, A. (2018). Bioengineering Strategies for Protein-Based Nanoparticles. *Genes*, *9*(7). https://doi.org/10.3390/GENES9070370

Du, X., Wang, J., Zhou, Q., Zhang, L., Wang, S., Zhang, Z., & Yao, C. (2018). Advanced physical techniques for gene delivery based on membrane perforation. *Drug Delivery*, *25*(1), 1516–1525. https://doi.org/10.1080/10717544.2018.1480674

Dutriaux, A., Diazzi, S., Caburet, S., Bresesti, C., Hardouin, S., Deshayes, F., Collignon, J., & Flagiello, D. (2023). *LADON*, a natural antisense transcript of NODAL, promotes an invasive behaviour in melanoma cells. *Non-coding RNA, 9(6), 71.*

Edwardson, T. G. W., Levasseur, M. D., Tetter, S., Steinauer, A., Hori, M., & Hilvert, D. (2022). *Protein Cages: From Fundamentals to Advanced Applications*. https://doi.org/10.1021/acs.chemrev.1c00877

Edwardson, T. G. W., Mori, T., & Hilvert, D. (2018). Rational Engineering of a Designed Protein Cage for siRNA Delivery. *J. Am. Chem. Soc*, *140*, 10439–10442. https://doi.org/10.1021/jacs.8b06442

Elzoghby, A. O., Samy, W. M., & Elgindy, N. A. (2012). Albumin-based nanoparticles as potential controlled release drug delivery systems. *Journal of Controlled Release*, *157*(2), 168–182.

Farooqi, Z. H., Akram, M. W., Begum, R., Wu, W., & Irfan, A. (2021). Inorganic nanoparticles for reduction of hexavalent chromium: Physicochemical aspects. *Journal of Hazardous Materials*, *402*(July 2020), 123535. https://doi.org/10.1016/j.jhazmat.2020.123535

Frascotti, G., Galbiati, E., Mazzucchelli, M., Pozzi, M., Salvioni, L., Vertemara, J., & Tortora, P. (2021). The vault nanoparticle: A gigantic ribonucleoprotein assembly involved in diverse physiological and pathological phenomena and an ideal nanovector for drug delivery and therapy. *Cancers*, *13*(4), 1–37. https://doi.org/10.3390/cancers13040707

Galbiati, E., Avvakumova, S., La Rocca, A., Pozzi, M., Messali, S., Magnaghi, P., Colombo, M., Prosperi, D., & Tortora, P. (2018). A fast and straightforward procedure for vault nanoparticle purification and the characterization of its endocytic uptake. *Biochimica et Biophysica Acta - General Subjects*, *1862*(10), 2254–2260. https://doi.org/10.1016/j.bbagen.2018.07.018

Goldsmith, L. E., Pupols, M., Kickhoefer, V. A., Rome, L. H., & Monbouquette, H. G. (2009). Utilization of a Protein "Shuttle" To Load Vault Nanocapsules with Gold Probes and Proteins. *Acs Nano, 3(10), 3175-3183*. https://doi.org/10.1021/nn900555d

Goldsmith, L. E., Yu, M., Rome, L. H., & Monbouquette, H. G. (2007). Vault nanocapsule dissociation into halves triggered at low pH. *Biochemistry*, *46*(10), 2865–2875. https://doi.org/10.1021/bi0606243

Gradishar, W. J., Tjulandin, S., Davidson, N., Shaw, H., Desai, N., Bhar, P., Hawkins, M., & O'Shaughnessy, J. (2005). Phase III trial of nanoparticle albumin-bound paclitaxel compared with polyethylated castor oil–based paclitaxel in women with breast cancer. *Journal of Clinical Oncology*, *23*(31), 7794–7803.

Guerra, P., González-Alamos, M., Llauró, A., Casañas, A., Querol-Audí, J., de Pablo, P. J., & Verdaguer, N. (2022). Symmetry disruption commits vault particles to disassembly. *Science Advances*, *8*(6). https://doi.org/10.1126/sciadv.abj7795

Güneş, H., & Çalık, P. (2016). Oxygen transfer as a tool for fine-tuning recombinant protein production by Pichia pastoris under glyceraldehyde-3-phosphate dehydrogenase promoter. *Bioprocess and Biosystems Engineering*, *39*, 1061–1072.

Hahne, J. C., Lampis, A., & Valeri, N. (2021). Vault RNAs: hidden gems in RNA and protein regulation. In *Cellular and Molecular Life Sciences* (Vol. 78, Issue 4, pp. 1487–1499). Springer Science and Business Media Deutschland GmbH. https://doi.org/10.1007/s00018-020-03675-9

Han, M., Kickhoefer, V. A., Nemerow, G. R., & Rome, L. H. (2011). Targeted vault nanoparticles engineered with an endosomolytic peptide deliver biomolecules to the cytoplasm. *ACS Nano*, *5*(8), 6128–6137. https://doi.org/10.1021/nn2014613

Herrera Estrada, L. P., & Champion, J. A. (2015). Protein nanoparticles for therapeutic protein delivery. *Biomaterials Science*, *3*(6), 787–799. https://doi.org/10.1039/c5bm00052a

Herrmann, C., Golkaramnay, E., Inman, E., Rome, L., & Volknandt, W. (1999). Recombinant major vault protein is targeted to neuritic tips of PC12 cells. *The Journal of Cell Biology*, *144*(6), 1163–1172.

Hidai, C., & Kitano, H. (2018). Nonviral Gene Therapy for Cancer: A Review. *Diseases*, *6*(3). https://doi.org/10.3390/diseases6030057

Hong, S., Choi, D. W., Kim, H. N., Gwon Park, C., Lee, W., & Park, H. H. (2020). Protein-Based Nanoparticles as Drug Delivery Systems. *Pharmaceutics*. https://doi.org/10.3390/pharmaceutics12070604

Hou, S., Hasnat, M., Chen, Z., Liu, Y., Muhammad Faran Ashraf Baig, M., Liu, F., & Chen, Z. (2022). Application Perspectives of Nanomedicine in Cancer Treatment. *Frontiers in Pharmacology*, *13*(909526). https://doi.org/10.3389/fphar.2022.909526

Hou, X., Zaks, T., Langer, R., & Dong, Y. (2021). Lipid nanoparticles for mRNA delivery. *Nature Reviews Materials*, *6*(12), 1078–1094.

Huang, J.-Y., Gao, Y., Cutlar, L., O'Keeffe-Ahern, J., Zhao, T., Lin, F.-H., Zhou, D., McMahon, S., Greiser, U., Wang, W., & Wang, W. (2015). Tailoring highly branched poly(β-amino ester)s: a synthetic platform for epidermal gene therapy. *Chem. Commun.*, *51*(40), 8473–8476. https://doi.org/10.1039/C5CC02193F

Ijaz, I., Gilani, E., Nazir, A., & Bukhari, A. (2020). Detail review on chemical, physical and green synthesis, classification, characterizations and applications of nanoparticles. *Green Chemistry Letters and Reviews*, *13*(3), 59–81. https://doi.org/10.1080/17518253.2020.1802517

Ikeda, R., Nishizawa, Y., Tajitsu, Y., Minami, K., Mataki, H., Masuda, S., Furukawa, T., Akiyama, S.-I., Yamada, K., & Takeda, Y. (2014). Regulation of major vault protein expression by upstream stimulating factor 1 in SW620 human colon cancer cells. *Oncology Reports*, *31*(1), 197–201.

Iravani, S., & Varma, R. S. (2023). Vault, viral, and virus-like nanoparticles for targeted cancer therapy. *Material Advances* https://doi.org/10.1039/d3ma00171g

Jain, A., Singh, S. K., Arya, S. K., Kundu, S. C., & Kapoor, S. (2018). Protein nanoparticles: promising platforms for drug delivery applications. *ACS Biomaterials Science & Engineering*, *4*(12), 3939–3961.

Jarvis, D. L. (2009). Baculovirus–insect cell expression systems. *Methods in Enzymology*, *463*, 191–222.

Jeevanandam, J., Barhoum, A., Chan, Y. S., Dufresne, A., & Danquah, M. K. (2018). Review on nanoparticles and nanostructured materials: history, sources, toxicity and regulations. *Beilstein J. Nanotechnol*, *9*, 1050–1074. https://doi.org/10.3762/bjnano.9.98

Jeong, J. H., Mok, H., Oh, Y.-K., & Park, T. G. (2009). siRNA Conjugate Delivery Systems. *Bioconjugate Chemistry*, *20*(1). https://doi.org/10.1021/bc800278e

Jones, C. H., Hill, A., Chen, M., & Pfeifer, B. A. (2015). Contemporary approaches for nonviral gene therapy. *Discovery Medicine*, *19*(107), 447–454.

Karikó, K., Muramatsu, H., Welsh, F. A., Ludwig, J., Kato, H., Akira, S., & Weissman, D. (2008). Incorporation of pseudouridine into mRNA yields superior nonimmunogenic vector with increased translational capacity and biological stability. *Molecular Therapy : The Journal of the American Society of Gene Therapy*, *16*(11), 1833–1840. https://doi.org/10.1038/mt.2008.200

Kedersha, N. L., Heuser, J. E., Chugani, D. C., & Rome, L. H. (1991). Vaults. III. Vault ribonucleoprotein particles open into flower-like structures with octagonal symmetry. *Journal of Cell Biology*, *112*(2), 225–235. https://doi.org/10.1083/jcb.112.2.225

Kedersha, N. L., Miquel, M. C., Bittner, D., & Rome, L. H. (1990). Vaults. II. Ribonucleoprotein structures are highly conserved among higher and lower eukaryotes. *Journal of Cell Biology*, *110*(4), 895–901. https://doi.org/10.1083/jcb.110.4.895

Kedersha, N. L., & Rome, L. H. (1986). Isolation and characterization of a novel ribonucleoprotein particle: Large structures contain a single species of small RNA. *Journal of Cell Biology*, *103*(3), 699–709. https://doi.org/10.1083/jcb.103.3.699

Kickhoefer, V. A., Garcia, Y., Mikyas, Y., Johansson, E., Zhou, J. C., Raval-Fernandes, S., Minoofar, P., Zink, J. I., Dunn, B., Stewart, P. L., & Rome, L. H. (2005). Engineering of vault nanocapsules with enzymatic and fluorescent. *Proceedings of the National Academy of Sciences of the United States of America*, *102*(12), 4348–4352. https://doi.org/10.1073/pnas.0500929102

Kickhoefer, V. A., Han, M., Raval-Fernandes, S., Poderycki, M. J., Moniz, R. J., Vaccari, D., Silvestry, M., Stewart, P. L., Kelly, K. A., & Rome, L. H. (2009). Targeting vault nanoparticles to specific cell surface receptors. *ACS Nano*, *3*(1), 27–36. https://doi.org/10.1021/nn800638x

Kickhoefer, V. A., Liu, Y., Kong, L. B., Snow, B. E., Stewart, P. L., Harrington, L., & Rome, L. H. (2001). The Telomerase/Vault-associated Protein TEP1 Is Required for Vault RNA Stability and Its Association with the Vault Particle. In *The Journal of Cell Biology* (Vol. 152, Issue 1). http://www.jcb.org/cgi/content/full/152/1/157

Kickhoefer, V. A., Rajavel, K. S., Scheffer, G. L., Dalton, W. S., Scheper, R. J., & Rome, L. H. (1998). Vaults are up-regulated in multidrug-resistant cancer cell lines. *Journal of Biological Chemistry*, *273*(15), 8971–8974. https://doi.org/10.1074/jbc.273.15.8971

Kickhoefer, V. A., Siva, A. C., Kedersha, N. L., Inman, E. M., Ruland, C., Streuli, M., & Rome, L. H. (1999). The 193-kD Vault Protein, VPARP, Is a Novel Poly(ADP-ribose) Polymerase. *The Journal of Cell Biology*, *146*(5), 917–928. http://www.jcb.org

Kickhoefer, V. A., Stephen, A. G., Harrington, L., Robinson, M. O., & Rome, L. H. (1999). Vaults and telomerase share a common subunit, TEP1. *Journal of Biological Chemistry*, *274*(46), 32712–32717. https://doi.org/10.1074/jbc.274.46.32712

Kolev, N. G., Rajan, K. S., Tycowski, K. T., Toh, J. Y., Shi, H., Lei, Y., Michaeli, S., & Tschudi, C. (2019). The vault RNA of Trypanosoma brucei plays a role in the production of trans-spliced mRNA. *Journal of Biological Chemistry*, *294*(43), 15559–15574. https://doi.org/10.1074/jbc.RA119.008580

Kong, L. B., Siva, A. C., Kickhoefer, V. A., Rome, L. H., & Stewart, P. L. (2000). RNA location and modeling of a WD40 repeat domain within the vault. *RNA (New York, N.Y.)*, *6*(6), 890–900. https://doi.org/10.1017/S1355838200000157

Kong, L. B., Siva, A. C., Rome, L. H., & Stewart, P. L. (1999). Structure of the vault, a ubiquitous cellular component. *Structure*, *7*(4), 371–379. https://doi.org/10.1016/S0969-2126(99)80050-1

Krayem, O. Ben. (2017). Hydrophobic Engineering of a Bacterial Nanodimensional Capsule Protein, Thesis

Lai, C.-Y., Wiethoff, C. M., Kickhoefer, V. A., Rome, L. H., & Nemerow, G. R. (2009). Vault Nanoparticles Containing an Adenovirus-Derived Membrane Lytic Protein Facilitate Toxin and Gene Transfer. *ACS Nano*, https://doi.org/10.1021/nn8008504

Liu, L., Yang, J., Men, K., He, Z., Luo, M., Qian, Z., Wei, X., & Wei, Y. (2018). Current Status of Nonviral Vectors for Gene Therapy in China. *Human Gene Therapy*, *29*(2), 110–120. https://doi.org/10.1089/hum.2017.226

Liu, Y., Snow, B. E., Hande, M. P., Baerlocher, G., Kickhoefer, V. A., Yeung, D., Wakeham, A., Itie, A., Siderovski, D. P., Lansdorp, P. M., Robinson, M. O., & Harrington, L. (2000). Telomerase-Associated Protein TEP1 Is Not Essential for Telomerase Activity or Telomere Length Maintenance In Vivo. *Molecular and Cellular Biology*, *20*(21), 8178–8184. https://doi.org/10.1128/mcb.20.21.8178-8184.2000

Liu, Y., Snow, B. E., Kickhoefer, V. A., Erdmann, N., Zhou, W., Wakeham, A., Gomez, M., Rome, L. H., & Harrington, L. (2004). Vault Poly(ADP-Ribose) Polymerase Is Associated with Mammalian Telomerase and Is Dispensable for Telomerase Function and Vault Structure In Vivo. *MOLECULAR AND CELLULAR BIOLOGY*, *24*(12), 5314–5323. https://doi.org/10.1128/MCB.24.12.5314-5323.2004

Llauró, A., Guerra, P., Irigoyen, N., Rodríguez, J. F., Verdaguer, N., & De Pablo, P. J. (2014). Mechanical stability and reversible fracture of vault particles. *Biophysical Journal*, *106*(3), 687–695. https://doi.org/10.1016/j.bpj.2013.12.035

Llauró, A., Guerra, P., Kant, R., Bothner, B., Verdaguer, N., & De Pablo, P. J. (2016). Decrease in pH destabilizes individual vault nanocages by weakening the inter-protein lateral interaction. *Scientific Reports*, *6*(October), 1–10. https://doi.org/10.1038/srep34143

Lötsch, D., Steiner, E., Holzmann, K., Spiegl-Kreinecker, S., Pirker, C., Hlavaty, J., Petznek, H., Hegedus, B., Garay, T., Mohr, T., Sommergruber, W., Grusch, M., & Berger, W. (2013). Major vault protein supports glioblastoma survival and migration by upregulating the EGFR/PI3K signalling axis. *Oncotarget*, *4*(11), 1904–1918. https://doi.org/10.18632/oncotarget.1264

Madej, M., Kurowska, N., & Strzalka-Mrozik, B. (2022). Polymeric Nanoparticles—Tools in a Drug Delivery System in Selected Cancer Therapies. *Applied Sciences*, *12*(19). https://doi.org/10.3390/app12199479

Marques, A. C., Costa, P. J., Velho, S., & Amaral, M. H. (2020). Functionalizing nanoparticles with cancer-targeting antibodies: A comparison of strategies. *Journal of Controlled Release*, *320*, 180–200. https://doi.org/https://doi.org/10.1016/j.jconrel.2020.01.035

Matsumoto, N. M., Buchman, G. W., Rome, L. H., & Maynard, H. D. (2015). Dual pH- and temperature-responsive protein nanoparticles. *European Polymer Journal*, *69*, 532–539. https://doi.org/10.1016/j.eurpolymj.2015.01.043

McNamara, K., & Tofail, S. A. M. (2017). Nanoparticles in biomedical applications. *Advances in Physics: X*, *2*(1), 54–88. https://doi.org/10.1080/23746149.2016.1254570

Meyron-Holtz, E. G., Moshe-Belizowski, S., & Cohen, L. A. (2011). A possible role for secreted ferritin in tissue iron distribution. *Journal of Neural Transmission (Vienna, Austria : 1996)*, *118*(3), 337–347. https://doi.org/10.1007/s00702-011-0582-0

Mikyas, Y., Makabi, M., Raval-Fernandes, S., Harrington, L., Kickhoefer, V. A., Rome, L. H., & Stewart, P. L. (2004). Cryoelectron microscopy imaging of recombinant and tissue derived vaults: Localization of the MVP N termini and VPARP. *Journal of Molecular Biology*, *344*(1), 91–105. https://doi.org/10.1016/j.jmb.2004.09.021

Mirón-Barroso, S., Domènech, E. B., & Trigueros, S. (2021). Nanotechnology-Based Strategies to Overcome Current Barriers in Gene Delivery, *International Journal of Molecular Sciences,* https://doi.org/10.3390/ijms22168537

Mitchell, M. J., Billingsley, M. M., Haley, R. M., Wechsler, M. E., Peppas, N. A., & Langer, R. (2021). Engineering precision nanoparticles for drug delivery. *Nature Reviews Drug Discovery*, *20*(2), 101–124. doi.org/10.1038/s41573-020-0090-8

Molino, N. M., & Wang, S.-W. (2014). Caged protein nanoparticles for drug delivery. *Current Opinion in Biotechnology*, *28*, 75–82.

Morales, J. C., Li, L., Fattah, F. J., Dong, Y., Bey, E. A., Patel, M., Gao, J., & Boothman, D. A. (2014). Review of poly (ADP-ribose) polymerase (PARP) mechanisms of action and rationale for targeting in cancer and other diseases. *Critical Reviews in Eukaryotic Gene Expression*, *24*(1), 15–28. https://doi.org/10.1615/CritRevEukaryotGeneExpr.2013006875

Mrazek, J., Toso, D., Ryazantsev, S., Zhang, X., Zhou, Z. H., Fernandez, B. C., Kickhoefer, V. A., & Rome, L. H. (2014). Polyribosomes are molecular 3D

nanoprinters that orchestrate the assembly of vault particles. *ACS Nano*, *8*(11), 11552–11559. https://doi.org/10.1021/nn504778h

Muñoz-Juan, A., Carreño, A., Mendoza, R., & Corchero, J. L. (2019). Latest advances in the development of eukaryotic vaults as targeted drug delivery systems. In *Pharmaceutics* (Vol. 11, Issue 7). MDPI AG. https://doi.org/10.3390/pharmaceutics11070300

Nagasawa, D. T., Yang, J., Romiyo, P., Lagman, C., Chung, L. K., Voth, B. L., Duong, C., Kickhoefer, V. A., Rome, L. H., & Yang, I. (2020). Bioengineered recombinant vault nanoparticles coupled with NY-ESO-1 glioma-associated antigens induce maturation of native dendritic cells. *Journal of Neuro-Oncology*, *148*(1), 1–7. https://doi.org/10.1007/s11060-020-03472-1

Nandy, C., Mrázek, J., Stoiber, H., Grässer, F. A., Hüttenhofer, A., & Polacek, N. (2009). Epstein–Barr virus-induced expression of a novel human vault RNA. *Journal of Molecular Biology*, *388*(4), 776–784.

Nguewa, P. A., Fuertes, M. A., Valladares, B., Alonso, C., & Pérez, J. M. (2005). Poly(ADP-Ribose) Polymerases: Homology, Structural Domains and Functions. Novel Therapeutical Applications. *Progress in Biophysics and Molecular Biology*, *88*(1), 143–172. https://doi.org/10.1016/J.PBIOMOLBIO.2004.01.001

Niazi, S. K. (2023). *RNA Therapeutics: A Healthcare Paradigm Shift*. https://doi.org/10.3390/biomedicines11051275

Nobel. (2023). *Scientific background 2023 Discoveries concerning nucleoside base modifications that enabled the development of effective mRNA vaccines against COVID-19*.

*Noble Nanomedicine: Celebrating Groundbreaking mRNA Vaccine Innovations*. (n.d.). https://doi.org/10.1021/acsnano.3c09781

Pan, X., Veroniaina, H., Su, N., Sha, K., Jiang, F., Wu, Z., & Qi, X. (2021). Applications and developments of gene therapy drug delivery systems for genetic diseases. *Asian Journal of Pharmaceutical Sciences*, *16*(6), 687–703. https://doi.org/10.1016/j.ajps.2021.05.003

Pelaz, B., Alexiou, C., Alvarez-Puebla, R. A., Alves, F., Andrews, A. M., Ashraf, S., Balogh, L. P., Ballerini, L., Bestetti, A., Brendel, C., Bosi, S., Carril, M., Chan, W. C. W., Chen, C., Chen, X., Chen, X., Cheng, Z., Cui, D., Du, J., … Parak, W. J. (2017). Diverse Applications of Nanomedicine. *ACS Nano*, *11*(3), 2313–2381. https://doi.org/10.1021/acsnano.6b06040

Perera, B., Wu, Y., Nguyen, N. T., & Ta, H. T. (2023). Advances in drug delivery to atherosclerosis: Investigating the efficiency of different nanomaterials employed for different type of drugs. *Materials Today Bio*, *22*(April), 100767. https://doi.org/10.1016/j.mtbio.2023.100767

Poderycki, M. J., Kickhoefer, V. A., Kaddis, C. S., Raval-Fernandes, S., Johansson, E., Zink, J. I., Loo, J. A., & Rome, L. H. (2006). The Vault Exterior Shell is a Dynamic Structure that Allows Incorporation of Vault Associated Proteins into its Interior †. *Biochemistry*, *45*(39), 12184–12193. https://doi.org/10.1021/bi0610552

Polack, F. P., Thomas, S. J., Kitchin, N., Absalon, J., Gurtman, A., Lockhart, S., Perez, J. L., Pérez Marc, G., Moreira, E. D., Zerbini, C., Bailey, R., Swanson, K. A., Roychoudhury, S., Koury, K., Li, P., Kalina, W. V, Cooper, D., Frenck, R. W. J., Hammitt, L. L., … Gruber, W. C. (2020). Safety and Efficacy of the BNT162b2 mRNA Covid-19 Vaccine. *The New England Journal of Medicine*, *383*(27), 2603–2615. https://doi.org/10.1056/NEJMoa2034577

Pu, X., Li, J., Qiao, P., Li, M., Wang, H., Zong, L., Yuan, Q., & Duan, S. (2019). Mesoporous Silica Nanoparticles as a Prospective and Promising Approach for Drug Delivery and Biomedical Applications. *Current Cancer Drug Targets*, *19*(4), 285–295. https://doi.org/10.2174/1568009619666181206114904

Querol-Audí, J., Casañas, A., Usón, I., Luque, D., Castón, J. R., Fita, I., & Verdaguer, N. (2009). The mechanism of vault opening from the high resolution structure of the N-terminal repeats of MVP. *The EMBO Journal*, *28*(21), 3450–3457. https://doi.org/10.1038/emboj.2009.274

Redmond, K. A., Nguyen, T.-S., & Ryan, R. O. (2007). All-trans-retinoic acid nanodisks. *International Journal of Pharmaceutics*, *339*(1–2), 246–250. https://doi.org/10.1016/j.ijpharm.2007.02.033

Roberts, T. C., Langer, R., & Wood, M. J. A. (2020). Advances in oligonucleotide drug delivery. In *Nature Reviews Drug Discovery* (Vol. 19, Issue 10, pp. 673–694). Nature Research. https://doi.org/10.1038/s41573-020-0075-7

Rome, L. H., & Kickhoefer, V. A. (2013). Development of the Vault Particle as a Platform Technology. In *ACS Nano* (Vol. 7, Issue 2, pp. 889–902). American Chemical Society. https://doi.org/10.1021/nn3052082

Ryan, R. O. (2008). Nanodisks: hydrophobic drug delivery vehicles. *Expert Opinion on Drug Delivery*, *5*(3), 343–351. https://doi.org/10.1517/17425247.5.3.343

Scheffer, G., Wijngaard, P., Flens, M., Izquierdo, M. A., Slovak, M. L., Pinedo, H. M., Meijer, C. J. L. M., Clevers, H. C., & Scheper, R. J. (1995). The drug resistance-related LRP is the human major vault protein. *Nature Medicine*.

Slesina, M., Inman, E. M., Moore, A. E., Goldhaber, J. I., Rome, L. H., & Volknandt, W. (2006). Movement of vault particles visualized by GFP-tagged major vault protein. *Cell and Tissue Research*, *324*(3), 403–410. https://doi.org/10.1007/s00441-006-0158-8

Song, W., Das, M., & Chen, X. (2020). Nanotherapeutics for Immuno-Oncology: A Crossroad for New Paradigms. *Trends in Cancer*, *6*(4), 288–298. https://doi.org/10.1016/j.trecan.2020.01.011

Stadler, P. F., Chen, J. J. L., Hackermüller, J., Hoffmann, S., Horn, F., Khaitovich, P., Kretzschmar, A. K., Mosig, A., Prohaska, S. J., Qi, X., Schutt, K., & Ullmann, K. (2009). Evolution of vault RNAs. *Molecular Biology and Evolution*, *26*(9), 1975–1991. https://doi.org/10.1093/molbev/msp112

Steiner, E., Holzmann, K., Elbling, L., Micksche, M., & Berger, W. (2006). Cellular Functions of Vaults and their Involvement in Multidrug Resistance. *Current Drug Targets*, *7*(8), 923–934. https://doi.org/10.2174/138945006778019345

Stephen, A. G., Raval-Fernandes, S., Huynh, T., Torres, M., Kickhoefer, V. A., & Rome, L. H. (2001). Assembly of Vault-like Particles in Insect Cells Expressing only the Major Vault Protein. *Journal of Biological Chemistry*, *276*(26), 23217–23220. https://doi.org/10.1074/jbc.C100226200

Suprenant, K. A. (2002). Vault ribonucleoprotein particles: Sarcophagi, gondolas, or safety deposit boxes? *Biochemistry*, *41*(49), 14447–14454. https://doi.org/10.1021/bi026747e

Tanaka, H. (2009). The structure of rat liver vault at 3.5 angstrom resolution (Science (384)). *Science*, *323*(5919), 1290. https://doi.org/10.1126/science.323.5919.1290

Tanaka, H., & Tsukihara, T. (2012). Structural studies of large nucleoprotein particles, vaults. In *Proceedings of the Japan Academy Series B: Physical and Biological Sciences* (Vol. 88, Issue 8, pp. 416–433). https://doi.org/10.2183/pjab.88.416

Tenchov, R., Bird, R., Curtze, A. E., & Zhou, Q. (2021). Lipid Nanoparticles─From Liposomes to mRNA Vaccine Delivery, a Landscape of Research Diversity and Advancement. *ACS Nano*, *15*(11), 16982–17015. https://doi.org/10.1021/acsnano.1c04996

van Zon, A., Mossink, M. H., Schoester, M., Houtsmuller, A. B., Scheffer, G. L., Scheper, R. J., Sonneveld, P., & Wiemer, E. A. C. (2003). The formation of vault-tubes: A dynamic interaction between vaults and vault PARP. *Journal of Cell Science*, *116*(21), 4391–4400. https://doi.org/10.1242/jcs.00749

Voltà-Durán, E., Parladé, E., Serna, N., Villaverde, A., Vazquez, E., & Unzueta, U. (2023). Endosomal escape for cell-targeted proteins. Going out after going in. *Biotechnology Advances*, *63*(January). https://doi.org/10.1016/j.biotechadv.2023.108103

Wang, H., Jiang, Y., Peng, H., Chen, Y., Zhu, P., & Huang, Y. (2015). Recent progress in microRNA delivery for cancer therapy by non-viral synthetic vectors. *Advanced Drug Delivery Reviews*, *81*, 142–160. https://doi.org/10.1016/j.addr.2014.10.031

Wang, J. W., & Roden, R. B. S. (2013). Virus-like particles for the prevention of human papillomavirus-associated malignancies. *Expert Review of Vaccines*, *12*(2), 129–141. https://doi.org/10.1586/erv.12.151

Wang, M., Kickhoefer, V. A., Rome, L. H., Foellmer, O. K., & Mahendra, S. (2018). Synthesis and assembly of human vault particles in yeast. *Biotechnology and Bioengineering*, *115*(12), 2941–2950. https://doi.org/10.1002/bit.26825

Wiethoff, C. M., Wodrich, H., Gerace, L., & Nemerow, G. R. (2005). Adenovirus protein VI mediates membrane disruption following capsid disassembly. *Journal of Virology*, *79*(4), 1992–2000. https://doi.org/10.1128/JVI.79.4.1992-2000.2005

Wittrup, A., & Lieberman, J. (2015). Knocking down disease: a progress report on siRNA therapeutics. *Nature Reviews. Genetics*, *16*(9), 543–552. https://doi.org/10.1038/nrg3978

Xu, S., Yang, K., Li, R., & Zhang, L. (2020). mRNA Vaccine Era-Mechanisms, Drug Platform and Clinical Prospection. *International Journal of Molecular Sciences*, *21*(18). https://doi.org/10.3390/ijms21186582

Yahya, E. B., & Alqadhi, A. M. (2021). Recent trends in cancer therapy: A review on the current state of gene delivery. *Life Sciences*, *269*(January), 119087. https://doi.org/10.1016/j.lfs.2021.119087

Yang, J., Srinivasan, A., Sun, Y., Mrazek, J., Shu, Z., Kickhoefer, V. A., & Rome, L. H. (2013). Vault nanoparticles engineered with the protein transduction domain, TAT48, enhances cellular uptake. *Integrative Biology : Quantitative Biosciences from Nano to Macro*, *5*(1), 151–158. https://doi.org/10.1039/c2ib20119d

Yang, Z., & Zhang, Z. (2018). Engineering strategies for enhanced production of protein and bio-products in Pichia pastoris: A review. In *Biotechnology Advances* (Vol. 36, Issue 1, pp. 182–195). Elsevier Inc. https://doi.org/10.1016/j.biotechadv.2017.11.002

Zhang, W., Wei, J., & Hui, A.-M. (2022). *The Delivery of mRNA Vaccines for Therapeutics*. https://doi.org/10.3390/life12081254

# Chapter 1

# Addressing critical issues related to storage and stability of the vault nanoparticle expressed and purified from *Komagataella phaffi*

The results have been published in *International Journal of Molecular Sciences*, as:

*Addressing critical issues related to storage and stability of the vault nanoparticle expressed and purified from Komagataella phaffi.*

Giulia Tomaino[1,2,†], Camilla Pantaleoni[1,†], Diletta Ami[1], Filomena Pellecchia[1‡], Annie Dutriaux[2], Linda Barbieri[1], Stefania Garbujo[1], Antonino Natalello[1], Paolo Tortora[1,*], Gianni Frascotti[1,*]

[1] Department of Biotechnology and Biosciences, University of Milano-Bicocca, I-20126 Milano, Italy

[2] Université Paris Cité, CNRS, Institut Jacques Monod, F-75013 Paris, France

* Correspondence: PT, paolo.tortora@unimib.it; GF, gianni.frascotti@unimib.it

† These authors contributed equally to this work

Int. J. Mol. Sci. 2023, 24, 4214. https://doi.org/10.3390/ijms24044214

## Abstract

The vault nanoparticle is a eukaryotic assembly consisting of 78 copies of the 99-kDa major vault protein. They generate two cup-shaped symmetrical halves, which *in vivo* enclose protein and RNA molecules. Overall, this assembly is mainly involved in pro-survival and cytoprotective functions. It also holds a remarkable biotechnological potential for drug/gene delivery, thanks to its huge internal cavity and the absence of toxicity/immunogenicity. The available purification protocols are complex, partly because they use higher eukaryotes as expression systems. Here, we report a simplified procedure that combines human vault expression in the yeast *Komagataella phaffii*, as described in a recent report, and a purification process we have developed. This consists of RNase pretreatment followed by size-exclusion chromatography, which is far simpler than any other reported to date. Protein identity and purity was confirmed by SDS-PAGE, Western blot and transmission electron microscopy. We also found that the protein displayed a significant propensity to aggregate. We thus investigated this phenomenon and the related structural changes by Fourier transform spectroscopy and dynamic light scattering, which led us to spot out the most suitable storage conditions. In particular, the addition of either trehalose or Tween-20 ensured the best preservation of the protein in native, soluble form.

**Keywords:** vault nanoparticle purification; major vault protein; *Komagataella phaffii* expression system; transmission electron microscopy; Fourier transform infrared spectroscopy

# 1 Introduction

Vaults are natural ribonucleoprotein nanoparticles found in several eukaryotes (Kedersha and Rome, 1986; Frascotti *et al.*, 2021). In their molecular assembly, the 99-kDa major vault protein (MVP) is present in 78 copies and generates a barrel-like, natural "nanocapsule" consisting of two symmetrical halves (Kedersha *et al.*, 1991), which encloses other molecular components, i.e., the 193 kDa vault poly(ADP-ribose) polymerase, the 290 kDa telomerase-associated protein-1 (TEP1) and one or more small untranslated RNAs (Kickhoefer *et al.*, 1993, 1998; Kickhoefer, Siva, *et al.*, 1999; Kickhoefer, Stephen, *et al.*, 1999; Van Zon *et al.*, 2001). Overall, the molecular mass of vault particles amounts to about 13 MDa, their size is 72.5 × 41 × 41 nm, with an internal cavity volume of $5 \times 10^4$ $nm^3$. A well-assembled vault structure can be also produced by expressing the sole MVP, as originally shown in insect cells (Stephen *et al.*, 2001; Mrazek *et al.*, 2014). Although the physiological roles of this nanocomplex are only partially understood, numerous reports highlight, nevertheless, its involvement in several pro-survival and cytoprotective actions (Berger *et al.*, 2009).

Thanks to the aforementioned properties, this macromolecular assembly has attracted a huge interest as a tool for drug/gene/vaccine delivery often targeted to cancer cell lines (Anderson *et al.*, 2007; Ng *et al.*, 2008; Rome and Kickhoefer, 2013). Actually, not only can it accommodate large amounts of cargo molecules, including toxic and hydrophobic ones (Buehler *et al.*, 2011), but can also be targeted to specific cell surface receptors, provided it is bound to suitable peptides or antibodies via chemical (Benner *et al.*, 2017) or genetical approaches. In particular, a vault variant was genetically engineered so as to carry a protein A fragment at the C-terminus. It could bind IgGs with high affinity, thus representing a general tool to target the nanoparticle to specific surface antigens (Kickhoefer *et al.*, 2009). Likewise, an MVP variant was produced in fusion with the peptide pVI at the C-terminus, which allows endosomal escape and improves penetration into target cells (Wiethoff *et al.*, 2005).

Nevertheless, the standard production protocol of vault nanoparticles is still burdensome and labor intensive due to the complexity of both the aforementioned baculovirus–insect cell expression system and the

purification procedure so far available, which includes different ultracentrifugation and gradient centrifugation steps (Stephen *et al.*, 2001). Recently, a more simplified procedure was developed by expressing a $His_6$-tagged vault variant in human embryonic kidney cells, which made it possible to affinity-purify the nanocomplex (Martín *et al.*, 2022). The same research group subsequently reported an *Escherichia coli*-based protocol, which unquestionably represents a substantial improvement in terms of process simplification (Fernández *et al.*, 2022). Yet, it might suffer from obvious restraints related to the production of a non-natural, $His_6$-tagged variant, mainly in view of its employment as a nanovector to be administered to cells or whole organisms.

Thus, the most manageable expression system available to date for the production of authentic vault is based on the use of the methylotrophic yeast *Komagataella phaffii* (formerly *Pichia pastoris*) due to the ease of yeast cultivation compared with insect and mammalian cells (Wang *et al.*, 2018). Furthermore, we recently developed a straightforward purification procedure of the vault nanoparticle expressed in the baculovirus–insect cell system, which only consisted of a dialysis and a size-exclusion chromatography (SEC) (Galbiati *et al.*, 2018). Here, we present a novel procedure, whereby human vault expressed in *K. phaffii* was purified via a simple, SEC-based protocol, which also includes an RNase pretreatment of cell-free extracts obtained as supernatants from homogenate centrifugation. Pure preparations of authentic vault nanoparticles were thus obtained, as shown by SDS-PAGE, Western blotting and transmission electron microscopy (TEM). The ethidium bromide staining of agarose gel also demonstrated virtually complete removal of contaminating RNA.

## 2 Results

### Production Procedure of Pure Vault Particle from *K. phaffii*

One major requirement in experimental designs that make use of the vault nanoparticle for either biological investigations or biotechnological applications is the availability of a manageable procedure to produce pure preparations. We formerly developed a protocol that, starting from transfected insect cell extracts (Stephen *et al.*, 2001), led to the isolation of pure human protein through a purification procedure only consisting of a dialysis and a subsequent Sepharose CL-6B SEC (Galbiati *et al.*, 2018). Here, we present a novel protocol that takes advantage of the formerly developed yeast-based expression system (Wang *et al.*, 2018). This is far simpler than that based on insect cells and, no less important, should also allow a much easier scale up. We harvested the cells in the late exponential phase, when the culture attained its maximum biomass density and disrupted them, as described in Material and Methods (Section 4.4). In preliminary experiments, after cell disruption, we centrifuged the resulting homogenate at 20,000 × g and directly subjected the supernatant (henceforth referred to as cell extract) to Sepharose CL-6B SEC, thus obtaining apparently pure preparations, as assessed in SDS-PAGE. However, we became aware of a major RNA contamination, quite likely ribosomal, as revealed by DNase-resistant ethidium bromide staining in agarose gel electrophoreses of the eluted fractions. To remove this contaminant, we adopted, with minor modifications, a previously published procedure (Stephen *et al.*, 2001), whereby we incubated the cell extract with RNases A and T1 (Section 4.4).

Following this treatment, agarose gel electrophoresis actually revealed an almost complete disappearance of a broad, ethidium bromide-stained band and an equally migrating Coomassie-stained one (Figure 1A), which quite plausibly represent ribosomal contaminants. In contrast, the vault protein, which was detected in the same lanes as a slower-migrating Coomassie-stained band and identified by Western blotting, was completely unaffected by the treatment. The RNase-treated extract was then subjected to SEC and the eluted fractions again analyzed by agarose gel electrophoresis

and subsequent staining according the same protocol adopted for the cell extract. This revealed virtually complete absence of RNA contaminants in the void-volume fraction, whereas residual RNA components were still visible in the second-eluted fraction (Figure 1B)

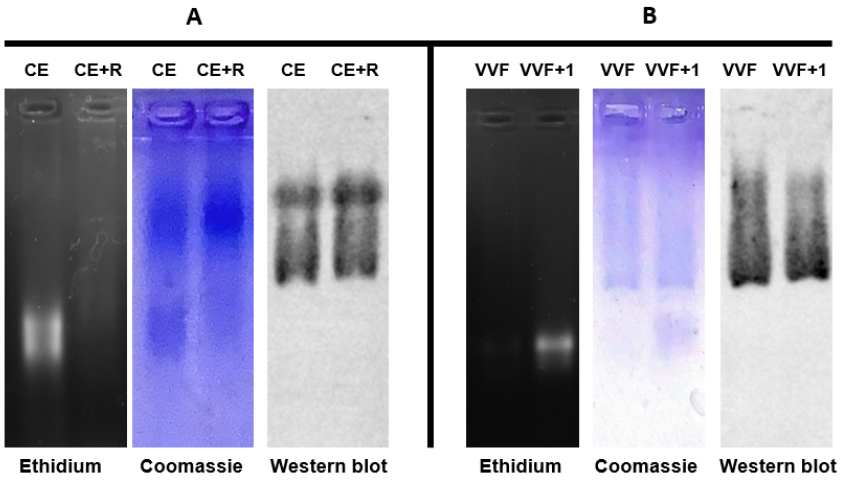


***Figure 1.*** *Electrophoretic characterization of a cell-free extract from the vault-expressing K. phaffii strain (A) and the purified vault (B). Agarose gel electrophoresis (0.7% gel) was performed on the extract before (CE) and after (CE+R) RNase treatment. Then, the gel was subjected to ethidium bromide and Coomassie staining, and Western blotting. Void-volume fraction (VVF) and the following one (VVF+1) from SEC of the RNase-treated extract was subjected to the same analytical procedures. Other details are reported in Materials and Methods (par. 4.6).*

Finally, we checked by SDS-PAGE the SEC-eluted fractions for possible protein contaminations (Figure 2). Coomassie staining revealed a major band both in the void-volume fraction and in the following one, positively identified as MVP in Western blotting, and negligible amounts of protein contaminants. However, the latter fraction had to be discarded, due to RNA contamination, as detected in agarose gel electrophoresis (Figure 1B). Based on these observations, in our purification protocol we routinely identified and discarded RNA-containing fractions and recovered pure, RNA-free vault in the void-volume fraction, typically yielding 1.5 mg of protein per g of yeast wet weight.

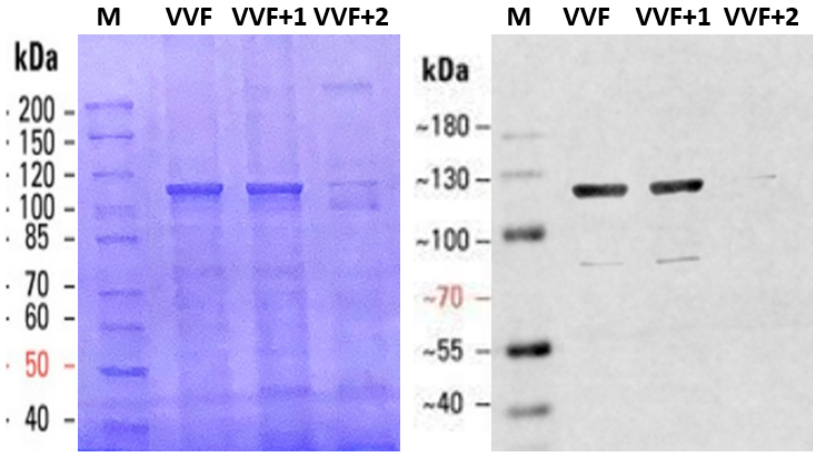


***Figure 2.*** *SDS-PAGE (8% gel) of vault eluted from the SEC column. The void-volume fraction (VVF) and the following ones (VVF+1 and VVF+2) were subjected to electrophoresis, Coomassie stained (left panel) and Western blotted (right panel). M: standard proteins with the respective molecular weights (kDa). Other details are reported in Materials and Methods (par. 4.6).*

**Transmission electron microscopy reveals well-assembled vault NPs.**

TEM of specimens from the void-volume fraction only displayed nanoparticles whose morphology and size were consistent with the one expected, thus confirming both the homogeneity of the preparation and the occurrence of correctly assembled MVP, yielding authentic vault nanoparticle (Figure 3A1). The second-eluted fraction revealed instead several particles unrelated to vault in size and morphology (Figure 3A2). In keeping with our electrophoretic analyses (Figure 1B), we assume that they are aggregated ribosomal proteins released by RNase treatment. Indeed, it is well documented that such proteins undergo aggregation, once the partner RNA components are degraded (Aarum *et al.*, 2020). The two fractions were also subjected to DLS, the relevant spectra being shown in Figures 3B1 and B2 as number-based particle size distribution. Actually, it is suggested that, when comparing size assessments obtained by electron microscopy with DLS measurements, the number distribution is more suitable for comparisons (Nobbmann and Morfesis, 2009). At the same rate, it is generally agreed that this parameter will provide reliable estimates provided the relevant autocorrelation profile displays a single exponential decay, diagnostic of a monodisperse preparation. As shown in Figure S1, this is the case for the

samples analyzed. The analysis detected a distinctly smaller hydrodynamic radius in the second-eluted fraction as compared to the first one, in keeping with the TEM images. Overall, these observations highlight the substantial role of RNase treatment in obtaining pure vault preparations.

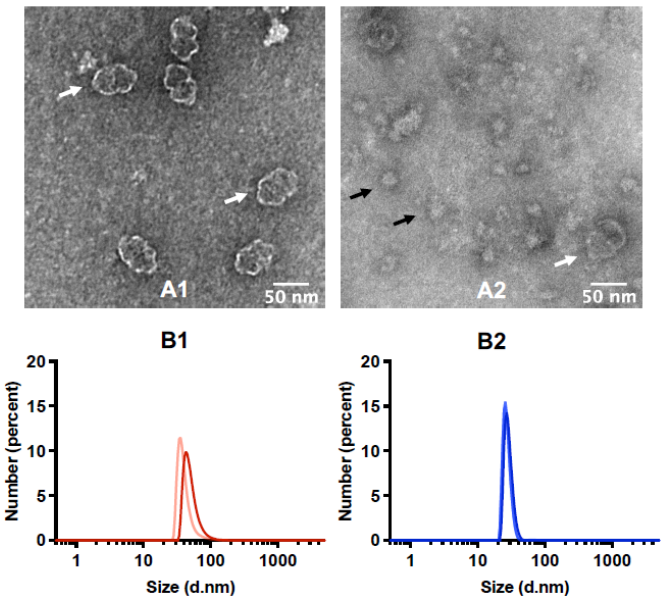


***Figure 3.*** *TEM images of vault nanoparticles stained by uranyl acetate, as detected in the void-volume fraction (A1) and in the following one (A2). The fractions were analyzed after centrifuging at 20,000 x g and discarding the pellet. Vault particles are indicated by white arrows; contaminating matter, quite likely ribosomal components, by black arrows. DLS of the void-volume fraction and the following one are shown in B1 and B2, respectively. Results are presented as number-weighted particle size distributions. B1: size 51.3 ± 15.6 (mean ± std. dev.); polydispersity index (PDI): 0.203. B2: size 28.9 ± 4.0; PDI 0.263. Result quality: good. In each panel, two replicates of the measurement are shown. The relevant intensity and autocorrelation plots are presented in Figure S1.*

## Spotting out by FTIR and DLS the optimal conditions for vault storage and stability

When freshly eluted from the SEC column, vault preparations did not display any detectable protein loss in the supernatants upon centrifugation at 20,000 x g for 20 min, although tiny amounts of precipitated protein could be anyway revealed in FTIR analysis, as discussed below, thanks to the remarkable sensitivity of this analytical technology. In contrast, when either

incubated at +4 °C or frozen and thawed under different conditions, the same preparations displayed a significant propensity to generate precipitates, suggestive of ongoing aggregation. We thus set out to explore vault's stability in solution under different storage conditions, with the aim of both spotting out those compatible with the best recovery of soluble, native protein and providing insight into the structural changes responsible for its aggregation (Table 1). When incubated at +4 °C, an about two-thirds protein loss in the supernatant was observed after only one week. Thus, this condition was proven to be unsuitable for long-term storage.

Upon incubation under frozen conditions, a better preservation of soluble protein was generally achieved. In particular, frozen vault was subjected to short- and long-term storage (1 day and 7 weeks, respectively), under different conditions, including the addition of either trehalose or the non-ionic surfactant Tween-20. In the presence of trehalose, we also assessed the recovery of soluble protein after sample lyophilization and reconstitution (Table 1). Actually, this sugar has been employed as an additive in vault lyophilization (Kickhoefer *et al.*, 2009). Likewise, the capability of Tween-20 to prevent protein aggregation and improve thermodynamic stability is well documented (Kerwin *et al.*, 1998; Chou *et al.*, 2005).

The different freezing-thawing treatments also resulted in a significant decrease in soluble protein, in the range 35-55%, as assessed after a one-day storage. A further, smaller decline in soluble protein was detected in the frozen samples at the longest storage time, i.e., 7 weeks, the best recoveries being obtained in the presence of Tween-20. These observations make it apparent that protein loss mainly takes place during the freezing process, rather than during the subsequent storage.

***Table 1.*** *Residual protein content in supernatants of vault preparations stored under different conditions.*

| Storage conditions[1] | 1 day | 1 week | 7 weeks |
|---|---|---|---|
| + 4 °C | 51 ± 4 | 35 ± 2 | |
| - 20 °C | 44 ± 2 | | 31 ± 7 |
| - 80 °C | 52 ± 5 | | 43 ± 6 |
| - 80 °C in 10 mg/mL trehalose | 56 ± 6 | | 50 ± 3 |
| - 80 °C in 10 mg/mL trehalose, lyophilized and reconstituted | 50 ± 8 | | 45 ± 5 |
| - 80 °C in 0.05% Tween 20 | 64 ± 4 | | 59 ± 5 |

[1] *After storage for the indicated times, frozen samples were thawed and centrifuged at 20,000 x g for 20 min. Then, residual protein in the supernatants was determined using the bicinchoninic acid (BCA) assay and expressed as percentage relative to zero time. Figures are mean values ± standard deviation (n ≥ 3).*

To further characterize structurally the vault nanoparticle after incubation under the above-described conditions, as well as to provide insight into possible structural changes related to protein precipitation, both supernatants and pellets were investigated by FTIR in attenuated total reflection (ATR) mode (Figure 4). In particular, we analyzed the Amide I band in the second derivatives of the protein IR absorption spectra. This band is due to the C=O stretching vibration of the peptide bond and is sensitive to the protein secondary structures as well as to the formation of intermolecular β-sheets in protein aggregates (Ami and Natalello, 2022; Ami, Mereghetti and Natalello, 2022).

The second derivative spectrum of the freshly purified vault (Figure 4A) displayed a main peak at ~1655 cm-1 that can be assigned to α-helical and random coil structures. Less intense peaks were observed at ~1638 cm-1, due to the native β-sheets, and at ~1688 cm-1. This latter broad band can be assigned to -sheet and β-turn structures. The relative intensities of the ~1655 cm-1 and ~1638 cm-1 Amide I components are well in agreement with the structural data currently available for the native protein (Ding *et al.*, 2018), indicating an overall higher content of α-helix and random coil structures (~51%) as compared with β-sheets (~28%). The spectrum of the supernatant was almost superimposable to that of the total sample (Figure S2), whereas the pellet spectrum displayed a slightly reduced intensity of the Amide I

components assigned to the native protein structures and a new component at ~1629 cm-1, which appears as a very low intensity shoulder and can be assigned to the formation of intermolecular β-sheet structures typical of protein aggregates. Interestingly, the strong intensity of the peaks associated with the native structures in the pellet suggests that, rather unusually, a substantial fraction of native conformation is present in the aggregated protein.

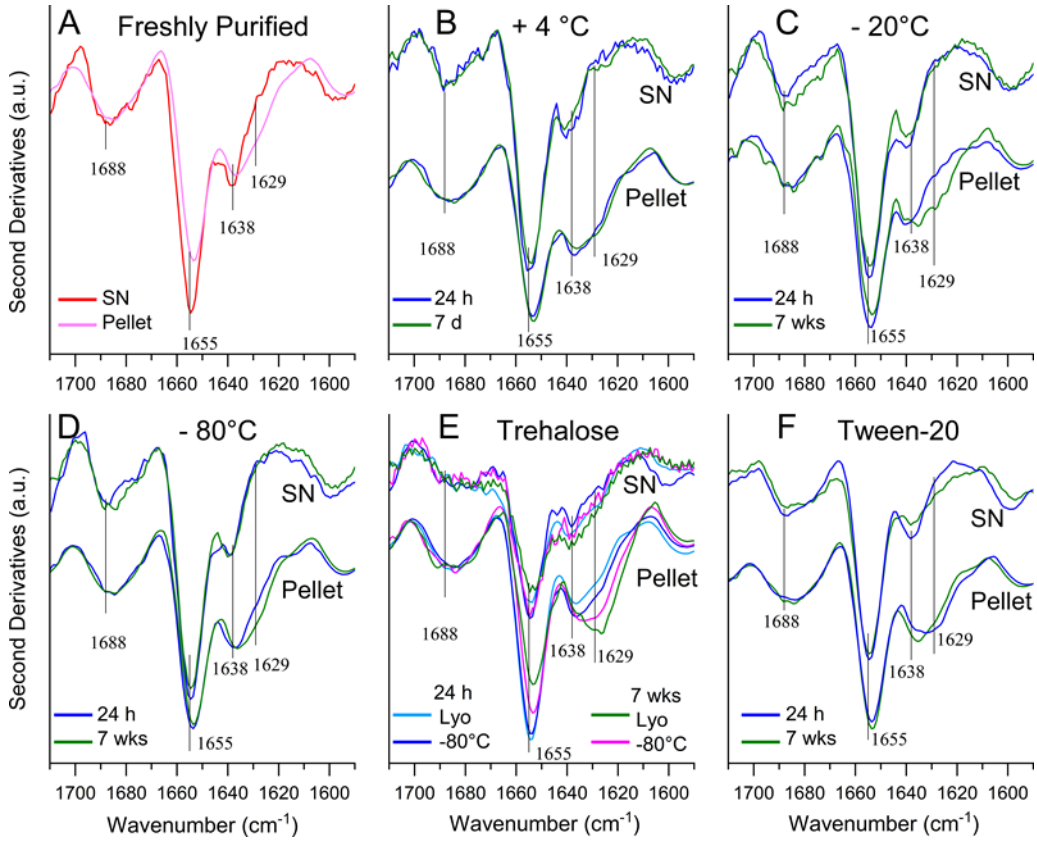


***Figure 4.*** *FTIR analysis of vault protein preparations. Samples were stored for the indicated times and under the indicated conditions, as shown in the individual panels. Then, second derivatives of the IR absorption spectra of supernatants N) and pellets after centrifugation at 20,000 x g were analyzed. A) sample freshly eluted from the SEC column; B) sample incubated at 4 °C; C-F) samples frozen and thawed, except for panel E), wherein the sample was frozen at -80 °C in 10 mg/mL trehalose and either thawed or lyophilized and reconstituted yo) before the analysis; F) sample frozen at -80 °C in 0.05% Tween-20. The main peak positions are reported. Spectra of total samples (analyzed prior to centrifugation) are shown in Figure S2.*

The ATR-FTIR analysis was also performed on vault preparations subjected to storage either at 4 °C or after freezing under different conditions. The spectra of the supernatants were essentially indistinguishable from one another as well as from that of fresh protein and were representative of a protein in the native state (Figure 4B-F).

However, for sake of completeness it should be also noted that the slight spectral differences observed in the supernatant samples in the presence of trehalose as compared with the others (Figure 4E), may be well accounted for by an instrumental constraint. Specifically, they essentially result from the so-called z-dilution, namely protein dilution along the z-axis due to the presence of the sugar, with resulting reduced protein accumulation in the immediate vicinity of the ATR interface (Goormaghtigh, Raussens and Ruysschaert, 1999). Likewise, the supernatant spectrum collected in the presence of Tween-20 displayed a slightly reduced ratio of β-sheet to $\alpha$-helix peak intensities (Figure 4F). Although we have no obvious interpretation for this result, the spectrum collected confirms anyway that under these conditions the protein also retains a native conformation. We speculate that this result may reflect the dynamic structure of the protein, as documented by its capability of adopting at least two different conformations (Ding *et al.*, 2018). Nevertheless, the protein preparations incubated in the presence of Tween-20 as well as of trehalose were also subjected to TEM analysis after spinning down at 20,000 x g possible aggregates, which made it possible to detect the typical vault morphology under both conditions (Figure S3).

Furthermore, as already observed in the case of fresh protein, we found that under all employed storage conditions the pelleted protein also retained a large fraction of native conformation, as documented by the relevant spectra that display the Amide I components observed in the respective supernatants (Figure 4B-F). Concurrently, in such samples the ~1629 $cm^{-1}$ component, which is representative of intermolecular β-sheets, only appeared as a shoulder and not as a well-resolved peak, albeit more intense than that detected in the pellet of the fresh protein (Figure 4A). These findings clearly show that a native-like structure must be largely prevailing in the pellet, wherein the vault molecules must otherwise interact with one another in some way to give rise to insoluble matter. Thus, intermolecular β-sheets,

which are a typical hallmark of denaturation-induced aggregation both *in vitro* and *in vivo* (Chiti and Dobson, 2017), are scarcely represented in the pellets. Currently, we do not have any obvious interpretation for this phenomenon. However, we deem it worth mentioning that even TEM images of soluble preparations are frequently suggestive of vaults' propensity to generate clusters with no ordered aggregation pattern, wherein the individual nanoparticles retain otherwise their typical conformation (Galbiati *et al.*, 2018). On the other hand, the dynamic nature of the vault nanoparticle is well documented, as above mentioned, and also results in several modes of interaction, quite likely of physiological relevance such as, for instance, *in vivo* formation of intracellular tube-like structures, whereby MVP molecules interact with one another via their coiled-coil domains (van Zon *et al.*, 2003), MVP subunit exchange (Yang *et al.*, 2010), and vault opening (Guerra *et al.*, 2022).

Finally, we also subjected our preparations to DLS analysis in order to assess their homogeneity, focusing on the frozen, long-term incubated samples, namely the ones which are more likely to be employed for any predictable application. In line with the criteria outlined when discussing Figure 3, in Figure 5 the number-based particle size distribution is presented, and the respective correlograms and intensity plots are shown in Figure S4. The correlograms generally fitted with a single exponential decay, with the exception of the sample stored at -20 °C, the only one displaying a somewhat larger size and some degree of polydispersity, as documented by the relevant PDI. Except for this condition, which was therefore judged unsatisfactory for long-term storage, we determined nanoparticle dimensions reasonably in agreement with those determined in previous reports (Matsumoto *et al.*, 2015; Martín *et al.*, 2022).

Unfortunately, inconsistent DLS measurement were obtained when analyzing vault samples incubated in the presence of 0.05% Tween-20, which prevented us from collecting reliable data under these conditions. This effect is plausibly justified by the well-known propensity of non-ionic detergents to generate a heterogeneous micelle population, wherein different numbers of protein molecules may be recruited into different micelles (Aivaliotis *et al.*, 2003). However, as already mentioned above, TEM analysis of the vault

incubated in the presence of the detergent did not reveal any gross morphological alteration (Figure S3).

Overall, our investigations highlight a critical issue related to vault purification and handling, i.e., its propensity to aggregate, but also provide the most suitable approaches to cope with. The implications of these results are analyzed in the Section Discussion.

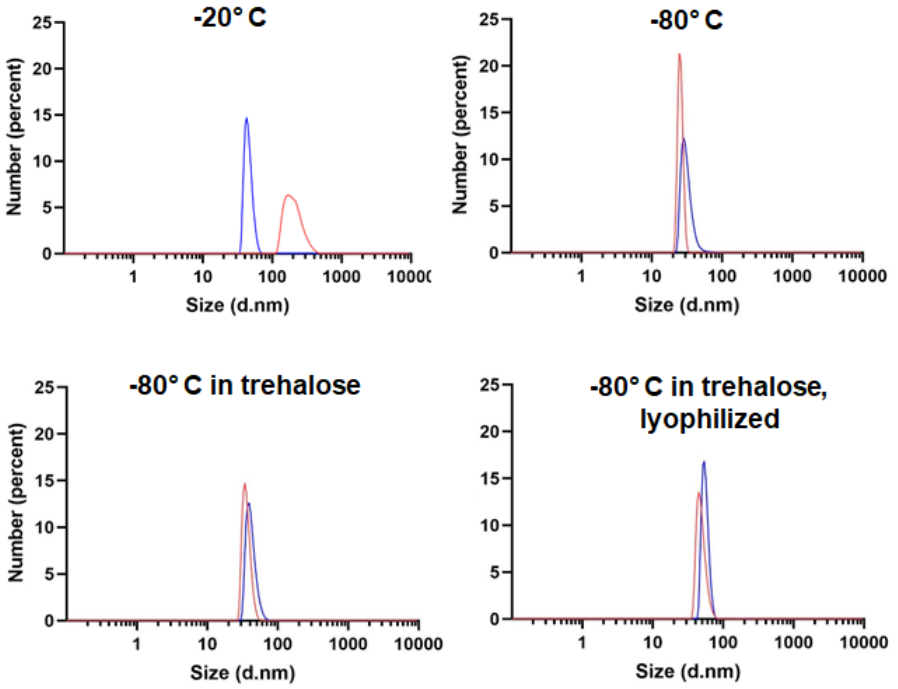


***Figure 5.*** *DLS of the 20,000 x g supernatants of vault samples incubated for 7 days and otherwise as indicated in the respective panels. Results are presented as number-weighted particle size distribution. -20 °C: size 204.8 ± 17.9 (mean ± std. dev.) nm, PDI: 0.332; -80 °C: size 94.00 ± 9.09 nm, PDI 0.007; - 80 °C plus trehalose: size 120.30 ± 11.89, PDI 0.044; - 80 °C plus trehalose, lyophilized and reconstituted: size 148.20 ± 19.24, PDI 0.145. Result quality: good. In each panel, two replicates of the measurement are shown. The relevant intensity and autocorrelation plots are presented in Figure S4.*

## 3 Discussion

In the last decades, the vault nanoparticle has attracted a considerable interest for both its multifaceted and as yet only partially elucidated biological roles, and its potential as a nanovector for drug/gene delivery (Muñoz-Juan *et al.*, 2019; Frascotti *et al.*, 2021). Nevertheless, most protocols available for vault production have still to cope with major constraints regarding both the expression systems and the purification procedures, which are lengthy and multistep. In particular, the baculovirus-insect cell system is complex and time-consuming (Stephen *et al.*, 2001), whereas the human-cell based procedure is definitely simpler (Martín *et al.*, 2022), but both of them hardly can lend themselves to a significant scale up. Conversely, the recently developed *E. coli*-based protocol actually allows a substantial simplification of the process but only enables the production of a vault variant consisting of $His_6$-tagged MVP subunits (Fernández *et al.*, 2022). The present contribution reports a novel protocol that overcomes these limitations by combining the use of an engineered *K. phaffi* strain as the expression system of authentic vault (Wang *et al.*, 2018) with a purification procedure that represents a modification of a previously reported one (Galbiati *et al.*, 2018), now essentially consisting of RNase treatment of yeast cell-free extracts and a subsequent SEC. This avoids the need for multiple cycles of ultracentrifugation (Stephen *et al.*, 2001), as well as for a dialysis step (Galbiati *et al.*, 2018). In this way, we were able to produce about 1.5 mg of pure vault per g of yeast wet weight, which corresponds to about 50-60 mg/L culture. This yield is significantly better than that previously reported using the same host organism (Wang *et al.*, 2018). Other published protocols based on insect (Stephen *et al.*, 2001) or human cells (Martín *et al.*, 2022) are not likely to perform better, given the inherent limitations related to the production of the starting cellular material, regardless of the complexity of the purification procedure.

It should be also pointed out that the vault nanoparticle could be expressed constitutively thanks to its lack of toxicity in yeast cells. This made it possible to grow cells in the absence of inducers, which are generally very expensive, making a process hardly scalable.

Based on different analytical methods we demonstrated that our vault preparations are essentially pure and, no less important, correctly folded so as to display the expected morphology, as substantiated by TEM images and DLS measurements. Thus, they are apparently of suitable quality for virtually all of the potential applications they may be destined for.

However, a critical issue became apparent during the present experimentation, namely a significant propensity of vault preparations to generate insoluble aggregates. They appeared on incubation at 4 °C, as well as after freezing-thawing under different conditions. Also, under all assayed conditions, they displayed a typical FTIR peak at ~1629 $cm^{-1}$, which is representative of intermolecular β-sheets. This is a signature of protein aggregation, a process envisaging a progressive recruitment of the involved proteins via the initial formation of small oligomers, which subsequently evolve into large aggregates (Chiti and Dobson, 2017). This is paralleled by a time-dependent increase in intermolecular β-sheets and accordingly of the relevant peak at ~1629 $cm^{-1}$. In contrast, we surprisingly observed that the pellets collected after a one-day and a one-week incubation at 4 °C displayed virtually indistinguishable spectra (Figure 4B), which does not fit with a pattern entailing progressive structural changes, as expected during protein aggregation. Rather, it points to a two-state conversion from a soluble to an aggregated form, the latter being richer in intermolecular β-sheets. This phenomenon deserves further investigations in order to provide insight into the mode of vault association and its possible physiological relevance.

Besides the aforementioned investigations, which led to a partial characterization of structural features distinctive of the aggregates, we set out to select the most suitable storage conditions to prevent their appearance, with the obvious intent of ensure the best recovery of soluble, native vault during long-term storage. As shown in Table 1, it is apparent that, on the one hand most (but not all) protein loss resulted from the freezing process; on the other hand, significant differences in soluble vault recovery were detected depending on the adopted conditions, although none of them ensured full recovery of soluble protein. In merely descriptive terms, it is apparent that a storage at -80 °C, rather than at 4 °C or -20 °C, is better capable of preserving the soluble form along with its native size and secondary structure content.

Also, trehalose addition improved to some extent the recovery of soluble protein, in keeping with a previous report (Kickhoefer *et al.*, 2009). Noteworthy, our results also confirm that in the presence of the sugar vault preparations can withstand long-term storage in lyophilized form. Nevertheless, vault solubility was best preserved when stored at -80 °C in the presence of 0.05% Tween-20, a non-ionic detergent that in our preliminary experiments was selected among others due to its better capability to prevent aggregation. As already mentioned, (Kerwin *et al.*, 1998; Chou *et al.*, 2005), its stabilizing and solubilizing effect on proteins is well known. Also, it did not detectably perturb vault's overall morphology, as apparent in TEM images (Figure S3). Based on these results, we conclude that its stability and solubility can be better preserved when stored in the presence of either trehalose or Tween-20. However, in view of possible vault administration to cell cultures or tissues, caution should be taken when using this latter compound, due to the well-known cell lytic effects exerted by detergents, even non-ionic (Linke, 2009).

To the best of our knowledge, no stability data under the conditions described in Table 1 were reported prior to the present contribution. We assume, however, that our purification procedure should ensure a very good preservation of protein stability thanks to its simplicity, in particular if compared with others encompassing several centrifugation steps. This is also attested by the fact that the vault nanoparticle did not undergo any appreciable aggregation when freshly eluted from the SEC column. Thus, the relative instability subsequently detected under different conditions (Table 1) does not seem to be related to the previous handling.

In conclusion, the achievements of the present investigation not only deliver the most practical purification procedure to date of authentic vault, but also provide further hints regarding its structure dynamics, which might have both theoretical and practical implications.

# 4 Materials and Methods

*Strain and growth media*

For the production of the MVP protein, the vacuolar aspartyl protease PEP4 deficient *K. phaffii* SMD1168 (his4, ura3, pep4::URA3) strain was used (Gleeson *et al.*, 1998). The strain is available from Invitrogen (Carlsbad, CA). *K. phaffii* was grown in flask in BMDY medium (10 g/L yeast extract, 20 g/L bacto peptone, 20 g/L dextrose, 100 mM potassium phosphate buffer, pH 5.8, 13.4 g/L yeast nitrogen base without amino acids, 0.4 mg/L biotin) (Weidner, Taupp and Hallam, 2010; Wu *et al.*, 2012). All media were from Biolife; monobasic potassium phosphate, yeast nitrogen base without amino acids and biotin were from Sigma-Aldrich. Standard liquid and plate growth were performed on YPD medium (10 g/L yeast extract, 20 g/L bacto peptone, 20 g/L dextrose, 20 g/L agar omitted in liquid medium) with or without 100 μg/mL zeocin. After electroporation, YPDS plates containing 1 M sorbitol and 100 μg/mL Zeocin were used for the selection of the transformants.

*MVP gene cloning*

The cDNA sequence coding for human Major Vault Protein (MVP, Gene Bank accession no. BC015623.2) was PCR-amplified using the forward primer JB183 – AATTAGAATTCACCATGGCAACTGAAGAGTTCATC (Eurofins), the reverse primer JB184 – ATTAGGTACCTTAGCGCAGTACAGGCAC-CACG (Eurofins) and the pVL1393-MVP vector (Galbiati *et al.*, 2018) as the template. The PCR product was then digested with EcoRI and KpnI and subcloned downstream of the glyceraldehyde 3-phosphate dehydrogenase promoter (pGAP) in the EcoRI/KpNI digested pGAPZB yeast vector DNA (Invitrogen, Carlsbad, CA) to form pGAPZB-MVP. The construct was confirmed by Sanger sequence analysis carried out by Eurofins.

*Transformation and selection of positive clones*

The plasmid pGAPZB-MVP was linearized with BspHI and transformed into *K. phaffii* SMD1168 protease-deficient strain, using Gene Pulser II electroporator (Biorad Laboratories, Hercules, CA), following the procedure previously described (Wang *et al.*, 2018), with minor modifications. Briefly, electroporation was performed at 1.5 kV, 400 Ω, and 25 μF by a single pulse.

The transformation mixture was plated on YPDS selective agar plates. To make sure that the pGAPZ B-MVP plasmid had correctly integrated within the yeast genome, a colony PCR was performed on the Zeocin resistant clones. A cell suspension was obtained by resuspending a small amount of cells from colonies in 10 μL of RNAse-free water. The enzyme Wonder Taq polymerase (Euroclone) was used for the amplification. The correct integration of the plasmid was also confirmed by agarose electrophoresis (2% gel). Cells were collected, lysed and subjected to sodium dodecyl sulfate-polyacrylamide gel electrophoresis (SDS-PAGE), followed by Coomassie staining and Western Blot analysis. The most productive clones were selected, stored at-80 °C as glycerol stock and used in all the subsequent experiments.

*Cell growth and collection, and cell-free extract production*

The best-producing clone was streaked on YPD plates with 100 μg/mL zeocin and incubated at 30 °C for two days. A 1-mL suspension in sterile water of cells grown on plates was used to inoculate at $OD_{600}$ 0.4 a 1000-mL Erlenmeyer flask containing 200 mL of BMDY medium. The flask was incubated at 30 °C under stirring at 160 rpm. After approximately 24-30 h, 100-mL aliquots of cell cultures were collected and washed with cold milli-Q water through repeated sedimentation cycles for 5 min at 5,000 x g in a bench-top centrifuge (Eppendorf 5430R) in pre-weighted 50-mL test tubes (Falcon). The pellets were weighed, wet weight recorded and stored at -80 °C. Then, they were resuspended in breaking buffer (3 mL/g wet weight; 50 mM sodium phosphate buffer, pH 7.4, 5% glycerol (v/v), 1 mM EDTA, 1 mM dithiothreitol, 1 mM PMSF, Pierce™ Protease Inhibitor Mini Tablets EDTA-free according to the producer's recommendations). 2-mL aliquots of cell suspensions were transferred into 10-mL round bottom tubes containing 1 mL of glass beads (425-600 μm diameter). Cells were disrupted by vigorous vortexing for ten periods of 1 min each, with idle intervals of 1 min in ice. The homogenate was withdrawn and centrifuged for 20 min at 20,000 x g, 4 °C (Eppendorf 5430R). The cell-free extract was then incubated with RNase A and RNase T1 (0.5 mg and 50 U per mL of extract, respectively) for 20 min at room temperature under stirring. Then, it was centrifuged for 20 min at

20,000 x g and 4 °C to eliminate insoluble ribosomal protein (Stephen *et al.*, 2001). Finally, the supernatant was collected to be destined for vault purification.

*Vault purification*

RNase-treated cell-free extract (approximately 70 mg protein content in 6 mL) was loaded onto a Sepharose CL-6B column (Healthcare Life Sciences; fractionation range 10 kDa-4 MDa; 206 mL bed volume, 42 cm height) pre-equilibrated with 20 mM Hepes, pH 7.4, 75 mM NaCl, 0.5 mM $MgCl_2$. Elution was performed at 4 °C using the same buffer at a flow rate of 2 mL/min and 6 mL fractions were collected. Both in extract and in the individual 6 mL fractions, protein was assayed by the bicinchoninic acid assay using the KIT QPRO-BCA (Cyanagen) and bovine serum albumin as the calibration standard. Typically, the first 8 eluted aliquots (around 50 ml) yielded no measurable protein content. Thus, the first 50 ml eluted were usually discarded and only the subsequential 6 ml fractions were collected and subjected to SDS PAGE.

*Electrophoretic analyses*

The eluted fractions were subjected to SDS-PAGE (8% gel). Typically, 6-12 μg samples were applied. Gels were stained by Coomassie brilliant blue R-250 following a standard protocol. MVP identity was confirmed by western blot analysis on PVDF membrane Immobilon (Millipore) using a primary anti-MVP antibody (rabbit monoclonal; 1:10000 dilution in PBS-5% skim milk; Abcam) and a fluorescent secondary anti-rabbit IR-800 antibody (1:16000 dilution in PBS-5% skim milk; LI-COR Biosciences). Immunoreactive signal was revealed by Odyssey Fc instrument (LI-COR Biosciences). For nucleic acid detection, samples (typically 3 to 10 μg protein) were run in 0.7% agarose and TAE buffer (40 mM Tris base, 20 mM acetic acid, 1 mM EDTA, pH 8.3-8.5) and ethidium bromide-stained. Staining was revealed using a Uvidoc HD6 transilluminator (Uvitec).

*Transmission electron microscopy*

TEM images of vault particles were obtained using a Tecnai12 (RH42B) microscope (Accelerating voltage: 120 kV - Filament: LaB6). Samples were deposited on carbon-coated copper grids, 400 Mesh, after plasma activation for 20 sec, by floating the grid onto the protein drop (20 μL, 0.5 mg/mL) for 1-2 min. The grid was then dried from liquid excess by filter paper and put on a drop of uranyl acetate (1% in PBS, pH 5.0) for 1-2 min, depending on sample concentration. Finally, the grids were dried with Whatman filter paper and analyzed.

*Fourier transform infrared spectroscopy*

FTIR measurements were performed in ATR mode using 2 μL of the protein preparations, which were deposited on the diamond plate of the single reflection ATR device (Quest, Specac, USA). Spectra were recorded after solvent evaporation as previously described (Ami and Natalello, 2022). The Varian 670-IR spectrometer (Varian Australia Pty Ltd., Mulgrave VIC, AU) was employed under the following conditions: 1024 scan coadditions, 2 $cm^{-1}$ spectral resolution, 25 kHz scan speed, triangular apodization, and nitrogen-cooled Mercury Cadmium Telluride (MCT) detector. Absorption spectra, after subtraction of the buffer spectra and, when necessary, after water vapor correction, were normalized at the Amide I band area and were smoothed using the Savitsky–Golay method (25 points) before the second-derivative calculation (Resolutions-Pro software, Varian Australia Pty Ltd.).

*Dynamic light scattering*

Dynamic Light Scattering (DLS) measurements were performed by a Zeta Sizer Nano Instrument (Malvern Instruments Ltd., Amesbury, UK) operating at 4 mW of a HeeNe 633 nm laser, using a scattering angle of 90°. A disposable cuvette with 1 cm optical path length was used for the measurements. Each sample was allowed to equilibrate for 2 min prior to measurement. Three independent measurements of 60 s duration were performed at 25 °C. Calculations of the hydrodynamic diameter were performed using the Mie theory, considering the absolute viscosity and the refractive index of the material set to 1.450, Abs 0.001. Number-based

hydrodynamic diameter and the autocorrelation function were determined, the latter being diagnostic of sample homogeneity, insofar as a single exponential decay profile is detected.

**Author Contributions:** conceptualization, G.F. and P.T.; methodology, G.T., D.A. and A.N.; validation, C.P. and G.T.; investigation, D.A., A.N., L.B., A.D., S.G. and F.P.; resources, G.F.; data curation, G.T. and C.P.; writing—original draft preparation, P.T.; writing—review and editing, G.F., G.T. and C.P.; supervision, C.P. and G.T.; funding acquisition, P.T. All authors have read and agreed to the published version of the manuscript.

**Funding:** this work was funded by the Italian Ministry of University and Research (PRIN 2017: "Development of a biotechnological nanoparticle platform for the delivery of antitumor therapies using Patient Derived-Organoid library of Breast Cancer"). G.T. is a PhD student in Converging Technologies for Biomolecular Systems (TeCSBi), funded by CHRONOS (CHROnical multifactorial disorders explored by Novel integrated Strategies) excellence project of the Department of Biotechnology and Bioscience. D.A. benefits from a post-doctoral research fellow (Assegno di Ricerca) from the University of Milano-Bicocca.

**Data Availability Statement**: not applicable.

**Acknowledgments:** We gratefully acknowledge Dr. Fabio Lapenta for helpful suggestions. The skilful technical assistance of Mr. Davide Valsecchi is acknowledged. We also acknowledge the core imaging facility of the Institut Jacques Monod (ImagoSeine facility, member of the France BioImaging infrastructure supported by grant ANR-10-INBS-04 from the French National Research Agency).

**Conflicts of Interest:** the authors declare no conflict of interest.

## Supplementary Information

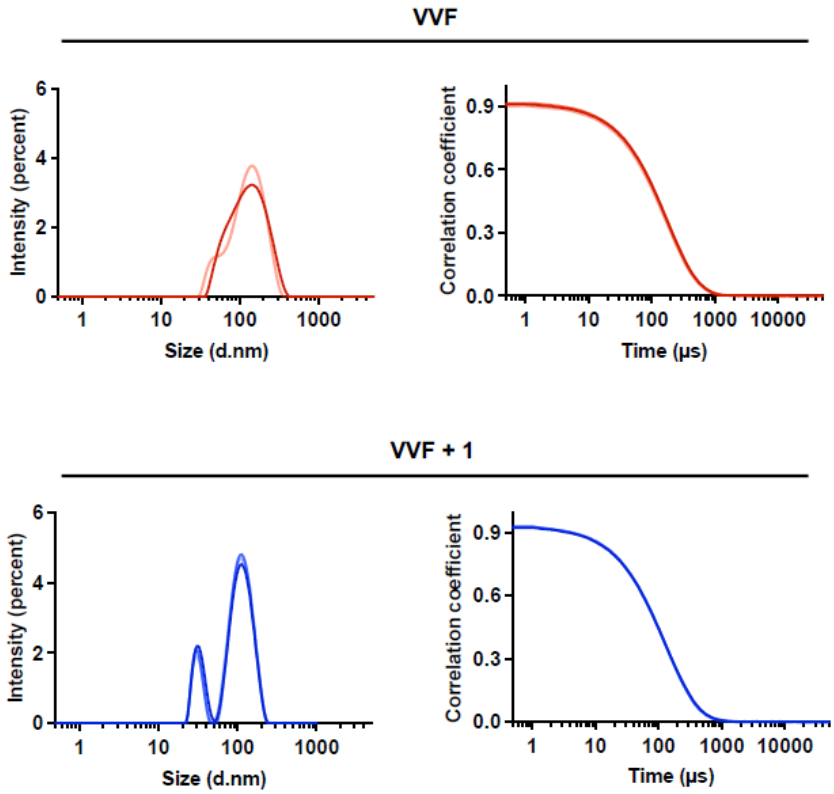


***Figure S1***. *DLS of the 20,000 x g supernatants of freshly purified vault from the SEC void-volume fraction (VVF) and the following one (VVF + 1). Intensity-weighted particle size distribution and autocorrelation function are presented.*

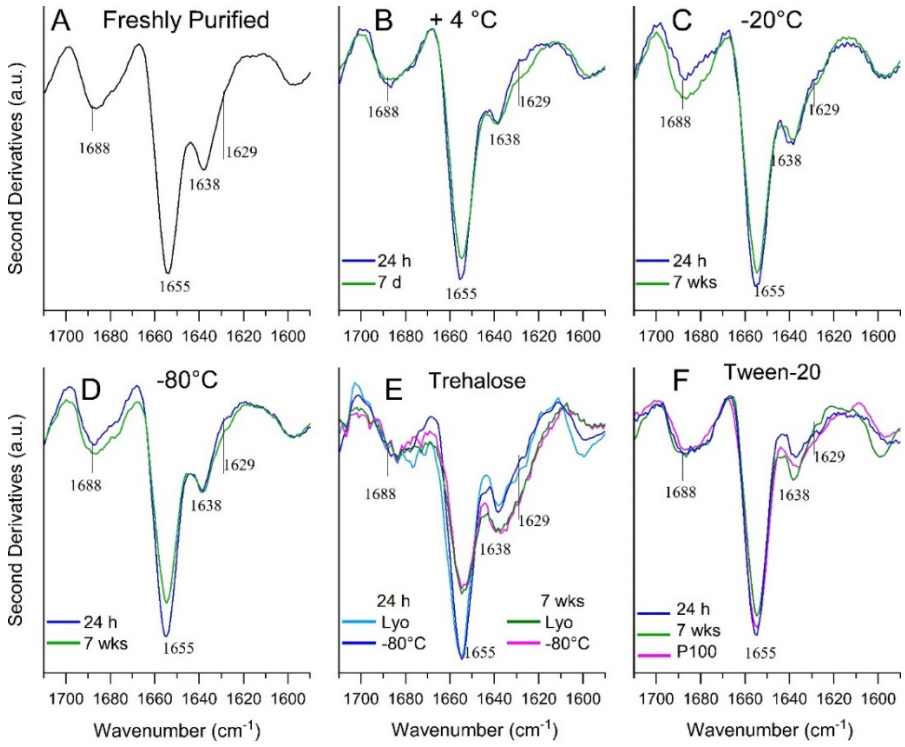


***Figure S2***. *FTIR analysis of whole samples of vault protein preparations. Analyses were performed prior to protein centrifugation and otherwise as described in the legend to Figure 4, except that after a 7-weeks incubation in 0.05% Tween-20 under frozen conditions, the sample was thawed, centrifuged at 100,000 x g for 2 h, and the pellet analyzed (P100, panel F).*

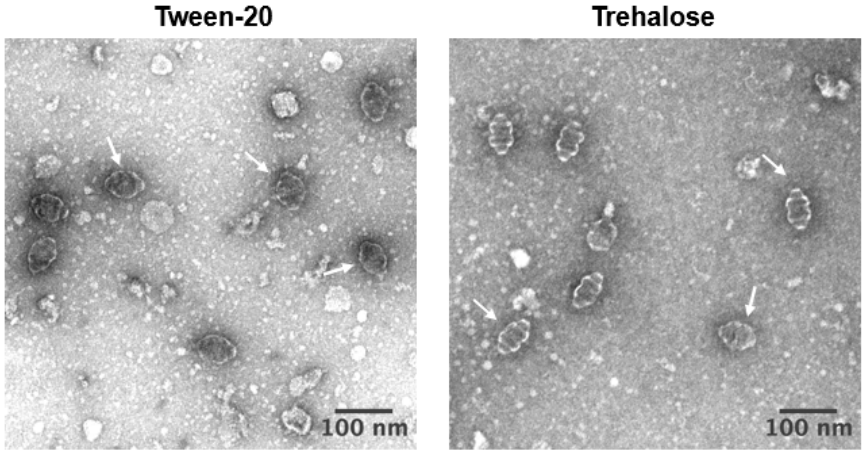


***Figure S3***. *TEM images of vault nanoparticles stained by uranyl acetate, as detected in samples frozen at -80 °C in the presence of either 0.05% Tween 20 or 10 mg/mL trehalose and stored for 7 weeks. The fractions were analyzed after centrifuging at 20,000 x g for 20 min and discarding the pellet. Some vault particles are indicated by white arrows.*

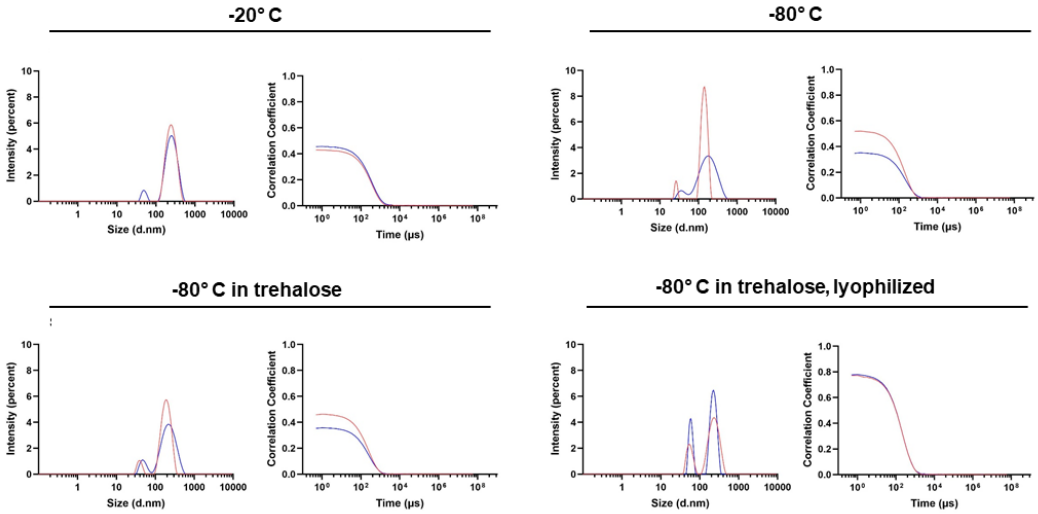


***Figure S4**. DLS of the 20,000 x g supernatants of vault samples incubated for 7 weeks and otherwise as indicated in the respective panels. Intensity-weighted particle size distribution and autocorrelation function are presented. In each panel, two replicates of the same measurement are shown.*

## References


Aarum, J., Cabrera, C. P., Jones, T. A., Rajendran, S., Adiutori, R., Giovannoni, G., Barnes, M. R., Malaspina, A., & Sheer, D. (2020). Enzymatic degradation of RNA causes widespread protein aggregation in cell and tissue lysates. *EMBO Reports*, *21*(10), e49585. https://doi.org/10.15252/EMBR.201949585

Aivaliotis, M., Samolis, P., Neofotistou, E., Remigy, H., Rizos, A. K., & Tsiotis, G. (2003). Molecular size determination of a membrane protein in surfactants by light scattering. *Biochimica et Biophysica Acta (BBA) - Biomembranes*, *1615*(1–2), 69–76. https://doi.org/10.1016/S0005-2736(03)00208-6

Ami, D., Mereghetti, P., & Natalello, A. (2022). Contribution of Infrared Spectroscopy to the Understanding of Amyloid Protein Aggregation in Complex Systems. *Frontiers in Molecular Biosciences*, *9*, 822852. https://doi.org/10.3389/FMOLB.2022.822852/BIBTEX

Ami, D., & Natalello, A. (2022). Characterization of the Conformational Properties of Soluble and Insoluble Proteins by Fourier Transform Infrared Spectroscopy. *Methods in Molecular Biology (Clifton, N.J.)*, *2406*, 439–454. https://doi.org/10.1007/978-1-0716-1859-2_26

Anderson, D. H., Kickhoefer, V. A., Sievers, S. A., Rome, L. H., & Eisenberg, D. (2007). Draft Crystal Structure of the Vault Shell at 9-Å Resolution. *PLOS Biology*, *5*(11), e318. https://doi.org/10.1371/JOURNAL.PBIO.0050318

Benner, N. L., Zang, X., Buehler, D. C., Kickhoefer, V. A., Rome, M. E., Rome, L. H., & Wender, P. A. (2017). Vault Nanoparticles: Chemical Modifications for Imaging and Enhanced Delivery. *ACS Nano*, *11*(1), 872–881. https://doi.org/10.1021/ACSNANO.6B07440/ASSET/IMAGES/LARGE/NN-2016-07440S_0005.JPEG

Berger, W., Steiner, E., Grusch, M., Elbling, L., & Micksche, M. (2009). Vaults and the major vault protein: Novel roles in signal pathway regulation and immunity. *Cellular and Molecular Life Sciences*, *66*(1), 43–61. https://doi.org/10.1007/S00018-008-8364-Z/METRICS

Buehler, D. C., Toso, D. B., Kickhoefer, V. A., Zhou, Z. H., & Rome, L. H. (2011). Vaults Engineered for Hydrophobic Drug Delivery. *Small*, *7*(10), 1432–1439. https://doi.org/10.1002/SMLL.201002274

Chiti, F., & Dobson, C. M. (2017). Protein Misfolding, Amyloid Formation, and Human Disease: A Summary of Progress Over the Last Decade. *Annurev-Biochem*, *86*, 27–68. https://doi.org/10.1146/ANNUREV-BIOCHEM-061516-045115

Chou, D. K., Krishnamurthy, R., Randolph, T. W., Carpenter, J. F., & Manning, M. C. (2005). Effects of Tween 20® and Tween 80® on the Stability of Albutropin During Agitation. *Journal of Pharmaceutical Sciences*, *94*(6), 1368–1381. https://doi.org/10.1002/JPS.20365

Ding, K., Zhang, X., Mrazek, J., Kickhoefer, V. A., Lai, M., Ng, H. L., Yang, O. O., Rome, L. H., & Zhou, Z. H. (2018). Solution Structures of Engineered Vault Particles. *Structure*, *26*(4), 619-626.e3. https://doi.org/10.1016/J.STR.2018.02.014

Fernández, R., Carreño, A., Mendoza, R., Benito, A., Ferrer-Miralles, N., Céspedes, M. V., & Corchero, J. L. (2022). Escherichia coli as a New Platform for the Fast Production of Vault-like Nanoparticles: An Optimized Protocol. *International Journal of Molecular Sciences 2022, Vol. 23, Page 15543*, *23*(24), 15543. https://doi.org/10.3390/IJMS232415543

Frascotti, G., Galbiati, E., Mazzucchelli, M., Pozzi, M., Salvioni, L., Vertemara, J., & Tortora, P. (2021). The Vault Nanoparticle: A Gigantic Ribonucleoprotein Assembly Involved in Diverse Physiological and Pathological Phenomena and an Ideal Nanovector for Drug Delivery and Therapy. *Cancers 2021, Vol. 13, Page 707*, *13*(4), 707. https://doi.org/10.3390/CANCERS13040707

Galbiati, E., Avvakumova, S., La Rocca, A., Pozzi, M., Messali, S., Magnaghi, P., Colombo, M., Prosperi, D., & Tortora, P. (2018). A fast and straightforward procedure for vault nanoparticle purification and the characterization of its endocytic uptake. *Biochimica et Biophysica Acta (BBA) - General Subjects*, *1862*(10), 2254–2260. https://doi.org/10.1016/J.BBAGEN.2018.07.018

Gleeson, M. A., White, C. E., Meininger, D. P., & Komives, E. A. (1998). Generation of protease-deficient strains and their use in heterologous protein expression. *Methods in Molecular Biology (Clifton, N.J.)*, *103*, 81–94. https://doi.org/10.1385/0-89603-421-6:81

Goormaghtigh, E., Raussens, V., & Ruysschaert, J. M. (1999). Attenuated total reflection infrared spectroscopy of proteins and lipids in biological membranes. *Biochimica et Biophysica Acta (BBA) - Reviews on Biomembranes*, *1422*(2), 105–185. https://doi.org/10.1016/S0304-4157(99)00004-0

Guerra, P., González-Alamos, M., Llauró, A., Casañas, A., Querol-Audí, J., de Pablo, P. J., & Verdaguer, N. (2022). Symmetry disruption commits vault particles to disassembly. *Science Advances*, *8*(6), 7795. https://doi.org/10.1126/SCIADV.ABJ7795/SUPPL_FILE/SCIADV.ABJ7795_SM.

Kedersha, N. L., Heuser, J. E., Chugani, D. C., & Rome, L. H. (1991). Vaults. III. Vault ribonucleoprotein particles open into flower-like structures with octagonal symmetry. *Journal of Cell Biology*, *112*(2), 225–235. https://doi.org/10.1083/JCB.112.2.225

Kedersha, N. L., & Rome, L. H. (1986). Isolation and characterization of a novel ribonucleoprotein particle: large structures contain a single species of small RNA. *The Journal of Cell Biology*, *103*(3), 699–709. https://doi.org/10.1083/JCB.103.3.699

Kerwin, B. A., Heller, M. C., Levin, S. H., & Randolph, T. W. (1998). Effects of Tween 80 and Sucrose on Acute Short-Term Stability and Long-Term Storage at − 20 C of a Recombinant Hemoglobin. *Journal of Pharmaceutical Sciences*, *87*(9), 1062–1068. https://doi.org/10.1021/JS980140V

Kickhoefer, V. A., Han, M., Raval-Fernandes, S., Poderycki, M. J., Moniz, R. J., Vaccari, D., Silvestry, M., Stewart, P. L., Kelly, K. A., & Rome, L. H. (2009). Targeting vault nanoparticles to specific cell surface receptors. *ACS Nano*, *3*(1), 27–36. https://doi.org/10.1021/NN800638X/SUPPL_FILE/NN800638X_SI_001.PDF

Kickhoefer, V. A., Rajavel, K. S., Scheffer, G. L., Dalton, W. S., Scheper, R. J., & Rome, L. H. (1998). Vaults Are Up-regulated in Multidrug-resistant Cancer Cell Lines. *Journal of Biological Chemistry*, *273*(15), 8971–8974. https://doi.org/10.1074/JBC.273.15.8971

Kickhoefer, V. A., Searles, R. P., Kedersha, N. L., Garber, M. E., Johnson, D. L., & Rome, L. H. (1993). Vault ribonucleoprotein particles from rat and bullfrog contain a related small RNA that is transcribed by RNA polymerase III. *Journal of Biological Chemistry*, *268*(11), 7868–7873. https://doi.org/10.1016/S0021-9258(18)53038-6

Kickhoefer, V. A., Siva, A. C., Kedersha, N. L., Inman, E. M., Ruland, C., Streuli, M., & Rome, L. H. (1999). The 193-Kd Vault Protein, Vparp, Is a Novel Poly(Adp-Ribose) Polymerase. *Journal of Cell Biology*, *146*(5), 917–928. https://doi.org/10.1083/JCB.146.5.917

Kickhoefer, V. A., Stephen, A. G., Harrington, L., Robinson, M. O., & Rome, L. H. (1999). Vaults and Telomerase Share a Common Subunit, TEP1. *Journal of Biological Chemistry*, *274*(46), 32712–32717. https://doi.org/10.1074/JBC.274.46.32712

Linke, D. (2009). Detergents: an overview. *Methods in Enzymology*, *463*(C), 603–617. https://doi.org/10.1016/S0076-6879(09)63034-2

Martín, F., Carreño, A., Mendoza, R., Caruana, P., Rodriguez, F., Bravo, M., Benito, A., Ferrer-Miralles, N., Céspedes, M. V., & Corchero, J. L. (2022). All-in-one biofabrication and loading of recombinant vaults in human cells. *Biofabrication*, *14*(2), 025018. https://doi.org/10.1088/1758-5090/AC584D

Matsumoto, N. M., Buchman, G. W., Rome, L. H., & Maynard, H. D. (2015). Dual pH- and temperature-responsive protein nanoparticles. *European Polymer Journal*, *69*, 532–539. https://doi.org/10.1016/J.EURPOLYMJ.2015.01.043

Mrazek, J., Toso, D., Ryazantsev, S., Zhang, X., Zhou, Z. H., Fernandez, B. C., Kickhoefer, V. A., & Rome, L. H. (2014). Polyribosomes are molecular 3D nanoprinters that orchestrate the assembly of vault particles. *ACS Nano*, *8*(11), 11552–11559. https://doi.org/10.1021/NN504778H/SUPPL_FILE/NN504778H_SI_001.PDF

Muñoz-Juan, A., Carreño, A., Mendoza, R., & Corchero, J. L. (2019). Latest Advances in the Development of Eukaryotic Vaults as Targeted Drug Delivery Systems. *Pharmaceutics 2019, Vol. 11, Page 300*, *11*(7), 300. https://doi.org/10.3390/PHARMACEUTICS11070300

Ng, B. C., Yu, M., Gopal, A., Rome, L. H., Monbouquette, H. G., & Tolbert, S. H. (2008). Encapsulation of semiconducting polymers in vault protein cages. *Nano Letters*, *8*(10), 3503–3509.

https://doi.org/10.1021/NL080537R/ASSET/IMAGES/LARGE/NL-2008-00537R_0007.JPEG

Nobbmann, U., & Morfesis, A. (2009). Light scattering and nanoparticles. *Materials Today*, *12*(5), 52–54. https://doi.org/10.1016/S1369-7021(09)70164-6

Rome, L. H., & Kickhoefer, V. A. (2013). Development of the Vault Particle as a Platform Technology. *ACS Nano*, *7*(2), 889–902. https://doi.org/10.1021/NN3052082/ASSET/IMAGES/LARGE/NN-2012-052082_0007.JPEG

Stephen, A. G., Raval-Fernandes, S., Huynh, T., Torres, M., Kickhoefer, V. A., & Rome, L. H. (2001). Assembly of Vault-like Particles in Insect Cells Expressing Only the Major Vault Protein. *Journal of Biological Chemistry*, *276*(26), 23217–23220. https://doi.org/10.1074/JBC.C100226200

van Zon, A., Mossink, M. H., Schoester, M., Houtsmuller, A. B., Scheffer, G. L., Scheper, R. J., Sonneveld, P., & Wiemer, E. A. C. (2003). The formation of vault-tubes: a dynamic interaction between vaults and vault PARP. *Journal of Cell Science*, *116*(21), 4391–4400. https://doi.org/10.1242/JCS.00749

Van Zon, A., Mossink, M. H., Schoester, M., Scheffer, G. L., Scheper, R. J., Sonneveld, P., & Wiemer, E. A. C. (2001). Multiple Human Vault RNAs: EXPRESSION AND ASSOCIATION WITH THE VAULT COMPLEX. *Journal of Biological Chemistry*, *276*(40), 37715–37721. https://doi.org/10.1074/JBC.M106055200

Wang, M., Kickhoefer, V. A., Rome, L. H., Foellmer, O. K., & Mahendra, S. (2018). Synthesis and assembly of human vault particles in yeast. *Biotechnology and Bioengineering*, *115*(12), 2941–2950. https://doi.org/10.1002/BIT.26825

Weidner, M., Taupp, M., & Hallam, S. J. (2010). Expression of recombinant proteins in the methylotrophic yeast Pichia pastoris. *Journal of Visualized Experiments : JoVE*, *36*. https://doi.org/10.3791/1862

Wiethoff, C. M., Wodrich, H., Gerace, L., & Nemerow, G. R. (2005). Adenovirus Protein VI Mediates Membrane Disruption following Capsid Disassembly. *Journal of Virology*, *79*(4), 1992–2000. https://doi.org/10.1128/JVI.79.4.1992-2000.2005/ASSET/8DE5A532-17B1-4D74-9362-17706A862A11/ASSETS/GRAPHIC/ZJV0040557710008.JPEG

Wu, D., Chu, J., Hao, Y. Y., Wang, Y. H., Zhuang, Y. P., & Zhang, S. L. (2012). Incomplete protein disulphide bond conformation and decreased protein expression result from high cell growth during heterologous protein expression in Pichia pastoris. *Journal of Biotechnology*, *157*(1), 107–112. https://doi.org/10.1016/J.JBIOTEC.2011.08.032

Yang, J., Kickhoefer, V. A., Ng, B. C., Gopal, A., Bentolila, L. A., John, S., Tolbert, S. H., & Rome, L. H. (2010). Vaults are dynamically unconstrained cytoplasmic nanoparticles capable of half vault exchange. *ACS Nano*, *4*(12), 7229–7240. https://doi.org/10.1021/NN102051R/ASSET/IMAGES/LARGE/NN-2010-02051R_0009.JPEG

# Chapter 2

# Exploring Human Recombinant Vault Ability to Load INT-fused Cargo Molecules: GFP-INT as a Model for Loading Strategy and Binding Stoichiometry Evaluation

The following researchers also participated in the study:
Annie Dutriaux[2], Camilla Pantaleoni[1], Domenico Flagiello[2], Paolo Tortora[1], Gianni Frascotti[1]

[1] Department of Biotechnology and Biosciences, University of Milano-Bicocca, I-20126 Milano, Italy
[2] Université Paris Cité, CNRS, Institut Jacques Monod, F-75013 Paris, France

## Abstract

One valuable characteristic of vaults is their ability to encapsulate cargo proteins by fusing them to the INT peptide (a vault-targeting domain from the vault-interacting vPARP protein). Encapsulation approaches reported in literature require the previous construction of recombinant baculoviruses encoding either the MVP or the INT-tagged protein, before co-infecting Sf9 cells.

We explored the putative encapsulation of a cargo protein within vault particles expressed and purified with our simplified procedure. Encapsulation of purified GFP-INT, chosen as a reporter cargo protein, into vault was achieved by just mixing purified vault and GFP-INT, taking advantage of the "breathing" event described for vaults. Western blot analysis on the mixes of vault incubated with GFP-INT and GFP, used as control, proved that only GFP-INT is pelleted and stably associated with vault. To assess the stoichiometry of GFP-INT loading into vault lumen, densitometric analysis on SDS-PAGE has been conducted on increasing molar ratio GFP-INT: vault, resulting in a saturation of the binding site with around 20 copies of GPF INT. Recombinant vaults can be internalized in vitro via macro-pinocytosis or endocytosis. To evaluate GFP-INT-carrying vault uptake by cancer cell lines, confocal analysis has been conducted on Melanoma A375 cancer cell line incubated with vault carrying GFP-INT. Signal of GFP-INT inside of the cells proved the ability of vault of delivering the cargo molecule inside of the cells.


**Keywords:** Vault particle, Drug delivery system, INT domain, cargo, vault "breathing"

# 1 Introduction

One valuable characteristic of vaults is their ability to encapsulate cargo proteins by fusing them to the interaction domain (INT), the 162 amino acid C-terminal fragment of the vault-interacting vPARP protein (vPARP residues 1563-1724) (Kickhoefer *et al*., 2005). The association between INT-fused protein and vault is made possible by the ability of the INT domain to bind MVP on specific sites, as demonstrated by a previous study that utilized MVP as the bait in a yeast two-hybrid analysis (Kickhoefer *et al*., 1999). INT domain has been proved to enable the encapsulation of several fused protein into vault lumen (Rome & Kickhoefer, 2013).

In the past, the association between INT-fused protein and vault was thought to take place during the assembly of the vault MVP shell, when MVP expression directs the self-assembly of vault-like particles on polyribosomes (Mrazek *et al*., 2014). Recombinant vaults were routinely produced in *Spodoptera frugiperda* (Sf9) insect cells (Stephen *et al*., 2001) through Baculovirus expression system, being the most used for vault expression as described in Chapter 1. INT-tagged proteins have been successfully encapsulated within recombinant vaults by the co-infection of Sf9 cells with recombinant baculovirus encoding MVP and the INT-tagged cargo protein (Kickhoefer *et al*., 2005). However, this approach requires the previous construction of the respective recombinant baculoviruses before the co-infection. Nevertheless, the packaging process has been further examined and proved not to require co-translation of INT-fused protein with MVP (Poderycki *et al*., 2006), being instead a process that can occurs after vault protein has reached stable conformation. This is possible thanks to the transient half-vault/whole-vault dynamic of vault in solution that shows transient open and closed states, a mechanism that can explain the encapsulation of vault-interacting proteins (Poderycki *et al*., 2006). In particular, the packaging of INT fusion protein into vault is thought to occur via vault "breathing", a process already described for virus particles (Broo *et al*., 2001). Purified INT fusion proteins were found to be packaged inside purified recombinant vaults by simply mixing the two components.

As reported in the Chapter 1, we have optimized a simpler and faster procedure for vault production exploiting the yeast *K. phaffii* combined with

a size exclusion method for vault purification (Tomaino *et al*., 2023). Thus, in this chapter, we investigate whether the recombinant vault particles, expressed in *K. phaffii* and purified with our simplified procedure, maintained the natural ability of encapsulating INT-fused cargo protein.

The *Aequorea coerulescens* green fluorescent protein (AcGFP1) fused in frame with INT domain (GFP-INT), was chosen as reporter cargo protein, thanks to its stability and monomeric nature (Gurskaya *et al*., 2003). $His_6$-tagged GFP-INT has been expressed in M15 *E. coli* strain and purified through IMAC. Encapsulation of purified GFP INT into purified vault has been achieved just by mixing both purified vault and GFP INT, by taking advantage of the "breathing" event described for vaults (Kickhoefer *et al*., 2005). Densitometric analyses were conducted to study the stoichiometry of GFP-INT loading into vault lumen. To evaluate GFP-INT-carrying vault uptake by cancer cell lines, confocal analysis has been conducted on Melanoma A375 cancer cell line incubated with vault carrying GFP-INT. Signal of GFP-INT inside of the cells proved the ability of vault of delivering the cargo molecule inside of the cells.

## 2 Results

### GFP-INT Production and Solubility

GFP-INT was expressed in *E. coli* strain M15 upon IPTG induction and incubation overnight at either 37°C or 25°C. Aliquots of 1 $OD_{600}$ were harvested at 0 time and after the overnight (O/N) induction. Suitable amounts of sample were loaded on gel to be analyzed through electrophoresis and western blot. Under both conditions, GFP-INT of the expected molecular mass (approx. 45 kDa) was produced and accumulated within the cells after the induction (Figure 1A).

To evaluate GFP-INT solubility at the two temperatures, induced cells were lysed, and soluble and insoluble fractions were also analyzed by SDS-PAGE ad Western blot. As shown in Figure 1B, at 25°C GFP-INT found in the soluble fraction is about 40% more (measured on western blot (WB)) compared to the amount of soluble GFP-INT produced at 37°C. For this

reason and despite the remaining presence of GFP-INT in the insoluble fraction, induction at 25°C was chosen to produce recombinant GFP-INT.

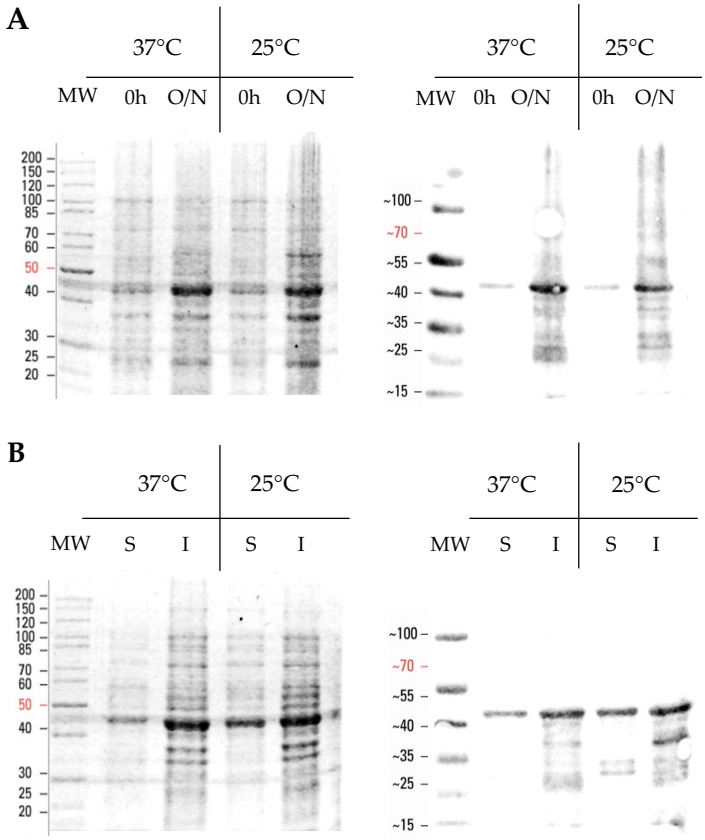


***Figure 1.*** *Production (A) and solubility (B) of GFP-INT expressed under two different inducing conditions. Samples of total cell pellets of induced M15/GFP-INT cultures O/N at 37 °C and 25 °C (A), and their corresponding soluble (S) and insoluble (I) cell fractions (B) were analyzed by SDS-PAGE (left panels) and western-blot (right panels) developed with anti-GFP antibody. MW: PageRuler™ Protein Ladder (Thermofisher) unstained (for SDS PAGE) or pre-stained (for WB).*

## GFP-INT Purification

GFP-INT purification was carried out using nickel-based immobilized metal affinity chromatography (IMAC). Following induction, the pelleted cells were lysed and purified on Nickel Sepharose 6 Fast Flow resin (Materials and Methods 3.2.5). The eluted fractions were analyzed by SDS-PAGE and GFP-INT identity was confirmed by Western blot, using anti-GFP primary antibody. The results (Figure 2) confirmed that GFP-INT is captured

by the resin, since is not found in the flowthrough and in the washes while is present in the eluted fractions (at high imidazole concentration). Fractions containing the highest amount of pure protein, quantified by UV vis as shown in Figure 2C, were collected and buffer exchanged on PBS. Purified GFP-INT yields 2.8 mg per g of wet weight corresponding to 10% of the total soluble protein.

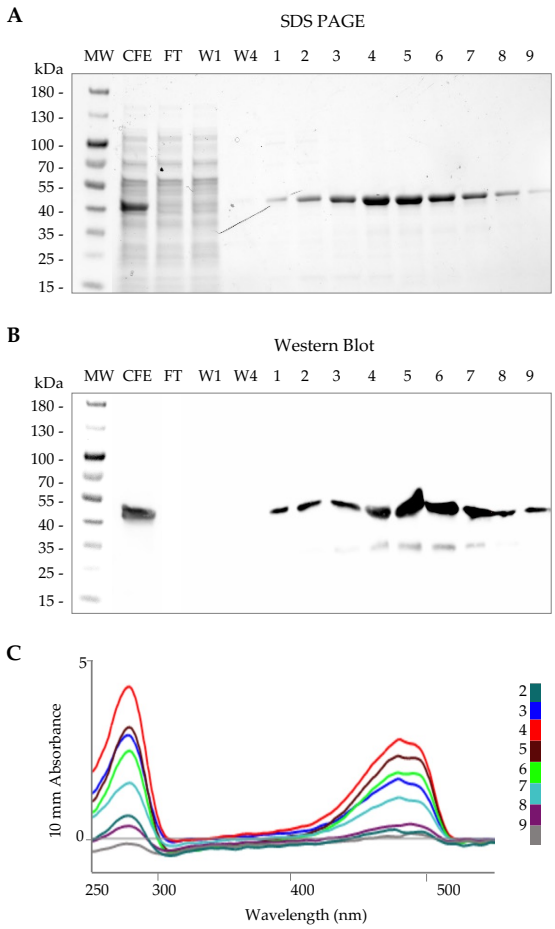


***Figure 2.*** *SDS-PAGE (A), Western blot (B) and Uv vis analysis (C) of GFP-INT purification. MW: standard proteins with the respective molecular weights (kDa). FT: flow through, W: wash, numbers 1-9 indicate eluted 1-mL fractions at the highest concentration of imidazole (300 mM) when GFP-INT elution occurs. Eluted fractions with imidazole concentration between 100 mM and 250 mM are not shown. An aliquot of 10 µL of cell free extract (CFE) (corresponding to 15 µg of total protein), FT and washes was loaded on the gel. 1-3 µg of purified GFP-INT samples were applied on the gel and normalized at the same volume. Uv vis analysis was conducted on 1 µL of sample. Other details are reported in Materials and Methods (Section 4.6).*

## GFP-INT Encapsulation

The encapsulation of purified GFP-INT into vault was achieved by mixing the two purified proteins (O/N 4°C), taking advantage of the "breathing" event described for vaults. A first round of ultracentrifugation at 100,000 x g showed that control samples of GFP-INT and GFP alone cannot be found in the pellet (spun at 5000 x g to remove possible insoluble aggregate, P100 S5), while GFP-INT is retained in the sedimentation at 100,000 g, indicative of its loading within vault. Giving that a little signal of GFP was detected in the pellet together with vault, another step of ultracentrifugation was added, to completely remove GFP unbound or bound in a non-specific way. Western blot and fluorimeter analysis on the $P100_2$ S5 of vaults incubated with GFP-INT and GFP proved that only GFP-INT is pelleted and stably associated to vault (Figure 3).

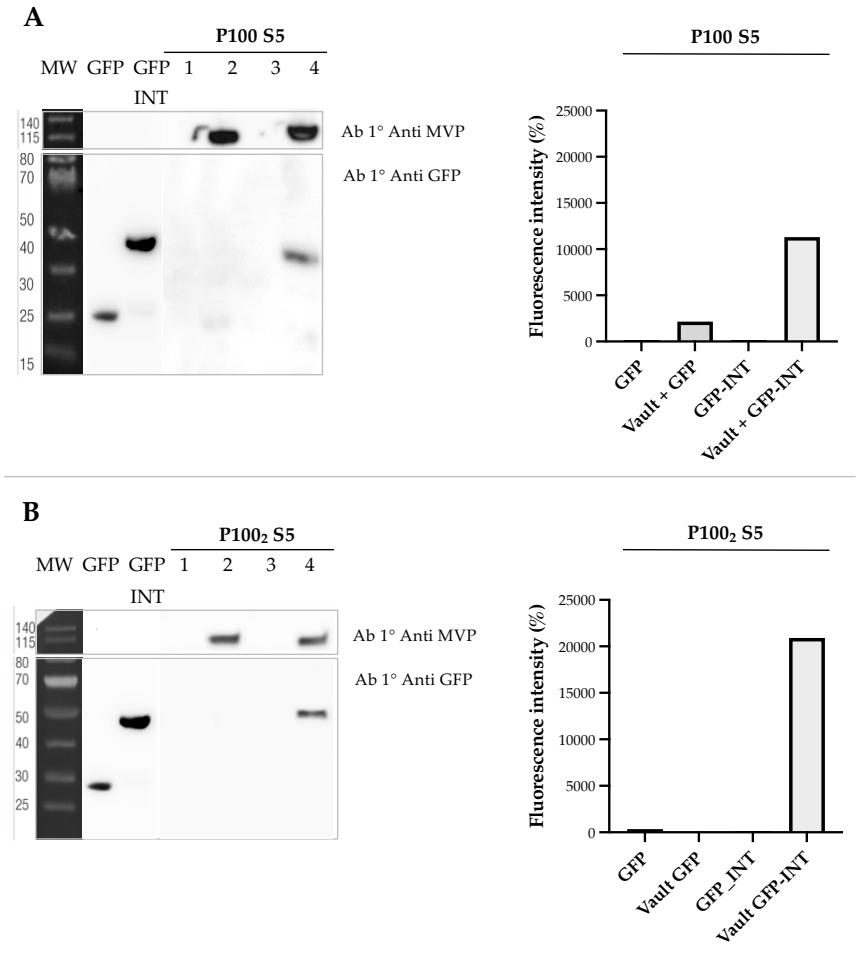

***Figure 3.*** *Encapsulation of GFP-INT into vault analyzed by Western blot (left) and fluorimeter analysis at 520 nm (right). Comparison between P100 S5 (A) and P100₂ S5 (B). On the gels, samples are normalized on volume (15 µl) except for GFP and GFP-INT that are used as control lanes (1-2 µg). 1) GFP; 2) vault + GFP; 3) GFP-INT 4) vault + GFP-INT. Error bar not shown because fluorometric analysis was conducted in single.*

## Binding stoichiometry of GFP-INT loading into vault

To assess the stoichiometry of GFP-INT loading into vault lumen, densitometric analysis on SDS-PAGE has been conducted: vault has been incubated with GFP-INT in increasing molar excess (5, 10, 25, 50). After the incubation (O/N, 4°C) the samples were ultra-centrifuged twice as described in materials and methods. Once resuspended, the reaction mixes were spun down 5 min at 5000 x g and suitable amounts thereof dissolved in SDS-PAGE sample buffer and subjected to electrophoresis. Defined amounts of purified vault and GFP-INT were co-electrophoresed with the P100₂ S5 of the mixes to construct suitable calibration curves for both vault and GFP-INT, to measure the molar ratio of bound GFP-INT to vault in the P100₂ S5. Saturation of the binding sites was reached around 20 copies of GFP-INT (Figure 4).

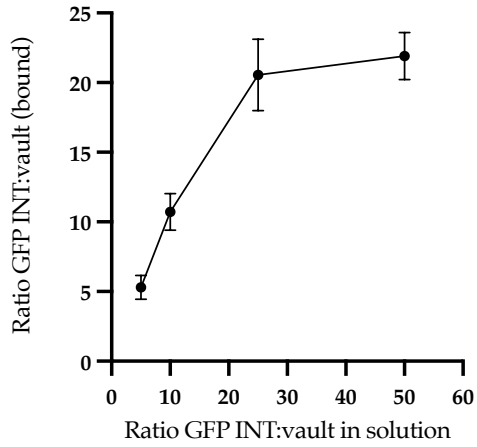


| **Molar ratio GFP INT:vault in solution** | **5** | **10** | **25** | **50** |
|---|---|---|---|---|
| Molar ratio GFP INT:vault (bound) | 5.3 ± 0.85 | 10.72 ± 1.32 | 20.55 ± 2.56 | 21.9 ± 1.69 |
| | 106% | 107% | 82% | 44% |

***Figure 4.*** *Stoichiometry of GFP-INT loading into vault. Densitometry analysis on SDS PAGE showing the plateau around 20 copies of GFP-INT per vault. The graph shows the molar ratio of GFP-INT bound to vault as a function of the molar ratio present in solution in the initial mix. Each point represents the mean of three biological replicates loaded on SDS-PAGE gels (examples are provided in the supplementary section, Figure S1). The percentage represents the quantity of GFP-INT in solution that is bound to vault.*

### GFP-INT co-migration with vault on native gel

Native agarose gel electrophoresis was conducted to visualize the interaction between GFP-INT and vault depending on the ratio of incorporation and the analyzed fractions $S100_2$ or $P100_2$ S5 (Figure 5). Vault is mainly retained in the well due to its size, meaning that it's correctly assembled ($P100_2$ S5). Half vaults or degraded particles (like monomers) are enriched in the supernatant of the ultra-centrifugation ($S100_2$) and move faster in the gel. Compared to vault, GFP-INT moves faster but its mobility decreases when incubated and pelleted with vault particles ($P100_2$ S5), proving that it is loaded within vault and therefore retained in the wells of the gels. At higher molar ratio between GFP-INT and vault the signal of GFP-INT in the well increases (second panel Figure 5).

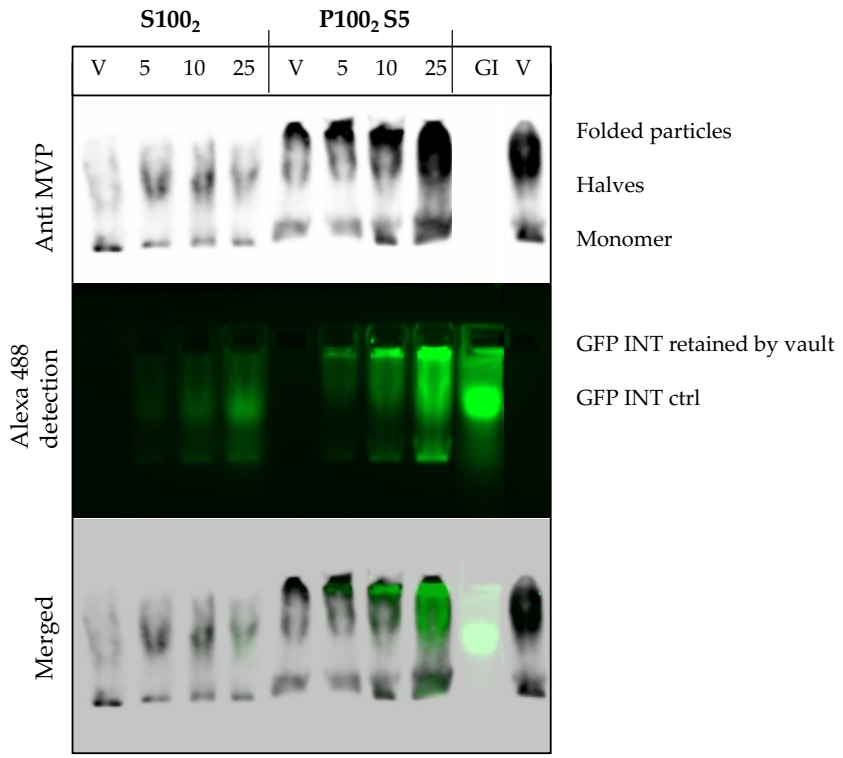


***Figure 5.*** *Native agarose gel electrophoresis showing the interaction between GFP-INT and vault depending on the ratio of incorporation and the analyzed fraction, supernatant $S100_2$ or pellet $P100_2$ S5). Samples are loaded on agarose 1.5% gel. V: vault, 5-10-25 indicate the mix with increasing ratio GFP-INT/vault. GI: GFP INT used as control lane. In the first panel the signal of vault is detected by immunoblotting with 1° Ab anti MVP and 2° Ab anti rabbit HRP. The second panel shows the signal of GFP-INT detected with the filter for Alexa 488 on Bio-Rad imaging system. Signals are merged in the last panel.*

**Vault-mediated, GFP-INT cell internalization**

The ability of GFP-INT encapsulated within vaults to be internalized in cancer cells was tested on Melanoma A375 cell line. GFP-INT-carrying vaults and GFP-INT were added to cultured A375 cells and incubated for 3 h and O/N, and their uptake was monitored using Airyscan microscopy. The results showed that the control GFP-INT was hardly internalized into A375 cells after 3 h of incubation (Figure 6.1). However, when GFP-INT protein was encapsulated within vaults, it was internalized into the cells creating a punctate pattern of fluorescence, similar to the one reported in literature (Kickhoefer *et al*., 2005) (Figure 6.2). Moreover, its uptake into cells increased O/N, suggesting that the uptake may be time dependent (Figure 6.3). To demonstrate effective uptake of the GFP-INT carrying vault, cells were also pretreated with chlorpromazine hydrochloride for 2 h at 37°C, to block endocytosis (Galbiati *et al*., 2018), prior to addition of the GFP-INT-carrying vault (Figure S2). This confirms the ability of vaults to enter melanoma A375 cells, even without a specific cell targeting, and further supports the well-established idea (Champion *et al*., 2009; Kar *et al*., 2011, 2012; Wang *et al*., 2015) that vaults are efficient DDS.

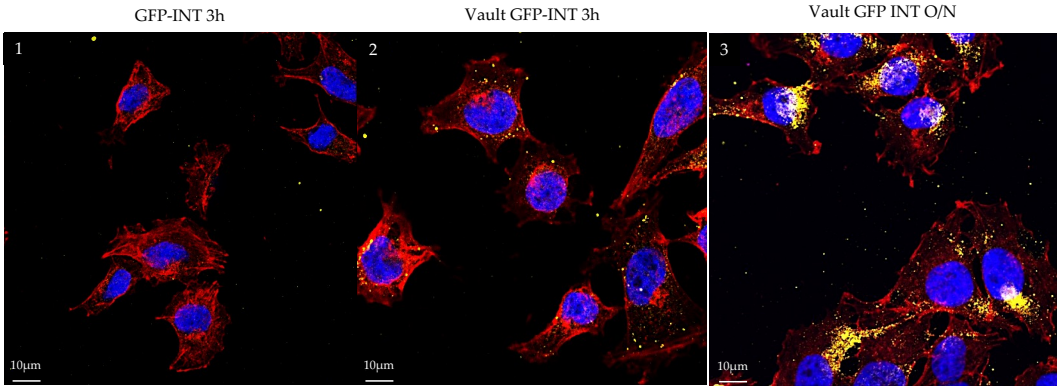


***Figure 6.*** *Vault-mediated GFP-INT endocytic uptake in A375, detected by Airyscan microscopy. The images show the merged signals of GFP-INT in yellow (detected by 1° antibody anti-GFP and 2° antibody anti chicken 488), actine and cytoskeleton stained with Alexa Fluor 647-coupled Phalloidin (red) and nuclei labeled with Hoechst Hoechst 33342 (blue). Other details are in Materials and Methods, Section*

## 3 Discussion

In the last decades, recombinant vaults have gained interest as promising nano-vectors for DDS thanks to all their features such as biocompatibility, particle size, dynamic structure, big cavity, and protection of the cargo molecules from external proteases (Frascotti *et al*., 2021; Muñoz-Juan *et al*., 2019). Among them, one of the interesting properties is their ability to encapsulate virtually any cargo protein by fusing the cargo to the INT peptide.

The association between INT-fused domain and vault have been fully studied in the literature, and different approaches have been proposed (Table 1). Co-translation of MVP and INT-fused protein have been proved to successfully enable the packaging of cargo protein into vault in insect cells (Kickhoefer *et al*., 2005). Yet this method requires the construction of respective baculoviruses and besides having been recently translated to mammalian cells (Martín *et al*., 2022), it only enabled the packaging into the $His_6$-tagged vault variant. Another packaging approach, based on the observation that co-translation is not required (Poderycki *et al*., 2006), foresees the mix of soluble fractions containing vault and INT-fused protein together, exploiting the natural "breathing" of vault in solution. Still, with this method, established with insect cells lysate (Poderycki *et al*., 2006) but used with yeast soluble fractions too (Wang *et al*., 2018), the purification of the final cargo-carrying vaults from the CFE requires the standard but onerous procedure of ultracentrifugation and sucrose gradient centrifugation. And even if the same loading strategy have been used with *E. coli* soluble fractions (Fernández *et al*., 2022), the produced vault-like particles not only were $His_6$-tagged but they didn't reflect the authentic morphology.

***Table 1:*** *Packaging methods of INT-fused protein described in literature.*

| Method | Vault | INT fused protein | Purification | Ref |
|---|---|---|---|---|
| Co - infection | Baculovirus-insect Mammalian | Baculovirus-insect Mammalian | Sucrose gradient IMAC | (Kickhoefer *et al*., 2005) (Martín *et al*., 2022) |
| Soluble fraction mix | Baculovirus-insect Yeast E. coli | Baculovirus-insect Yeast E. coli | Sucrose gradient Sucrose gradient IMAC | (Poderycki *et al*., 2006) (Wang *et al*., 2018) (Fernández *et al*., 2022) |

To overcome the drawbacks of the traditional procedure for vault production and purification, we set up a simpler and faster method, combining the production in *K. phaffii* with a purification based on SEC (as described in chapter 1). Consequently, in this chapter we demonstrated that vault obtained with our combined method preserved its natural ability of loading cargo protein. The reporter cargo protein, GFP-INT, was produced in *E. coli* M15 upon induction with IPTG overnight at 25°C instead of 37°C as initially tested. Production at 25°C yielded more soluble protein compared to production at 37°C. This result is coherent with previously reported research where production of a different variant of GFP-INT in *E. coli* was conducted at 20°C (Fernández *et al*., 2022), indicating that higher temperature might hamper the solubility of the recombinant GFP-INT.

To load GFP-INT into vault we took advantage of the dynamic structure of vault, by mixing the two purified protein. Two rounds of ultracentrifuge were enough to wash away all the a-specific bound GFP protein, used as control. Through densitometric analysis we determined the precise stoichiometry of GFP-INT protein in the vault, resulting in 20 copies of GFP-INT that can be loaded. Being the minimum INT binding domain an MVP monomer, the maximum number of INT binding sites per vault would be 78 like the number of monomers, but the size and any steric constraints that result from binding must be taken in consideration (Kickhoefer *et al*., 2005). For example, although vPARP copy numbers per vault are somewhat divergent (Poderycki *et al*., 2006; Yang *et al*., 2012), it has been estimated that around 8 copies of vPARP can interact with one single vault protein (Poderycki *et al*., 2006). Being vPARP (193 kDa) 4-fold bigger than GFP-INT (46 kDa) and considering vault internal volume of $5x10^7$ $Å^3$ (Kedersha & Rome, 1986) a maximum of 32 copies of GFP-INT could theoretically fit into vault in term of space. Evidence in literature reports that 1 mg of $His_6$-tagged vault can encapsulate approx. 15 μg of GFP-INT co-expressed with it in mammalian cells, resulting in a molar ratio around 3 of GFP-INT per vault (Martín *et al*., 2022). Our result of 20 copies of GFP-INT loaded, demonstrate not only that recombinant vault here produced maintained its carrier ability, but also that the packaging procedure here adopted is competitive with the other strategies reported in literature, allowing the loading of a number of

GFP-INT, 20, that is within the theoretical limit of space. Moreover, being able to load purified cargo into the vault could be advantageous: the INT-fused cargo could be modified or crosslinked with other non-protein molecules, allowing different molecules to be selectively targeted into the vault lumen. This perspective has been analyzed in the next chapter, where the possibility of having vault-mediated siRNA delivery has been addressed.

Lastly, we evaluate whether the human recombinant vault here produced from *K. phaffii* maintained the biological property of being internalized into cells and to release its cargo. Qualitative Airyscan microscopy analysis has been conducted on the metastatic melanoma A375 cell line, whose scientific relevance in this study is fully discussed in the next chapter, incubated with GFP-INT carrying vault. The presence of GFP-INT signal inside of the cells demonstrated that human recombinant vaults produced in *K. phaffii* are able to internalize and deliver the cargo protein to cancer cells, even without a specific targeting peptide. Evidence in the literature reports that recombinant vaults are taken up unspecifically by HeLa (Kickhoefer *et al*., 2005, Kickhoefer *et al*.,2009), glioblastoma cell lines by clathrin-mediated endocytosis (Galbiati *et al*., 2018) and recently by ovarian cancer cell (Martín *et al*., 2022). Yet in neither of these study, recombinant vault was produced in *K. phaffii* and purified with SEC. This confirms the ability of recombinant vaults to enter cells and thus further supports the well-described functionality (Champion *et al*., 2009; Kar *et al*., 2011, 2012; Wang *et al*., 2015) of recombinant vault as nanocarrier and efficient DDS.

## 4 Material and methods

### MVP cloning and vault production, purification, and storage

Authentic human MVP gene cloning and selection of best-producing clones has been previously described (Tomaino *et al*., 2023). Growth of the yeast clone expressing authentic vault and subsequent production of cell-free extracts was performed as reported in chapter 1. The purification of authentic vault was carried out according to the procedure we previously developed (Tomaino *et al*., 2023). It essentially consists of RNase treatment of cell-free

extracts, subsequent centrifugation to remove ribosomal contaminations, followed by size-exclusion chromatography (SEC) using Sepharose CL-6B as the matrix. To facilitate downstream processes, elution was performed at 4 °C using PBS instead of previously used Hepes buffer. Eluted protein was assayed by the bicinchoninic acid assay using the KIT QPRO-BCA (Cyanagen) and bovine serum albumin as the calibration standard.

## GFP-INT expression and purification

*Strain and growth media*

The *Escherichia coli* strain M15[pREP] (Quiagen), used as host strain, includes the pREP4 plasmid which confers kanamycin resistance and constitutively expresses the lac repressor protein encoded by the lacI gene. 2xTY medium (16 g/L tryptone, 10 g/L yeast extract, 5 g/L NaCl, 15 g/L Agar (solid medium only)) was used for maintaining the strain and for batch production in shake flasks with the addition of kanamycin (0.0025 g/L), to maintain the pREP4 plasmid and ampicillin (0.1 g/L) as described below to express the recombinant GFP-INT. The antibiotics ampicillin and kanamycin stock were filter-sterilized before being kept at −20 °C. *E. coli* M15 strains was stored at −80 °C in 30% glycerol.

*Plasmid construction and cloning*

To study protein encapsulation within vault, a "green fluorescence protein" has been used. The chosen one is the *Aequorea coerulescens* Green Fluorescence Protein (AcGFP1), an artificial derivative of the Aequorea coerulescens acGFPL gene (GenBank:AY151052), with spectral properties similar to those of Enhanced GFP (EGFP). AcGFP1 represents a better alternative for fusion applications because it is a monomer, compared to the *Aequorea victoria* GFP and EGFP, that form dimers (Chen *et al*., 2002; Jain *et al*., 2001). The coding sequence of AcGFP1 was fused to the interaction domain INT (GenBank accession No. AF158255, 162 amino acid, residues 1563 – 1724 of poly-(ADP-ribose) polymerase 4, PARP4 protein), which mediates the interaction of PARP4 with the MVP monomer, allowing PARP4 to be tightly bound within vault. AcGFP1-INT (henceforth referred to as GFP-INT) coding sequences were synthesized and cloned by Eurofins Genomics

(Ebersberg, Germany) in the pQE30 vector (3461 kbp, QIAGEN, Hilden, DE), between the BamHI and HindIII sites, in frame with a polyhistidine tag ($His_6$ tag) and under the control of the Lac promoter. The resulting plasmid expressing the recombinant protein GFP-INT (415 amino acids, molecular weight 46.3 kDa), carrying ampicillin resistance has been inserted into *E. coli* M15 according to the manufacturer's instructions.

*Recombinant proteins expression*

*E. coli* M15 cells carrying the plasmid pQE30/GFP-INT were inoculated in 20 mL of 2TY medium supplemented with 0.1 g $L^{-1}$ ampicillin and 0.025 g $L^{-1}$ kanamycin in 100 mL flask and were kept in an orbital shaker (200 rpm, 37°C) overnight. The pre-culture was then transferred in 400 mL of fresh medium and kept under agitation at 200 rpm at 37°C until mid-exponential phase was reached, around $OD_{600}$ 0.7. Then, production of recombinant GFP-INT was induced by isopropyl β-D-1-thiogalactopyranoside (IPTG) addition at a final concentration of 1 mM.

After induction, cells were incubated under two conditions, i.e., at 25 °C or at 37 °C, overnight (O/N) on an orbital shaker set at 200 rpm. To check protein expression, aliquots of 1 $OD_{600}$ from induced cultures were taken at 0 h and after the O/N incubation and centrifuged (16,000 x g, 5 min). Pellets were analyzed by SDS-PAGE.

*Cells lysis and solubility estimation*

Induced cells were collected in 100 mL aliquots and washed with cold Milli-Q water by repeated centrifugation in a JA-10 Beckman rotor at 4°C, 6000 x g for 15 min. The supernatant was discarded; the wet cells were weighted and stored at -80°C before being subjected to cell lysis.

Pellets were resuspended in binding buffer (5 mL/g wet weight; 20 mM $Na_2HPO_4$, 0.5 M NaCl, 10 mM imidazole, pH 7.4) with the addition of 1 mM lysozyme, Pierce™ Protease Inhibitor Mini Tablets EDTA-free according to the producer's recommendations. Cells were vortexed and placed in constant agitation for 30 min at RT before being disrupted by sonication in 8 cycles for 30 s (pulse ON/OFF: 30 s, 30% amplification, kept in ice). The CFE was obtained by centrifugation at 20,000 rpm for 30 min at 4°C.

To evaluate GFP-INT solubility at the tested temperatures, soluble (CFE) and insoluble fraction were loaded on SDS-PAGE. The pellets containing the insoluble fractions were resuspended with lysis buffer in the same volume as soluble fractions. 10 μg of total protein were loaded per lane.

*GFP-INT purification*

Recombinant GFP-INT was tagged to a histidine tail that possesses high affinity for nickel ions, therefore the purification was carried out using nickel-based IMAC with Nickel Sepharose 6 Fast Flow resin (Amersham Biosciences, slurry 20% ethanol) packed into a glass column (Healthcare Life Sciences, Ø 1.4 cm, 20 cm height).

The CFE from 200 mL of culture (around 3.5 g of wet weight) was filtered with 0.22 μm PES syringe filter (Sigma), loaded onto Nickel Sepharose 6 Fast Flow column (5 mL bed volume, previously washed with 5 bed volumes $H_2O$ MilliQ to remove ethanol present in the slurry and equilibrated with 5 bed volumes binding buffer), by adding 5 mL at a time, waiting 3 min, and then collecting the flowthrough. The loaded resin was then washed 4 times with 1 bed volume of washing buffer (20 mM $Na_2HPO_4$, 0.5 M NaCl, 20 mM imidazole, pH 7.4). To increase the purity of the eluted sample, the elution was carried out with an increasing and discontinuous imidazole gradient (100 mM, 150 mM, 200 mM, 250 mM, 300 mM, pH 7.4) collecting 1-mL fractions, one per each concentration, maintaining the highest concentration till the end. Protein amount in CFE and individual fractions was assayed by the bicinchoninic acid assay using the KIT QPRO-BCA (Cyanagen) and bovine serum albumin as the calibration standard. The eluted fractions were also analyzed with UV vis to measure GFP-INT concentration following the absorbance at 475 nm. Fractions containing the highest amount of pure protein were collected and washed with PBS in a protein concentrator (Pierce, 10 kDa cutoff) at 3200 x g until imidazole was removed. Recombinant GFP-INT both in the CFE and in the eluted fractions, has been detected and quantified by SDS-PAGE and western blot.

*Electrophoretic Analyses*

SDS-PAGE for GFP-INT protein detection was performed by using 4–20% Mini-PROTEAN® TGX Stain-Free™ Protein Gels (Bio-Rad). Samples were prepared by adding sample buffer (0.25 M Tris/HCl, pH 6.8, 2% SDS, 20% glycerol, 716.5 mM 2-mercaptoethanol, bromophenol blue) and then boiled at 100°C for 10 min to facilitate protein denaturation. Proteins were revealed using Chemi-Doc MP imaging system (Bio-Rad). GFP-INT identity was confirmed by Western blot analysis on PVDF membrane Immobilon (Millipore) using a primary anti-GFP antibody (rabbit monoclonal; 1:7500 Abcam) and an HRP secondary anti-rabbit antibody (1:15000; LI-COR Biosciences).

## GFP-INT protein encapsulation

The putative spontaneous encapsulation of GFP-INT protein into vault was assessed by mixing (4°C overnight) the two purified proteins (GFP-INT and vault) with GFP-INT in a molar excess of 100, in PBS 1 mM EDTA. As a control, the same quantity of purified vault (typically 1-1.5 mg) was mixed with GFP (his-tagged AcGFP1 previously produced and purified as GFP-INT, data not shown) in the same molar excess. After the incubation, the mixes were ultra-centrifuged at 100,000 x g for 1h 30 min (Beckman Ultima X, with 5 mL tubes) together with GFP and GFP-INT controls diluted in PBS at the same concentration. The pelleted samples (P100) were centrifuged at 5000 x g for 5 min (P100 S5) to remove possible insoluble aggregate and suitable amounts were loaded on 12% gel to be analyzed by Western Blot. To completely remove the excess of GFP and GFP-INT, either unbound or non-specifically bound, a second run of ultracentrifugation has been added. Pelleted samples, after being centrifuged 5000 x g for 5 min ($P100_2$ S5), were also analyzed by Western blot. MVP was detected using a primary anti-MVP antibody (rabbit monoclonal; 1:7500 dilution; Abcam) and an HRP anti-rabbit antibody (1:20000 dilution; LI-COR Biosciences). GFP and GFP-INT detection was carried out as described above. Fluorometric analysis to detect GFP and GFP-INT fluorescence at 520 nm have been conducted on the P100 S5 and $P100_2$ S5 of all the mixes, using Software SoftMax Pro on 96 MW plates.

*Densitometric assessment of stoichiometry binding ratio GFP-INT to vault.*

GFP-INT were mixed at different molar excess (5, 10, 25, 50) with a fixed amount of vault in PBS 1 mM EDTA and the molar ratios of loaded GFP-INT into vault were then determined as follows. After incubation overnight at 4°C, the mixes were ultracentrifuged twice at 100,000 x g for 1 h 30 min. The pellets ($P100_2$) resuspended in PBS EDTA and spun 5 min at 5000 g, were loaded on 4-20% stain-free gel to be subject to SDS PAGE as described in above.

GFP-INT and vault amounts were densitometrically estimated on SDS-PAGE by comparison with a standard curve prepared with known amounts of purified GFP-INT and vault. Samples and standards (measured by the BCA assay) to be quantitatively compared were run in the same gel and processed as a set. Densitometric analyses of the individual bands were performed with Image Lab™ software (version 6.1.0. built 7, Bio-Rad).

*Native agarose gel electrophoresis*

Pellet ($P100_2$ S5) and supernatant ($S100_2$) of vault and vault mixed with GFP-INT at different molar excess (5, 10, 25) were loaded on 1.5% agarose gel to conduct native electrophoresis. GFP-INT and vault aliquots were used as control lane. The gel was run 40 min at 90 V and was then analyzed with Chemi-Doc MP imaging system (Bio-Rad) to detect GFP-INT signal. After blotting the gel on PVDF membrane Immobilon (Millipore) vault signal was detected with western blot analysis as described in the paragraph above. Final images were analyzed with Image Lab™ software (version 6.1.0. built 7, Bio-Rad).

## GFP-INT cell internalization mediated by recombinant vaults.

*Cell cultures*

The metastatic melanoma cell line A375, a recognized cell culture model for this type of cancer, was kindly provided from Dr. Collignon (Institut Jacques Monod, Paris). Cells maintenance was conducted as described by (Dutriaux *et al.*, 2023). Briefly cells were grown in DMEM/F12 Glutamax (Invitrogen, Cergy-Pontoise, France) supplemented with antibiotics, penicillin (50 IU/mL), and streptomycin (50 mg/ mL), with 10% fetal bovine

serum at 37 °C in a humidified atmosphere with 5% $CO_2$. Cells were subcultured using trypsin/EDTA prior to confluence.

*Immunostaining and Airyscan microscopy*

Internalization of vaults loaded with GFP-INT in A375 melanoma cells was explored, by taking inspiration from experiments described by (Galbiati *et al*., 2018). A375 cells (1-2 x $10^4$) were seeded onto a 24x60 mm 10 well magnetic chamber (Chamlide®, Live Cell Instrument) and let grow overnight. The following days cells were incubated for different times (3 h and O/N) with 20 μg/mL of vault loaded with GFP-INT (20 molar excess, resulting in a concentration of GFP-INT around 50nM). As a control, cells were incubated 3 h with the same concentration of GFP-INT only. To demonstrate effective uptake of the GFP-INT carrying vault, cells were pretreated with chlorpromazine hydrochloride (14 μg/mL) for 2 h at 37°C, to block endocytosis, prior to addition of the GFP-INT -carrying vault (Figure S2). At the end of the incubation, cells were fixed in 4% formaldehyde solution and permeabilized with blocking solution (3% BSA 0.1% Triton X-100) 1 h 4°C to be then immunodecorated. For the immunostaining of GFP-INT, cells were incubated with the primary antibody chicken anti-GFP (1:2000 in blocking solution, Abcam) O/N at 4°C. Next, cells were washed twice with PBS and incubated with secondary antibody anti-chicken 488 (1:500 in blocking solution, Sigma Aldrich) together with Alexa Fluor 647-coupled Phalloidin (1:50, 2 h RT) to visualize F-actin. After the washes, the nuclei were labeled with Hoechst 33342 (1:2000). The Chamlide® wells were then further washed in PBS and treated with Fluoromount-G anti-fade (Southern Biotech). Images were acquired onto a Zeiss LSM980 spectral Airyscan 2 at ImagoSeine Imaging platform, with 40X glycerol (1.45 n) immersion objective (LC LCI Plan-Apochromat 40x /1.2 l mm Zeiss), using ZEN 2.6 pro software (Zeiss). Images were processed with Fiji for adjustment of contrast.

## Supplementary Information

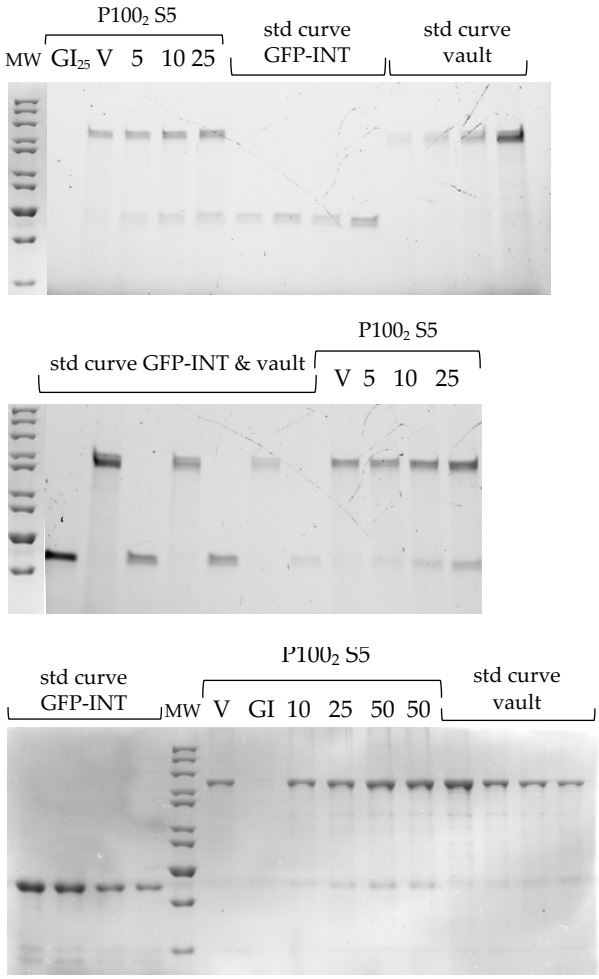


***Figure S1***. *Examples of SDS PAGE performed to assess the binding stoichiometry between GFP-INT and vault. V: P100$_2$ S5 vault, GI: P100$_2$ S5 GFP-INT, 5-10-25-50: P100$_2$ S5 of vault GFP-INT in different ratio, respectively 5, 10, 25 and 50.*

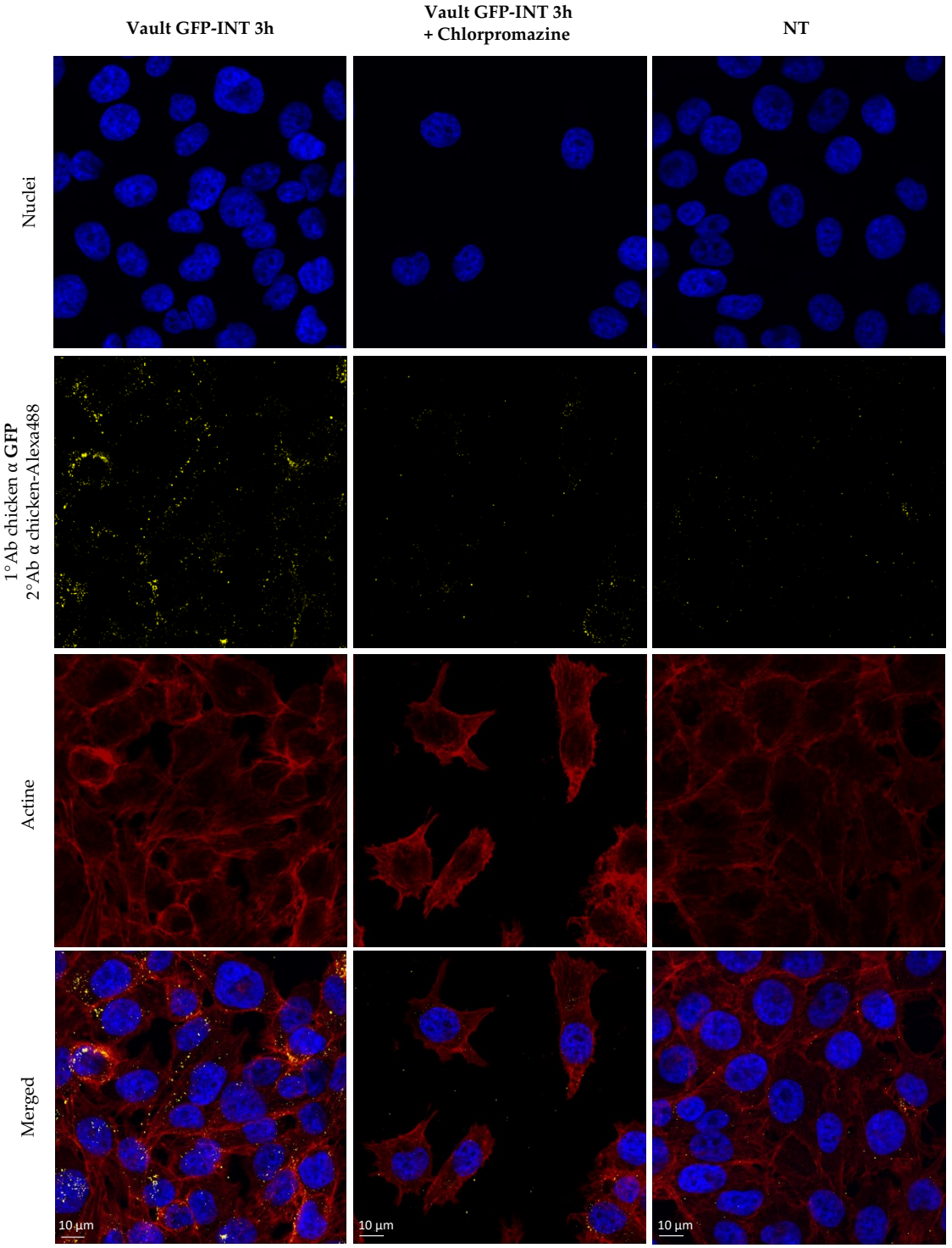
Vault GFP-INT 3h
Vault GFP-INT 3h
+ Chlorpromazine
NT
Nuclei
1°Ab chicken α GFP
2°Ab α chicken-Alexa488
Actine
Merged
10 µm
10 µm
10 µm

***Figure S2.*** *Airyscan microscopy analysis on A375 Melanoma cell line. Cells were pre-incubated in the presence or the absence of endocytosis inhibitor chlorpromazine for 2 h at 37 °C, then incubated with 20 μg/mL vault carrying GFP-INT (in 20 molar excess) for 3 h at 37 °C in complete medium. Chlorpromazine is a cationic amphiphilic compound that inhibits clathrin-mediated endocytosis, and it has been shown to inhibit vault uptake in different cell lines (Galbiati et al., 2018). The Figure shows split channels of nuclei (stained with Hoechst, in blue), GFP-INT (detected after incubation with 1° Ab chicken anti GFP, 2° Ab anti chicken-Alexa488, in yellow) and actine (labelled with Phalloidin 647nm, in red). Merged signals show that GFP-INT uptake occurred in present of vault, but decreases after pre-incubation with Chlorpromazine. The lower number of cells upon chlorpromazine incubation could be due to its toxicity towards cells. The experiment should be repeated with a lower concentration of chlorpromazine.*

## References

Broo, K., Wei, J., Marshall, D., Brown, F., Smith, T. J., Johnson, J. E., Schneemann, A., & Siuzdak, G. (2001). Viral capsid mobility: A dynamic conduit for inactivation. *Proceedings of the National Academy of Sciences*, *98*(5), 2274–2277. https://doi.org/10.1073/pnas.051598298

Champion, C. I., Kickhoefer, V. A., Liu, G., Moniz, R. J., Freed, A. S., Bergmann, L. L., Vaccari, D., Raval-Fernandes, S., Chan, A. M., Rome, L. H., & Kelly, K. A. (2009). A vault nanoparticle vaccine induces protective mucosal immunity. *PLoS ONE*, *4*(4). https://doi.org/10.1371/journal.pone.0005409

Chen, Y., Müller, J. D., Ruan, Q., & Gratton, E. (2002). Molecular brightness characterization of EGFP in vivo by fluorescence fluctuation spectroscopy. *Biophysical Journal*, *82*(1 Pt 1), 133. https://doi.org/10.1016/S0006-3495(02)75380-0

Dutriaux, A., Diazzi, S., Caburet, S., Bresesti, C., Hardouin, S., Deshayes, F., Collignon, J., & Flagiello, D. (2023). *LADON*, a natural antisense transcript of NODAL, promotes an invasive behaviour in melanoma cells. *Non-coding RNA*, *9*(6), 71.

Fernández, R., Carreño, A., Mendoza, R., Benito, A., Ferrer-Miralles, N., Céspedes, M. V., & Corchero, J. L. (2022). Escherichia coli as a New Platform for the Fast Production of Vault-like Nanoparticles: An Optimized Protocol. *International Journal of Molecular Sciences*, *23*(24), 15543. https://doi.org/10.3390/ijms232415543

Frascotti, G., Galbiati, E., Mazzucchelli, M., Pozzi, M., Salvioni, L., Vertemara, J., & Tortora, P. (2021). The vault nanoparticle: A gigantic ribonucleoprotein assembly involved in diverse physiological and pathological phenomena and an ideal nanovector for drug delivery and therapy. *Cancers*, *13*(4), 1–37. https://doi.org/10.3390/cancers13040707

Galbiati, E., Avvakumova, S., La Rocca, A., Pozzi, M., Messali, S., Magnaghi, P., Colombo, M., Prosperi, D., & Tortora, P. (2018). A fast and straightforward procedure for vault nanoparticle purification and the characterization of its endocytic uptake. *Biochimica et Biophysica Acta - General Subjects*, *1862*(10), 2254–2260. https://doi.org/10.1016/j.bbagen.2018.07.018

Gurskaya, N. G., Fradkov, A. F., Pounkova, N. I., Staroverov, D. B., Bulina, M. E., Yanushevich, Y. G., Labas, Y. A., Lukyanov, S., & Lukyanov, K. A. (2003). A colourless green fluorescent protein homologue from the non-fluorescent hydromedusa Aequorea coerulescens and its fluorescent mutants. *The Biochemical Journal*, *373*(Pt 2), 403–408. https://doi.org/10.1042/BJ20021966

Jain, R. K., Joyce, P. B. M., Molinete, M., Halban, P. A., & Gorr, S.-U. (2001). Oligomerization of green fluorescent protein in the secretory pathway of endocrine cells. *Biochemical Journal*, *360*(3), 645–649. https://doi.org/10.1042/BJ3600645

Kar, U. K., Jiang, J., Champion, C. I., Salehi, S., Srivastava, M., Sharma, S., Rabizadeh, S., Niazi, K., Kickhoefer, V., Rome, L. H., & Kelly, K. A. (2012). Vault nanocapsules as adjuvants favor cell-mediated over antibody-mediated immune responses following immunization of mice. *PLoS ONE*, *7*(7), 1–13. https://doi.org/10.1371/journal.pone.0038553

Kar, U. K., Srivastava, M. K., Andersson, Å., Baratelli, F., Huang, M., Kickhoefer, V. A., Dubinett, S. M., Rome, L. H., & Sharma, S. (2011). Novel ccl21-vault nanocapsule intratumoral delivery inhibits lung cancer growth. *PLoS ONE*, *6*(5). https://doi.org/10.1371/journal.pone.0018758

Kedersha, N. L., & Rome, L. H. (1986). Isolation and characterization of a novel ribonucleoprotein particle: Large structures contain a single species of small RNA. *Journal of Cell Biology*, *103*(3), 699–709. https://doi.org/10.1083/jcb.103.3.699

Kickhoefer, V. A., Garcia, Y., Mikyas, Y., Johansson, E., Zhou, J. C., Raval-Fernandes, S., Minoofar, P., Zink, J. I., Dunn, B., Stewart, P. L., & Rome, L. H. (2005). Engineering of vault nanocapsules with enzymatic and fluorescent. *Proceedings of the National Academy of Sciences of the United States of America*, *102*(12), 4348–4352. https://doi.org/10.1073/pnas.0500929102

Kickhoefer, V. A., Han, M., Raval-Fernandes, S., Poderycki, M. J., Moniz, R. J., Vaccari, D., Silvestry, M., Stewart, P. L., Kelly, K. A., & Rome, L. H. (2009). Targeting vault nanoparticles to specific cell surface receptors. *ACS Nano*, *3*(1), 27–36. https://doi.org/10.1021/nn800638x

Kickhoefer, V. A., Siva, A. C., Kedersha, N. L., Inman, E. M., Ruland, C., Streuli, M., & Rome, L. H. (1999). The 193-kD Vault Protein, VPARP, Is a Novel Poly(ADP-ribose) Polymerase. *The Journal of Cell Biology*, *146*(5), 917–928. http://www.jcb.org

Martín, F., Carreño, A., Mendoza, R., Caruana, P., Rodriguez, F., Bravo, M., Benito, A., Ferrer-Miralles, N., Céspedes, M. V., & Corchero, J. L. (2022). All-in-one biofabrication and loading of recombinant vaults in human cells. *Biofabrication*, *14*(2), 025018. https://doi.org/10.1088/1758-5090/ac584d

Mrazek, J., Toso, D., Ryazantsev, S., Zhang, X., Zhou, Z. H., Fernandez, B. C., Kickhoefer, V. A., & Rome, L. H. (2014). Polyribosomes are molecular 3D nanoprinters that orchestrate the assembly of vault particles. *ACS Nano*, *8*(11), 11552–11559. https://doi.org/10.1021/nn504778h

Muñoz-Juan, A., Carreño, A., Mendoza, R., & Corchero, J. L. (2019). Latest advances in the development of eukaryotic vaults as targeted drug delivery systems. In *Pharmaceutics* (Vol. 11, Issue 7). MDPI AG. https://doi.org/10.3390/pharmaceutics11070300

Poderycki, M. J., Kickhoefer, V. A., Kaddis, C. S., Raval-Fernandes, S., Johansson, E., Zink, J. I., Loo, J. A., & Rome, L. H. (2006). The Vault Exterior Shell is a Dynamic Structure that Allows Incorporation of Vault Associated Proteins into its Interior †. *Biochemistry*, *45*(39), 12184–12193. https://doi.org/10.1021/bi0610552

Rome, L. H., & Kickhoefer, V. A. (2013). Development of the Vault Particle as a Platform Technology. In *ACS Nano* (Vol. 7, Issue 2, pp. 889–902). American Chemical Society. https://doi.org/10.1021/nn3052082

Stephen, A. G., Raval-Fernandes, S., Huynh, T., Torres, M., Kickhoefer, V. A., & Rome, L. H. (2001). Assembly of Vault-like Particles in Insect Cells Expressing only the Major Vault Protein. *Journal of Biological Chemistry*, *276*(26), 23217–23220. https://doi.org/10.1074/jbc.C100226200

Tomaino, G., Pantaleoni, C., Ami, D., Pellecchia, F., Dutriaux, A., Barbieri, L., Garbujo, S., Natalello, A., Tortora, P., & Frascotti, G. (2023). Addressing Critical Issues Related to Storage and Stability of the Vault Nanoparticle Expressed and Purified from Komagataella phaffi. *International Journal of Molecular Sciences*, *24*(4). https://doi.org/10.3390/ijms24044214

Wang, M., Abad, D., Kickhoefer, V. A., Rome, L. H., & Mahendra, S. (2015). Vault Nanoparticles Packaged with Enzymes as an Efficient Pollutant Biodegradation Technology. *ACS Nano*, *9*(11), 10931–10940. https://doi.org/10.1021/acsnano.5b04073

Wang, M., Kickhoefer, V. A., Rome, L. H., Foellmer, O. K., & Mahendra, S. (2018). Synthesis and assembly of human vault particles in yeast. *Biotechnology and Bioengineering*, *115*(12), 2941–2950. https://doi.org/10.1002/bit.26825

Yang, J., Nagasawa, D. T., Spasic, M., Amolis, M., Choy, W., Garcia, H. M., Prins, R. M., Liau, L. M., & Yang, I. (2012). Endogenous Vaults and Bioengineered Vault Nanoparticles for Treatment of Glioblastomas. Implications for Future Targeted Therapies. In *Neurosurgery Clinics of North America* (Vol. 23, Issue 3, pp. 451–458). https://doi.org/10.1016/j.nec.2012.04.012

# Chapter 3

# Investigating the Untapped Potential of Vault Nanoparticles as a tool for siRNA Delivery

The following researchers also participated in the study:
Annie Dutriaux [2], Paolo Tortora [1], Domenico Flagiello [2], Gianni Frascotti[1]

[1] Department of Biotechnology and Biosciences, University of Milano-Bicocca, I-20126 Milano, Italy
[2] Université Paris Cité, CNRS, Institut Jacques Monod, F-75013 Paris, France

Manuscript in preparation

## Abstract

In the past decade, the rise of nucleic acid-based therapeutics has demanded better delivery, leading researchers to rely on NPs to tackle this issue. Leveraging recombinant vault particles as nano-drug delivery systems shows significant promise. This chapter explores the possibility of using vault as a tool for siRNA delivery. Our attempts focused on loading vault with siRNAs targeting *LADON*, a lncRNA known to promote tumor progression and invasion in melanoma. We pursued two strategies: one involves the potential loading of siRNA into the vault lumen by its chemical conjugation to INT domain. It requires the use of a suitable crosslinker allowing for a cleavable binding of INT-fused protein, GFP-INT in this case, and a modified siRNA that could be released in cells. So far, while crosslinking of GFP-INT was proved successful, the construction of the final product GFP-INT-siRNA is still on-going. The other approach entails the direct loading of siRNA into the vault. Endogenous vault particles carry untranslated RNAs (vRNA) into their lumen whose protection and stable is likely to be possible by the peculiar delta of positive charges inside the vault lumen. We explored the possibility of free fluorescent siRNA to be loaded and associated into the vault lumen. siRNA incubation with vault led to a partially co-migration with vault in native agarose gel, suggesting that an interaction could have occurred. We have demonstrated that recombinant vaults can mediate the delivery of naked siRNA molecules without additional formulation aiding the transfection, thus causing a biological effect.

**Keywords:** RNA therapeutics, siRNA delivery, vault nanoparticle, Melanoma, cancer treatment

# 1 Introduction

In the past few decades, gene therapy has emerged as an essential tool for the treatment of a wide range of diseases, including cancer, cardiovascular, neurological diseases (Blau & Springer, 1995; Jin & Ye, 2007; Mirón-Barroso *et al*., 2021). Gene therapy works by editing, replacing, or altering gene expression, introducing in cells, DNA or RNA therapeutic molecules. Although clinical trials are ongoing, and some treatments are already approved, achieving efficient delivery for gene therapeutic remains a challenge (Lu *et al*., 2016; Mirón-Barroso *et al*., 2021). Ideally, therapeutic nucleic acids should be targeted to specific cells, overcome physical cell barriers, avoid degradation, minimize toxicity, and be expressed or do their corrective function. Thus, the design of suitable delivery systems to accomplish a safe and effective delivery of gene therapeutics is highly demanded (Mirón-Barroso *et al*., 2021).

With the progress of nanotechnology and given the opportunities provided by gene therapy, NPs have attracted growing interest as tools for delivery of genetic elements as well as of other therapeutic molecules, thanks to their capability of encapsulating and protecting them en route to the respective cellular targets (Niazi, 2023; Roberts *et al*., 2020). A wide range of nanocarriers for nucleic acid drug delivery are at various stages of development including liposomes, polymeric NPs, and inorganic NPs that are among the most promising nanocarriers for mRNA delivery (Lu *et al*., 2016; Niazi, 2023).

In this context, naturally occurring bio-nanocapsules known as "vaults" are an attractive system candidate for the delivery (Iravani & Varma, 2023). Vaults are ribonucleoprotein NPs that possess a large internal cavity, making them suitable for encapsulating therapeutic molecules (Frascotti *et al*., 2021). Moreover, vault stability, monodispersity, non-immunogenicity, and biocompatibility make them ideal tool for the encapsulation and delivery of various cargo including drugs, probes as well as proteins, peptides, and possibly nucleic acids (Fernández *et al*., 2022; Frascotti *et al*., 2021; Martín *et al*., 2022; Muñoz-Juan *et al*., 2019) .

The use of recombinant vault particles as nano-drug delivery systems holds great potential for both drug and gene delivery. Indeed, evidence in

literature have underlined vault nanoparticle ability in aiding in the delivery of a cDNA plasmid (Lai *et al*., 2009; Yang *et al*., 2012). Nevertheless, the specific or direct loading into vault of nucleic acids molecules, even though potentially feasible as suggested by different vault features (discussed in this chapter), has not been accomplished or at least demonstrated yet.

To shed light onto this issue, we attempted the loading of siRNA into recombinant vault produced in *K. phaffii* and purified by our optimized technique as described in chapter 1.

Synthetic siRNAs are a type of RNA therapeutic of particular interest for the treatment of various infectious and genetic diseases including cancer (1, 2, 4) (Jeong *et al*., 2009; Roberts *et al*., 2020). These 19-23 base pairs double-stranded RNA molecules are the effector molecules of RNA interference (RNAi) pathways by which they mediate gene silencing via slicing of target mRNA transcripts or non-coding RNAs. The development of effective technologies for the delivery of siRNAs remains a major challenge. Different strategies have been proposed to enhance their delivery, including chemical modification of the backbone or terminal modifications (like phosphorylation of 5′ terminus of sense strand), bioconjugation with peptides, aptamers, antibodies, or sugars (GalNAc) together with various nanotechnology-based drug delivery systems such as dendrimers, micelles, carbon nanotubes, quantum dots, metal-based NPs, liposomes developed for cancer treatment (Chakraborty *et al*., 2017; Jain *et al*., 2018).

The specific target of the siRNA used in this study is *LADON*, a long non-coding RNA that plays a critical role in melanoma tumor progression and metastasis. The deletion of *LADON* in cells from the metastatic melanoma cell line A375 prevents them from undergoing the mesenchymal to amoeboid transition that is key to their adoption of an invasive behavior. Two anti-*LADON* siRNAs were found to reduce *LADON* expression in melanoma cells and to affect their behavior in the same way as the deletion of the gene (Dutriaux *et al*., 2023). One of these anti-*LADON* siRNAs has been used to test the ability of vault to target its delivery for therapeutic purposes.

To address the issue of loading siRNA vault we conducted two parallel strategies based on different considerations. It is worth reminding that the fusion of INT domain to proteins with therapeutic interest allows their

spontaneous encapsulation within vaults without affecting their biological activity (Frascotti *et al*., 2021). As extensively discussed in the second chapter, this mechanism has allowed the loading into vault of several proteins (Champion *et al*., 2009; Han *et al*., 2011; Kar *et al*., 2011, 2012; Muñoz-Juan *et al*., 2019). The idea of exploiting INT ability to enter and "dock" within the vault lumen, has been taken in consideration to sequester into vault compounds, not only drugs but inorganic molecules too, like Ni-NTA-nanogold (Goldsmith *et al*., 2007). Thus, a potential strategy for loading siRNA molecules into vaults could rely on the INT-fused cargo ability to be loaded into vault. Moreover, siRNA modification and conjugation to proteins have been already described and can be carried out with the use of a suitable crosslinker (Roberts *et al*., 2020).

Another approach relies upon the expectation of direct siRNA binding to the positively charged inner surface of the vault nanoparticle. Endogenous vault particles carry untranslated vRNAs in their lumen. The binding of vRNAs into vault is reported to be mediated by the protein TEP1 (Poderycki *et al*., n.d.). Despite this, stable association of RNA within the vault lumen is likely to be possible by the peculiar delta of positive charges inside the vault lumen (Ng *et al*., 2008a). For these reasons, we explored the possibility of siRNA to be loaded and associated into the vault lumen.

## 2 Results

### 2.1 Design of anti-*LADON* si*LADON*-Cy5 with intact activity

To investigate the possibility of loading siRNAs into vault, we designed a modified siRNA that could be used for both the chemical conjugation strategy and the direct interaction evaluation, thus carrying a fluorophore to follow its loading into vault and a functional group to be crosslinked. Among three already tested siRNA targeting *LADON* (Dutriaux *et al*., 2023), the 21-bp double strand sequence of the most efficient one in decreasing *LADON* expression was chosen. The final product, schematically represented in Figure 1A, was a 5′ Cyanine-5 labelled, 3′ amino modified siRNA targeting *LADON* (si*LADON*-Cy5). Notably, both modifications were inserted on the sense strand, to leave the antisense strand, stabilized by a phosphate on 5′

end (and carrying other modifications, under Dharmacon patent, that increase the specificity with its target), free to interact with the RISC complex.

RT-qPCR analysis was conducted to verify the ability of si*LADON*-Cy5 to decrease *LADON* expression, despite all the added modifications. Melanoma A375 cells were transfected (using Ribocellin as trasfectant agent) with anti-*LADON* si*LADON*-Cy5 or the control anti-*LADON* having the same sequence without the additional groups. Total RNA was extracted from both samples and from untreated cells as negative control. Comparison of *LADON* expression in untreated cells with the expression upon transfection with si*LADON*-Cy5, or siRNA, shown in Figure 1B, demonstrated that despite the modifications, si*LADON*-Cy5 maintained its activity.

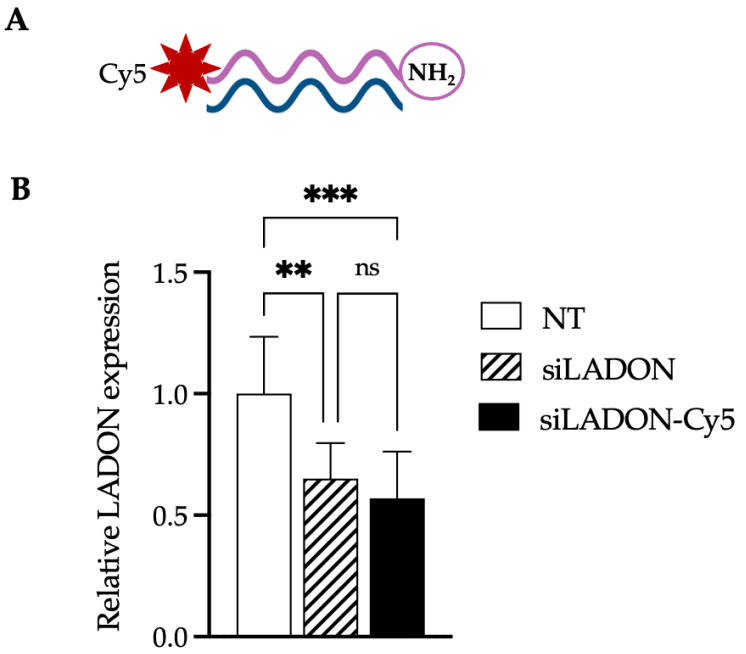


***Figure 1.*** *The modified siLADON-Cy5 anti LADON maintained its targeting ability. A) Schematic representation of the designed modified siLADON-Cy5 anti LADON carrying Cy5 on 5′ sense strand and $NH_2$ on 3′ sense strand. B) RT-qPCR measurements of LADON expression performed in metastatic melanoma cells (A375), after 72 h of culture. Comparison between the level of LADON expression in untreated cells, cells transfected with siRNA anti LADON (as control) and with siLADON-Cy5 here designed. LADON expression was normalized to that of endogenous GAPDH. Expression of LADON in the untreated cells is then normalized to 1. Histograms display mean values from three independent replicates. Error bars indicate std dev. The p-values were calculated by one-way ANOVA. ** $p < 0.01$, *** $p < 0.001$, ns: not significant.*

## 2.2 Chemical conjugation strategy

As mentioned in the introduction, a potential strategy for loading siRNA molecules into vaults relies on exploiting INT-fused cargo ability to be loaded into vault, thus seeing the INT domain as a carrier for the siRNA. This consideration, together with the technique outlined in chapter 2 for loading vaults with purified GFP-INT, presents an opportunity to establish the proof of concept of siRNA loaded into vault through a chemical conjugation with GFP-INT. To proceed with the chemical conjugation between GFP-INT, and si*LADON*-Cy5 just described in the previous paragraph, a suitable crosslinker is required.

Sulfosuccinimidyl-6-(3-(2-pyridyldithio) propionamido) hexanoate (sulfo-LC-SPDP) was chosen as crosslinker. This amine- and sulfhydryl-reactive heterobifunctional crosslinker can be used to form amine-to-amine or amine-to-sulfhydryl crosslinks among molecules, producing disulfide-containing linkages, which undergo spontaneous cleavage in the reducing intracellular milieu (Saito *et al*., 2003), thus releasing the linked molecule, in our case the siRNA. In this chapter, the followed strategy foresees an amine-to-amine crosslinking of GFP-INT and si*LADON*-Cy5, which first requires the modification of both molecules with the SPDP reagent. Figure 2 schematically represents the chemical crosslinking strategy between si*LADON*-Cy5 and GFP-INT. The first step consists in the crosslinking of GFP-INT amino groups with sulfo-LC-SPDP. Once obtained, the thiol activated GFP-INT (1) can be reduced with DTT to free the SH group (2). si*LADON*-Cy5 carrying the amino group is also crosslinked to sulfo-LC-SPDP (3) and then incubated with the reduced GFP-INT-SPDP. The final product (4) is ready to be loaded into vault, following the protocol described in chapter 2.

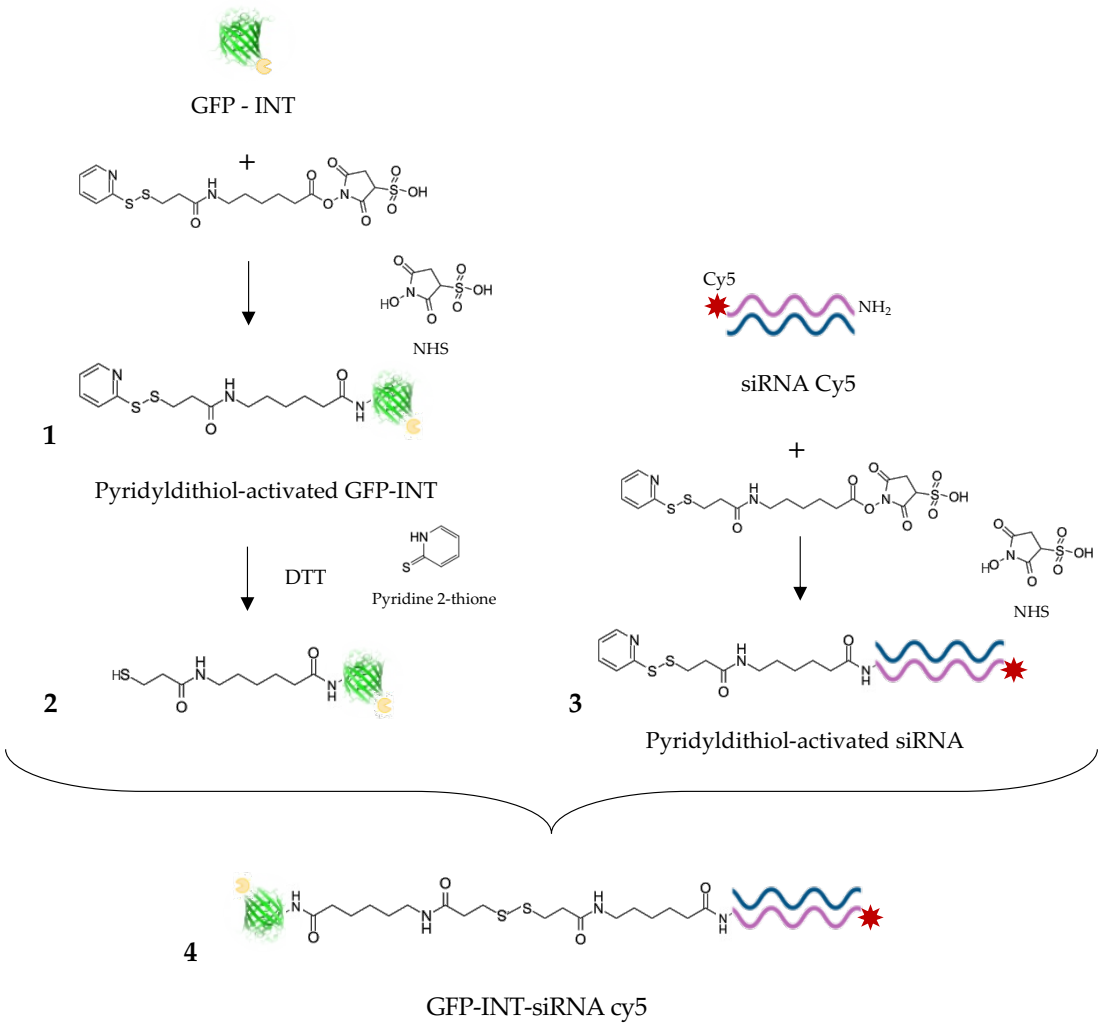


***Figure 2.*** *Schematic representation of chemical conjugation strategy. The formation of Pyridylthiol-activated GFP-INT (1) and Pyridylthiol-activated siLADON-Cy5 (3) occurs in parallel. The reduction of pyridylthiol on GFP-INT expose the thiol (2) that can react with Pyridylthiol-activated siLADON-Cy5 (3) to form the final compound (4).*

## 2.3 Thiol Activation of GFP-INT with sulfo-LC-SPDP

To obtain an amine-to-amine crosslinking of GFP-INT and si*LADON*-Cy5, the modification of both molecules with the sulfo-LC-SPDP reagent is required, thus introducing activated thiols on the surface. This is obtained through the reaction of the N-hydroxysuccinimide (NHS) ester moiety of sulfo-LC-SPDP with the pendant functional primary amine groups on the surface of both molecules.

To elucidate the 3D structure of GFP-INT and to estimate the number of available primary amine groups present on the surface that could be crosslinked, in silico 3D modelling were constructed, with the help of Dr. Vertemara. In the 3D structure of GFP-INT shown in Figure 3A1, as expected, the INT domain (in green) appears to be separated from the GFP core, in red. NHS ester crosslinking reagents like sulfo-LC-SPDP react principally with the α-amines at the N-terminals and the ε-amines of lysine residues (Hermanson, 2013). The filled structure (Figure 3A2) highlights the density of the INT-fused protein where lysine residues are colored in blue (positive) and negative charged aminoacids in red. The cysteine residues (in yellow), besides being potentially able to interact with the 2-pyridyldithio group of the crosslinker with their SH group, are not easily accessible from the surface, thus avoiding unwanted interaction with the crosslinker. On the other hand, between the ones exposed on the surfaces, around 5 – 6 lysine residues resulted not to be involved in ionic bonds with negative charged residues (Figure 3A3), thus they were considered available for the crosslinking. In the reaction, 1.5 mg of GFP-INT were mixed with a 10-fold molar excess of sulfo-LC-SPDP and incubated O/N at 4°C. Byproducts and the unconjugated sulfo-LC-SPDP were removed and the degree of SPDP molecules per GFP-INT was determined by measuring the concentration of pyridine-2-thione released from the crosslinker after incubation with DTT, as shown in Figure 3B. As shown in Figure 3D, a mean value of 2 sulfo-LC-SPDP crosslinker per GFP-INT was calculated.

To further validate the actual extent of GFP-INT conjugation with the crosslinker, a native gel electrophoresis was conducted. Protein mobility in native gel electrophoresis depends on protein size and charge. Taking this in consideration, we observed an increased mobility of GFP-INT-sulfo-LC-

SPDP on native gel, thus meaning that thiol-activation of GFP-INT could have neutralized the positive charges of the lysine residues, causing the faster migration on gel. Nevertheless, the folding stability of the protein seems not to be affected (data not shown) as well as its intrinsic fluorescence (Figure 3D). After the crosslinking, GFP-INT-sulfo-LC-SPDP was then reduced with DTT to be then linked to modified si*LADON*-Cy5.

## 2.4 Thiol Activation of si*LADON*-Cy5 and attempted crosslinking

As for GFP-INT, si*LADON*-Cy5 was incubated with sulfo-LC-SPDP to be crosslinked. Different ratios si*LADON*-Cy5 and sulfo-LC-SPDP were tested ranging between 5 and 20 molar excess of crosslinker. In all cases it was difficult to calculate the degree of sulfo-LC-SPDP per siRNA because the differences in the absorption at 343 nm after DTT incubation were barely detectable (Figure S1 A). NHS-ester reaction presents some drawbacks due to the poor stability of the NHS-ester in solution, which is pH dependent (Hermanson, 2013). Moreover, the concentration of the reacting molecules plays an important role (Solomatin & Herschlag, 2009). We thus tried increasing the pH of PBS-SPDP from 7.5 to 8 and we assembled the reaction with sulfo-LC-SPDP in 8-fold molar excess of siRNA at a concentration of 150 μM. A degree of sulfo-LC-SPDP per siRNA of 0.6 was calculated with absorbance assay and considering that each si*LADON*-Cy5 molecule carries 1 $NH_2$ group, this result sounded promising (Figure S1 B). Unfortunately, upon the loading on agarose gel of si*LADON*-Cy5 (Figure 3D lane 4) and si*LADON*-Cy5-sulfo-LC-SPDP (Figure 3D lane 5), no change emerged in the mobility of the two molecules, letting us doubt that si*LADON*-Cy5 was really crosslinked.

Nevertheless, we attempted the final crosslinking with the reduced form of GFP-INT-sulfo-LC-SPDP. However, on native agarose gel (Figure 3E) GFP-INT and the si*LADON*-Cy5 fluorescence are moving way apart one each other meaning that the crosslinking didn't occur. As GFP-INT crosslinking with the SPDP reagent was anyway successful, we are now exploring the possibility of conjugating the siRNA with a different crosslinker, while the re-setting of the reaction is ongoing.

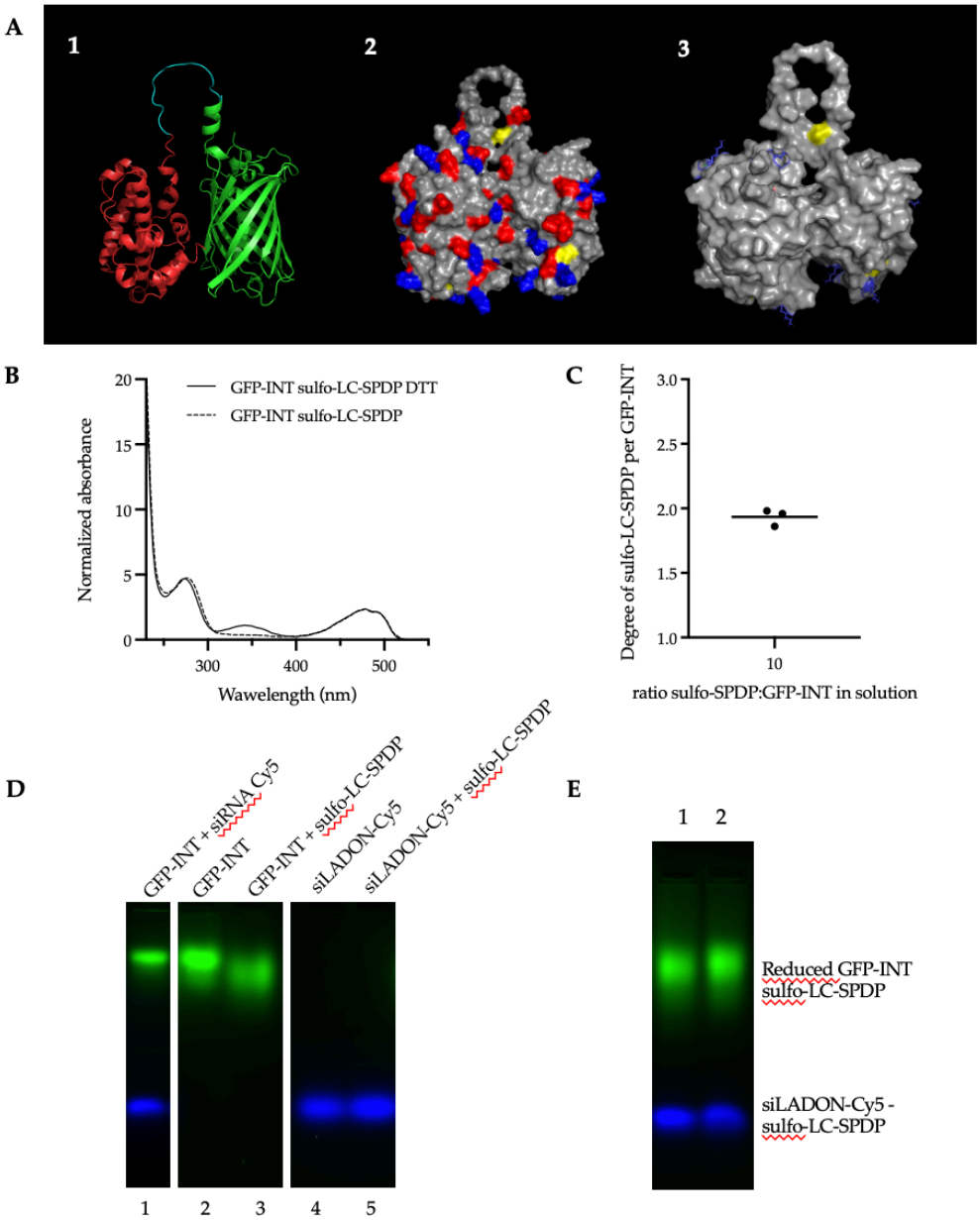


***Figure 3.*** *A) In silico 3D modelling provided by Dr. Jacopo Vertermara. 1) 3D structure of the fusion protein between GFP (in green) and INT domain (in red) connected by a linker. 2) Filled structure of GFP-INT. Blue: lysine residues (carrying NH2 group). Red: negative charged residues. Yellow: cysteine carrying thiolic group. 3) Filled structure of GFP-INT where the external available lysine residues are marked in blue B) Absorbance assay used to calculate the crosslinking degree of GFP-INT conjugation with sulfo-LC-SPDP. C) Degree of sulfo-LC-SPDP per GFP-INT over three biological replicates. D) Native 3% agarose gel. In green the fluorescence of GFP-INT, in blue siLADON-Cy5 fluorescence. The first lane is a negative control of the crosslinking where GFP-INT and siRNA are loaded on the gel together, without crosslinker. E) Attempted but failed crosslinked between reduced GFP-INT sulfo-LC-SPDP and siLADON-Cy5 modified. The numbers represent two replicates.*

## 2.5 Partial co-migration of si*LADON*-Cy5 with vault

The other strategy we adopted, to address the issue of loading siRNA into vault, was based on the idea that vault could naturally load siRNA molecules inside its lumen. Indeed, it is possible that a big complex like vault could naturally encapsulate inside its lumen molecules, preferably anionic, driven by the interaction with the positively charged interior (Ng *et al*., 2008).

To assess the direct loading of siRNA into vault, we incubated the Cy5 modified siRNA with vault and left O/N at 4°C. More precisely, we tested the direct interaction with two different molar ratios between vault and si*LADON*-Cy5, respectively 1:55 and 1:25 (Table 1, M&M section). The mixes were loaded on 1.5% agarose gel to conduct a native electrophoresis together with si*LADON*-Cy5 alone and vault alone as control. Vault was mainly retained in the well and signal on the western blot analysis presented the characteristic smear of vault mobility on native gel, similar to the one shown in chapter 2. Interestingly, besides signal of free si*LADON*-Cy5 was detected in all si*LADON*-Cy5-containing lanes (Figure 4A left panel), only when it was mixed with vault, a partial Cy5 signal detection was at the same height of vault signal. Thus, it seemed clear that the incubation of vault with si*LADON*-Cy5 causes a change in siRNA mobility resulting in a partial co-migration of si*LADON*-Cy5 with vault. In addition, when incubated with vault, the co-migrating signal of si*LADON*-Cy5 was similar in both molar excess (55 and 25), while vault loaded quantity was different (1.5 μg and 3 μg). To the lowest amount of vault is associated a higher amount of siRNA, proving that higher molar ratio between si*LADON*-Cy5 and vault leads to a bigger association si*LADON*-Cy5:vault.

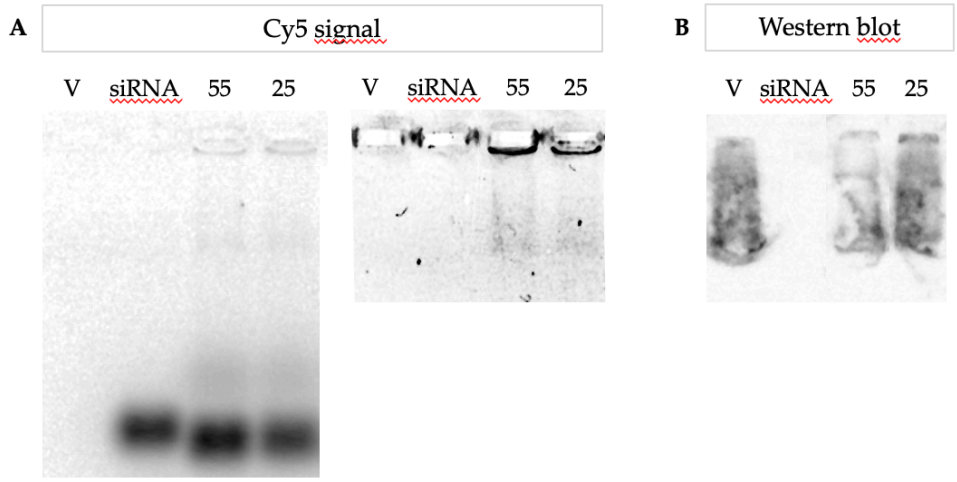


***Figure 4.*** *Native electrophoresis gel of siLADON-Cy5 + vault. siRNA: siLADON-Cy5 (10 pmol), V: vault (3 μg), 55 and 25 indicates respectively vault + siLADON-Cy5 in ratio 1:55 (10 pmol siRNA, 1.5 μg vault) and 1:25 (10 pmol siRNA, 3 μg vault), loaded after the incubation O/N at 4°C. A) Cy5 signal detection. Left) entire gel, right) gel has been cut to focus the attention on siLADON-Cy5: vault interaction and to increase the exposure on the ChemiDoc Image viewer. B) WB analysis with 1° antibody anti MVP and 2° antibody anti rabbit HRP.*

## 2.6 Vault si*LADON*-Cy5 transfection of melanoma A375 cells

Incubation of si*LADON*-Cy5 and vault resulted in a partial co-migration of si*LADON*-Cy5 with vault, indicating a possible association between the two molecules. To test whether this association could be functional and exploitable for the delivery of siRNA to cells, the melanoma cell line A375 was incubated with si*LADON*-Cy5-carrying vault (ratio 55:1), siRNA alone and siRNA with a transfectant. After 72 h of incubation cells were fixed and signal of Cy5-labeled siRNA was visualized through Airyscan microscopy. As shown in Figure 5.2, an increased intracellular fluorescence of Cy5 was detected in the cell transfected with si*LADON*-Cy5 carrying vault compared to siRNA alone (Figure 5.1). Si*LADON*-Cy5 transfection with Ribocellin, performed as control, showed a Cy5 signal inside of the cells comparable to that detected when cells were transfected with si*LADON*-Cy5 and vault (Figure S2). Preliminary measurement of the fluorescent signal of Cy5 inside the cells, performed with FIJI, confirmed the qualitative results that incubation of si*LADON*-Cy5 with vault mediates its uptake into cells (Figure 6).

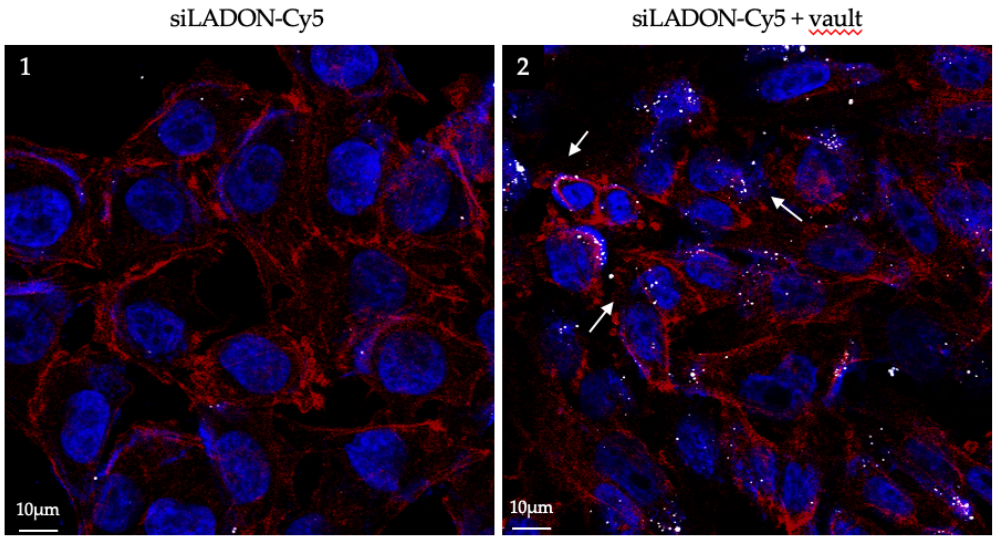


***Figure 5.*** *Airyscan microscopy on Melanoma A375 cells transfected with naked siLADON-Cy5 (1) and siLADON-Cy5 + vault (2). The images show the merged signals of siLADON-Cy5 (white) detected with Cy5 filter at 700 nm, actin and cytoskeleton stained with Alexa Fluor 647-coupled Phalloidin (red) and nuclei labeled with Hoechst 33342 (blue). siLADON-Cy5 is internalized in cells when associated with vault as indicated by white arrows. Other details can be found in Materials and Methods section.*

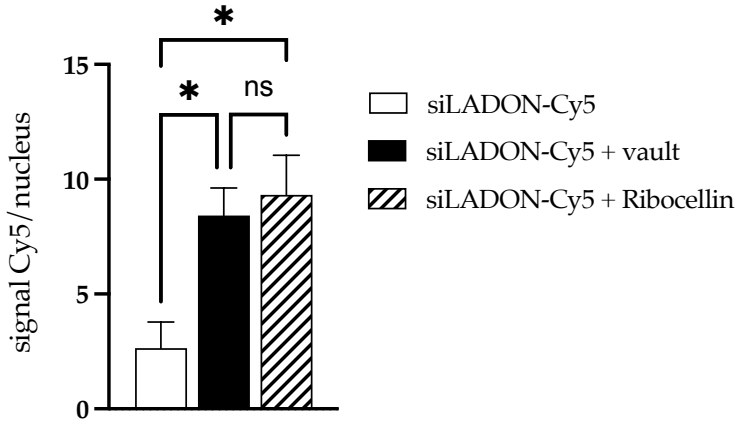


***Figure 6.*** *Preliminary measurement of siLADON-Cy5 signal vs nuclei. Semiautomatic counting of siLADON-Cy5 signal vs nuclei. Preliminary results show an increase of Cy5 signal vs nuclei when cells are treated with siLADON-Cy5 + vault and siLADON-Cy5 + Ribocellin, compared to the incubation with naked siLADON-Cy5. More information in M&M section. Statistical analysis with one-way ANOVA on two biological replicates. * $p < 0.05$; ns: non-significant.*

## 2.7 Vault mediates siRNA delivery causing a biological effect

Besides that, the qualitative Airyscan analysis conducted on A375 cells showed an increased signal of si*LADON*-Cy5 inside the cells when incubated with vault, we conducted RT-qPCR analysis of *LADON* expression to evaluate si*LADON*-Cy5 biological activity in causing a decrease in *LADON* expression upon transfection with vault. Melanoma A375 cells were incubated with si*LADON*-Cy5-carrying vault (ratios 55:1 and 25:1), siRNA alone and siRNA with a transfectant (Ribocellin). To see a biological effect, cells were lysed after 72 h of incubation and total RNA was extracted from all the samples and from untreated cells as negative control. Incubation with si*LADON*-Cy5 alone didn't cause a decrease in *LADON* expression, as for the control of untreated cells and of cells treated with vault alone (Figure S3). The level of *LADON* expression in cells treated with si*LADON*-Cy5 was set at 1 and compared with the level of *LADON* in the other samples. As shown in Figure 7 the incubation of vault with siRNA in ratio 1:55 causes a decrease of *LADON* similar to the effect of si*LADON*-Cy5 transfected with the transfectant Ribocellin. This difference in *LADON* expression was less evident for the treatment with vault si*LADON*-Cy5 ratio 1:25, although being still significant. Incubation ratio of 1:55 was already shown to allow a bigger association on native agarose gel. Moreover, considering that all samples were treated with the same amount of si*LADON*-Cy5 (20 pmol), the amount of vault when incubated with siRNA in 1:55 ratio was lower than the sample with ratio 1:25. Thus, cells treated with vault:siRNA ratio 1:55 were exposed to a lower number of vaults loaded with more si*LADON*-Cy5. In contrast, the ratio 1:25 delivered more vault to the cells with less si*LADON*-Cy5 loaded.

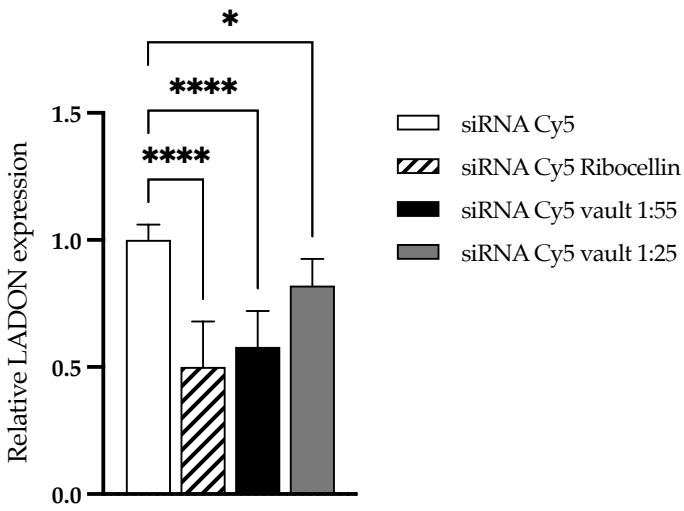


***Figure 7.*** *Vault mediates siRNA delivery causing a biological effect. RT-qPCR measurements of LADON expression in melanoma cells (A375), after 72 h of culture. Comparison between the level of LADON expression in cells transfected with siLADON-Cy5 anti LADON alone (as control), siLADON-Cy5 anti LADON with Ribocellin and siLADON-Cy5 incubated O/N with vault at two different molar ratio (1:55, 1:25). LADON expression was normalized to that of endogenous GAPDH. Expression of LADON in the untreated cells is then normalized to 1. Histograms display mean values from three independent replicates. Error Bars indicate std ved. The p-values were calculated by one-way ANOVA. * $p < 0.05$ **, **** $p < 0.0001$.*

## 3 Discussion

A variety of therapeutic delivery systems have been developed, including viruses, liposomes, polymers, proteins, and inorganic materials. While some of these systems have shown promises in cellular systems, their effectiveness in vivo has been limited by undesirable properties such as immunotoxicity, poor drug release, mis-targeting, and instability. Therefore, it is crucial to consider safety, capacity, targeting, and pharmacokinetics when evaluating a new therapeutic delivery system (Han *et al*., 2011). One potential option for therapeutic delivery is provided by vault NPs in that they possess several desirable characteristics for drug and gene delivery. They have a hollow, barrel-like structure with a large internal cavity, allowing for the encapsulation and transport of biomaterials. They are non-immunogenic and nontoxic. MVP can be easily modified at either end, offering flexibility for customization, as exemplified in Chapter 4. Furthermore, vault NPs have a dynamic structure that can "breathe" in solution, further enhancing their utility in drug/gene loading and delivery. Additionally, their low toxicity and immunogenicity make them an attractive option for therapeutic use (Muñoz-Juan *et al*., 2019).

Utilizing vault NPs for siRNA delivery holds great promise. SiRNAs are a powerful tool in gene therapy, but their efficient delivery to target cells remains a challenge (Roberts *et al*., 2020). In this study we investigated whether vault NPs could meet this challenge by encapsulation of siRNA within their internal cavity. The siRNA molecules that we designed, labelled with Cy5, and carrying a functional group, were able to decrease the expression of their target, *LADON*, in vitro, meaning that the added modifications didn't hamper its biological function.

*Loading of siRNA by chemical conjugation with INT-fused protein*

The encapsulation of siRNA into vault could be mediated by its interaction with the INT domain, derived from the vault-interacting protein vPARP. As reported in literature, INT domain can be exploited to encapsulate into vault a broad range of proteins (Muñoz-Juan *et al*., 2019), but also inorganic molecules such as gold NPs (Goldsmith *et al*., 2009). Thus, in this chapter we have set up a strategy for the chemical conjugation of siRNA

targeting *LADON* to an INT fused protein, GFP-INT, taking advantage of the technique outlined in chapter 2 for loading vaults with purified GFP-INT.

The crosslinker sulfo-LC-SPDP was chosen to link GFP-INT and siRNA by a disulfide bound. The reaction of GFP-INT with the SPDP reagent led to the crosslinking of 2 molecules of sulfo-LC-SPDP on the surface, in line with the number of lysine residues found available on the surface from a 3D modelling in silico of GFP-INT. The crosslinking of si*LADON*-Cy5 with SPDP reagent presented instead some obstacles. Reactions with NHS ester crosslinker are known to be challenging due to the poor stability of the NHS-ester in solution: NHS esters have a half-life on the order of hours at room temperature under physiological pH conditions. However, hydrolysis and amine reactivity both increase with increasing pH. For example, at 0°C and pH 7.0, the half-life is typically 4 to 5 h (Lomant & Fairbanks, 1976) while at pH 8.0 at 25°C it drops to 1 h (Staros, 1988). To try balancing these two reactions we increased the pH at 8, maintaining the incubation overnight at 4°C. Moreover, the concentration of the reacting molecules plays an important role especially for oligonucleotide crosslinking (Solomatin & Herschlag, 2009). Higher concentrations of RNA can result in better yields at the same dye-to-oligo ratio. We thus increased the concentration of si*LADON*-Cy5 at 150 μM, which allowed a crosslinking of 0.6 SPDP molecules for siRNA.

Despite this, the final crosslinking between si*LADON*-Cy5 – sulfo-LC-SPDP and GFP-INT carrying reduced sulfo-LC-SPDP has still to be achieved. For sure, reactions with even higher concentration of si*LADON*-Cy5 are likely to work better and are feasible, even if they imply the use of high amounts of si*LADON*-Cy5, resulting in unmanageable costs.

Moreover, the use of an alternative crosslinker has been proposed in order to avoid the cross-reaction between SPDP and reduced SPDP molecules and the step of DTT removal from the reduced GFP-INT SPDP. Indeed, the DTT used for reducing the SPDP reagent on one of the two modified molecules has to be removed, since the presence of a reductive agent like DTT could hamper the formation of the disulfide bond. Succinimidyl trans-4-(maleimidylmethyl)cyclohexane- 1-carboxylate (SMCC) crosslinker could be used to crosslink si*LADON*-Cy5 carrying $NH_2$ group. Then the crosslinked

si*LADON*-Cy5 could react with the reduced sulfo-LC-SPDP carrying GFP-INT, without removing the reductive agent DTT. Besides looking more viable, this reaction would lead to the formation of a more stable thioether bond between GFP-INT and si*LADON*-Cy5, thus preventing si*LADON*-Cy5 releasing in the cytosol.

Another option could be the design of a si*LADON*-Cy5 molecule carrying a sulfhydryl group (SH) instead of $NH_2$. In this way siRNA molecules could react directly with the 2-pyridyldithio group of the sulfo-LC-SPDP crosslinked on GFP-INT. Since SH group are reactive, this modification required the presence of a protective group. Thus, the si*LADON*-Cy5 would carry a more stable S-S that has to be deprotected afterwards. This step could cause damage to the fluorophore Cy5 linked at the 5′ terminal of the sense strand. To avoid this, two single strands siRNA could be designed both carrying one modification (either Cy5 or S-S). Being the antisense strand the one interacting with the RISC complex, modification on this strand is not recommended (Jeong *et al*., 2009). However, the integrity of the 5′- terminus, rather than that of the 3′-terminus of the antisense strand is essential for the initiation of an RNAi mechanism (18-20), thus leaving the possibility of modification on the 3′-terminus.

All of these considerations underline how challenging is the crosslinking of siRNA with molecules, making the entire strategy cumbersome.

*Exploring the putative ability of vault to load siRNA molecules*

Encapsulation of siRNA into vault might also be achieved by direct interaction between the two molecules. In general, recombinant vault nanoparticle has features that makes it an ideal tool for the delivery of drugs and nucleic acid like siRNA. Indeed, it is quite likely that a big complex like vault could naturally encapsulate nucleic acid molecules (Frascotti *et al*., 2021). This consideration is in line with its capability to open at low pH (Goldsmith *et al*., 2007), thus allowing the uptake of molecules, preferably anionic, driven by the interaction with the positively charged interior. Thus, as speculated by Ng and collaborators (Ng *et al*., 2008) polymeric, polyanionic compounds might represent ideal cargos to be loaded into vault, like DNA or RNA molecules. Nevertheless, the direct loading of nucleic acids

molecules in vault NP has not been reported yet, besides the well-known presence of untranslated vault RNA in the endogenous vault complex (Kickhoefer *et al*., 1998).

In this study we thus investigated whether the vault nanoparticle could be actually capable of loading nucleic acid molecules. To do so, we tested vault interaction with si*LADON*-Cy5, incubating the two molecules together at two different ratios (1:55 and 1:25). Observing the migration of vault and si*LADON*-Cy5 on native agarose gel we noticed a partial co-migration of si*LADON*-Cy5 with vault, more intense at a 55-fold molar excess of si*LADON*-Cy5 compared to 25. A similar co-migration pattern was observed incubating vault with another fluorescent siRNA (Cy3-siRNA), without the additional functional group, proving that the interaction was not due to the presence of the $NH_2$ group (Figure S4). The co-migration of si*LADON*-Cy5 with vault could be seen as a proof of vault–si*LADON*-Cy5 interaction. To test whether this interaction could lead to the delivery of siRNA into cells, we transfected melanoma cells A375 with si*LADON*-Cy5 vault. Analysis by qualitative Airyscan microscopy and RT q PCR, corroborated our hypothesis showing that vault alone can mediate the delivery of siRNA into A375 melanoma cells, at a similar extent as the commercial transfectant Ribocellin. Indeed, not only siRNA is transported inside the cells, but it also acts effectively on the expression of endogenous *LADON*.

Interestingly, a similar outlook has been reported by Lai *et al*., 2009 and then corroborated by Han *et al*., 2011. Vault carrying or in fusion with the membrane lytic domain of adenovirus protein VI has been demonstrated to facilitate the delivery of co-transfected calcium phosphate precipitated (CaPi) plasmid DNA to mouse macrophage cell. The presence of the pVI peptide enhanced the endosomal escape ability of vault that consequently co-delivered CaPi DNA through a nonspecific phagocytic uptake. Besides being important in understanding the mechanisms of drug releasing into the cells, these results do not corroborate possible direct interaction of the DNA with vault NPs. Moreover, the formulation of the DNA used in these studies (CaPi) provides an established classical method for transfecting plasmid DNA into mammalian cells, leaving to vault NPs the only task of aiding in the delivery.

Regarding our results, it is evident that further research is needed to elucidate the degree of interaction and extent of the association between vault and siRNA. It is still unclear whether this interaction could reach a saturation over which no more siRNA molecules could interact. For example, results obtained with the different molar excess of siRNA demonstrated that relative concentration of siRNA and vault in the pre-incubation mix might have an impact on the extent of the interaction. More precisely, in 1:25 and 1:55 mixes vault concentration was the same, while RNA molar excess was different even if it was still in the same total amount (50 pmol), thus the concentration of siRNA was affected and led to a more diluted mix 1:25 (Table 1). The results show that, besides having provided cells with the same amount (20 pmol) of siRNA, in the same final volume (100 μL of final mix was added to 1 mL culture medium) the degree of interaction with vault was different, thus leading to a better result with ratio 1:55. Figure S5 schematically explain this point.

With this study, we have demonstrated that recombinant vault particle can mediate the delivery of naked siRNA molecules without additional formulation aiding the transfection (as CaPi). For sure, to improve this delivery system, the insertion of pVI molecule on vault is needed and efforts have been made to create an engineered variant of vault carrying pVI domain. Unfortunately, the production of this variant has not been achieved in *K. phaffii* probably because of an issue in MVP assembly, but an alternative way to harness vault with pVI domain is proposed in chapter 4.

# 4 Materials and Methods

Production and purification of recombinant human vault have been conducted as in chapter 1 (Tomaino *et al*., 2023). Purification and storage in PBS were done to facilitate downstream processes, as reported in chapter 2. GFP-INT has been expressed in M15 *E. coli* and purified through IMAC as described in chapter 2.

## siRNAs design and transfection

The investigation on the loading of siRNA into vault was conducted following two strategies (chemical conjugation and direct interaction) both requiring the design of a suitable modified siRNA targeting *LADON*. Three anti-*LADON* siRNA have been proved to decrease *LADON* expression by Dutriaux *et al*., 2023. The targeting sequence of the most efficient siRNA among them was chosen as template. The design of the modified siRNA was conducted under technical advice of Dharmacon (Pittsburgh Pennsylvania, USA) customer service and the purchased final product was an RNAse-free, HPLC-purified 5′ Cyanine-5 labelled, 3′ amino modified siRNA targeting *LADON* (si*LADON*-Cy5). siRNA against *LADON* without modification was provided by Dr. Collignon (Institut Jacques Monod, Paris) and used as control. Sequences for siRNAs used in this study can be found in Table S1. For the standard transfection experiment, synthetic siRNAs were transfected with Ribocellin Transfection Reagent (Eurobio) according to the manufacturer's instructions. Lyophilized siRNAs were resuspended in RNase free water at a concentration of 100 µM and stored in aliquots at -80°C. RNA was quantified by absorbance at 260 nm using DS-11 spectrophotometer (DeNovix Inc, USA) in microvolume mode, with RNA setting. siRNAs were handled with gloves and plasticware and pipette tips were treated overnight with 0.1% diethyl pyrocarbonate (DEPC)-treated distilled water and autoclaved. Water used in all procedures was purified by passing through a MilliQ Millipore (Burlington, MA, USA) system.

## Chemical conjugation

*Crosslinker*

For the chemical conjugation of GFP-INT and si*LADON*-Cy5, the Sulfosuccinimidyl-6-(3'-(2-pyridyldithio)propionamido)hexanoate (sulfo-LC-SPDP) was chosen and purchased from CovaChem (Loves Park, IL, USA). Unlike NHS-ester reagents like SPDP (used in this study for preliminary experiments), sulfo-NHS-ester reagents like Sulfo-LC-SPDP are water-soluble and can be added directly to aqueous reaction mixtures. SPDP reagents are a group of amine- and sulfhydryl-reactive heterobifunctional crosslinkers that can be used to form amine-to-amine or amine-to-sulfhydryl crosslinks among molecules, producing disulfide-containing linkages that can be cleaved later with reducing agents such as dithiothreitol (DTT). Sulfo-LC-SPDP interact with amino residues through the N-hydroxysuccinimide (NHS) ester, while the 2-pyridyldithio group, reacts with sulfhydryls. In this study, the followed strategy foresees an amine-to-amine crosslinking of GFP-INT and si*LADON*-Cy5, which first require the modification of both the molecules with the SPDP reagent (Neurath & Strick, 1981).

*Thiol Activation of GFP-INT and siLADON-Cy5 with sulfo-LC-SPDP*

Activated thiols can be introduced on GFP-INT and siRNA through the reaction of the NHS ester moiety of sulfo-LC-SPDP with the pendant functional primary amine groups on the surface of both molecules. To estimate the number of available primary amine groups, present on the surface of GFP-INT, i*n silico* modelling of the 3D structure of GFP-INT have been constructed using Alphafold program and kindly provided as Pymol files by Dr. Jacopo Vertemara (University of Milan Bicocca). Around 6-7 lysine residues were colcated on the surfaces and were targeted for functionalization with sulfo-SPDP. For the reaction, a volume of 17.4 μL 0.020 M (0.35 μmol) sulfo-LC-SPDP was added to 1.5 mg of GFP-INT (0.035 μmol, 1.8 mg/mL), in order to have a 10-fold molar excess of sulfo-LC-SPDP over GFP-INT. 20 mM potassium phosphate, pH 7.5 with 150 mM NaCl and 1mM EDTA buffer (PBS-SPDP) was added to reach 1 mL of total volume giving a final concentration of 0.35 mM and 0.035 mM for GFP-INT and sulfo-LC-SPDP, respectively. The mix was kept under stirring overnight at 4 °C.

Byproducts and the unconjugated sulfo-LC-SPDP were removed with Pierce® protein concentrator 2 ml, 10 kDa cutoff (Thermo Scientific) using PBS-SPDP as final buffer. The final concentration of sulfo-LC-SPDP-conjugated GFP-INT (GFP-INT-SPDP) was quantified with Uv vis spectroscopy using DS-11 spectrophotometer (DeNovix Inc, USA) in microvolume mode. The degree of conjugation of sulfo-LC-SPDP on GFP-INT, as a mean of three biological replicates, was determined as described below.

As for GFP-INT, siRNA was incubated with sulfo-LC-SPDP to be crosslinked. This time, ratios between 5 and 20 molar excess of crosslinker have been tested and different siRNA concentrations were assayed (data not shown). Tipically, 1-5 µL of 20 mM sulfo-LC-SPDP was added to 100 µL of 100 µM siRNA and kept O/N at 4°C. Byproducts and the unconjugated sulfo-LC-SPDP were removed using Microcon spin filter 10 kDa (Merck), already reported to be used for siRNA purification (York *et al*., 2010). The degree of conjugation of sulfo-LC-SPDP on siRNA was determined as described below.

*Pyridine-2-Thione Assay to Determine Level of SPDP-modification*

The degree of sulfo-LC-SPDP derivatization was calculated following the protocol reported on the datasheet that consists in measuring the absorbance at 343 nm of pyridine-2-thione group before and after incubation for 15 min with DTT as reducing agent. The absorbance was measured with DS-11 spectrophotometer (DeNovix Inc, USA) in microvolume mode. Once the delta of absorbance has been measured, the molar ratio of sulfo-LC-SPDP to GFP-INT or siRNA can be calculated using the following equation:

$$Degree\ of\ derivatization = \frac{\Delta Abs\ 343\ nm}{8080} x\ \frac{MW\ of\ molecule}{{}^{mg}/_{ml}\ of\ molecule}$$

Where the value 8080 is the extinction coefficient for pyridine-2-thione at 343 nm: 8.08 x $10^3$ $M^{-1}$ $cm^{-1}$. MW of GPF-INT is 46000 g/mol, MW of si*LADON*-Cy5 is 14127 g/mol. GFP-INT concentration was determined from the absorbance at 475 nm (peak of absorption) according to the Lambert-Beer law, with 56000 $M^{-1}$ $cm^{-1}$ as the extinction coefficient of GFP-INT. siRNA concentration was measured with DS-11 spectrophotometer (DeNovix Inc, USA) with RNA setting program.

*GFP-INT / siLADON-Cy5 Crosslinking*

As mentioned above, to form amine-to-amine crosslinks using Sulfo-LC-SPDP reagent, the modification of both molecules with the SPDP reagent is required (Neurath & Strick, 1981). Having activated with thiol both GFP-INT and si*LADON*-Cy5, the reduction of the disulfide from one of the two modified molecules, causing the release of the pyridine-2-thione group, is necessary of obtain a free SH. Only at this point, after the removal of the released group and DTT, the resulting sulfhydryl-modified molecule is incubated with the SPDP-modified molecule to make the final conjugate as represented in Figure 2. Reduction of GFP-INT was performed in 20 mM potassium phosphate, pH 7.6, 150 mM NaCl, 1 mM EDTA and 50 mM DTT as reported in the datasheet. Excess of DTT was removed from GFP-INT-sulfo-LC-SPDP and si*LADON*-Cy5 – sulfo-LC-SPDP respectively using Pierce protein concentrator 10 kDa (Thermo Scientific) and Microcon 10 kDa (Merck).

*Agarose retention gel*

RNA retention gel electrophoresis was conducted on 3% native agarose gel using Tris-borate-EDTA (TBE) as running buffer. Aliquots of GFP-INT, siRNA and their Sulfo-LC-SPDP derivatized counterpart were loaded on gel to monitor their migration across the gel. A mix of GFP-INT and siRNA was used as a negative control of the crosslinking. Usually, 20 pmol of siRNA and 1 μg of GFP-INT were diluted with gel loading dye buffer (6X) containing 0.2% bromophenol blue and 1× TBE buffer and loaded on the gel. Gels were run 20 min at 90 V and were then stained with ethidium bromide (EtBr). EtBr signal and fluorescence of GFP-INT (excitation at 488 nm) si*LADON*-Cy5 (excitation at 650) were detected by ChemiDoc MP Image system (Bio-Rad). Final images were analyzed with Image Lab™ software (version 6.1.0. built 7, Bio-Rad).

## Vault and siRNA direct interaction

*Vault and siRNA incubation*

Preliminary experiment to evaluate the natural loading of siRNA into vault, was performed by mixing 0.9 pmol of vault (0.25 mg/ml) with 55 pmol of siRNA (100 μM) in a total volume of 28 μL and incubating the mix O/N at 4°C. The same incubation was performed with Cy3 labelled siRNA (siGLO RISC-Free Control siRNA, Dharmacon) that doesn't present the $NH_2$ modification. Notably, this siRNA is not targeting *LADON* or any other transcripts, thus has not been used for in vitro experiment. After the incubation, native electrophoresis was conducted to check the migration of vault and si*LADON*-Cy5. To better investigate the interaction between siRNA and vault, the same experiment was repeated with two different molar excess of si*LADON*-Cy5 per vault (55 and 25) and the following analyses were carried out on both two molar ratios. The pre-incubation mixes were assembles as shown in Table 1.

***Table 1.*** *Incubation mixes of vault with siLADON-Cy5 at the two different ratios 1:55 and 1:25. To maintain siLADON-Cy5 quantity fixed, we varied only the quantity of vault.*

| 1:55 | 1:25 |
|---|---|
| 50 pmol siRNA | 50 pmol siRNA |
| 0.9 pmol vault | 2 pmol vault |
| 28 μl tot | 62 μl tot |

*Native gel electrophoresis and western blot*

Native gel electrophoresis was carried out with 1.5% agarose gel using TBE buffer as running. All the support and plasticware were previously treated RNase AWAY™ (Thermofisher) to remove RNase contaminations. Typically, an aliquot containing 10-15 pmol of siRNA and 1.5 μg of vault, was diluted with gel loading dye buffer (6X) containing 0.2% bromophenol blue and 1× TBE buffer and loaded on the gel. Vault and siRNA aliquots were used as control lanes. Only in the preliminary experiments, samples were loaded in parallel in another gel stained with EtBr; this step was afterwards avoided to save materials. All gels were run 20 min at 90 V and were then analyzed with Chemi-Doc MP imaging system (Bio-Rad) to detect si*LADON*-Cy5

signal. Native agarose gel analysis has also been conducted on Cy3 labelled siRNA incubated with vault, to detect Cy3 signal. After blotting the gel on PVDF membrane Immobilon (Millipore), vault signal was detected with western blot analysis as described in chapter 2. Images were analyzed with Image Lab™ software (version 6.1.0. built 7, Bio-Rad).

*Cell cultures*

The melanoma cell line A375 was purchased from ATCC (Manassas, VA). Cells were grown in DMEM/F12 Glutamax (Invitrogen, Cergy-Pontoise, France) supplemented with antibiotics, penicillin (50 IU/mL), and streptomycin (50 mg/mL), with 10% fetal bovine serum at 37 °C in a humidified atmosphere with 5% $CO_2$. Cells were subcultured using trypsin/EDTA prior to confluence.

*Immostaining and Airyscan analysis*

For endocytic uptake evaluation of vault incubated with siRNA, A375 cells (1 x $10^4$) were seeded onto a 24x60 mm 10 well magnetic chamber (Chamlide®, Live Cell Instrument), grown overnight before incubation 20 h with vault preincubated with si*LADON*-Cy5 (ratio 1:55), si*LADON*-Cy5 alone or si*LADON*-Cy5 with Ribocellin. Notably, all samples were incubated with 20 pmol of si*LADON* in a final volume of 100 µL that was added to 1 mL of cell medium. At the end of the incubation, cells were fixed in 4% formaldehyde solution and permeabilized with blocking solution (3% BSA 0.1% Triton X-100) 1 h 4°C, to be then immunodecorated. Actin was labelled with Phalloidin-Alexa 555, nuclei stained with Hoechst. Image acquisition settings are described in chapter 2.

Preliminary measurements of si*LADON*-Cy5 signal vs nuclei have been conducted on IMAGEJ, following a semi-automatic procedure. The nuclei were identified by setting the threshold (21% threshold limit, size pixel$^2$: 10-infinity, circularity 0.05-1.00) on the binary 8-bit image of the Hoechst channel. The software is able to count the object (in this case nuclei). This procedure has been repeated to count the dots of si*LADON*-Cy5 signals (55% threshold limit, size pixel$^2$: 0.10-1.0, circularity 0.10-infinity). Next, number of dots were divided per number of nuclei.

*RNA extraction, reverse transcription (RT), Quantitative PCR (Q-PCR)*

For RNA extraction, cell aliquots (5 x$10^4$) were seeded in a 12-well plate and incubated O/N, at 37 °C in complete medium. Then, cells were transfected with siRNA alone, siRNA incubated with vault, vault alone and siRNA with Ribocellin Transfection Reagent (Eurobio). In all experiments, siRNA concentration in the well was 20 nM while the quantity of vault depended on the experiment. Two different ratios vault/si*LADON*-Cy5 were tested (1:55 and 1:25). The quantity of siRNA provided to the cells were the same for all the samples tested: aliquots of the pre-incubation mix (Table 1) containing 20 pmol of si*LADON*-Cy5 (with vault in different amounts) were brought to 100 µL and added to 1 mL of culture medium, thus maintaining constant the quantity of siRNA given to cells (Figure S5). Total RNA extraction (performed after 72 h of incubation), cDNA synthesis and Q-PCR were performed as described previously (Legent *et al*., 2006). For each RT PCR, values were normalized to the level of expression of the reference gene GAPDH. Primers for GAPDH and Nodal Exon2 are indicated in Table S1. The values were averaged over at least three independent measurements. Three independent RNA isolations were performed for all experiments.

*Statistical analysis*

Statistical analysis was performed using a one-way ANOVA for multiple comparisons. Data was collected and plotted using GraphPad Prism 6 (GraphPad Holdings, San Diego, CA, USA). P-values of less than 0.05 were considered statistically significant. Significance is indicated in the Figures as: * $p < 0.05$, ** $p < 0.01$, *** $p < 0.001$, **** $p < 0.0001$.

# Supplementary Information

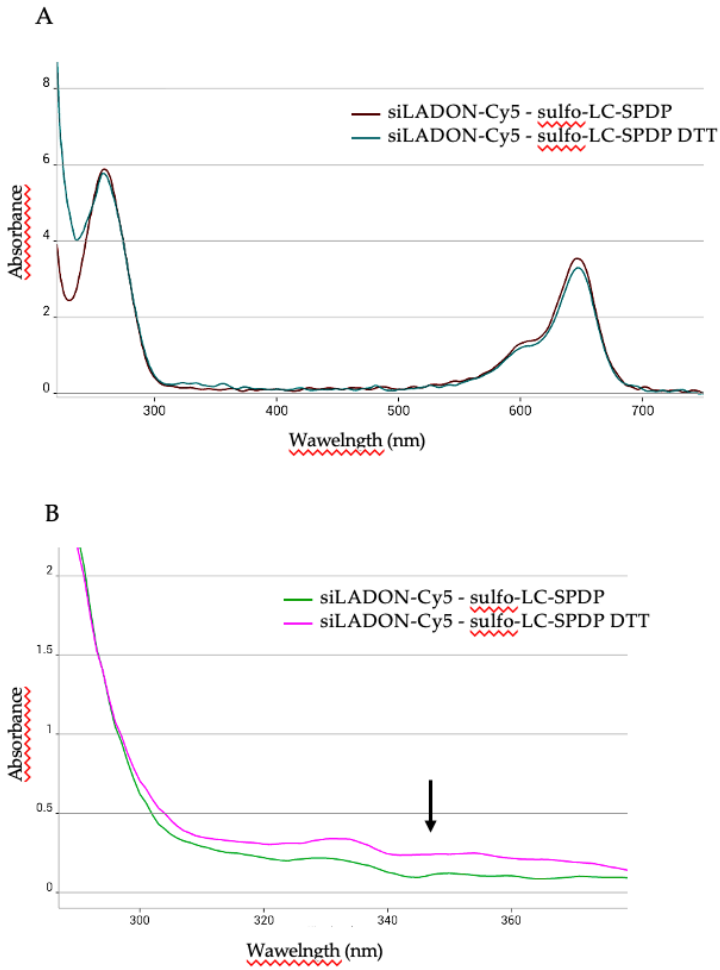


***Figure S1.*** *Absorbance assays on siRNA Cy5 sulfo-LC-SPDP. A) Example of barely detectable difference in the absorption upon reduction with DTT B) Changing pH and siRNA concentration, the absorbance at 343 of the reduced siLADON-Cy5 sulfo-LC-SPDP increased (black arrow), resulting in a degree of crosslinking of 1:0.6*

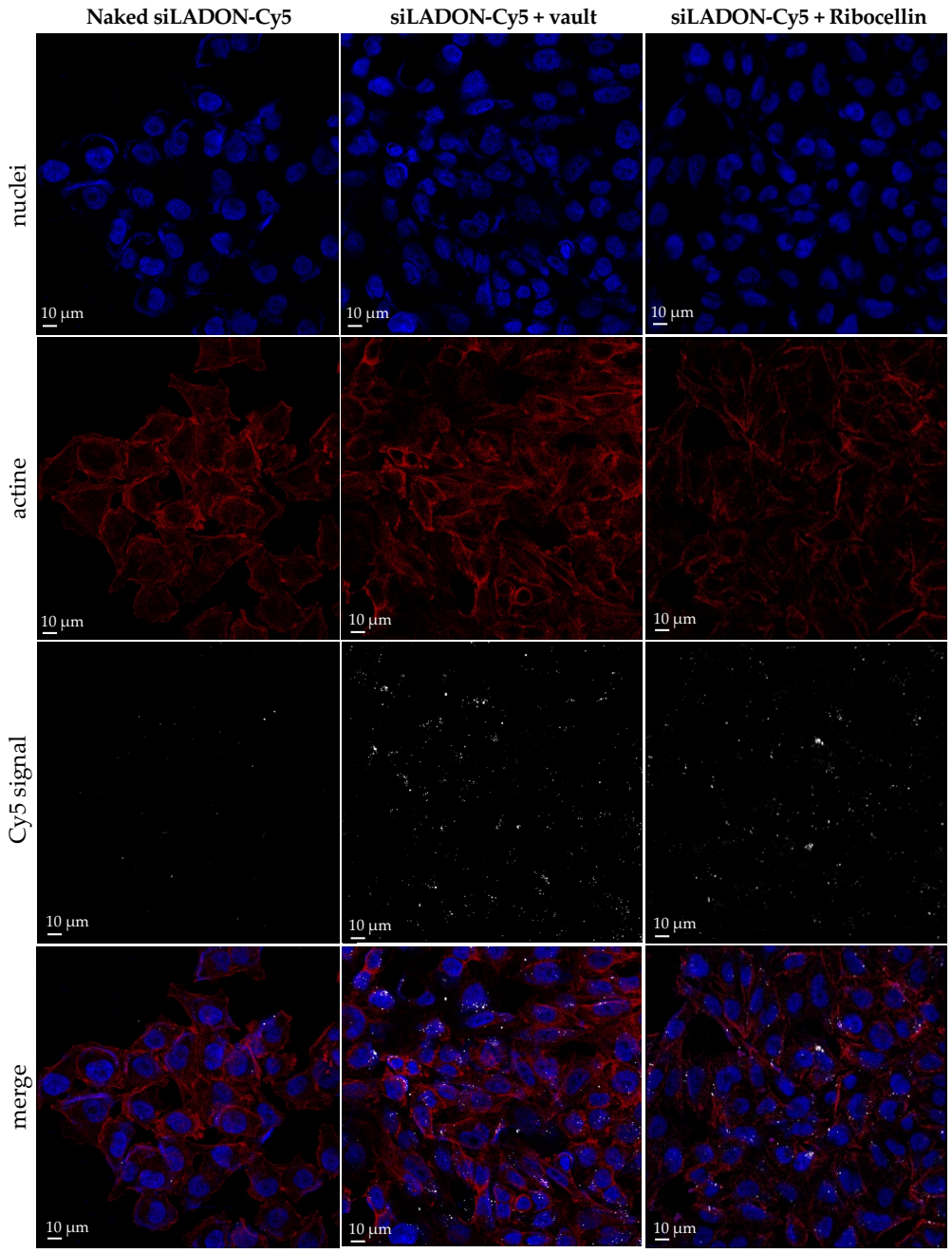


***Figure S2.*** *Airyscan microscopy on Melanoma A375 cells transfected with naked siLADON-Cy5 (left), siLADON-Cy5 + vault (center) and siLADON-Cy5 + Ribocellin (right). The images show split signals of nuclei labeled with Hoechst 33342 (blue); cytoskeleton stained with Alexa Fluor 647-coupled Phalloidin (red) and siLADON-Cy5 (white) detected with Cy5 filter at 700 nm. The last row shows merged signals. Signal of internalized siLADON-Cy5 when incubated with vault is comparable to the signal detected when cells are transfected with Ribocellin. Other details in M&M section.*

***Table S1.*** *qRT-PCR primers and siRNAs ordered and designed in this study*

| Amplicon/Name | Sequence |
|---|---|
| GAPDH | F- GAAGGTCGGAGTCAACGGATT<br>R- TGACGGTGCCATGGAATTTG |
| Nodal Exon2 | N2F - CTGCTTAGAGCGGTTTCAGATG<br>N2R - CGAGAGGTTGGAGTAGAGCATAA |
| siRNA *LADON* | CAGCUAAUGAGGAGUCAAAUU |
| Cy5 - anti *LADON* - 6NH2 siRNA | Sense: 5' Cy5.CAGCUAAUGAGGAGUCAAAUU.N6 3'<br>Antisense: 5' P.UUUGACUCCUCAUUAGCUGUU 3'<br>miRIDIAN, ON-TARGETplus, and Accell, siSTABLE product (Dharmacon) |

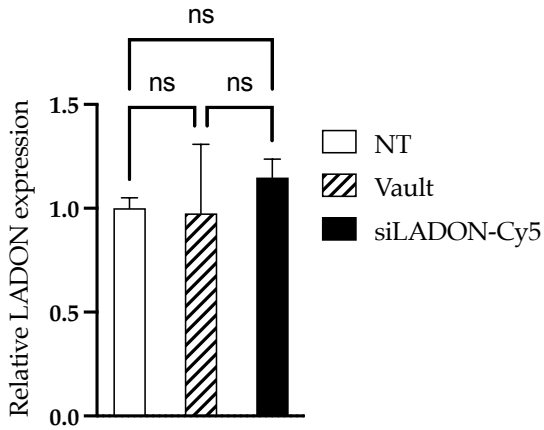


***Figure S3.*** *RT-qPCR showing non-significant differences in LADON expression in untreated cells (NT), cells incubated with naked siLADON-Cy5 and cells incubated with vault. Statistical analysis with one-way ANOVA on two biological replicates. ns: non significant.*

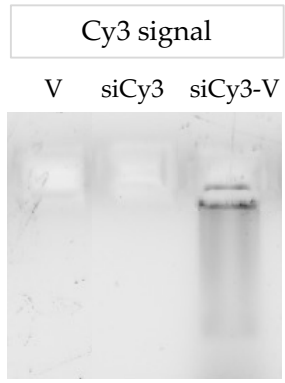


***Figure S4.*** *Native agarose gel (1.5%) electrophoresis of vault, Cy3 labelled siRNA (siCy3) and siCy3 incubated with vault (siCy3-V). Detection of Cy3 signal was performed with ChemiDoc Image system. More information in M&M section.*

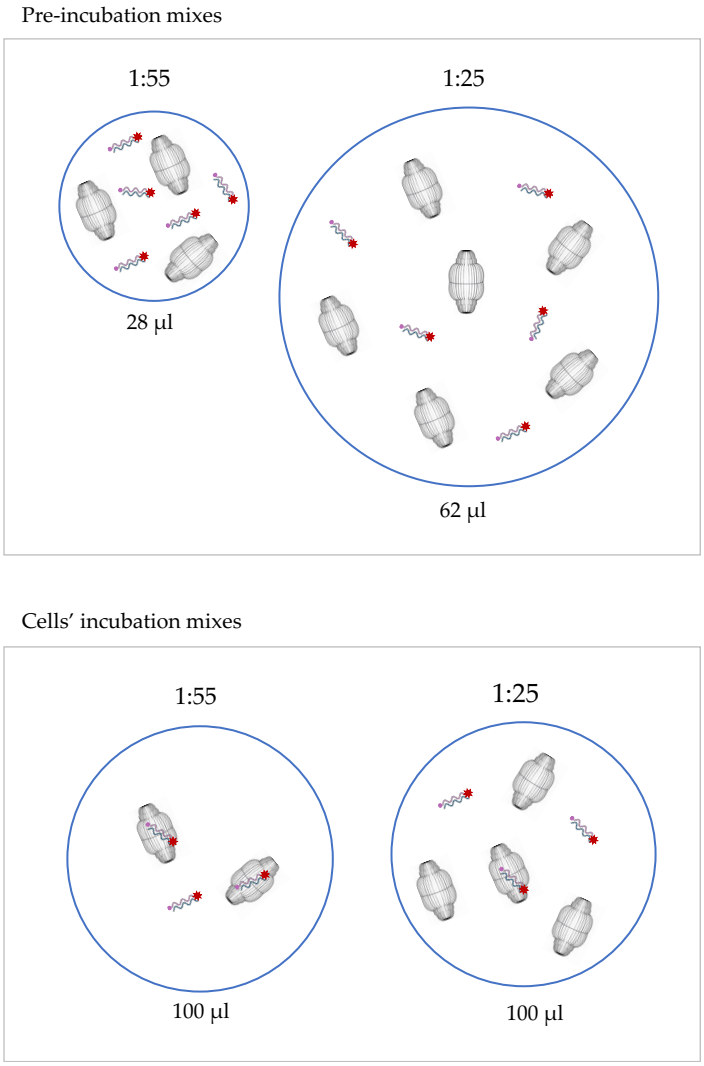


***Figure S5.*** *Graphical representation underlying the hypothetical role of the initial siRNA concentration in the mix. Upper panel: Illustration of the two pre-incubation mixes vault:siLADON-Cy5 1:55 and 1:25. The same amount of siLADON-Cy5 is present. Vault concentration is the same in the two mixes thus resulting in a less siLADON-Cy5 concentrated 1:25 mix (Table 1). The lower concentration could have hampered the loading of siLADON-Cy5 into vault NPs (besides the latter were more abundant compared to the mix 1:55. Thus, after the O/N incubation, the portion of siLADON-Cy5 associated with vault in the mix 1:55 is higher than in the other mix. Lower panel: cells' incubation mixes where an aliquot containing the same amount of siLADON-Cy5 (20 pmol) has been taken from both pre-incubation mixes. These aliquots were brought to 100 µL with cell medium, to provide to the cell the same volume. Notably, the aliquot from mix 1:55 is likely having higher siLADON-Cy5 associated with vault, thus resulting in a more efficient delivery of siLADON-Cy5 into cells that resulted in a more significant biological effect (Figure 6). Figure of vault and siLADON-Cy5 are not in scale.*

## References

Blau, H. M., & Springer, M. L. (1995). Gene Therapy — A Novel Form of Drug Delivery. *New England Journal of Medicine*, *333*(18), 1204–1207. https://doi.org/10.1056/nejm199511023331808

Chakraborty, C., Sharma, A. R., Sharma, G., Doss, C. G. P., & Lee, S. S. (2017). Therapeutic miRNA and siRNA: Moving from Bench to Clinic as Next Generation Medicine. *Molecular Therapy - Nucleic Acids*, *8*(September), 132–143. https://doi.org/10.1016/j.omtn.2017.06.005

Champion, C. I., Kickhoefer, V. A., Liu, G., Moniz, R. J., Freed, A. S., Bergmann, L. L., Vaccari, D., Raval-Fernandes, S., Chan, A. M., Rome, L. H., & Kelly, K. A. (2009). A vault nanoparticle vaccine induces protective mucosal immunity. *PLoS ONE*, *4*(4). https://doi.org/10.1371/journal.pone.0005409

Dutriaux, A., Diazzi, S., Caburet, S., Bresesti, C., Hardouin, S., Deshayes, F., Collignon, J., & Flagiello, D. (2023). *LADON*, a natural antisense transcript of NODAL, promotes an invasive behaviour in melanoma cells. *Non-coding RNA*, *9*(6), 71.

Fernández, R., Carreño, A., Mendoza, R., Benito, A., Ferrer-Miralles, N., Céspedes, M. V., & Corchero, J. L. (2022). Escherichia coli as a New Platform for the Fast Production of Vault-like Nanoparticles: An Optimized Protocol. *International Journal of Molecular Sciences*, *23*(24), 15543. https://doi.org/10.3390/ijms232415543

Frascotti, G., Galbiati, E., Mazzucchelli, M., Pozzi, M., Salvioni, L., Vertemara, J., & Tortora, P. (2021). The vault nanoparticle: A gigantic ribonucleoprotein assembly involved in diverse physiological and pathological phenomena and an ideal nanovector for drug delivery and therapy. *Cancers*, *13*(4), 1–37. https://doi.org/10.3390/cancers13040707

Goldsmith, L. E., Pupols, M., Kickhoefer, V. A., Rome, L. H., & Monbouquette, H. G. (2009). Utilization of a Protein "Shuttle" To Load Vault Nanocapsules with Gold Probes and Proteins. *Acs Nano, 3(10), 3175-3183*. https://doi.org/10.1021/nn900555d

Goldsmith, L. E., Yu, M., Rome, L. H., & Monbouquette, H. G. (2007). Vault nanocapsule dissociation into halves triggered at low pH. *Biochemistry*, *46*(10), 2865–2875. https://doi.org/10.1021/bi0606243

Han, M., Kickhoefer, V. A., Nemerow, G. R., & Rome, L. H. (2011). Targeted vault nanoparticles engineered with an endosomolytic peptide deliver biomolecules to the cytoplasm. *ACS Nano*, *5*(8), 6128–6137. https://doi.org/10.1021/nn2014613

Hermanson, G. T. (2013). The Reactions of Bioconjugation. *Bioconjugate Techniques*, 229–258. https://doi.org/10.1016/b978-0-12-382239-0.00003-0

Iravani, S., & Varma, R. S. (2023). Vault, viral, and virus-like nanoparticles for targeted cancer therapy. *Material Advances* https://doi.org/10.1039/d3ma00171g

Jain, S., Pathak, K., & Vaidya, A. (2018). Molecular therapy using siRNA: Recent trends and advances of multi target inhibition of cancer growth. *International Journal of Biological Macromolecules*, *116*, 880–892. https://doi.org/10.1016/J.IJBIOMAC.2018.05.077

Jeong, J. H., Mok, H., Oh, Y.-K., & Park, T. G. (2009). siRNA Conjugate Delivery Systems. *Bioconjugate Chemistry*, *20*(1). https://doi.org/10.1021/bc800278e

Jin, S., & Ye, K. (2007). *Nanoparticle-Mediated Drug Delivery and Gene Therapy*. https://doi.org/10.1021/bp060348j

Kar, U. K., Jiang, J., Champion, C. I., Salehi, S., Srivastava, M., Sharma, S., Rabizadeh, S., Niazi, K., Kickhoefer, V., Rome, L. H., & Kelly, K. A. (2012). Vault nanocapsules as adjuvants favor cell-mediated over antibody-mediated immune responses following immunization of mice. *PLoS ONE*, *7*(7), 1–13. https://doi.org/10.1371/journal.pone.0038553

Kar, U. K., Srivastava, M. K., Andersson, Å., Baratelli, F., Huang, M., Kickhoefer, V. A., Dubinett, S. M., Rome, L. H., & Sharma, S. (2011). Novel ccl21-vault nanocapsule intratumoral delivery inhibits lung cancer growth. *PLoS ONE*, *6*(5). https://doi.org/10.1371/journal.pone.0018758

Kickhoefer, V. A., Rajavel, K. S., Scheffer, G. L., Dalton, W. S., Scheper, R. J., & Rome, L. H. (1998). Vaults are up-regulated in multidrug-resistant cancer cell lines. *Journal of Biological Chemistry*, *273*(15), 8971–8974. https://doi.org/10.1074/jbc.273.15.8971

Lai, C.-Y., Wiethoff, C. M., Kickhoefer, V. A., Rome, L. H., & Nemerow, G. R. (2009). Vault Nanoparticles Containing an Adenovirus-Derived Membrane Lytic Protein Facilitate Toxin and Gene Transfer. *ACS Nano*, https://doi.org/10.1021/nn8008504

Legent, K., Mas, M., Dutriaux, A., Bertrandy, S., Flagiello, D., Piskur, J., & Silber, J. (2006). In Vivo Analysis of Drosophila Deoxyribonucleoside Kinase Function in Cell Cycle, Cell Survival and Anti-Cancer Drugs Resistance. In *Cell Cycle* (Vol. 5, Issue 7).

Lomant, A. J., & Fairbanks, G. (1976). Chemical probes of extended biological structures: Synthesis and properties of the cleavable protein cross-linking reagent [35S]dithiobis(succinimidyl propionate). *Journal of Molecular Biology*, *104*(1), 243–261. https://doi.org/10.1016/0022-2836(76)90011-5

Lu, H., Wang, J., Wang, T., Zhong, J., Bao, Y., & Hao, H. (2016). Recent Progress on Nanostructures for Drug Delivery Applications, *Journal of Nanomaterials*, https://doi.org/10.1155/2016/5762431

Martín, F., Carreño, A., Mendoza, R., Caruana, P., Rodriguez, F., Bravo, M., Benito, A., Ferrer-Miralles, N., Céspedes, M. V., & Corchero, J. L. (2022). All-in-one biofabrication and loading of recombinant vaults in human cells. *Biofabrication*, *14*(2), 025018. https://doi.org/10.1088/1758-5090/ac584d

Mirón-Barroso, S., Domènech, E. B., & Trigueros, S. (2021). Nanotechnology-Based Strategies to Overcome Current Barriers in Gene Delivery, *International Journal of Molecular Sciences,* https://doi.org/10.3390/ijms22168537

Muñoz-Juan, A., Carreño, A., Mendoza, R., & Corchero, J. L. (2019). Latest advances in the development of eukaryotic vaults as targeted drug delivery systems. In *Pharmaceutics* (Vol. 11, Issue 7). MDPI AG. https://doi.org/10.3390/pharmaceutics11070300

Neurath, A. R., & Strick, N. (1981). Enzyme-linked fluorescence immunoassays using β-galactosidase and antibodies covalently bound to polystyrene plates. *Journal of Virological Methods*, *3*(3), 155–165. doi.org/10.1016/0166-0934(81)90050-1

Ng, B. C., Yu, M., Gopal, A., Rome, L. H., Monbouquette, H. G., & Tolbert, S. H. (2008a). Encapsulation of semiconducting polymers in vault protein cages. *Nano Letters*, *8*(10), 3503–3509. https://doi.org/10.1021/nl080537r

Niazi, S. K. (2023). *RNA Therapeutics: A Healthcare Paradigm Shift*. https://doi.org/10.3390/biomedicines11051275

Poderycki, M. J., Rome, L. H., Harrington, L., & Kickhoefer, V. A. (2005). The p80 homology region of TEP1 is sufficient for its association with the telomerase and vault RNAs, and the vault particle. *Nucleic Acids Research, Vol. 33, No. 3* https://doi.org/10.1093/nar/gki234

Roberts, T. C., Langer, R., & Wood, M. J. A. (2020). Advances in oligonucleotide drug delivery. In *Nature Reviews Drug Discovery* (Vol. 19, Issue 10, pp. 673–694). Nature Research. https://doi.org/10.1038/s41573-020-0075-7

Solomatin, S., & Herschlag, D. (2009). Methods of site-specific labeling of RNA with fluorescent dyes. *Methods in Enzymology*, *469*, 47–68. https://doi.org/10.1016/s0076-6879(09)69003-0

Staros, J. V. (1988). Membrane-impermeant Cross-Linking Reagents: Probes of the Structure and Dynamics of Membrane Proteins. *Accounts of Chemical Research* **1988** *21* (12), 435-441 DOI: 10.1021/ar00156a001 .

Tomaino, G., Pantaleoni, C., Ami, D., Pellecchia, F., Dutriaux, A., Barbieri, L., Garbujo, S., Natalello, A., Tortora, P., & Frascotti, G. (2023). Addressing Critical Issues Related to Storage and Stability of the Vault Nanoparticle Expressed and Purified from Komagataella phaffi. *International Journal of Molecular Sciences*, *24*(4). https://doi.org/10.3390/ijms24044214

Yang, J., Nagasawa, D. T., Spasic, M., Amolis, M., Choy, W., Garcia, H. M., Prins, R. M., Liau, L. M., & Yang, I. (2012). Endogenous Vaults and Bioengineered Vault Nanoparticles for Treatment of Glioblastomas. Implications for Future Targeted Therapies. In *Neurosurgery Clinics of North America* (Vol. 23, Issue 3, pp. 451–458). https://doi.org/10.1016/j.nec.2012.04.012

# Chapter 4

# An engineered vault variant suitable for facile conjugation with finely adjustable amounts of antibodies or peptides

The following researchers also participated in the study:
Camilla Pantaleoni[1], Davide Cotugno[1,3], Davide Valsecchi[1], Carlo Santambrogio[1], Annalisa D'urzo[1] , Marco Vanoni[1,4], Paolo Tortora[1], Gianni Frascotti[1]

1 Department of Biotechnology and Biosciences, University of Milano-Bicocca, I-20126 Milano, Italy
2 Université Paris Cité, CNRS, Institut Jacques Monod, F-75013 Paris, France.
3 Current address : IEO, European Institute of Oncology IRCCS, 20139 Milan, Italy
4 ISBE-SYSBIO Centre of Systems Biology, Milan, Italy

Manuscript in preparation

## Abstract

To achieve specific targeting, NPs can be modified by addition of peptides and/or antibodies on their surface using different chemical functionalization methods. However, several of them are complex, time consuming and do not necessarily guarantee the correct orientation required for the targeting molecules, e.g. antibodies, to recognize a specific cell receptor. This issue has been addressed in the present chapter where we report the construction of a vault variant engineered to obtain a direct and oriented antibody-vault conjugation. This variant carries the 33-aa long, protein A-derived Z peptide, reported to tightly bind the Fc portion of human IgG1, genetically fused at the MVP C-terminus (vault-Z). This was produced in *K. phaffii*, purified following our optimized procedure, and displayed the same morphology and size of the wild type vault, as shown by DLS and TEM analyses. Moreover, an in-depth characterization of vault-Z/antibody affinity (performed by surface plasmon resonance analysis) and saturation profile (by densitometry on SDS-PAGE gels and mass spectrometry analyses), demonstrated that up to 10-12 antibody molecules per vault-Z were quantitatively and irreversibly bound. This was proved using Trastuzumab (Tz), a monoclonal antibody that recognizes HER2, a receptor1 overexpressed in several breast tumors. We thus observed that vault-Z conjugated to Tz was endowed with a substantially enhanced endocytosis by the HER2+ SKBR3 cell line, compared with the non-conjugated counterpart.

**Keywords:** targeted delivery, Z peptide, recombinant vault nanoparticle, mass spectrometry, surface plasmon resonance.

# 1 Introduction

The recent years have witnessed a growing impact of nanobiotechnologies in medicine, due to the remarkable therapeutic and diagnostic potential of NPs of diverse design [for extensive reviews see refs (Abdel-Mageed *et al*., 2021; Hong *et al*., 2020). They are frequently employed for the treatment of tumor diseases, being loaded for this purpose with specific anticancer drugs (Kim & Huang, 2012; Lohcharoenkal *et al*., 2014) and equipped with antibodies, proteins or peptides that selectively direct them to cancer cell lines (Avvakumova *et al*., 2014; D Friedman *et al*., 2013; Marques *et al*., 2020). In particular, this task may be fulfilled by a repertoire of antibodies that are capable of binding overexpressed cell surface receptors, which ensures a targeted delivery and endocytic uptake of the therapeutic agent (Schrama *et al*., 2006). Thus, a widely adopted strategy to actively target NPs to a specific cell line envisages their conjugation with specific antibodies (Marques *et al*., 2020). Several methods of functionalization are employed, including adsorption, covalent binding based on different protocols (e.g., using carbodiimide, maleidimide or click chemistry), or binding via adapter molecules. However, these methods suffer most often from major disadvantages in that they are complex and time consuming, and/or do not necessarily guarantee the correct orientation required for the antibody to effectively bind to the target molecule (Marques *et al*., 2020).

With regard to the nature of nano-sized materials available to date, there is a wide and diversified repertoire encompassing several varieties of NPs, such as metallic, magnetic, quantum dots, liposomes, as well as protein-based ones (Abdel-Mageed *et al*., 2021; Avvakumova *et al*., 2014; Hong *et al*., 2020). In particular, in the last decade the latter have gained a growing interest as drug delivery systems, due to the several advantages they offer as compared to the others, particularly in terms of lack of toxicity or immunogenicity, biodegradability, biocompatibility, size homogeneity, stability(Jain *et al*., 2018).

In this context, the vault NP stands out for its unique properties. Vaults are natural ribonucleoproteins found in several eukaryotes (Frascotti *et al*., 2021; Kedersha & Rome, 1986). In their molecular assembly, the 97-kDa major vault protein (MVP) is present in 78 copies and generates a barrel-like,

natural "nanocapsule" consisting of two symmetrical halves whose C-termini form two protruding caps at both ends (Anderson *et al*., 2007; Kedersha *et al*., 1991). Vaults also enclose other molecular components, i.e., the 193 kDa vault poly(ADP-ribose) polymerase, the 290 kDa telomerase-associated protein-1 (TEP1) and one or more small untranslated RNAs (Kickhoefer *et al*., 1993, 1998; Kickhoefer, Siva, *et al*., 1999; Kickhoefer, Stephen, *et al*., 1999; Van Zon *et al*., 2001). Overall, the molecular mass of vault particles amounts to about 13 MDa, their size is 72.5 × 41 × 41 nm and the internal cavity volume is $5 \times 10^4$ $nm^3$. A well-assembled vault structure can be also produced by expressing the sole MVP, as originally shown in insect cells (Mrazek *et al*., 2014; Stephen *et al*., 2001). Although the physiological roles of this nanocomplex is only partially understood, numerous reports highlight, nevertheless, its involvement in several pro-survival and cytoprotective actions (Berger *et al*., 2009; Frascotti *et al*., 2021).

Thanks to the aforementioned characteristics, this macromolecular assembly has attracted a remarkable interest as a tool for drug/gene delivery often directed to cancer cell lines (Muñoz-Juan *et al*., 2019). Actually, it was shown that the sole MVP can assemble into "empty" vault, which not only can accommodate large amounts of cargo molecules but can be also targeted to specific cell surface receptors, provided it is bound to suitable peptides or antibodies via genetical (Kickhoefer *et al*., 2009) or chemical approaches (Benner *et al*., 2017). Of remarkable interest, in this respect, is the development of a vault variant carrying at the MVP C-terminus a staphylococcal protein A-derived sequence referred to as Z domain (vault-Z and MVP-Z, respectively), 33 residues in length, which has been reported to tightly bind the Fc portion of human IgG1 (Braisted & Wells, 1996a; Kickhoefer *et al*., 2009). The resulting recombinant vaults expose these domains at both caps, thus enabling conjugation with any desired antibody (Kickhoefer *et al*., 2009). Besides tight antibody binding, these molecular assemblies offer therefore the remarkable advantage of ensuring the proper antibody orientation, whereby the antigen-binding sites are fully available to the interaction with the cognate antigen, thus circumventing one major drawback associated with many other conjugation methodologies (Marques *et al*., 2020).

Based on these premises, we expressed human vault in the methylotropic yeast *Komagataella phaffii* (formerly *Pichia pastoris*) (Tomaino *et al*., 2023) following a previously described protocol (Wang *et al*., 2018). With a view to explore its potential as a platform to be variously harnessed to optimize drug delivery, we then produced pure protein following a procedure consisting of a RNase pretreatment of cell-free extracts followed by size exclusion chromatography (SEC) (Tomaino *et al*., 2023). This, in turn, represents a modification of the one formerly developed in our lab starting from transfected insect cell extracts (Galbiati *et al*., 2018).

Here, we have cloned, expressed in *K. phaffi* and purified the human vault-Z variant, aiming at undertaking an in-depth characterization of its antibody binding affinity and saturation profile. The investigation was carried out by conjugating vault-Z with Trastuzumab (Tz), a monoclonal antibody that recognizes the human epidermal growth factor receptor 2 (HER2 receptor) and is overexpressed in a number of breast tumors (Hudis, 2007). We thus found out that up to at least 10 antibody molecules per vault-Z were bound in a virtually irreversible and quantitative fashion, whereas the affinity declined at higher molar ratios.

Lastly, we investigated whether antibody conjugation increased cell targeting of the vault, by directing the nanoassembly to a mammary carcinoma cell line (SKBR3). As the constant portion (Fc) antibodies domain also bound irreversibly to vault-Z, we used it as a molecular scaffold for fluorofore vault labelling, thus avoiding vault-Z manipulation and the inherent stability-related issues. Specifically, vault-Z was conjugated to Alexa 488-labeled Fc. Cytofluorimetric analyses have been conducted on SKBR3 cells incubated with vault-Z carrying labeled Fc alone or with Tz. The results show that Tz conjugation substantially increased vault-Z endocytosis as shown by cytofluorimetric analyses.

## 2 Results

### The production and purification vault-Z variant

The protocol for authentic vault purification from *K. phaffi* and an in depth-characterization of its purity and properties have been previously described in chapter 1 (Tomaino *et al.*, 2023). In particular, the purification procedure relies upon an RNase pretreatment of cell-free extracts followed by a SEC using Sepharose CL-6B as the matrix. Here, the same protocol has been used for vault-Z production and purification. Purified fractions were subjected to SDS-PAGE and western blot analysis to confirm identity and purity of the protein (Figure S1), which were also checked by TEM and DLS (Figure 1): These analyses displayed the expected morphology and one, essentially symmetrical peak, respectively.

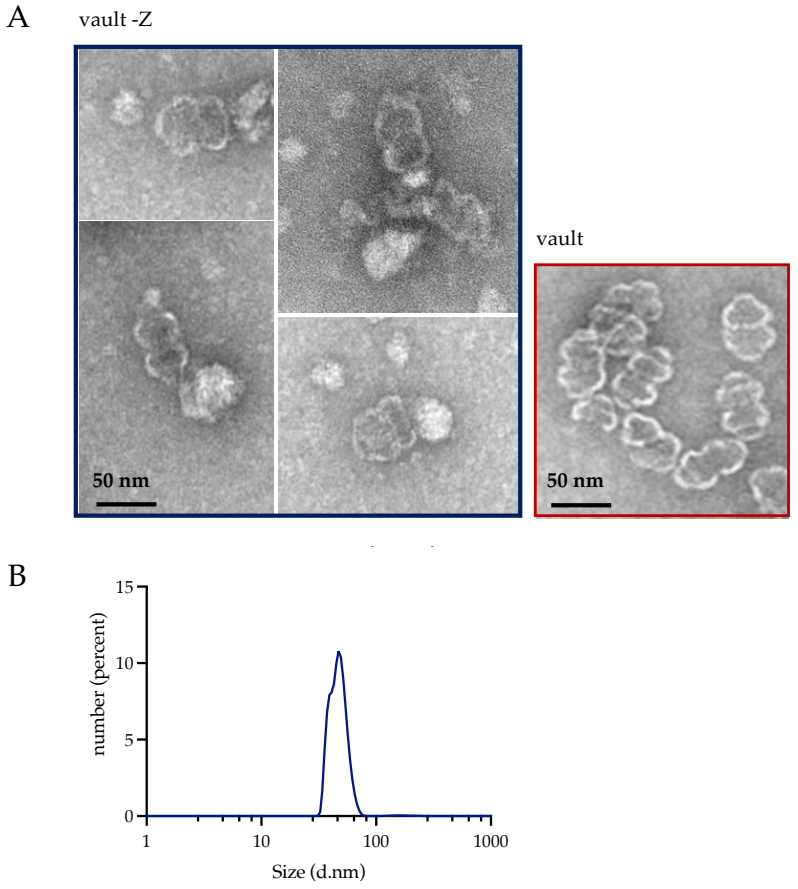

***Figure 1.*** *TEM and DLS analysis of purified vault-Z. Purified samples were analyzed after centrifuging at 20,000 x g and discarding the pellet. A) TEM images of some vault-Z NPs stained by uranyl acetate (left) compared to vault image from chapter 1 (right). B) DLS analysis of Vault-Z NPs. Results are presented as number-weighted particle size distributions. Size: 52.27 ± 6.21 nm (99.4%); 191.00 ± 43.08 nm (0.6%); polydispersity index (PDI): 0.272. Result quality: good. The graph represents the mean of three replicates.*

## Investigating Trastuzumab binding mode to either vault-Z or the sole Z domain by surface plasmon resonance analysis

To determine Tz affinity for vault-Z, as well as the relevant binding and release rate constants, surface plasmon resonance (SPR) analysis was performed using a Biacore X100 apparatus, the antibody being immobilized on a CM3 sensor chip via amine-coupling chemistry, so as to attain 1220 response units (RU), which is in the range recommended by the producer. Besides vault-Z, authentic vault and the Z domain in isolation were also analyzed. The reverse setup, i.e., vault immobilization, was not feasible as this procedure must be effectued at a pH value of 4.5 (see Materials and Methods), which is incompatible with the preservation of vault structural integrity. In each case, the real-time association and dissociation rates of the individual analytes to Tz was recorded. Binding kinetics were reproducible in the different experiments.

As a negative control, we assayed authentic vault, which showed virtually complete absence of interaction with the antibody (Figure 2). In contrast, vault-Z was capable of binding with high affinity. In particular, scalar Tz concentrations in the range 1-60 nM were manually injected in sequence in the multi-cycle kinetics mode (MCK) and binding and release kinetics recorded (Figure 3). To preserve protein stability the samples were stored in ice before injection, then injected at room temperature.

Simultaneous fitting of sensorgrams by the software BIAevalutation 4.1 matches a Langmuir 1:1 binding model, in keeping with a simple bi-molecular reaction between the ligand and the analyte. From each binding-release profile, the association ($k_{on}$) and dissociation ($k_{off}$) rate constants, along with the relevant equilibrium dissociation constant ($K_D$) were determined (Table 1).

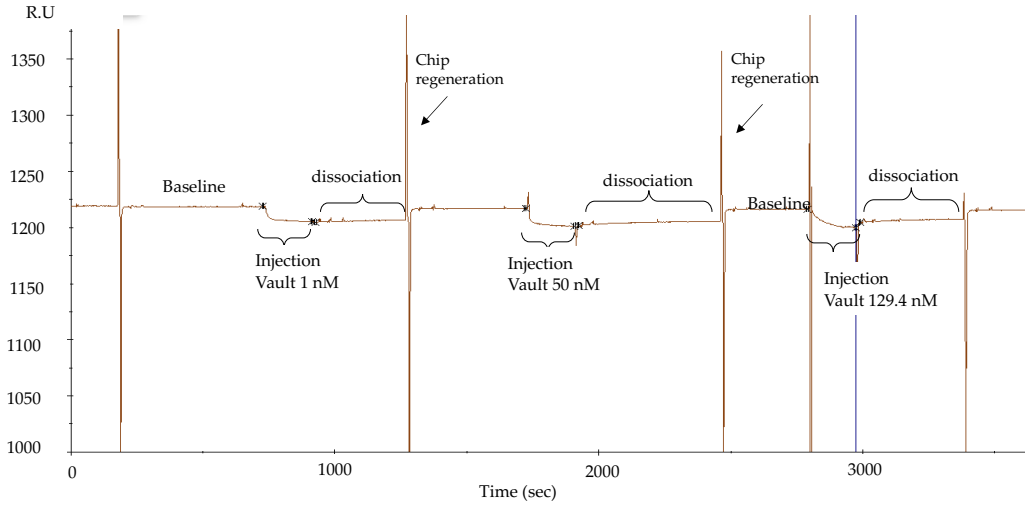


***Figure 2.*** *Association-dissociation binding kinetics between authentic vault and Tz**.** Vault was injected in running buffer on CM3 chip at different concentration at different concentrations (1 nM, 50nM, 129.4 nM) then displaced by injecting the sole running buffer. Flow rate: 30uL/min; Association Contact time: 3 minutes, T =25°C, Running Buffer: HBS-EP+, chip regeneration: NaOH 50mM.*

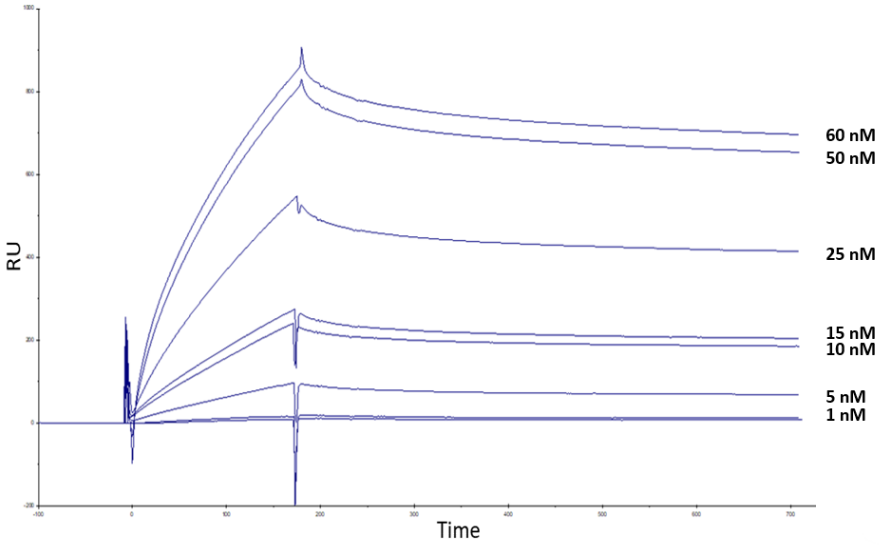


***Figure 3.*** *Association-dissociation binding kinetics between vault-Z and Tz**.** Vault-Z was injected in running buffer at growing concentrations as indicated in Figure, then displaced by injecting the sole running buffer.*

The mean ± standard deviation of $K_D$, as determined on the basis of the values shown in Table 1 (excluding the measurement at 1 nM Tz, an obvious outlier, quite plausibly due to poor signal), was 2.51 nM ± 0.40.

***Table 1.*** *Rate and equibrium constants of Tz binding to vault-Z-Tz as determined by the SPR analysis shown in Figure2.*

| **Vault-Z (nM)** | **$k_{on}$ ($M^{-1}$ $s^{-1}$)** | **$k_{off}$ ($s^{-1}$)** | **$K_D$ (nM)** |
|---|---|---|---|
| 60 | $8.57\ 10^4$ | $2.50\ 10^{-4}$ | 2.92 |
| 50 | $10.4\ 10^4$ | $2.47\ 10^{-4}$ | 2.38 |
| 25 | $12.9\ 10^4$ | $2.51\ 10^{-4}$ | 1.95 |
| 15 | $9.90\ 10^4$ | $2.86\ 10^{-4}$ | 2.87 |
| 10 | $10.3\ 10^4$ | $2.49\ 10^{-4}$ | 2.41 |
| 1 | $8.66\ 10^4$ | $6.30\ 10^{-4}$ | 7.27 |

We then determined kinetic and equibrium binding constants of Tz to the Z domain in isolation. Again, a CM3 sensor carrying immobilized antibody was used along with a Fit Kinetics Simultaneous that performs a global fit of association and dissociation of all concentrations (Conrad *et al*., 2022) (Figure 4). Based on the recorded profiles, the following values were determined: $k_{on}$ ($M^{-1}$ $s^{-1}$): $6.53\ 10^5$; $k_{off}$ ($s^{-1}$): $1.63\ 10^{-2}$; $K_D$ (nM): 24.9 nM. It is apparent that the dissociation constant of the Z domain in isolation is about one order of magnitude higher than the one determined for the whole vault-Z.

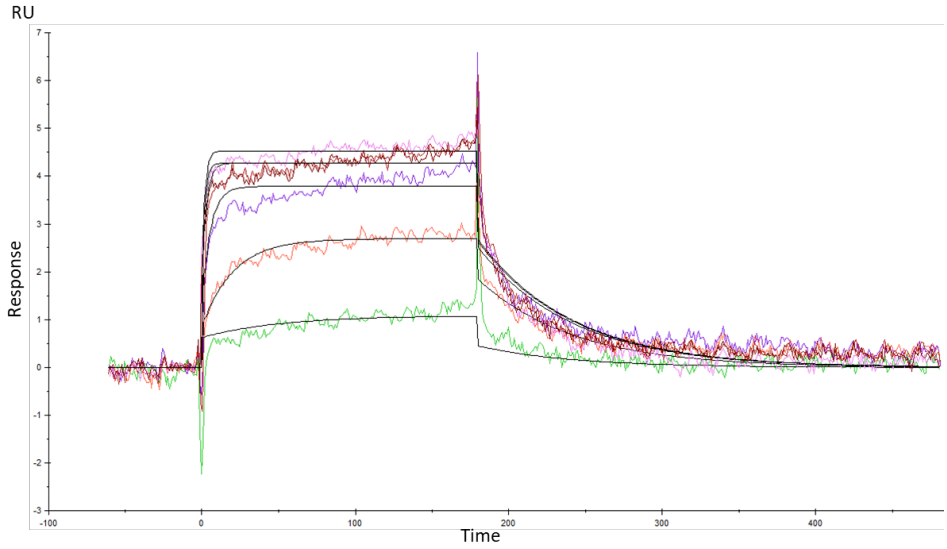


***Figure 4.*** *Sensorgrams of Z peptide and Ab Trastuzumab interaction analysis by Multi cycle kinetics. Fit binding 1:1, Kinetics simultaneous Kon /Koff. The overall curve selection used for data extrapolation is observed (in black). Peptide Z was injected in running buffer at growing concentrations 5, 50, 250, 500 e 770 nM, then displaced by injecting the sole running buffer.*

For a better understanding of the above results, some remarks should be made. First, based on Tz density on the CM3 chip, we have estimated an average distance among adjacent antibodies of about 17 nm. As vault's cap ring has a 13 nm diameter (Ding *et al*., 2018), this makes it quite unlikely that an individual vault-Z molecule can interact with more than one Tz at a time, even more if one takes into account that conjugation at the chip surface occurs with a random orientation. Thus, only a subpopulation of bound antibodies has a proper orientation for binding. Second, either chain composing the antibody's Fc portion has a facing-outward binding site for Protein A (Deisenhofer, 1981; Yang *et al*., 2018). Of course, this must also hold true for the Protein A-derived Z domain, so it is expected that up to two Z domains can bind to a single antibody molecule. Third, based on the $K_D$ values, it can be determined that the free energy binding values of Z domain and Tz to vault-Z at 25 °C are 43.4 and 49.1 kj $mol^{-1}$, respectively, the latter (Figure 4) being well below the one expected when assuming an additive contribution of the two binding sites to the overall binding energy. This can be plausibly accounted for by the fact that vault cap ring's geometry is by no means

designed for optimal interaction with Fc binding sites, so the second binding event must pay a substantial penalty in terms of entropy loss and/or structural strain. Yet the increase in affinity by an order of magnitude resulting from dual binding plays a substantial role in accomplishing an extremely stable interaction between the two molecular partners, as also documented in the following sections.

**Binding stoichiometry to vault-Z of Tz and saturation-dependent affinity decline are assessed by densitometric and mass spectrometry analyses.**

To explore the actual binding mode of Tz to vault-Z in solution, we incubated 8.27 nM vault-Z (corresponding to 645 nM MVP-Z) with different Tz concentrations, 40 to 320 nM. After a 1-h incubation at 25 °C, the reaction mixes were spun down at 100,000 x g for 2 h at 4 °C, suitable amounts of pellets dissolved in SDS-PAGE sample buffer and subjected to electrophoresis. Under these conditions, Tz co-precipitated with vault-Z, whereas no detectable amounts of antibodies were pelleted when vault-Z was replaced by authentic vault (Figure S2_A highlighted in the rectangle). Furthermore, suitable calibration curves for Tz and vault-Z quantification were constructed by co-electrophoresing the pellets with defined amounts of the two proteins (2 examples are provided in Figure S2). Based on this approach, we could quantify the molar ratio of bound antibody to vault-Z (Figure 4).

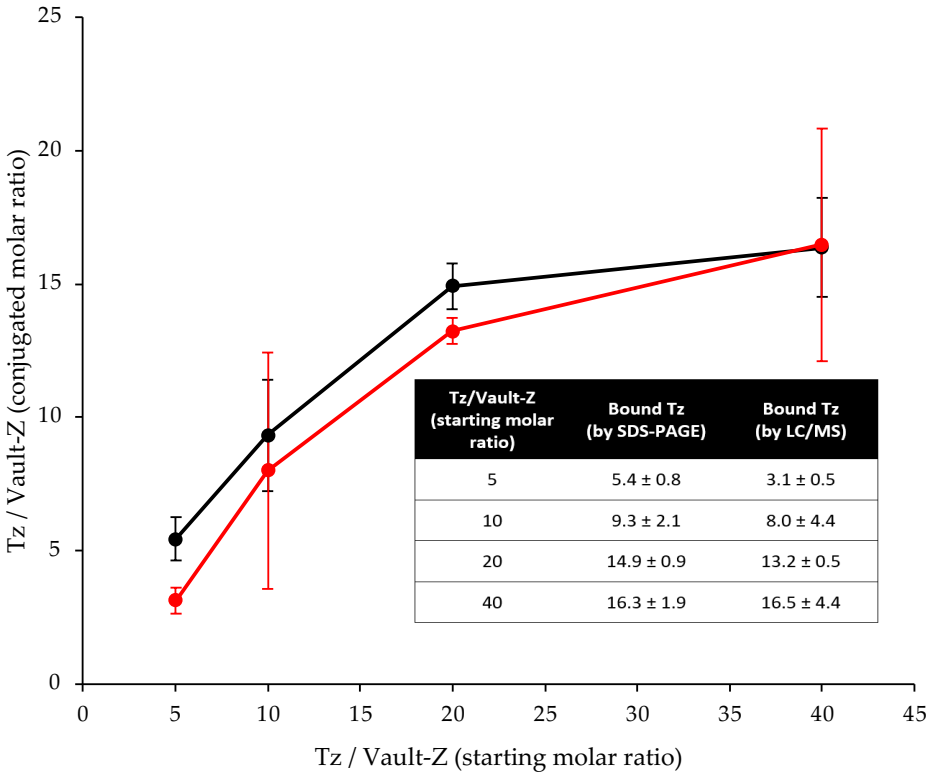


| Tz/Vault-Z (starting molar ratio) | Bound Tz (by SDS-PAGE) | Bound Tz (by LC/MS) |
|---|---|---|
| 5 | 5.4 ± 0.8 | 3.1 ± 0.5 |
| 10 | 9.3 ± 2.1 | 8.0 ± 4.4 |
| 20 | 14.9 ± 0.9 | 13.2 ± 0.5 |
| 40 | 16.3 ± 1.9 | 16.5 ± 4.4 |

***Figure 4.*** *Binding stoichiometry of Tz/vault-Z conjugates as a function of in-solution molar ratios, as assessed by either SDS-PAGE densitometry (black line) or LC/MS (red line). Error bars correspond to the standard deviation over three independent experiments. The gray circle represents the negative control performed by LC/MS analysis of authentic vault protein (devoid of the Z peptide). Inset: in-solution versus bound Tz at the adopted Tz/vault-Z molar ratios, as determined by both densitometry and LC/MS.*

To confirm the above results, an orthogonal method was also adopted, i.e. mass spectrometry. First, a calibration profile was created using the relative intensities of Tz and vault-Z peptides resulting from the digestion of mixtures of the two proteins at defined molar ratios (Figure S3). Then, the profile was used to estimate the binding stoichiometries of the conjugates digested under the same conditions.

Densitometric and MS approaches displayed saturation profiles in satisfactory agreement with each other (Figure 4)., showing almost quantitative antibody binding up to a molar ratio Tz/vault-Z up at least 10, well in agreement with the nanomolar affinity assessed by SPR measurements. In contrast, binding was only partial above this threshold

(inset to Figure 4), with a substantial decline in the apparent affinity, as determined on the basis of the saturation fraction (moles of bound Tz per mole of vault-Z. See Additional File 1, Materials and Methods). Based on the mathematical model we have developed, we estimated apparent $K_D$ values of 200 and 694 nM at molar ratios Tz/vault-Z of 20 and 40, respectively. At the lowest molar ratios, i.e., 5 and 10, this same approach was more strongly affected by statistical variability, which made it unfeasible to determine reliable Figures under conditions close to quantitative binding. The picture emerging from these data quite plausibly suggests that Tz overcrowding at the level of vault-Z cap rings is responsible for the dramatic drop in affinity at the highest molar ratios. In practical terms, one can confidently rely upon tight, operationally irreversible antibody binding up to 10 (or somewhat more) molecules loaded per vault-Z.

**Cytofluorimetric analysis of Tz-mediated vault targeting to SKBR3 cells at different Tz/vault-Z molar ratios**

We conducted cytofluorimetric analyses to evaluate whether vault-Z conjugation with Tz could stimulate its endocytosis by a mammary adenocarcinoma cell line (SKBR3), also assessing possible dependence of the process on the extent of antibody conjugation. Our experimental setup was based on the assumption that each vault-Z NP can tightly bind to a maximum of 10 antibody and Fc molecules, on the whole, as determined in the previous paragraph.

Preliminarily, fluorescent labeling of vault-Z was performed by binding it to Alexa Fluor 488 TPF-conjugated Fc (molar ratio vault-Z/Fc: 1:3). Then, following the protocol described by Galovic *et al*. (2011), SKB3 cells were incubated for 1 h at 4°C with either vault-Z (as the control) or with distinct vault-Z preparations conjugated with three different vault-Z:Tz ratios, i.e., 1:2, 1:5, 1:10. Next, the cells were incubated 20 min at 37°C to enable the endocytic process.

Data analysis of fluorescence intensities normalized to the cell autofluorescence demonstrated an about 4-fold higher uptake of Tz-conjugated vault-Z compared to the non-conjugated one, no significant difference being detected among the three Tz-conjugated vault samples

(Figure 5). This latter observation suggests that a 1:2 conjugation molar ratio already allows maximal endocytosis, at least under our working conditions. Of course, this conclusion does not necessarily apply to other cellular targets and antibodies, for which the best conditions must be identified individually, following the same procedure detailed in the present paragraph.

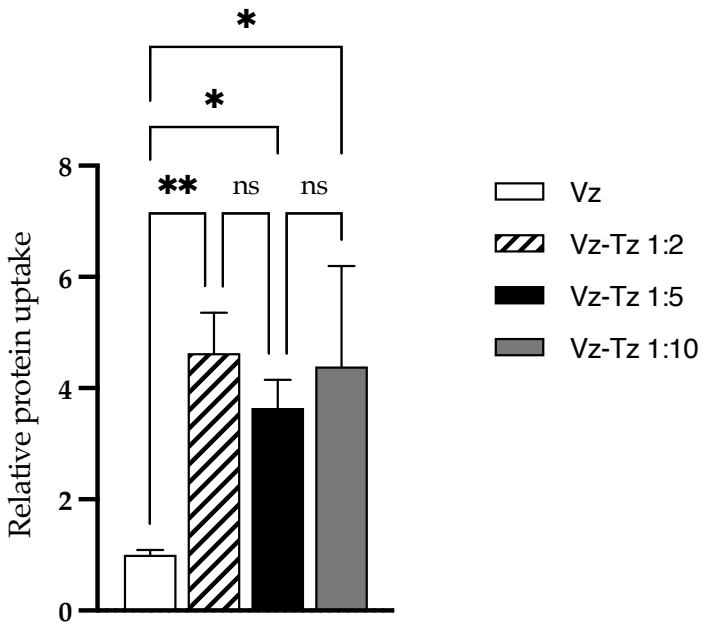


***Figure 5.*** *Vault-Z uptake by different cells lines, as assessed by cytofluorimetric analysis measuring the fluorescence intensity of Alexa 488 nm. Cells were incubated with 488-Fc-labeled-vault-Z (control) and with 488-Fc-labeled-vault-Z-Tz at three different ratios, specifically 1:2, 1:5, 1:10. Measurements were normalized to the autofluorescence emission in the absence of vault and otherwise under the same conditions. Data are the mean ± std. deviation of three biological replicates, each of them being obtained from the mean of three technical replicates. Statistical analyses were performed using the One-way ANOVA test. *p < .05; **p < .01.*

## 3 Discussion

To achieve precise targeting, nanoparticles (NPs) can be tailored by incorporating peptides and antibodies onto their surfaces using various functionalization methods. However, these approaches have to cope with inherent drawbacks such as complexity, time consumption, and inability of controlling the correct orientation required for the targeting molecules, like antibodies, to effectively fulfill their functions. To address these limitations, we produced an engineered vault variant in *K. phaffii* that carries the Z peptide by fusing it at the C-terminal of MVP. Notably, the vault-Z displayed the same morphology and size as the wild-type vault, as confirmed by dynamic light scattering (DLS) and transmission electron microscopy (TEM).

Subsequently, we conducted an in-depth analysis of the number of antibodies that could be bound to the vault-Z surface. We discovered that up to about 10 antibody molecules could be bound in a virtually irreversible and quantitative manner. Further exploration involved cytofluorimetric analysis on SKBR3 cells to assess endocytosis of both vault-Z and Tz-conjugated vault-Z. Whereas Tz conjugation resulted in an about four-fold increase compared to non-conjugated vault, no significant difference was apparent depending on the extent of conjugation within a range of molar ratios vault-Z:Tz 1:2 to 1:10. So, even two bound antibody molecules were sufficient to attain maximal endocytic stimulation. This result holds promise for future applications of this nanoassembly, as the remaining binding sites can be utilized for attaching peptides or other molecules, such as fluorophores, as in our study.

Indeed, here we harnessed the constant portion (Fc) of antibody, which also binds irreversibly to vault-Z, as a molecular scaffold for labeling vault, thereby eliminating the need for further manipulation of vault-Z. Noteworthy, the Fc domain can be also conjugated with various peptides at defined molar ratios (typically 1:1) using a click-chemistry approach (Lallana *et al*., 2011).

Thus, based on these remarks, not only could vault-Z NPs be conjugated with specific antibodies, but also with other peptides e.g. with cell-targeting peptides, greatly expanding the potential applications of our vault-Z-based platform. Importantly, a wide array of such peptides, often identified

through phage display technology, possess high affinity and specificity for distinct cellular targets (Mousavizadeh *et al*., 2017).

Alternatively, this platform could be used to bind other peptides like pVI, which is crucial for enhancing the endosomal escape of vault-Z. This approach could represent a possibly better option compared with incorporating pVI fused to INT and then loading it inside the vault, or fusing pVI to the N-terminal of MVP. Both methods have limitations, with pVI-INT taking up space that could otherwise house additional cargo molecules and pVI-vault demonstrating toxicity to treated cells, likely due to the high pVI content. Consequently, conjugating pVI on the surface of the vault, leveraging the interaction between Fc and peptide Z, emerges as a viable alternative. This approach allows for the cargo loading into the vault's lumen while avoiding the associated pVI toxicity that characterized pVI-vault.

In conclusion, the experimental scenario outlined by our cytofluorimetric analyses is indeed highly promising in view of enlarging the scope of application of our vault-based platform. Specifically, not only can the Z peptides at vault's C-terminus be exploited to stably bind antibodies at different molar ratios so as to optimize the endocytic process, but also Fc-bound cell-targeting peptides can be similarly handled, as planned in our ongoing research. No less important, the Fc moiety can be exploited as a scaffold for fluorophore conjugation as already accomplished in the present experimentation.

## 4 Materials and Methods

### MVP-Z cloning and vault-Z production, purification,

*Strain and growth media*

For the production of the MVP protein, the vacuolar aspartyl protease PEP4-deficient *K. phaffii* SMD1168 (his4, ura3, pep4::URA3) strain was used (Gleeson *et al*., 1998). The strain is available from Invitrogen (Carlsbad, CA, USA). *K. phaffii* was grown in a flask in BMDY medium (10 g/L yeast extract, 20 g/L bacto peptone, 20 g/L dextrose, 100 mM potassium phosphate buffer, pH 5.8, 13.4 g/L yeast nitrogen base without amino acids, 0.4 mg/L biotin). All media were from Biolife; monobasic potassium phosphate, yeast nitrogen

base without amino acids and biotin were from Sigma-Aldrich. Standard liquid and plate growth were performed on YPD medium (10 g/L yeast extract, 20 g/L bacto peptone, 20 g/L dextrose, 20 g/L agar omitted in liquid medium) with or without 100 μg/mL zeocin. After electroporation, YPDS plates containing 1 M sorbitol and 100 μg/mL Zeocin were used for the selection of the transformants.

*MVP-Z gene cloning and selection of positive clones*

Authentic human MVP gene cloning and selection of best-producing clones has been previously described (Tomaino *et al*., 2023). The MVP gene variant encoding the Z peptide at the C-terminus (MVP-Z) was cloned as follows. The C-terminal sequence of MVP was removed from pGAPZ B MVP vector, previously constructed (Tomaino *et al*., 2023) by digestion with SacI and NotI. Electrophoresis of the digestion mix on 1% agarose gel, with TAE as running buffer was run 45 min at 90 V and gel stained with EtBr 2000X and confirmed the digestion of the plasmid. The NotI/SacI digested pGAPZB carrying the N-terminal sequence of MVP was purified from gel using Gel Extraction Kit (QIAGEN) and quantified with NanoDrop (NanoDrop 2000c Spectrophotomer, Thermo Scientific). The amino acid sequence used for addition of the Z33 peptide to the C-terminus of MVP was FNMQQQRRFYEALHDPNLNEEQRNAKIKSIRDD (Braisted & Wells, 1996b). The nucleotide sequence encoding this peptide was fused in frame with the C terminal of MVP and designed to have terminal regions homologous to those adjacent to extremity of the NotI/SacI digested plasmid. The complete synthetized sequence, purchased from Eurofins (Ebersberg, Germany) and reported in table S1, was cloned in the purified NotI/SacI digested pGAPZB carrying the N-terminal sequence of MVP, using NEBuilder® HiFi DNA Assembly Master Mix method, requiring the presence of homologous ends. The sequence was confirmed by Sanger sequencing, which was commissioned to Eurofins Genomics (Ebersberg, Germany). Transformation of *K. phaffii* and selection of MVP-Z-positive clones was performed as previously reported when handling authentic MVP (Tomaino *et al*., 2023).

*Cell growth, collection, and cell-free extract production*

Growth of the yeast clone expressing authentic vault and subsequent production of cell-free extracts was performed as previously described in chapter 1 (Tomaino *et al*., 2023). Likewise, production of vault-Z-containing extracts was achieved following the same procedure.

*Vault-Z purification*

The purifications of both authentic vault and vault-Z were carried out according to the procedure we previously developed, essentially consisting of RNase treatment of cell-free extracts, subsequent centrifugation to remove ribosomal contaminations, followed by size-exclusion chromatography (SEC) using Sepharose CL-6B as the matrix (Tomaino *et al*., 2023). Eluted protein was assayed by the bicinchoninic acid assay using the KIT QPRO-BCA (Cyanagen) and bovine serum albumin as the calibration standard.

*Electrophoretic Analyses*

The purified vault-Z samples were subjected to SDS-PAGE (8% gel). Typically, 6–12 μg samples were applied. Gels were stained with Imperial Protein Stain (Thermo Scientific). MVP identity was confirmed by Western blot analysis on PVDF membrane Immobilon (Millipore) using a primary anti-MVP antibody (rabbit monoclonal; 1:10000 dilution in PBS-5% skim milk; Abcam) and a fluorescent secondary anti-rabbit IR-800 antibody (1:16000 dilution in PBS-5% skim milk; LI-COR Biosciences). The signal of MVP was revealed using an Odyssey Fc instrument (LI-COR Biosciences).

## Vault-Z characterization

*TEM analysis*

TEM images of vault particles were obtained using a Tecnai12 (RH42B) microscope (Accelerating voltage: 120 kV—Filament: LaB6) at *ImagoSeine* platform, Institute Jacques Monod (Paris). Sample preparation and analysis have been conducted as previously described in chapter 1 (Tomaino *et al*., 2023). Samples were deposited on carbon-coated copper grids, 400 mesh, after plasma activation for 20 sec, by floating the grid onto the protein drop

(20 μL, 0.5 mg/mL) for 1–2 min. The grid was then dried from liquid excess by filter paper and put on a drop of uranyl acetate (1% in PBS, pH 5.0) for 1–2 min, depending on sample concentration. Finally, the grids were dried with Whatman filter paper and analyzed.

*Dynamic light scattering analysis*

Dynamic Light Scattering (DLS) measurements were performed by a Zeta Sizer Nano Instrument (Malvern Instruments Ltd., Amesbury, UK) operating at 4 mW of a HeeNe 633 nm laser, using a scattering angle of 90°. A disposable cuvette with 1 cm optical path length was used for the measurements. Each sample was allowed to equilibrate for 2 min prior to measurement. The measurements were acquired as described in chapter 1 (Tomaino *et al*., 2023). Briefly, three independent measurements of 60 s duration were performed at 25 °C. Mie theory was used to perform calculations of the hydrodynamic diameter, considering the absolute viscosity and the refractive index of the material set to 1.450, Abs 0.001. The number-based hydrodynamic diameter based and the autocorrelation function were evaluated, with the latter serving as an indicator of sample uniformity, as it reveals a single exponential decay profile when observed.

## Analysis of Vault-Z/Ab binding

*Surface plasmon resonance for the determination of Z peptide-antibody and vault-Z-antibody binding affinities*

A BIACORE X100 system (Cytiva-Pall, Marlborough [HQ], MA, USA) was used to analyze molecular interactions by means of SPR. Tz antibody was coupled to a carboxymethylated dextran surface of CM3 sensor chip by using amine-coupling chemistry. The amine coupling procedure was performed setting the instrumentation temperature at 25°C, by using the running buffer HBS-EP+ (0.01 M HEPES, 0.15 M NaCl, 0.003 M EDTA and 0.05% v/v Surfactant P20 pH 7.4) at a flow rate of 5 μL/min and with the following three steps as recommended by the producer (Biacore Sensor Surface handbook BR100571) and adapted for our purposes. First step, the CM3 chip was activated by injecting EDC/NHS (1/1) on both flow cells 1 and

2 for 7 min; second step, Ab Tz was diluted in 10 mM sodium acetate pH 4.5 at a final concentration of 20μg/mL and injected on flow cell 2 until reaching a surface density of 1220 RU; third step, 1M ethanolamine- HCl, pH 8.5, was injected on both cells.

Appropriate, multiple concentrations of authentic vault, vault-Z and peptide Z (purchased from ProteoGenix) were injected for 3 min at 25°C and at a flow rate of 30 μL/min in running buffer (10 mM HEPES, pH 7.4, 150 mM NaCl, 3 mM EDTA containing 0.005% [v/v] Surfactant P20). After injection, analyte solutions were replaced by running buffer at a continuous flow rate of 30 μL/min. Surface regeneration was accomplished by injecting 50 mM NaOH for a contact time of 1 min. Each sensorgram was subtracted for the response observed in the control flow cell (no immobilized protein) and normalized to a baseline of 0 RU.

The sensorgram curves were acquired by setting the BiacoreX100 Control software, 2.0.2 (Cytiva-Pall, Marlborough [HQ], MA, USA) in manual run mode for authentic vault, vault-Z and immobilization procedure injections; multi cycle kinetics mode for peptide Z. The interaction rate constants were calculated by fitting the sensorgrams to the model Langmuir Binding 1:1 and using the Bia Evaluation software 2.0.2 (Cytiva-Pall, Marlborough [HQ], MA, USA) for Peptide Z and BIA evaluation 4.1 software (GE Healthcare Life Sciences, Little Chalfont, England) for Vault-Z.

### *Densitometric and Mass spectrometric determination of vault-Z-antibody binding stoichiometry*

Different amounts of antibody were mixed with a fixed amount of vault-Z and the molar ratios of bound antibody to vault-Z were then determined as follows. Briefly, 8.27 nM vault-Z (corresponding to 645 nM MVP-Z) was incubated with scalar concentrations (40 to 320 nM) of Tz at 4°C for 1 h in 12 mM sodium phosphate, pH 7.2, 0.14 M NaCl, 2.7 mM KCl, in a final volume of 7.5 ml. Then, the mixes were centrifuged for 2 h at 4 °C and 100,000 x g. The pellets were dissolved in SDS-PAGE sample buffer and suitable amounts were subjected to electrophoresis (12% gel). Gels were stained with Imperial Protein Stain (Thermo Scientific) and images were acquired by Odyssey Fc instrument (LI-COR Biosciences). Vault-Z and Tz protein content of the

individual bands were determined densitometrically using the program ImageJ and scalar amounts of purified vault-Z and Tz (quantified by the BCA assay) to construct the calibration curves.

The binding stoichiometry of Tz conjugated to MVP-Z was also assessed by reverse phase liquid chromatography mass spectrometry (LC/MS). For this purpose, a calibration curve was first constructed by mixing vault-Z and Tz at predefined molar ratios, reducing, alkylating and digesting the mixtures by a standard in-solution protocol for MS [ref]. The resulting peptides were then desalted by a C18 ziptip column (Millipore) and injected in an Orbitrap Fusion mass spectrometer coupled with an EASY-1000 LC system (Thermo Fischer). Peptides were separated by a 50-cm C18 EASY-Spray column (Thermo Fisher) employing a 1-h gradient (0-80% acetonitrile), detected in the orbitrap analyzer and fragmented by high-energy collision-induced dissociation (HCD) in the iontrap analyzer of the instrument. Peptides were identified and quantified by a label-free approach using the Proteome Discoverer software (Thermo Fisher). Based on signal intensities and missed cleavages rates, six peptides for each protein were selected to create the calibration curve for the MVP-Tz relative quantification. To assess the binding stoichiometries, Tz-vault-Z conjugates were previously collected by ultracentrifugation at 100,000 for 2 h at 4 °C, dissolved in SDS sample buffer (0.4 % SDS), then subjected to the above procedure, using the calibration curve to quantify the two molecular partners.

## Endocytosis studies

*Fluorescent Fc and Trastuzumab vault conjugation*

Alexa Fluor 488 TPF (Themo Fisher) was added to 0.9 mg of Fc in 20 mM KPi, 0.137 M NaCl, pH 8, at molar ratio 10:1 (10 mg/mL fluorophore stock solution in DMSO) and incubated for 1 h at room temperature under shaking. The reaction mixture was purified with Zeba™ Dye and Biotin Removal Spin Columns (Thermo Fisher). 3 molar excess of fluorescent Fc (Fc488) was added to 1 mg vault-Z in phosphate buffer saline (PBS) (0.14 M NaCl, 27 mM KCl, 100 mM Na2HPO4, 10 mM KH2PO4) and incubated for 1 h at 4°C under shaking. 0.25 mg of the resulting vault-Z-Fc488 was then conjugate with Tz at different vault-Z-Fc488:Tz molar ratio (1:2, 1:5, 1:10), for 1 h at 4°C under

shaking. The resulting concentration of conjugates was determined with UV-VIS, on NanoDrop. Vault-Z-Fc488 and vault-Z-Fc488-Tz conjugates had been stored overnight at 4°C. Immediately before incubation for endocytosis analysis, vault-Z-Fc488 and vault-Z-Fc488-Tz conjugates were diluted in basic buffer (DMEM with 0.1% BSA, 20 mM Hepes pH 7.4) to a final concentration of 20 μg/mL (binding buffer).

*Cell culture*

The mammary carcinoma cell line SKBR3, obtained from ATCC (Manasses, VA), was cultured in 50% Dulbecco's Modified Eagle's Medium High Glucose (DMEM-HG) and 50% HAM'S F12, supplemented with 10% fetal bovine serum, L-glutamine (2 mM), penicillin (50 IU/mL), and streptomycin (50 mg/mL) and incubated at 37 °C in a humidified atmosphere containing 5% CO2 and subcultured using trypsin/EDTA prior to confluence.

*Endocytosis analysis*

To measure vault-Z-Fc488 and vault-Z-Fc488-Tz internalization in SKBR3 cells, cytofluorimetric analyses were conducted. The incubation was performed following a previously described protocol (Galovic *et al*., 2011). Briefly, 3 x $10^5$ cell aliquots were seeded in a 12-well plate and incubated 40 h at 37°C. Cells were then preincubated for 4 h with 1 ml/well basic buffer at 37°C. Subsequently, the basic buffer was removed, and 1 ml/well ice-cold binding buffer (DMEM with 0.1% BSA, 20 mM Hepes, pH 7.4, and 20 μg/mL of vault-Z-Fc488 or vault-Z-Fc488-Tz) was added. Cells were incubated with binding buffer for 1 h at 4°C under slow shaking. Cold medium was replaced by 1 ml/well warm basic buffer and cells transferred to 37°C for 20 min. Afterwards, they were washed twice with ice-cold PBS with $Ca^{2+}$ and $Mg^{2+}$ and incubated with acidic wash buffer (0.2 M acetic acid, pH 2.8, 0.5 M NaCl) for 5 min at 4°C under slow shaking, to eliminate surface-bound protein. After the incubation, cells were washed with PBS without $Ca^{2+}$ and $Mg^{2+}$, then with trypsin-EDTA to detach them. Complete medium was added, and samples centrifuged at 1300 rpm for 5 min. Pellets were washed twice with PBS without $Ca^{2+}$ and $Mg^{2+}$ and resuspended in 0.5 mL of PBS with 2 mM EDTA. Flow cytometer analysis was performed with CytoFLEX Flow

Cytometer (Beckman coulter) and samples were analyzed using the CytExpert Software (Beckman coulter).

## Supplementary Information

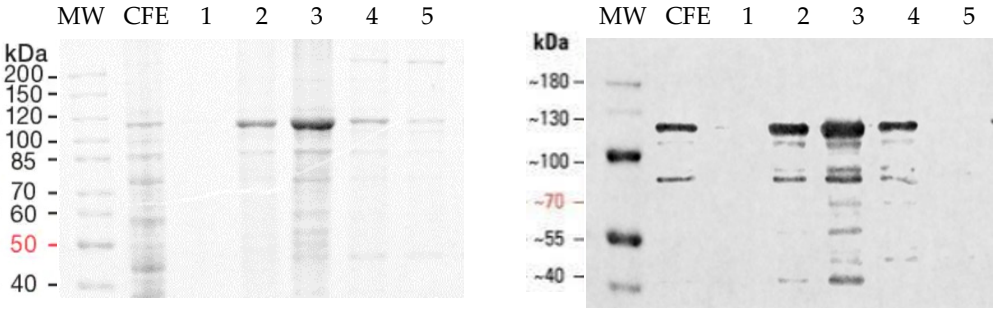


***Figure S1.*** *SDS-PAGE (8% gel) of vault-Z eluted from the SEC column. Cell free extract (CFE) and eluted fractions (1-5) were subjected to electrophoresis, Coomassie stained (left panel) and Western blotted (right panel). MW: standard proteins with the respective molecular weights (kDa). About 16μg of CFE and 20 μL of each eluted fraction were loaded.*

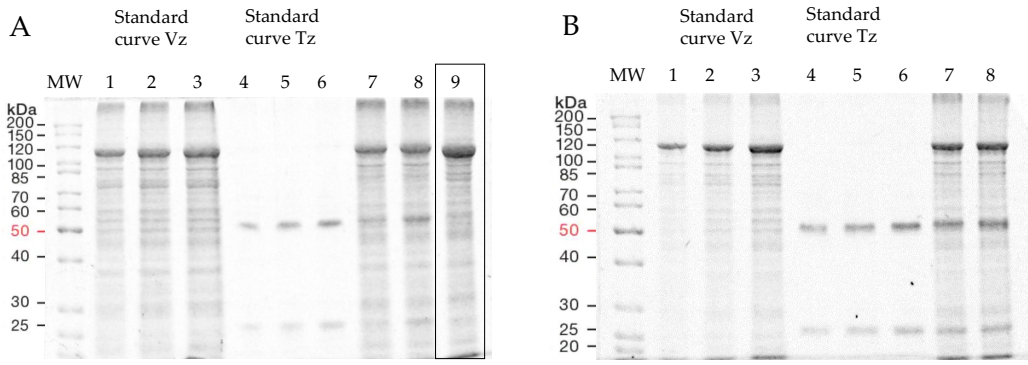


***Figure. S2.*** *Representative gel electrophoresis of 100,000 x g pellets collected after co-incubation of vault-Z (A-B) or authentic vault with Tz (A, highlighted in the rectangle). The samples were co-electrophoresed in the presence of scalar amounts of vault-Z and Tz. SDS PAGE (12%) MW: PageRuler™ Unstained Protein Ladder (Thermo Scientific). Staining: Imperial Protein Stain (Thermo Scientific). A) lanes 1-3: vault-Z (6.5 μg – 13 μg), and 4-6: Tz (0.7 – 1.7 μg) in defined amounts for creating the respective calibration profiles. Lanes 7, 8: 100,000 x g pellets of vault-Z-Tz incubation mixtures at the molar ratios 1:5, 1:10. 9: 100,000 x g pellets of vault + Tz incubation mixtures at the molar ratio 1:40 B) lanes 1-3: vault-Z (1.5 μg – 6 μg), and 4-6: Tz (1 – 1.8 μg) in defined amounts for creating the respective calibration profiles, lanes 7 and 8. 100,000 x g pellets of vault-Z-Tz incubation mixtures at the molar ratios 1:20 and 1:40, respectively.*

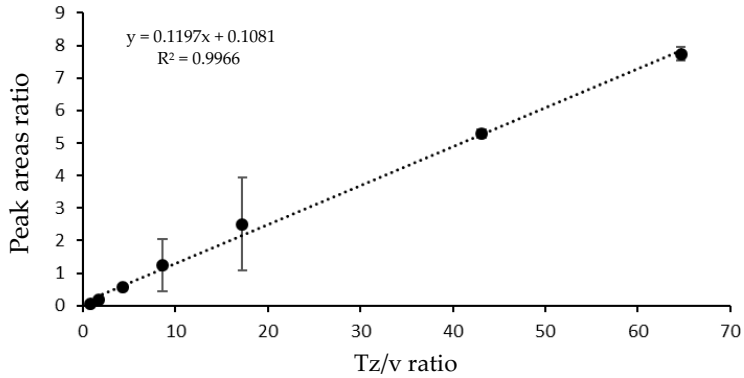


***Figure S3.*** *Calibration curve of Tz/v ratio constructed on the relative intensities of six peptides for both Tz and vault-Z protein, selected from the digestion of mixtures of the two proteins at defined molar ratios*

## References

Abdel-Mageed, H. M., AbuelEzz, N. Z., Radwan, R. A., & Mohamed, S. A. (2021). Nanoparticles in nanomedicine: a comprehensive updated review on current status, challenges and emerging opportunities. *Journal of Microencapsulation*, *38*(6), 414–436. https://doi.org/10.1080/02652048.2021.1942275

Anderson, D. H., Kickhoefer, V. A., Sievers, S. A., Rome, L. H., & Eisenberg, D. (2007). Draft crystal structure of the vault shell at 9-Å resolution. *PLoS Biology*, *5*(11), e318.

Avvakumova, S., Colombo, M., Tortora, P., & Prosperi, D. (2014). Biotechnological approaches toward nanoparticle biofunctionalization. *Trends in Biotechnology*, *32*(1), 11–20. https://doi.org/10.1016/j.tibtech.2013.09.006

Benner, N. L., Zang, X., Buehler, D. C., Kickhoefer, V. A., Rome, M. E., Rome, L. H., & Wender, P. A. (2017). Vault Nanoparticles: Chemical Modifications for Imaging and Enhanced Delivery. *ACS Nano*, *11*(1), 872–881. https://doi.org/10.1021/acsnano.6b07440

Berger, W., Steiner, E., Grusch, M., Elbling, L., & Micksche, M. (2009). Vaults and the major vault protein: Novel roles in signal pathway regulation and immunity. In *Cellular and Molecular Life Sciences* (Vol. 66, Issue 1, pp. 43–61). https://doi.org/10.1007/s00018-008-8364-z

Braisted, A. C., & Wells, J. A. (1996a). Minimizing a binding domain from protein A. *Proceedings of the National Academy of Sciences*, *93*(12), 5688–5692.

Braisted, A. C., & Wells, J. A. (1996b). Minimizing a binding domain from protein A. *Proceedings of the National Academy of Sciences of the United States of America*, *93*(12), 5688–5692. https://doi.org/10.1073/pnas.93.12.5688

Conrad, M., Fechner, P., Proll, G., & Gauglitz, G. (2022). Comparison of methods for quantitative biomolecular interaction analysis. *Analytical and Bioanalytical Chemistry*, 1–13.

D Friedman, A., E Claypool, S., & Liu, R. (2013). The smart targeting of nanoparticles. *Current Pharmaceutical Design*, *19*(35), 6315–6329.

Deisenhofer, J. (1981). Crystallographic refinement and atomic models of a human Fc fragment and its complex with fragment B of protein A from Staphylococcus aureus at 2.9-and 2.8-. ANG. resolution. *Biochemistry*, *20*(9), 2361–2370.

Ding, K., Zhang, X., Mrazek, J., Kickhoefer, V. A., Lai, M., Ng, H. L., Yang, O. O., Rome, L. H., & Zhou, Z. H. (2018). Solution Structures of Engineered Vault Particles. *Structure*, *26*(4), 619-626.e3. https://doi.org/10.1016/j.str.2018.02.014

Frascotti, G., Galbiati, E., Mazzucchelli, M., Pozzi, M., Salvioni, L., Vertemara, J., & Tortora, P. (2021). The vault nanoparticle: A gigantic ribonucleoprotein assembly involved in diverse physiological and pathological phenomena and an ideal nanovector for drug delivery and therapy. *Cancers*, *13*(4), 1–37. https://doi.org/10.3390/cancers13040707

Galbiati, E., Avvakumova, S., La Rocca, A., Pozzi, M., Messali, S., Magnaghi, P., Colombo, M., Prosperi, D., & Tortora, P. (2018). A fast and straightforward

procedure for vault nanoparticle purification and the characterization of its endocytic uptake. *Biochimica et Biophysica Acta - General Subjects*, *1862*(10), 2254–2260. https://doi.org/10.1016/j.bbagen.2018.07.018

Galovic, M., Xu, D., Areces, L. B., van der Kammen, R., & Innocenti, M. (2011). Interplay between N-WASP and CK2 optimizes clathrin-mediated endocytosis of EGFR. *Journal of Cell Science*, *124*(12), 2001–2012. https://doi.org/10.1242/jcs.081182

Gleeson, M. A. G., White, C. E., Meininger, D. P., & Komives, E. A. (1998). Generation of protease-deficient strains and their use in heterologous protein expression. *Pichia Protocols*, 81–94.

Hong, S., Choi, D. W., Kim, H. N., Gwon Park, C., Lee, W., & Park, H. H. (2020). Protein-Based Nanoparticles as Drug Delivery Systems. *Pharmaceutics*. https://doi.org/10.3390/pharmaceutics12070604

Hudis, C. A. (2007). Trastuzumab—mechanism of action and use in clinical practice. *New England Journal of Medicine*, *357*(1), 39–51.

Jain, A., Singh, S. K., Arya, S. K., Kundu, S. C., & Kapoor, S. (2018). Protein nanoparticles: promising platforms for drug delivery applications. *ACS Biomaterials Science & Engineering*, *4*(12), 3939–3961.

Kedersha, N. L., Heuser, J. E., Chugani, D. C., & Rome, L. H. (1991). Vaults. III. Vault ribonucleoprotein particles open into flower-like structures with octagonal symmetry. *Journal of Cell Biology*, *112*(2), 225–235. https://doi.org/10.1083/jcb.112.2.225

Kedersha, N. L., & Rome, L. H. (1986). Isolation and characterization of a novel ribonucleoprotein particle: Large structures contain a single species of small RNA. *Journal of Cell Biology*, *103*(3), 699–709. https://doi.org/10.1083/jcb.103.3.699

Kickhoefer, V. A., Han, M., Raval-Fernandes, S., Poderycki, M. J., Moniz, R. J., Vaccari, D., Silvestry, M., Stewart, P. L., Kelly, K. A., & Rome, L. H. (2009). Targeting vault nanoparticles to specific cell surface receptors. *ACS Nano*, *3*(1), 27–36. https://doi.org/10.1021/nn800638x

Kickhoefer, V. A., Rajavel, K. S., Scheffer, G. L., Dalton, W. S., Scheper, R. J., & Rome, L. H. (1998). Vaults are up-regulated in multidrug-resistant cancer cell lines. *Journal of Biological Chemistry*, *273*(15), 8971–8974. https://doi.org/10.1074/jbc.273.15.8971

Kickhoefer, V. A., Searles, R. P., Kedersha, N. L., Garber, M. E., Johnson, D. L., & Rome, L. H. (1993). Vault ribonucleoprotein particles from rat and bullfrog contain a related small RNA that is transcribed by RNA polymerase III. *Journal of Biological Chemistry*, *268*(11), 7868–7873.

Kickhoefer, V. A., Siva, A. C., Kedersha, N. L., Inman, E. M., Ruland, C., Streuli, M., & Rome, L. H. (1999). The 193-kD vault protein, VPARP, is a novel poly (ADP-ribose) polymerase. *The Journal of Cell Biology*, *146*(5), 917–928.

Kickhoefer, V. A., Stephen, A. G., Harrington, L., Robinson, M. O., & Rome, L. H. (1999). Vaults and telomerase share a common subunit, TEP1. *Journal of Biological Chemistry*, *274*(46), 32712–32717.

Kim, S. K., & Huang, L. (2012). Nanoparticle delivery of a peptide targeting EGFR signaling. *Journal of Controlled Release*, *157*(2), 279–286. https://doi.org/https://doi.org/10.1016/j.jconrel.2011.08.014

Lallana, E., Riguera, R., & Fernandez-Megia, E. (2011). Reliable and efficient procedures for the conjugation of biomolecules through Huisgen azide–alkyne cycloadditions. *Angewandte Chemie International Edition*, *50*(38), 8794–8804.

Lohcharoenkal, W., Wang, L., Chen, Y. C., & Rojanasakul, Y. (2014). Protein Nanoparticles as Drug Delivery Carriers for Cancer Therapy. *BioMed research international*, *2014*, 180549. https://doi.org/10.1155/2014/180549

Marques, A. C., Costa, P. J., Velho, S., & Amaral, M. H. (2020). Functionalizing nanoparticles with cancer-targeting antibodies: A comparison of strategies. *Journal of Controlled Release*, *320*, 180–200. https://doi.org/https://doi.org/10.1016/j.jconrel.2020.01.035

Mousavizadeh, A., Jabbari, A., Akrami, M., & Bardania, H. (2017). Cell targeting peptides as smart ligands for targeting of therapeutic or diagnostic agents: A systematic review. *Colloids and Surfaces B: Biointerfaces*, *158*, 507–517.

Mrazek, J., Toso, D., Ryazantsev, S., Zhang, X., Zhou, Z. H., Fernandez, B. C., Kickhoefer, V. A., & Rome, L. H. (2014). Polyribosomes are molecular 3D nanoprinters that orchestrate the assembly of vault particles. *ACS Nano*, *8*(11), 11552–11559. https://doi.org/10.1021/nn504778h

Muñoz-Juan, A., Carreño, A., Mendoza, R., & Corchero, J. L. (2019). Latest advances in the development of eukaryotic vaults as targeted drug delivery systems. In *Pharmaceutics* (Vol. 11, Issue 7). MDPI AG. https://doi.org/10.3390/pharmaceutics11070300

Schrama, D., Reisfeld, R. A., & Becker, J. C. (2006). Antibody targeted drugs as cancer therapeutics. *Nature Reviews Drug Discovery*, *5*(2), 147–159.

Stephen, A. G., Raval-Fernandes, S., Huynh, T., Torres, M., Kickhoefer, V. A., & Rome, L. H. (2001). Assembly of Vault-like Particles in Insect Cells Expressing only the Major Vault Protein. *Journal of Biological Chemistry*, *276*(26), 23217–23220. https://doi.org/10.1074/jbc.C100226200

Tomaino, G., Pantaleoni, C., Ami, D., Pellecchia, F., Dutriaux, A., Barbieri, L., Garbujo, S., Natalello, A., Tortora, P., & Frascotti, G. (2023). Addressing Critical Issues Related to Storage and Stability of the Vault Nanoparticle Expressed and Purified from Komagataella phaffi. *International Journal of Molecular Sciences*, *24*(4). https://doi.org/10.3390/ijms24044214

Van Zon, A., Mossink, M. H., Schoester, M., Scheffer, G. L., Scheper, R. J., Sonneveld, P., & Wiemer, E. A. C. (2001). Multiple human vault RNAs: expression and association with the vault complex. *Journal of Biological Chemistry*, *276*(40), 37715–37721.

Wang, M., Kickhoefer, V. A., Rome, L. H., Foellmer, O. K., & Mahendra, S. (2018). Synthesis and assembly of human vault particles in yeast. *Biotechnology and Bioengineering*, *115*(12), 2941–2950. https://doi.org/10.1002/bit.26825

Yang, X.-H., Huan, L.-M., Chu, X.-S., Sun, Y., & Shi, Q.-H. (2018). A comparative investigation of random and oriented immobilization of protein A ligands on the binding of immunoglobulin G. *Biochemical Engineering Journal*, *139*, 15–24.

# Conclusions

The purpose of this work was to establish a platform based on vault nanoparticles for loading and targeted delivery of therapeutic molecules like proteins and nucleic acids to the cell surface.

The optimization of production and purification processes, as discussed in Chapter 1, was a successful initial outcome, streamlining production and enhancing yields. The resulting protein was characterized, and ideal storage conditions were identified. Chapter 2 focused on the validation of vault functionality in transporting cargos, such as GFP-INT, and established useful cargo loading stoichiometry whose understanding was a key outcome, providing insight for the delivery of other molecules, which could be chemically conjugated for stable loading into vaults. One of the primary goals of this research was to investigate vault mediated siRNA delivery against *LADON*, a lncRNA in melanoma. Chapter 3 addressed this issue and presented two approaches: one involving chemical conjugation of siRNA with GFP-INT and the other the direct interaction between siRNA and vault. While chemical conjugation is still in progress, potential solutions are proposed. In parallel, the alternative strategy explored the inherent capacity of vaults to load siRNA, theoretically possible thanks to vault spacious cavity lined by positive charges. Studies revealed that siRNA incubated with vaults co-migrated, and this incubation allowed both siRNA entry into cells and the expected biological effect. Additionally, the results showed that siRNA incubation with vaults enabled cell transfection, comparable to common transfection agents like Lipofectamine. Notably, it appears that the effectiveness of this process is primarily influenced by the quantity of siRNA associated with vaults rather than the absolute amount provided to cells, as shown in Chapter 3. These are preliminary findings, and further research is required to better understand the mode of RNA-vault interaction. Future studies may include binding affinity assessment to explore this association. For sure, the degradation rate of vault-bound siRNA, as assessed by addition of a RNase to the medium, could be indicative of how tight siRNA binding is. Moreover other in vitro assays such as cytofluorimetric analysis and migration assays on melanoma are now ongoing.

The production of the variant vault-Z introduces new applications. Research on binding affinity and stoichiometry has identified the maximum number of stably bound antibodies. Furthermore, low levels of conjugated antibodies were found to already provide cell targeting activity, indicating that the binding potential of vault-Z can be harnessed in various ways: the Fc portion of antibodies, also binding the Z peptide, can be utilized for attaching not only fluorophores but also targeting peptides, such as the cardiomyocyte-penetrating peptide, or pVI peptide for enhancing endosomal escape. The next steps involve the combination of delivery and targeting properties: loading Vault-Z with siRNA and directing it to the cells.

It's important to note that handling this macromolecule has to cope with different challenges. While some stability issue has been faced and progress has been made in identifying ideal storage conditions, the full potential of vaults remains partly unexplored or obscured due to the proprietary nature of much of the vault literature (Muñoz-Juan *et al*., 2019). This notwithstanding, ongoing preclinical studies suggest the potential applications of vaults in the medical field that, along with their exploration in various fields beyond drug delivery, such as bioremediation and other areas, make them an attractive subject for continued research.

# List of pubblications

2023

**Tomaino, G**.; Pantaleoni, C.; Ami, D.; Pellecchia, F.; Dutriaux, A.; Barbieri, L.; Garbujo, S.; Natalello, A.; Tortora, P.; Frascotti, G. Addressing Critical Issues Related to Storage and Stability of the Vault Nanoparticle Expressed and Purified from *Komagataella phaffi*. *Int. J. Mol. Sci.* **2023**, *24*, 4214.

https://doi.org/10.3390/ijms24044214

2022

Cerri, F.; Giustra, M.; Anadol, Y.; **Tomaino, G**.; Galli, P.; Labra, M.; Campone, L.; Colombo, M. Natural Products from Mangroves: An Overview of the Anticancer Potential of *Avicennia marina*. *Pharmaceutics* **2022**, *14*, 2793.

https://doi.org/10.3390/pharmaceutics14122793

Salvioni, L.; Testa, F.; Barbieri, L.; Giustra, M.; Bertolini, J.A.; **Tomaino, G**.; Tortora, P.; Prosperi, D.; Colombo, M. Saporin Toxin Delivered by Engineered Colloidal Nanoparticles Is Strongly Effective against Cancer Cells. *Pharmaceutics* **2022**, *14*, 1517.

https://doi.org/10.3390/pharmaceutics14071517

# Posters and Oral presentations

10-16/12/2023 Sestriere, Italy

**Oral presentation at BIOCUBE Workshop**

Sestriere (IT)

Oral presentation at 2nd BIOCUBE Workshop and Winter School in BioPhotonics, BioElectronics & BioMechanics (BIOCUBE 2023) Sestriere (IT). Title: *Development and biophysical characterization of vault-based nanoparticles for the targeted delivery of therapeutic molecules.*

24-27/09/2023 Avigliana (TO), Italy - Milan

**Oral presentation at the 15th Annual PhD Meeting**

Certosa 1515, Avigliana (TO) – Mario Negri Institute (Milan)

PhD course in Converging Technologies for Biomolecular Systems, Annual meeting THE One Health 2.0. Title: *Recombinant vault nanoparticle: a potential tool for the targeted delivery ofsiRNA as therapeutic molecules.*

05/07/2023 Thessaloniki, Greece

**Invited presentation at "20th Conference of Nanotechnology & Nanomedicine"**

20th International Conference on Nanosciences & Nanotechnologies (NN23) 4-7 July 2023, Thessaloniki, Greece

Invited presentation entitled: *Recombinant vault nanoparticle: a potential tool for the targeted delivery of siRNA as therapeutic molecules*.

13/02/2023 Paris, France

**Invited presentation at the "IJM Internal Seminar"**

Université Paris Cité, CNRS, Institut Jacques Monod

G. Tomaino, A. Dutriaux, P. Tortora, M. Vanoni, G. Frascotti, J. Collignon, D. Flagiello. *Title: Recombinant vault nanoparticle: a potential tool for the targeted delivery of therapeutic molecules*

15/12/2022 Paris, France

**Oral presentation at "Young Scientist Club"**

Université Paris Cité, CNRS, Institut Jacques Monod

G. Tomaino, A. Dutriaux, P. Tortora, M. Vanoni, G. Frascotti, J. Collignon, D. Flagiello. Title: *Recombinant vault nanoparticle: a potential tool for the targeted delivery of therapeutic molecules*

25-28/09/2022 Avigliana (TO), Italy

**Best Oral presentation at the 14th Annual PhD Meeting**

Certosa 1515, Avigliana (TO)

PhD course in Converging Technologies for Biomolecular Systems (TeCSBi), Annual meeting. Title: *Recombinant vault nanoparticle: a potential tool for the targeted delivery of therapeutic molecules*

20-25/07/2022 Erice (TP), Italy

**Oral presentation at the 5th Course of the International School of Nanomedicine on "Advanced nano- and micro-structured materials for medical applications"**

"Ettore Majorana" foundation and center for scientific culture

Giulia Tomaino, Domenico Flagiello, Marco Vanoni, Paolo Tortora, Gianni Frascotti. Title: *Recombinant vault nanoparticle: a potential tool for the targeted delivery of therapeutic molecules*

05/07/2022 Paris, France

**Poster presentation at "Journée scientique de l'UFR Sciences du vivant"**

Université Paris Cité, CNRS, Institut Jacques Monod

G. Tomaino, A. Dutriaux, P. Tortora, M. Vanoni, G. Frascotti, J. Collignon, D. Flagiello. Title: *Recombinant vault nanoparticle: a potential tool for the targeted delivery of therapeutic molecules*

06/04/2022 Nova Gorica, Slovenia

**Invited lecture in the frame of the PhD program Molecular Genetics and Biotechnology, Graduate School of the University of Nova Gorica**

Molecular Genetics and Biotechnology, Graduate School – University of Nova Gorica

On-line lecture. Title: *Recombinant vault nanoparticle: a potential tool for the targeted delivery of therapeutic molecules*

15/12/2021 Milan, Italy

**Poster Presentation at Btbs day 2021**

Biotechnology and Bioscience Department – University of Milano-Bicocca

G. Tomaino, M. Vanoni, P. Tortora, G. Frascotti. Title: *Development and characterization of vault-based nanovectors in Pichia pastoris*

09/2021 Milan, Italy

**Poster Presentation at TeCSBi - 13th PhD meeting**

Biotechnology and Bioscience Department – University of Milano-Bicocca

PhD course in Converging Technologies for Biomolecular Systems (TeCSBi), Annual meeting. Title: *Development and characterization of vault-based nanocarriers in Pichia pastoris*

12/2020 Milan, Italy

**Poster Presentation at Btbs day 2020**

Biotechnology and Bioscience Department – University of Milano-Bicocca

G. Tomaino, M. Pozzi, M. Mazzucchelli, A. Agresta, M. Vanoni, G. Frascotti, P. Tortora. Title: *Development of vault-based nanovectors in Pichia pastoris and antibody-mediated targeting investigation on cancer cell lines*